

See discussions, stats, and author profiles for this publication at: <https://www.researchgate.net/publication/342550979>

Gaussian Quantum Trajectories for the variational simulation of Open Quantum Systems, with Photonic applications

Thesis · June 2020

DOI: 10.13140/RG.2.2.18971.08480

CITATIONS

0

READS

361

1 author:



Wouter Verstraelen

Nanyang Technological University

15 PUBLICATIONS 61 CITATIONS

SEE PROFILE



UNIVERSITEIT ANTWERPEN

FACULTEIT WETENSCHAPPEN – DEPARTEMENT FYSICA

THEORY OF QUANTUM SYSTEMS AND COMPLEX SYSTEMS

**Gaussian quantum trajectories for
the variational simulation of open
quantum systems
with photonic applications**

Proefschrift voorgelegd met het oog op het behalen van de graad van *Doctor
in de Wetenschappen: Fysica* door
Wouter VERSTRAELEN

Promotor
prof. dr. MICHIEL WOUTERS

Antwerpen, 24 juni 2020

Jury members:

prof. dr. Francois Peeters (chair)

Condensed Matter Theory, University of Antwerp

prof. dr. Michiel Wouters (advisor)

Theory of Quantum Systems and Complex Systems, University of Antwerp

prof. dr. Paul Scheunders

Vision Lab, University of Antwerp

prof. dr. Peter Kirton

Computational Nonlinear & Quantum Optics Group, University of Strathclyde

prof. dr. Michał Matuszewski

Polariton group, Polish Academy of Sciences

Samenvatting

Gaussische kwantumtrajecten voor de variationele simulatie van open kwantumsystemen, met fotonische toepassingen

Sinds de opkomst van de kwantummechanica, nu een eeuw geleden, heeft de fysica een enorme vooruitgang geboekt. Enkele fundamentele vragen zijn nog steeds grotendeels onbeantwoord: denk aan de interpretatie van het meetproces (mensen zijn zelf een deel van de kwantumwereld, hoe kunnen we dan het idee hebben dat metingen zo speciaal zijn en in het dagelijks leven klassiek gedrag observeren?) of het consistent maken met algemene relativiteit (hoe kan een golfpakket de ruimtetijd buigen?).

Operationeel is kwantummechanica echter bijzonder succesvol gebleken, en heeft allerlei tests met bijzonder hoge precisie doorstaan. Naast fundamenteel onderzoek heeft kwantummechanica dan ook steeds meer praktische toepassingen gevonden. Een groot toepassingsveld lag bijvoorbeeld in de vastestoffysica, waar materiaaleigenschappen konden (en kunnen) worden bepaald; en in het verlengde daarvan de volledige hedendaagse chemie.

De technologische vooruitgang staat echter niet stil, en we staan in de 21e eeuw voor nieuwe ontwikkelingen, waar kwantumeigenschappen niet meer louter worden gezien als noodzakelijke correcties om theoretische beschrijvingen te verfijnen. Het besef is meer en meer gaan groeien –na de vroege suggestie van Feynman– dat net die echte, tegenintuitieve, kwantumeigenschappen kunnen geogst worden voor zinvolle doeleinden.

Het gaat dan onder meer over de computationele oplossing van complexe problemen die moeilijk zijn op te lossen op een klassieke computer (uitgedrukt in klassen zoals *NP-hard*). Er worden enkele verschillende strategieën bestudeerd in deze context. De eerste is *kwantumsimulatie*: voor een belangrijk maar complex kwantumprobleem uit bijvoorbeeld de biochemie of hoge-energiefysica realiseert men zich dat de relevante Hilbertruimte exact afgebeeld kan worden op de Hilbertruimte in een ander kwantumsysteem waar een veel grotere experimentele controle over bestaat. Wanneer een experiment op dit tweede systeem wordt uitgevoerd, kan

daar, na het uitvoeren van de omgekeerde afbeelding, veel uit worden geleerd over het oorspronkelijk systeem.

De tweede strategie is volledige (universele) *kwantumcomputing*: hierbij zoekt men naar kwantumalgoritmes, die wegens de grotere flexibiliteit dan klassieke systemen moeten toelaten om taken die zwaar zijn voor klassieke computers (e.g. berekening van permanenten) uit te voeren, zogeheten *quantum supremacy*.

Als hardware zoekt men objecten die een mesoscopische coherentie kunnen vertonen, het kan dan onder meer gaan over koude atoomcondensaten, Rydbergatomen, ionen in een val, fotonen of een combinatie van deze elementen. Een zeer belangrijke factor in deze context, is dat zulke kwantumsystemen nooit compleet gesloten zijn, maar onvermijdelijk met hun omgeving interageren. Hoewel dit aanvankelijk als een obstakel werd gezien, is gaandeweg het besef gegroeid dat zulk gedrag ook nuttig toegepast kan worden.

Deze nood om te werken met een beschrijving als open quantumstelsel is het sterkst bij de fotonische systemen, waar steeds een deel weglekt dat moet gecompenseerd worden met een pomplaser, wat leidt tot zogeheten *gedreven-dissipatieve* systemen. Inderdaad is de studie van open quantumstelsels eind vorige eeuw voortgekomen uit de kwantumoptica. Nieuw in het laatste decennium is dat het onderzoeksgebied zich meer en meer uitbreidt richting open veeldeeltjessystemen. Behalve in het geval waar de interactie met de omgeving puur thermisch is, leidt dat automatisch tot niet-evenwichtsfysica, waar een groot deel van de gekende statistische fysica niet geldig is. Dit maakt dat dezelfde systemen ook uit fundamenteel oogpunt heel interessant zijn omdat er fenomenen opduiken die er in evenwicht niet zijn.

Een huidige beperking bij de studie van zulke open veeldeeltjessystemen met mogelijke toepassingen in kwantuminformatica is, ietwat ironisch, dat deze bijna per definitie moeilijk te simuleren zijn op een klassieke computer. Desalniettemin kunnen numerieke simulaties vaak wel helpen zulke systemen beter te begrijpen, zeker ook vanuit fundamentele interesse. Ook in gesloten niet-klassieke systemen worden al geruime tijd benaderende simulatiemethoden toegepast die dikwijls de belangrijke fysica vatten.

Eén zo'n methode in gesloten systemen staat bekend als *Hartree-Fock-Bogoliubov (HFB)*. Dit is een variationele methode waar een Gaussische toestand wordt gebruikt als ansatz voor de golf functie. Deze slaagt er in om complexiteit die exponentieel groeit met systeemgrootte, te reduceren tot louter kwadratische schaling.

In deze thesis breiden we de HFB methode uit naar open systemen. Een groot verschil is dat de Schrödingervergelijking in open systemen stochastisch wordt, op een manier die sterk gerelateerd is aan het optreden van metingen. De resulterende golffuncties staan bekend als kwantumtrajecten (*quantum trajectories*). Zoals we zullen zien, zullen noch de precieze manifestatie van ruis (*unraveling*), noch de Gaussische ansatz (kwadratuurvariabelen of dichtheid-fase) zelf uniek zijn, en kan deze vrijheid uitgebuit worden in verschillende situaties.

In Deel I van deze thesis geven we een gedetailleerdere achtergrond van open quantumsystemen en de recentere ontwikkelingen op het vlak van veeldeeltjessystemen in deze context, inclusief een overzicht van bestaande simulatiemethodes. We herhalen ook de basiseigenschappen van Gaussische toestanden. Daarna tonen we expliciet hoe de Gaussische aanname en het quantum trajectory formalisme gecombineerd kunnen worden. Aan de hand van twee problemen in een enkele gedreven-dissipatieve caviteit, vergelijken we de performantie van de verschillende keuzes die gemaakt kunnen worden en in het bijzonder de overeenkomst met de exacte oplossing die hier nog verkregen kan worden. We bespreken kort de numerieke schaling van de methodes.

In Deel II bestuderen we een meer geavanceerde toepassing: met name een rooster van gedreven-dissipatieve Kerr-caviteiten met twee-foton pomp. In dit systeem treedt spontane symmetriebreking op voor toenemende pompsterkte, een dissipatieve tweede-orde faseovergang. Het was reeds bekend dat deze fase-overgang tot de universaliteitsklasse van het *kwantum-(transvers-)Isingmodel* behoort in de limiet van lage verliezen en beperkte dichtheid: dit betekent dat correlaties tussen de caviteiten hoofdzakelijk een kwantumkarakter hebben, ook wel gekend als ‘verstrengeling’. Niet alleen bevestigen we dit resultaat met de Gaussische-trajectorymethode (tot iets grotere roosters dan voorheen), we zien ook dat in een parameterregime met hogere dichtheid en verliezen, waar andere methodes ontoereikend zijn, via deze methode dat de universaliteitsklasse verandert naar die van het *klassieke(thermische) Isingmodel*. We kunnen hier alvast uit leren dat de rol van dissipatie bij niet-evenwichtssystemen kan overeenkomen met een effectieve temperatuur. Vervolgens onderzoeken we de dynamische aspecten van de fase-overgang. We merken dat onder quenches (plotse verandering van een parameter) van het systeem er een duidelijke *kritische vertraging* optreedt die via het *Kibble-Zurek* effect tot de vorming van verschillende ‘magnetische’ domeinen leidt in de geordende fase. De grootte van deze domeinen correspondeert ook met de *dynamische kritische exponent* die met metropolisdynamica in het klassieke

Isingmodel overeenkomt. Dezelfde dynamische kritische exponent vinden we verder optreden in de *Liouwilliaanse gap*, die, zoals we aantonen, dezelfde universele schalingsrelaties heeft als de gewone (Hamiltoniaanse) gap voor kwantumfaseovergangen in een gesloten systeem.

Deel III tenslotte is gewijd aan een andere toepassing: een Bose-Einsteincondensaat van fotonen in een caviteit van verfmoleculen. Hier was reeds geruime tijd een heuristisch fasormodel in gebruik voor de numerieke beschrijving. Met Gaussische trajectories slagen we erin de geldigheid ervan te verifiëren. Een bijzondere eigenschap van een fotoncondensaat is dat het aantal deeltjes niet behouden blijft: in de limiet van een groot reservoir van verfmoleculen leidt dit zelfs tot *grootcanonische* statistiek waar deeltjesfluctuaties arbitrair groot kunnen worden. Het is dan ook geen triviaal gegeven dat condensatie kan plaatsvinden onder deze omstandigheden. We breiden de bestaande kennis van de deeltjesstatistiek uit met een studie van de invloed van foton-fotoninteracties, pomp en verliezen. In het bijzonder observeren we hoe interacties de deeltjesfluctuaties (tweede-orde coherentie) reduceren en sneller doen vervallen. De pomp en verliezen zorgen dan weer voor het merkwaardige effect dat enige tijd ná een fluctuatie met bovengemiddeld veel deeltjes, er gemiddeld minder fotonen zullen zijn dan gemiddeld. Vervolgens bestuderen we de fasecoherentie (eerste-orde coherentie). De twee voornaamse limitaties op lijnbreedte van pakweg een laser worden uitgebreid naar dit grootcanonisch regime. Dit zijn het *Schawlow-Townes* effect waarvan we zien dat het in de grootcanonische limiet slechts twee keer sneller gaat, en in het geval van interacties een bijkomende *Henry-diffusie* die deeltjesfluctuaties omzet in fasefluctuaties.

Voorwoord

Met deze thesis sluit ik de vierjarige periode in mijn leven, genaamd het doctoraat, af. Ik heb gedurende deze onderneming bij momenten gezweet (en een enkele keer zelfs eens gevloekt). Maar alles samen heb ik het in de eerste plaats als een bijzonder boeiende en leerrijke tocht ervaren. Dit is verre van louter mijn eigen verdienste. Ik dank **prof. dr. Michiel Wouters** om mij in dienst te nemen bij de groep en mij een thesisonderwerp te geven dat mij lag en waarop ik me goed heb kunnen uitleven. Ook het gemak waarmee hij bereikbaar was wanneer nodig voor hulp en heel interessante discussies maar ook vrijheid gaf, is noemenswaardig. En vooral ook om het voorbeeld te stellen van wat het betekent om een goede wetenschapper te zijn. Ik dank ook **dr. Wim Casteels** die me in gang heeft geholpen bij het uiterste begin van dit onderzoek.

Bij uitbreiding dank ik heel de groep *Theorie van kwantumsystemen en complexe systemen (TQC)*, de leuke bende met wie het een voorrecht was om onderzoek te doen. In het bijzonder mijn directe collega's Dolf, Mathias, Lennart en Vladimir; en kantoorgenoot Dietrich.

Gedurende bepaalde onderdelen van het onderzoek ben ik inhoudelijk nog met anderen in contact geweest. Voor het onderzoek naar de kwadratisch gedreven Kerr roosters heb ik bijvoorbeeld het genoeg gehad een viermaandelijke onderzoeksstage naar EPFL uit te voeren. Ook hier dank ik de groep (**LTPN**) voor de aangename tijd. Meerbepaald heb ik hier intensief samengewerkt met **dr. Riccardo Rota** en **prof. dr. Vincenzo Savona**, van wie me de georganiseerde aanpak en snel strategisch inschattingsvermogen zijn bijgebleven. Voor het onderzoek toegepast op fotoncondensatie, zijn discussies met **dr. Julian Schmitt** en **prof. dr. Martin Weitz** dan weer heel nuttig geweest. Ik dank ook de leden van de jury voor de constructieve opmerkingen die me de thesis nog verder hebben doen verbeteren tot deze finale versie.

CHAPTER 0 - VOORWOORD

Los van het wetenschappelijke aspect, dank ik ook alle vrienden en familie (deze houdt, naast mijn ouders en grootouders, ook mijn zus in van wie ik vier jaar lang heb moeten horen dat ik ze niet heb vermeld in het dankwoord van mijn masterthesis ;)) voor de steun, afleiding en interesse. Tot slot is er natuurlijk u, de lezer. Veel plezier!

Contents

Samenvatting	iii
Voorwoord	vii
1 Overview	1
1.1 Introduction: driven-dissipative many-body systems	1
1.2 The Gaussian Trajectory Approach	2
1.3 Application to specific models	3
1.3.1 Dissipative phase transition in quadratically-driven Kerr lattices	3
1.3.2 Temporal coherence of a dye-microcavity photon condensate	4
I Describing open quantum systems with Gaussian quantum trajectories	5
2 Fundamentals of open quantum systems	7
2.1 What is an open quantum system?	7
2.2 Preliminary notions	8
2.2.1 Wavefunction and Hilbert space	8
2.2.2 Mixed quantum states	9
2.2.3 Time-evolution	9
2.2.4 Composite systems	10
2.2.5 Measurements	11
2.3 Evolution of the density matrix: the Lindblad master equation . .	12
2.4 Quantum trajectories and stochastic simulation	14
2.4.1 First benefit of quantum trajectories: closer connection to experiment	16
2.4.2 Second benefit of quantum trajectories: stochastic simulation needs less computational resources	17

2.4.3	Distinguishing quantum- and classical fluctuations	17
2.4.4	Correspondence with other concepts from quantum mechanics	18
2.5	Example: dissipation from an optical cavity	18
2.5.1	The photon-counting unraveling	20
2.5.2	Other unravelings	21
2.6	Two-time correlation functions: the Onsager-Lax quantum regression theorem	22
2.7	Further extensions	22
2.7.1	Non-markovian dissipation	22
2.7.2	Relativistic methods	23
3	Many-body open quantum systems and their numerical description	25
3.1	Many-body open quantum systems	25
3.2	Experimental platforms	27
3.2.1	Non-equilibrium physics of atomic condensates	27
3.2.2	Exciton-polariton condensates	27
3.2.3	Dye-microcavity photon condensates	28
3.2.4	Superconducting quantum optics	28
3.2.5	Other experimental platforms	29
3.3	Contemporary analytical and numerical methods	29
3.3.1	Exact diagonalization	29
3.3.2	Mean-field	30
3.3.3	Locally exact master-equation based approaches	30
3.3.4	Locally exact trajectory-based approaches	31
3.3.5	Cumulant expansion	32
3.3.6	Phase-space methods	32
3.3.7	Other methods	33
4	Gaussian states	35
4.1	The Gaussian distribution in classical statistics	35
4.2	Gaussian states in quantum optics	36
4.2.1	Quantum-optical phase space	36
4.2.2	Squeezed and displaced light	40
4.3	Gaussian states in quantum information	44
4.4	As a variational ansatz: Hartree-Fock-Bogoliubov method	44
4.4.1	A note on the term 'variational'	45

4.5	Density-phase Gaussian states	45
5	Gaussian Quantum Trajectories for the variational simulation of open quantum systems	47
5.1	Combining quantum trajectories with a Gaussian ansatz	47
5.1.1	Quantum trajectories for expectation values	47
5.1.2	Closing at Gaussian level	49
5.2	Optical bistability and the XP -Gaussian methods	49
5.2.1	Benchmarks on a dimer	53
5.3	Phase diffusion and the $N\Theta$ -Gaussian method	54
5.3.1	Phase space evolution	54
5.3.2	$N\Theta$ -Gaussian states	55
5.4	Numerical considerations	60
5.5	Discussion and summary	62
II	Kerr lattices with quadratic driving: an application of the XP-Gaussian method	65
6	Driven-dissipative phase transition in Kerr lattices with two-photon driving	67
6.1	Dissipative phase transitions	67
6.1.1	Introduction: Phases of matter	67
6.1.2	From classical and quantum phase transitions to dissipative phase transitions	69
6.1.3	State-of-the-art on dissipative phase transitions	69
6.1.4	Structure of Part II	71
6.2	Quadratically-driven Kerr resonators	71
6.2.1	Single cavity	72
6.2.2	Arrays	73
6.2.3	Further state-of-the-art in two-photon-driven systems	75
6.3	Annealing and spin models	75
7	Describing quadratically driven kerr lattices with Gaussian trajectories	77
7.1	Accessing the high-loss regime with the GTA method	77
7.2	Implementation and performance	78

7.3	Is TWA a valid alternative?	80
8	The critical behaviour of quadratically driven photonic lattices	85
8.1	The GTA reproduces quantum critical behaviour in the low-loss limit	85
8.2	New result: classical critical behaviour in the high-loss regime . .	88
8.2.1	Failure of the TWA method	95
8.3	Interpretation: losses act as an effective temperature	96
9	Dynamical scaling in quadratically driven kerr-lattices: the Kibble-Zurek effect	99
9.1	Dynamics of phase transitions	99
9.2	Kibble-Zurek scaling for a linear quench	100
9.3	The Liouvillian gap scales with the same exponent	103
	Quadratically driven lattices: Summary and outlook	109
III	The dye-cavity photon condensate: an application of the $N\Theta$-Gaussian method	113
10	Condensation of Photons with dye-molecules	115
10.1	Condensation of photons using dye	115
10.1.1	Comparison with a laser	117
10.1.2	Interactions in a Photon BEC	119
10.1.3	Miscellaneous state-of-the art in photon BECs	120
10.1.4	Structure of Part III	120
10.2	Fluctuations in photon BECs	121
10.2.1	Model for a driven-dissipative, interacting photon condensate	122
10.3	The heuristic phasor model	124
10.3.1	A semiclassical model	124
10.3.2	Predictions	125
11	Describing photon condensates with $N\Theta$ Gaussian trajectories	127
11.1	The condensate as an open quantum system	127
11.2	The variational evolution	130
11.3	How to use a phase operator even though it doesn't exist? Transitions between exact and variational regimes	131
11.3.1	From variational to exact	131

11.3.2	From exact to variational	132
11.4	Predictions	133
12	Coherence of a photon condensate	137
12.1	Number statistics: effect of interactions and losses	137
12.1.1	number distribution	137
12.1.2	Decay of second-order correlations	141
12.1.3	Long- τ (delayed) antibunching	143
12.2	First-order coherence	144
12.2.1	The Grand-Canonical Schawlow-Townes effect, formerly known as 'phase jumps'	144
12.2.2	Henry diffusion in an interacting condensate	146
12.3	Further results	147
12.3.1	Arrays of photon condensates	147
12.3.2	Improved characterization of the number fluctuations	150
	Photon condensation: Summary and outlook	151
IV	Conclusions	153
13	Conclusions and Outlook	155
13.1	Results from quadratically driven lattices	155
13.2	Results from photon condensates	156
13.3	The GTA method: overall outlook	157
A	Unravelings	159
A.1	Photon Counting	159
A.2	Homodyne detection	159
A.3	Heterodyne detection	161
B	Coefficients	163
C	Numerical implementation	167
C.1	Software	167
C.2	Numerical solution of Stochastic processes	167

List of abbreviations

BEC	Bose-Einstein condensate
Cavity QED	Cavity Quantum electrodynamics
Circuit QED	Circuit Quantum electrodynamics
CPT	Classical phase transition
GTA	Gaussian trajectory approach
Het.	Heterodyne unraveling
Hom. (X)	Homodyne unraveling of the X -quadrature
HPM	Heuristic phasor model
KZ	Kibble-Zurek
LO	Local oscillator
θ_{PB}	Pegg-Barnett phase
PC	Photon counting unraveling
PDP	Piecewise-deterministic process
POVM	Positive-operator valued measurement
$N\Theta$ -Gaussian	State that is Gaussian in density and phase
QCP	Quantum-critical point
QCR	Quantum-critical region (regime)
QPT	Quantum phase transition
RateEq	Stochastic rate equations
SDE	Stochastic differential equation
SS	Steady state
$\langle \cdot \rangle_{\text{sym}}$	Symmetrized expectation value
TWA	Truncated Wigner approximation
W/E	Coherence functions of polariton condensates, as obtained by Whittaker and Eastham [1]
W-function	Wigner function
XP -Gaussian	State that is Gaussian in the quadrature variables, or, equivalently, the field operators

CHAPTER 1

Overview

In this thesis, we will introduce the Gaussian Trajectory Approach (GTA) as a novel numerical technique to study driven-dissipative many-body quantum systems. It combines insights about open quantum systems with the Gaussian ansatz that has been commonly used before in closed and equilibrium systems. We will then apply the method to two different systems: quadratically-driven Kerr lattices and a dye-microcavity photon condensate. Accordingly, the body of this thesis constitutes three main parts: on the GTA itself and on both applications. Finally, there is the conclusion section and appendices containing additional information (related to measurement schemes, perturbative coefficients that will arise, and numerical aspects).

1.1 Introduction: driven-dissipative many-body systems

In the first half of Part I, we outline the background by introducing the kinds of systems that we aim to study. Quantum mechanics has been very successful over the last century in describing a variety of physical phenomena in closed systems, including many-body physics in the solid state. In the late 20th century however, the field of quantum optics started to surge, studying individual photonic modes (harmonic oscillators) and their interaction with some atoms. An important consideration with these systems was that light easily leaks out to the environment (*dissipation*), such that it is a manifestly *open* quantum system. The compensation mechanism (pumping or driving) that replaces the photons, will typically drive the system out of equilibrium. Accordingly, theoretical tools had to be introduced to deal with such ‘openness’. First, there is the master equation approach for the ensemble. Tracing out the environment degrees of freedom from the full dynamics

leads to a loss of information (entropy increase). Second, consider continuous measurement on all leaking photons, therefore keeping track of all information that comes out of the system. The evolution *conditioned on this measurement record* can be studied, to retain a Schrödinger-like evolution for pure states: quantum trajectories. Ensemble-evolution can be reconstructed by averaging over many of these quantum trajectories, each with a different (random) measurement record.

At the dawn of the 21st century, the ever-increasing experimental controllability has allowed for a variety of studies regarding nonequilibrium phenomena in many-body physics. For many of these platforms (e.g. exciton-polaritons, cold atoms, Rydberg states, superconducting circuits...), dissipation is again an important aspect. There are at least two reasons why such systems are interesting. The first one is the fundamental condensed matter interest: the nonequilibrium nature gives rise to novel phenomena forbidden by equilibrium thermodynamics. The second one is that such systems are promising candidates for quantum technologies as quantum computing (solving a variety of algorithms on a quantum architecture) or quantum simulation (mapping another interesting quantum system on one which is more experimentally accessible). Indeed, one of the most important aspects in such quantum technologies is that they should combine being sufficiently mesoscopic to be accessible, while still being resilient to decoherence. This decoherence is strongly related to dissipation, although dissipation can also be engineered to maintain coherence as good as possible.

The quest for more exotic many-body phenomena, as well as increasing the interaction strengths to a level where quantum information processing becomes relevant, pushes the systems away from parameter regimes where reliable results are obtained by mean-field theory. Therefore, the many-body approach must be synthesized with the theoretical methodology for open quantum systems.

1.2 The Gaussian Trajectory Approach

Many successful results in closed-system many-body physics, both regarding stationary properties and the dynamics, are obtained from variational methods, where the true state is approximated by the one 'as close as possible' within a class of variational states with few parameters. An important example of such a variational class of states are the *Gaussian states*, which are entirely characterized by the expectation values and two-point correlators of the field operators. All higher order moments can be decomposed using Wick's theorem. The GTA methods that

we introduce simply combine quantum trajectories with such Gaussian ansatzes. Computationally, the advantage is that classical fluctuations can still be easily sampled, as for exact trajectories, but the computational cost for a trajectory reduces from exponentially large to only quadratic with system size. When working with quantum trajectories, there is some freedom involved related to the kind of measurement that is performed on the leaking light (the unraveling). Furthermore, we introduce ‘density-phase’ Gaussian states in addition to the normal Gaussian states. We will carefully examine the benefits and drawbacks of these different ansatzes and unravelings. As a first proof-of-principle study, we illustrate the method with a study on the bistability and dephasing in a single driven-dissipative Kerr-nonlinear cavity.

1.3 Application to specific models

1.3.1 DISSIPATIVE PHASE TRANSITION IN QUADRATICALLY-DRIVEN KERR LATTICES

In Part II, we study a lattice of such driven-dissipative Kerr resonators, that could for example be implemented with superconducting circuits. Furthermore, we use a specific two-photon pump for the driving. This model exhibits a symmetry-breaking second-order *dissipative* phase transition as function of the pump strength. Using finite-size scaling approaches, we determine the universality classes of the transition. In the low-loss regime, the method reproduces quantum-critical behaviour that was previously obtained with a different method, showing that the GTA is able to capture important long-range quantum correlations. We will then move on to a different parameter regime with higher loss rate, that is inaccessible with other methods. By application of the GTA we find out that the transition now belongs to a classical universality class. More specifically, these classes relate to Ising-spin models. The combination of both classes depending on the dissipation rate, shows that the losses take a role very similar to finite temperature.

In a following step, we study dynamical properties related to this dissipative phase transition. First, by performing linear quenches, we see that ‘magnetic’ domains are formed by the photons. The size of these domains is described by the celebrated Kibble-Zurek mechanism and allows us to extract the dynamical critical exponent. Second, from the relaxation time to equilibrium, we extract the gap of the *Liouvillian* superoperator. It scales with the same dynamical exponent,

which implies that its scaling relations are the same as for the Hamiltonian gap for quantum phase transitions in closed systems. The value of this dynamical exponent corresponds to the metropolis algorithm common for the simulation of spin lattices.

1.3.2 TEMPORAL COHERENCE OF A DYE-MICROCAVITY PHOTON CONDENSATE

Bose-Einstein condensation has been achieved on a variety of platforms. This includes photons in a cavity, which thermalize because of frequent absorption and emission processes with a dye-molecule reservoir. Unlike other condensates, the particle number is not conserved, leading to grand-canonical statistics in certain parameter regimes. Further subtleties affecting the system are interactions, and the fact that also the combined photon+dye system is weakly driven-dissipative.

In Part III, we construct a hybrid GTA+exact trajectory model to study the statistics and coherence properties in this system, in combination with analytical derivations. If one is only interested in the number statistics, the trajectory model reduces to stochastic rate equations. Interactions both decrease the amount of number fluctuations in the system and increase their decay rate (second-order temporal coherence). At longer timescales, we surprisingly find anticorrelations in photon number, that can be attributed to the finite photon losses through the mirrors. For the first-order coherence that includes phase information, we find with the help of trajectories and analytical expressions that the temporal decay of correlations is only twice as fast in the grand-canonical regime, compared to the canonical regime where the Schawlow-Townes mechanism determines the decay rate similar to lasers. This is in contrast with reasoning based on dominating ‘phase jumps’ when the photon number vanishes. Kerr interactions will further cause an additional Gaussian Henry phase diffusion. For both the number and phase correlations, we find that a heuristic phasor model, originally introduced for the study of laser physics, is able to provide quantitatively accurate results for the experimentally relevant parameters studied here, despite some conceptual difficulties.

PART

I

DESCRIBING OPEN QUANTUM
SYSTEMS WITH GAUSSIAN QUANTUM
TRAJECTORIES

W. Verstraelen and M. Wouters, “Gaussian quantum trajectories for the variational simulation of open quantum-optical systems”, *Applied Sciences* **8**, *feature paper*, 1427 (2018).

Fundamentals of open quantum systems

For many systems, weak coupling with an environment is highly relevant to their properties, and a Schrödinger equation alone is insufficient. Such systems can be described either with the Lindblad master equation for the density matrix, or with the stochastic quantum trajectory method that lays at the basis of the Gaussian trajectory method which is the central topic of this thesis.

2.1 What is an open quantum system?

Quantum mechanics has been a cornerstone of physical research in the 20th century [2]. It is widely regarded as a successful fundamental theory with a strong mathematical framework. This is largely despite the counterintuitive aspects of quantum mechanics that become explicit in (thought or real) experiments such as the Stern-Gerlach and double-slit experiment (because of which quantum mechanics has acquired an almost mythical status as ‘very weird and difficult’ in popular culture). These aspects are manifestations of the concept of Heisenberg uncertainty at the very heart of quantum mechanics. Despite the objections of big physicists such as Albert Einstein (“As I have said so many times, God doesn’t play dice with the world” [3]), we can say that quantum mechanics is inherently probabilistic, there are always ‘quantum fluctuations’¹.

However, this basic picture where everything can be described by the Schrödinger equation and Born’s rule [2] is often very optimistic in practical setups, in the

¹There is still some ambiguity in the *interpretation* of quantum mechanics. Strictly speaking, *non-local* hidden variable theories cannot be ruled out, these would be fully deterministic at the cost of violating locality. For an overview of the different interpretations, see e.g. Refs. [4, 5].

sense that it only applies to isolated systems. Ultimately, all quantum mechanical systems are open, as they are necessarily embedded in an environment [6]. In fact, the same holds for classical Hamiltonian mechanics, with the difference that the latter is often, in its realm of applicability (think for example of celestial bodies), much less sensitive to external influences.

In classical systems, tracing out the environment yields the Hamiltonian descriptions incomplete and gives the system a stochastic nature (with as a textbook example, the case of Brownian motion). Similarly, we will see that the openness of a quantum system leads to additional ‘classical’ fluctuations. Interestingly, the description of open quantum systems has a strong connection with quantum measurement theory [7], as an open quantum system can be formally seen as ‘continuously measured’ by its environment [8]. From this realization, it can be understood that the boundary between ‘quantum’ and ‘classical’ fluctuations is not uniquely defined, but depends on the measurement protocol.

In this chapter, we focus on the fundamentals of open quantum systems as the field emerged to large extent with quantum optics experiments up to the 1990s and early 2000s, including the ‘quantum trajectories’ method in section 2.4. A number of comprehensive books have been devoted to this subject on a fundamental level [6, 8], focussing on the practical application [9, 10] and starting from measurement theory [7]. From a pedagogical point, Ref. [11] is also very convenient in that, using a simple model of interacting q-bits in discrete time, it strips the physics down to its bare essence without the need for particular quantum optics background, and discusses the relation with alternative interpretations of quantum mechanics (although the Copenhagen interpretation is sufficient for the formalism). Here, we will only provide a brief overview and refer to these works for further background. In the next chapter 3, we then turn to the more recent study of open many-body systems and numerical approaches.

2.2 Preliminary notions

Before we move on to open quantum systems, a brief recap on quantum mechanics in closed systems [2] may be appropriate.

2.2.1 WAVEFUNCTION AND HILBERT SPACE

According to the common mathematical framework, any quantum system is characterized by its *Hilbert space* \mathcal{H} (a complete vector space endowed with an

inner product). The (pure) state of the system then corresponds to a *ket* $|\psi\rangle \in \mathcal{H}$, a state vector of the Hilbert space (modulo multiplicative constants), also known as the *wavefunction*. The space of linear functionals mapping states back to numbers is the dual space \mathcal{H}^* , of which elements $\langle\psi| \in \mathcal{H}^*$ are called *bra's*.

Physical observables are self-adjoint operators $\hat{A} = \hat{A}^\dagger$, of which the expectation value for state $|\psi\rangle$ is equal to $\langle\hat{A}\rangle = \langle\psi|\hat{A}|\psi\rangle$. Importantly, unless $|\psi\rangle$ is an eigenvector of \hat{A} , a finite uncertainty (the variance $\text{Var}\hat{A} = \langle\hat{A}^2\rangle - \langle\hat{A}\rangle^2$) remains. This directly relates to the *Heisenberg uncertainty relation*

$$\text{Var}(\hat{A}) \text{Var}(\hat{B}) \geq \frac{1}{4} |[\hat{A}, \hat{B}]|^2, \quad (2.1)$$

where $[\hat{A}, \hat{B}]$ is the commutator $\hat{A}\hat{B} - \hat{B}\hat{A}$.

The full Hilbert space of a many-body system can be parametrized in two ways: eigenbases are either constructed by starting with all particles and putting them in all possible modes (first quantization), or by starting with all the modes and giving them all possible occupations (second quantization). The latter approach has the advantages that symmetrization of the wavefunction is less cumbersome and that the particle number does not need to remain conserved.

2.2.2 MIXED QUANTUM STATES

In a generalized framework, mixed states are introduced as the ones where there is additional *classical* uncertainty. If we know the system to be in state $|\psi_i\rangle$ with probability p_i , then the mixed state is described by the *density matrix*

$$\hat{\rho} = \sum_i p_i |\psi_i\rangle \langle\psi_i|. \quad (2.2)$$

Some notions of mixedness are the purity $\mu = \text{tr}[\hat{\rho}^2]$ (1 for a pure state) and von Neumann-entropy $S_{\text{vn}} = -\text{Tr}[\hat{\rho} \log \hat{\rho}]$ (0 for a pure state and in first order equal to the linear entropy $S_{\text{lin}} = 1 - \mu$). Importantly, if $\hat{\rho}$ is mixed, its decomposition in pure states is not unique. Expectation values are computed in terms of density matrices as $\langle\hat{A}\rangle = \text{tr}[\hat{\rho}\hat{A}]$.

2.2.3 TIME-EVOLUTION

Physical symmetries in closed quantum systems map to unitary transformations, that conserve purity. In particular, kets in a closed quantum system evolve

according to the Schrödinger equation (we set $\hbar = 1$ for the remainder of this thesis).

$$\partial_t |\psi\rangle = -i \hat{H} |\psi\rangle. \quad (2.3)$$

This leads to

$$|\psi(t)\rangle = \hat{U} |\psi(0)\rangle, \quad (2.4)$$

where $\hat{U} = \exp[-i \hat{H} t]$ and we have assumed Hamiltonian \hat{H} to be time-independent for simplicity.

In terms of density matrices, one has the Von Neumann-Liouville equation

$$\partial_t \hat{\rho} = -i [\hat{H}, \hat{\rho}], \quad (2.5)$$

or

$$\hat{\rho}(t) = \hat{U} \hat{\rho}(0) \hat{U}^\dagger. \quad (2.6)$$

The picture above, where the quantum state evolves (keeping observables constant) is known as the *Schrödinger picture*. An equivalent formulation is the *Heisenberg picture* where the quantum state itself ($|\psi\rangle$ or $\hat{\rho}$) remains stationary, while instead

$$\partial_t \hat{A} = -i [\hat{A}, \hat{H}] \quad (2.7)$$

for all observables \hat{A} . Finally, there is the *interaction picture* where the observables evolve according to a ‘non-interacting’ part of the Hamiltonian, and the quantum state evolves to an ‘interaction’ term of the Hamiltonian. Its main advantage is that it allows for working perturbatively in this interaction term in a straightforward manner.

2.2.4 COMPOSITE SYSTEMS

Now, consider two quantum systems 1 and 2 with respective Hilbert spaces \mathcal{H}_1 and \mathcal{H}_2 . If the systems are coupled, the total quantum state lives in the combined Hilbert space $\mathcal{H}_{\text{tot}} = \mathcal{H}_1 \otimes \mathcal{H}_2$. This combined state can possibly be pure, but can in any case be described by a density matrix $\hat{\rho}_{\text{tot}}$.

If one is only interested in the first subsystem, one can work with the *reduced* density matrix

$$\hat{\rho}_1 = \text{tr}_2 \hat{\rho}, \quad (2.8)$$

where subsystem 2 is traced out. Importantly, this tracing out degrees of freedom implies a loss of information. This means that $S_1 + S_2 \geq S_{1+2}$. In particular, even when $\hat{\rho}$ is a pure state, $\hat{\rho}_1$ is not. In fact, in this case, $S_{\text{ent}} = -\text{tr}\{\hat{\rho}_1 \log \hat{\rho}_1\} = -\text{tr}\{\hat{\rho}_2 \log \hat{\rho}_2\}$, the *entanglement entropy* is a widely used concept to quantify the extent to which subsystems 1 and 2 are correlated.

2.2.5 MEASUREMENTS

Assume $|\psi\rangle = \sum_i c_i |\phi_i\rangle$, where $\{|\phi_i\rangle\}$ is a set of eigenvectors of observable \hat{A} , with corresponding eigenvalues a_i . Performing a *strong (projective) measurement* will yield a measurement outcome a_i with probability $|c_i|^2$ and then leave the system in state $|\phi_i\rangle$ (Born's rule). This can be formalized with projector operators $\hat{\mathcal{P}}_i$ satisfying

$$\hat{\mathcal{P}}_i \hat{\mathcal{P}}_{i'} = \delta_{ii'} \quad (2.9)$$

and

$$\sum_i \hat{\mathcal{P}}_i = \mathbb{1} : \quad (2.10)$$

The probabilities are given by $p_i = \langle \hat{\mathcal{P}}_i \rangle$ and bring the state to $\hat{\mathcal{P}}_i |\psi\rangle / \sqrt{p_i}$ or $\hat{\mathcal{P}}_i \hat{\rho} \hat{\mathcal{P}}_i / p_i$.

In realistic experimental setups, measurement devices have a limited resolution, meaning that complete projection on an eigenstate does not take place. To account for these cases, there is the more general notion of a *Positive-Operator Valued Measurement (POVM)* that generalizes projective measurements. These can also be understood as the effect of a projective measurement on an ancillary system to which the system of interest is connected: we will study an explicit example later. The projector operators are now replaced by more general positive operators \hat{E}_i satisfying $\sum_i \hat{E}_i = \mathbb{1}$. The property of positivity means that there exists a set of operators $\{\hat{A}_{ij}\}$ such that

$$\hat{E}_i = \sum_j \hat{A}_{ij}^\dagger \hat{A}_{ij}. \quad (2.11)$$

In a POVM, one observes with probability $p_i = \langle E_i \rangle$ the state

$$\frac{1}{p_i} = \sum_j \hat{A}_{ij} \hat{\rho} \hat{A}_{ij}^\dagger. \quad (2.12)$$

In the case where the POVM yields only little information on subsystem 1, and consequently causes only a little perturbation, it is called a *weak measurement*.

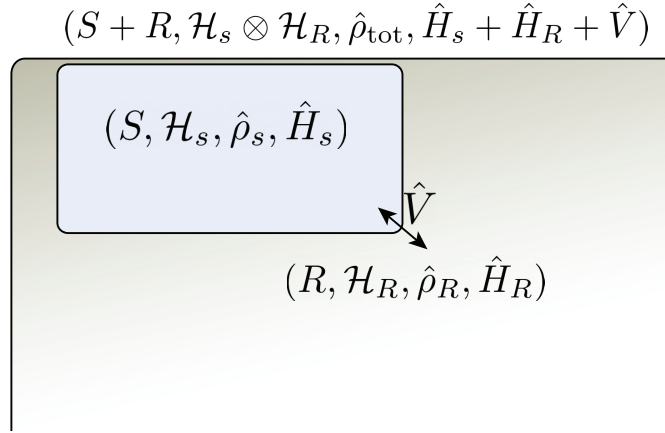


FIGURE 2.1: An open quantum system S is weakly coupled to an infinite reservoir R with a coupling Hamiltonian \hat{V}

2.3 Evolution of the density matrix: the Lindblad master equation

Consider a large quantum system $(S + R)$ with density matrix $\hat{\rho}_{\text{tot}}$ in Hilbert space $\mathcal{H}_S \otimes \mathcal{H}_R$, which consists of a subsystem S of interest (Hilbert space \mathcal{H}_S , reduced density matrix $\hat{\rho}_S$), via coupling Hamiltonian \hat{V} , weakly coupled with a reservoir R ($\mathcal{H}_R, \hat{\rho}_R$) with infinitely many degrees of freedom (Figure 2.1).

In order to study S , we are particularly interested in the evolution of $\hat{\rho}_S = \text{tr}_R \hat{\rho}_{\text{tot}}$. This immediately implies that we should expect $\hat{\rho}_S$ to become a mixed state (except in the trivial case where S and R are decoupled), even if $\hat{\rho}_{\text{tot}}$ is a pure state. This confirms that a wavefunction description is insufficient and a density-matrix description open quantum systems is necessary.

Comparing the evolution of a closed quantum system (governed by *quantum* fluctuations)

$$\partial_t |\psi\rangle = -i \hat{H} |\psi\rangle \quad (2.13)$$

with the evolution of probability for a classical Markov process for a probability vector \vec{p} (governed by *classical* fluctuations)

$$\partial_t \vec{p} = \mathcal{W} \vec{p}, \quad (2.14)$$

and observing the similarity, we might be hopeful that the evolution of an open quantum system, where both quantum and classical fluctuations are present, can

also be written as a first order linear differential equation that is local in time, i.e.

$$\partial_t \hat{\rho}_s = \mathcal{L} \hat{\rho}_s. \quad (2.15)$$

This conjecture turns out to be valid under quite general circumstances that allow writing $\hat{\rho}(t) \approx \hat{\rho}_s(t) \otimes \hat{\rho}_R$. This can be justified in microscopic models from a clear separation of timescales (Markov-Born approximation) and generates the so-called *quantum-dynamical semigroup* [6, 8, 12]. \mathcal{L} is a superoperator that goes under the name *Liouville operator* or *Liouvillian* and takes an analogous role to the Hamiltonian in closed quantum systems as the generator of time-evolution (it is a generalization of (2.5))².

We have, however, so far not obtained an explicit, useful form for \mathcal{L} . We require that \mathcal{L} is a linear operation that, to be physically acceptable, preserves hermiticity, the trace of $\hat{\rho}_s$ and its positivity. In fact, \mathcal{L} must be completely positive, meaning that for any other subsystem $\hat{\rho}'_s$, joint evolution $\mathcal{L}_s \otimes \mathbb{1}'_s$ is also a positive map. Under these circumstances, \mathcal{L} is a valid *quantum map*, meaning it can be written (compare with (2.6) for a closed system) as

$$\hat{\rho}_s(t) = \sum_{\mu} \hat{M}_{\mu} \hat{\rho}_s(0) \hat{M}_{\mu}^{\dagger}, \quad (2.16)$$

where $\{\hat{M}_{\mu}\}$ is a (non-unique) set of *Kraus operators* [8, 12].

For an infinitesimal time-evolution (first order in dt), we can rewrite (2.16) as

$$\hat{M}_0 = \mathbb{1} - i \hat{H}_{\text{eff}}(t) dt \quad (2.17)$$

$$\hat{M}_{\mu \geq 1} = \hat{L}_{\mu}(t) \sqrt{dt}. \quad (2.18)$$

Operators $\hat{L}_{\mu}(t)$ are known as the Lindblad or *jump operators*. From requiring trace preservation ($\sum_{\mu} \hat{M}_{\mu}^{\dagger} \hat{M}_{\mu} = \mathbb{1}$), we obtain that

$$\hat{H}_{\text{eff}} = \hat{H} - \frac{i}{2} \sum_{\mu} \hat{L}_{\mu}^{\dagger} \hat{L}_{\mu}, \quad (2.19)$$

where \hat{H} can be identified as the Hamiltonian of S . Putting everything together,

²Some authors prefer to use an explicit mapping $\hat{\rho}_s \in \mathcal{H} \otimes \mathcal{H}^* \leftrightarrow |\rho\rangle\rangle \in \mathcal{H} \otimes \mathcal{H}$. This procedure goes under the name of *third quantization* [13], and $|\rho_s\rangle\rangle$ is now a superket. The practical use of this symmetry is that it allows writing an explicit matrix representation \mathbb{L} for \mathcal{L} for which standard tools from linear algebra apply.

this leads to the *Lindblad equation*

$$\frac{d\hat{\rho}}{dt} = \mathcal{L}\hat{\rho} = -i[\hat{H}, \hat{\rho}] + \sum_{\mu} \left[\frac{-1}{2}(\hat{L}_{\mu}^{\dagger}\hat{L}_{\mu}\hat{\rho} + \hat{\rho}\hat{L}_{\mu}^{\dagger}\hat{L}_{\mu}) + \hat{L}_{\mu}\hat{\rho}\hat{L}_{\mu}^{\dagger} \right], \quad (2.20)$$

where we have now dropped the subscript s . Although equations of this form have appeared earlier in particular setups [14], the generality of the equation (2.20) has been shown by Gorini, Kossakowski, Sudarshan [15] and Lindblad [16]. It is also referred to as the *GKSL-equation*, although we will not use that terminology in this thesis.

2.4 Quantum trajectories and stochastic simulation

In the preceding section, we have seen that, in analogy with classical Markov processes, one can evolve the ensemble $\hat{\rho}$ with a Master equation. However, such construction assumes a complete loss of information; in reality one is (keeping track of information) always in a single realization (‘single shot’) of the Markov chain. A similar observation can be made for the open quantum system [6, 8, 12].

According to the *Von Neumann-scheme of measurement*, a measurement on a quantum system S happens as follows, where we take the example of a single spin-1/2 particle for simplicity. Initially, it is in a pure y -polarized state $|\uparrow\rangle + i|\downarrow\rangle$ (disregarding normalization for simplicity), corresponding to a density matrix

$$\hat{\rho}_{s,i} = |\uparrow\rangle\langle\uparrow| + |\downarrow\rangle\langle\downarrow| + i|\downarrow\rangle\langle\uparrow| - i|\uparrow\rangle\langle\downarrow|. \quad (2.21)$$

A macroscopic measurement device D (we will use a pointer as example) is now coupled with S , bringing the total state of $S + D$ to the maximally entangled state $|\uparrow\rangle_S |x_1\rangle_D + i|\downarrow\rangle_S |x_2\rangle_D$. D is however a macroscopic object and hence subject to decoherence. Therefore, we will quickly end up in a classical mixture $\hat{\rho}_{\text{tot},f} = (|\uparrow\rangle\langle\uparrow|_S (|x_1\rangle\langle x_1|)_D + |\downarrow\rangle\langle\downarrow|_S (|x_2\rangle\langle x_2|)_D)$ or, if we are interested in S alone,

$$\hat{\rho}_{s,f} = |\uparrow\rangle\langle\uparrow| + |\downarrow\rangle\langle\downarrow|. \quad (2.22)$$

Now, a crucial insight is that this procedure defines a quantum map on S . In fact, we see that $\hat{\rho}_{s,f}$ is obtained from $\hat{\rho}_{s,i}$ by choosing as Kraus operators $\{\hat{M}_{\mu}\}$ the two projection operators in the spin- z basis, meaning that interaction with an environment is equivalent to an unread measurement (this is consistent with our remarks when introducing POVMs in subsection 2.2.5). There is more, though.

What if we do read out the measurement (look at the pointer)? Then, we know, from the position of x on D , with certainty the spin of s , the 'measured' spin is now either

$$\hat{\rho}_{s,m} = |\uparrow\rangle\langle\uparrow| \quad \text{or} \quad |\downarrow\rangle\langle\downarrow|. \quad (2.23)$$

In fact, because S is in a pure state after reading out the measurement, there is no longer a need to work with density matrices and the system after measurement can be characterized by a wavefunction $|S\rangle$ alone! For the former example, we have used projectors as Kraus operators, but in fact the argument holds for all POVM measurement procedures (for example, when the spin and the pointer are not fully correlated). Now, what is the importance of this with respect to our story on the dynamics of open quantum systems? We note that the Lindblad equation (2.20) can be written in an equivalent form as

$$\frac{d\hat{\rho}}{dt} = -i[\hat{H}_{\text{eff}}, \hat{\rho}] + \sum_{\mu} \hat{L}_{\mu} \hat{\rho} \hat{L}_{\mu}^{\dagger}. \quad (2.24)$$

The first term describes an evolution with an effective (non-unitary) Hamiltonian, while the second term is known as the 'recycling' term. An important insight is that, since (2.24) is linear, $\hat{\rho}$ can be sampled with pure states, for which the evolution can be described in terms of wavefunctions. The effective Hamiltonian leads to a deterministic Schrödinger-like evolution

$$\frac{d|\tilde{\psi}\rangle}{dt} = -i \hat{H}_{\text{eff}} |\tilde{\psi}\rangle, \quad (2.25)$$

where the tilde denotes that the norm of $|\tilde{\psi}\rangle$ is in general not conserved under this evolution. The recycling terms enter the evolution as

$$|\tilde{\psi}\rangle \rightarrow \hat{L}_{\mu} |\tilde{\psi}\rangle. \quad (2.26)$$

The fact that the corresponding Kraus operator scales with \sqrt{dt} , as Wiener noise does, hints that process (2.26) has a stochastic nature. This turns out to be true, either in the form of discrete jumps at random times, leading to $|\tilde{\psi}\rangle$ being a piecewise-deterministic process (PDP), or in the form of continuous Wiener noise. In this thesis, all stochastic calculus is performed in the Itô sense, although it is in principle possible to translate it to the Stratonovic sense as well.

This procedure of writing the Lindblad evolution in terms of wavefunctions is known as an *unraveling*, while $|\psi\rangle(t)$ is a *quantum trajectory* and the method as

wavefunction monte-carlo. In practice, this nomenclature is used interchangeably, though.

There is one more important aspect to quantum trajectories which we have not yet discussed. As noted in subsection 2.2.2, density matrices don't have a unique decomposition in pure states. For the spin above, the same $\hat{\rho}_{s,f}$ would have been obtained by coupling the x -components of the spins for example (the analogy should not be carried to far, as it does not hold for the z -component for this initial state). This illustrates also, as already remarked, that the choice of Kraus operators is not uniquely defined by the decoherence mechanism (for example, in (2.17) alternative sets of Kraus operators can be obtained by adding a constant to operators \hat{L}_μ and simultaneously subtracting it from \hat{H}_{eff}). For our purposes, this means that a master equation has no unique unraveling. Different measurement procedures give measurement records that can look qualitatively entirely different, *but the average evolution of the ensemble is identical*. After preliminary work by Davies [17], the quantum trajectory formalism was developed in the early 90s by a number of different groups (Dalibard, Castin and Mølmer [18]; Dum, Zoller and Ritsch [19]; Carmichael [20] and Barchielli and Belavkin [21]) in a quantum-optical context.

In the quantum-optical context, we will study such an example where leaking photons are measured, and depending on if one uses photon-counting or homodyne/heterodyne measurement schemes, this gives a single-shot PDP or Wiener process. But let us first highlight some more general features of the quantum trajectory method.

2.4.1 FIRST BENEFIT OF QUANTUM TRAJECTORIES: CLOSER CONNECTION TO EXPERIMENT

There are two important reasons why one would prefer working with quantum trajectories over the master equation. The first is that the formalism allows studying qualitative features of single-shot real measurements, and can thus provide more complete experimental predictions. We will explicitly use a hybrid trajectory/GTA model in this context in Part III. Related to this, quantum trajectories allow for more flexibility than the master equation such as the study of feedback processes based on the measurement record [7, 22, 23].

2.4.2 SECOND BENEFIT OF QUANTUM TRAJECTORIES: STOCHASTIC SIMULATION NEEDS LESS COMPUTATIONAL RESOURCES

Second, wavefunctions $|\psi\rangle$ are elements of a Hilbert space \mathcal{H} that is quadratically smaller (dimension D) than the Hilbert space $\mathcal{H} \otimes \mathcal{H}^*$ of $\hat{\rho}$ (dimension D^2). In numerical simulations, the dimension directly relates to the computational complexity of the problem, it is the amount of numbers that must be stored in computer memory and computed each timestep. One sees that quantum trajectories (from a virtual measurement) here have a large benefit, harvesting this in practice is also known as the *stochastic simulation method*. The expense is of course that the trajectory simulations must be repeated until statistical convergence if one wants to recover the statistics of the full ensemble $\hat{\rho}$ [10, 24].

2.4.3 DISTINGUISHING QUANTUM- AND CLASSICAL FLUCTUATIONS

The variance of an operator \hat{O} in quantum mechanics is defined as

$$\text{Var}(\hat{O}) = \text{tr}[\hat{\rho} \hat{O}^2] - [\text{tr}(\hat{\rho} \hat{O})]^2 = \frac{1}{N_{\text{traj}}} \sum_{\alpha} \langle \hat{O}^2 \rangle_{\alpha} - \left[\sum_{\alpha} \frac{\langle \hat{O} \rangle_{\alpha}}{N_{\text{traj}}} \right]^2. \quad (2.27)$$

In the context of quantum trajectories, it is useful to note that this quantity can be decomposed in two contributions $\text{Var} \hat{O} = \text{Var}_1(\hat{O}) + \text{Var}_2(\hat{O})$, respectively defined as [6]

$$\text{Var}_1(\hat{O}) = \frac{1}{N_{\text{traj}}} \sum_{\alpha} \left[\langle \hat{O}^2 \rangle_{\alpha} - \langle \hat{O} \rangle_{\alpha}^2 \right], \quad (2.28)$$

$$\text{Var}_2(\hat{O}) = \sum_{\alpha} \frac{\langle \hat{O} \rangle_{\alpha}^2}{N_{\text{traj}}} - \left[\sum_{\alpha} \frac{\langle \hat{O} \rangle_{\alpha}}{N_{\text{traj}}} \right]^2. \quad (2.29)$$

$\text{Var}_1(\hat{O})$ is a measure for the quantum uncertainty on \hat{O} within a trajectory, whereas $\text{Var}_2(\hat{O})$ is the stochastic variance between trajectories. We will refer to these quantities as the *intra-trajectory variance* and *inter-trajectory variance*, respectively. While $\text{Var} \hat{O}$ is uniquely defined by the master equation, the weights of $\text{Var}_1 \hat{O}$ and $\text{Var}_2 \hat{O}$ can strongly depend on the unraveling. In particular, if an unraveling corresponds to measurements of \hat{O} , then $\text{Var}_1 \hat{O}$ tends to be small (and $\text{Var}_2 \hat{O}$ large) as $|\psi\rangle$ is close to an eigenstate of \hat{O} . Meanwhile, for a conjugate

observable \hat{O}' , we expect a large $\text{Var}_1 \hat{O}$. These considerations are useful to take into account when choosing an unraveling for the stochastic simulation method as they can strongly affect the statistical convergence of the method. In general, this discussion makes our earlier remark on the interchangeability of classical and quantum fluctuations more precise.

2.4.4 CORRESPONDENCE WITH OTHER CONCEPTS FROM QUANTUM MECHANICS

In deriving quantum trajectory theory, we have been relying only on the Copenhagen interpretation of quantum mechanics (even the decoherence used in the von Neumann measurement scheme is consistent with Born's rule [8]). Nevertheless, there are natural connections with some alternative interpretations. *Stochastic collapse models* assume that all natural objects are constantly subject to a very weak measurement, and naturally very similar formulas to the ones of quantum trajectories have arisen in this context. The most famous example is *quantum state diffusion*, which has shown to be mathematically equivalent with the heterodyne unraveling (see subsection 2.5.2). Furthermore, the *consistent (decoherent) histories interpretation* of quantum mechanics assumes that the importance of individual measurement events is overstated, but rather the whole history of a system is important. This also naturally connects with the quantum trajectory formalism [11]. Unfortunately, the term *quantum trajectory* is sometimes also used in the different context of de Broglie-Bohm (pilot-wave) theory [25]. We wish to highlight that this is an entirely different notion, as unlike in pilot-wave theory, the quantum trajectories referred to in this work do *not* interfere with each other. In fact, the time-evolution of an open quantum system can be described by a stochastic path integral over quantum trajectories in Hilbert space. This should not be confused with the coherent Feynman-Vernon path integral over classical paths in configuration space or phase space [6] .

2.5 Example: dissipation from an optical cavity

The discussions in the previous section have outlined a generic formalism to understand open quantum systems, but could not give a specific recipe to obtain the proper Lindblad operators for a given system. To make the methods a bit more concrete, we now turn to the particular setup of a leaky optical cavity [6, 12, 26, 27], which will be important for this thesis. The study of systems for which such

description is relevant is known as *Cavity quantum electrodynamics (cavity QED)* and can include individual atoms in a cavity as well as more extensive solid-state structures [28]. From Figure 2.1, recall that the total Hamiltonian is

$$\hat{H}_{\text{tot}} = \hat{H}_S + \hat{H}_R + \hat{V}. \quad (2.30)$$

In the interaction picture, the total density matrix evolves as

$$\frac{d\hat{\rho}_{\text{tot}}}{dt} = -i[\hat{V}, \hat{\rho}_{\text{tot}}]. \quad (2.31)$$

From iterative integration, we find

$$\hat{\rho}_{\text{tot}}(t+\Delta t) = \hat{\rho}_{\text{tot}}(t) + \sum_{n=1}^{\infty} (-i)^n \int_t^{t+\Delta t} dt_1 \int_t^{t_1} dt_2 \cdots \int_t^{t_{n-1}} dt_n [\hat{V}, [\hat{V}, \cdots [\hat{V}, \hat{\rho}_{\text{tot}}]]]. \quad (2.32)$$

For $\text{tr}_R(\hat{V}\hat{\rho}_R) = 0$, the first term in the expansion of $\hat{\rho}_s = \text{tr}_R \hat{\rho}_{\text{tot}}$ vanishes. When studying evolution in a short time t we should therefore consider the second term, leading to

$$\frac{\Delta \hat{\rho}_s}{\Delta t} = - \int_t^{t+\Delta t} dt_1 \text{tr}_R [\hat{V}, [\hat{V}, \hat{\rho}_{\text{tot}}(t)]] \quad (2.33)$$

$$\approx \int_t^{t+\Delta t} dt_1 \text{tr}_R \hat{\rho}_R [-\hat{V}^2 \hat{\rho}_s(t_1) - \hat{\rho}_s(t_1) \hat{V}^2 + 2\hat{V} \hat{\rho}_s(t_1) \hat{V}], \quad (2.34)$$

where we have used the Born-Markov approximation $\hat{\rho}_{\text{tot}}(t) = \hat{\rho}_s(t) \otimes \hat{\rho}_r$ in the second equality. For short Δt , $t_1 \approx t$ and we start recognizing the Lindblad form. Assuming a simple interaction Hamiltonian coupling the electromagnetic fields inside and outside the cavity (for notational simplicity, we drop dependencies on all degrees of freedom other than ω),

$$\hat{V} = -\hat{D} \cdot \hat{E} = \int d\omega g(\omega) (\hat{a} + \hat{a}^\dagger) (\hat{b}(\omega) + \hat{b}^\dagger(\omega)) \quad (2.35)$$

$$\approx g\Delta_\omega (\hat{a} \hat{b}^\dagger + \hat{a}^\dagger \hat{b}). \quad (2.36)$$

(Rotating-wave and Markov approximations), where \hat{b}, \hat{b}^\dagger are the annihilation and creation operators of the reservoir (free space with $\hat{H}_R = \int_\omega d\omega c(\omega) \omega f \hat{b}^\dagger(\omega) \hat{b}(\omega)$). If free space has temperature zero, $\text{tr}_R(\hat{b}^\dagger \hat{b}) = \text{tr}_R(\hat{b} \hat{b}) = \text{tr}_R(\hat{b}^\dagger \hat{b}^\dagger) = 0$ while $\text{tr}_R(\hat{b} \hat{b}^\dagger) = 1$. Upon defining $\gamma := 2g^2 \Delta_\omega^2$, we readily obtain the Lindblad equation

$$\partial_t \hat{\rho}_s = \frac{\gamma}{2} \left(2 \hat{a} \hat{\rho} \hat{a}^\dagger - \hat{a}^\dagger \hat{a} \hat{\rho} - \hat{\rho} \hat{a}^\dagger \hat{a} \right), \quad (2.37)$$

or returning to the Schrödinger picture

$$\partial_t \hat{\rho} = -i \left[\hat{H}, \hat{\rho} \right] + \frac{\gamma}{2} \left(2 \hat{a} \hat{\rho} \hat{a}^\dagger - \hat{a}^\dagger \hat{a} \hat{\rho} - \hat{\rho} \hat{a}^\dagger \hat{a} \right). \quad (2.38)$$

Expression (2.38) is clearly of the form (2.20), where we see that the jump operator associated with this process is $\sqrt{\gamma} \hat{a}$. In the following, we will refer to γ as the *dissipation rate*.

2.5.1 THE PHOTON-COUNTING UNRAVELING

Let us now take a look at this process from the quantum trajectory perspective. The most straightforward continuous measurement is direct photodetection: an (idealized) detector will, at any infinitesimal timestep dt either detect one photon ('click') or none³. Therefore, the stochastic Schrödinger equation for these trajectories is a Poisson process

$$|\widetilde{\psi}\rangle = \left[1 - \left(i \hat{H} + \frac{\gamma}{2} \hat{a}^\dagger \hat{a} \right) dt + \left(\frac{\hat{a}}{\|\hat{a} |\widetilde{\psi}\rangle\|} - 1 \right) dN \right] |\widetilde{\psi}\rangle, \quad (2.39)$$

where $dN^2 = dN$, $E[dN] = \gamma \langle \hat{n} \rangle dt$.

Note that the Poisson increment dN for an infinitesimal timestep is either 0 (with probability $1 - \gamma \langle \hat{n} \rangle dt$) or 1 (with probability $\gamma \langle \hat{n} \rangle dt$). Hence, as long as dt is sufficiently small, we can replace the random generation of a Poisson integer each timestep by a random real number ξ from a uniform $[0, 1]$ distribution and perform a jump if $\xi < \gamma \langle \hat{n} \rangle dt$. As long as no jump has been performed, the same number ξ can however be reused. The probability of m subsequent timesteps without a jump is $(1 - \gamma \langle \hat{n} \rangle dt)^m \approx e^{-\gamma \langle \hat{n} \rangle m dt} = e^{-\gamma \langle \hat{n} \rangle t}$. This latter quantity is equal to the decrease of the norm according to the deterministic part of (2.39).

This leads to the following, practical procedure that has turned out to be beneficial in many cases [10]:

1. Pull a random number ξ from a uniform $[0, 1]$ distribution

³Two things to note that may seem counterintuitive: (1) the absence of a click is also a measurement result that gives information on the system (2) Clicks don't always decrease the expectation value of the photon number in the cavity: although one particle is lost it signals that there were a lot in there as well [10].

2. Perform a deterministic evolution of the unnormalized state according to

$$i\partial_t|\widetilde{\psi}\rangle = \left(\hat{H} - i\frac{\gamma}{2}\hat{a}^\dagger\hat{a}\right)|\widetilde{\psi}\rangle, \quad (2.40)$$

3. when the norm has decreased to $\| |\widetilde{\psi}\rangle \|^2 = \xi$, a jump is performed

$$|\widetilde{\psi}\rangle \rightarrow \hat{a}|\widetilde{\psi}\rangle / \|\hat{a}|\widetilde{\psi}\rangle\| \quad (2.41)$$

4. Repeating of the procedure.

2.5.2 OTHER UNRAVELINGS

The most important other unravelings for this process are the *dyne* (*homodyne/heterodyne*) detection schemes that measure the interference of this leaking light with a macroscopic reference beam and are able to provide phase information as well. The combined photon current of signal and reference beam is now macroscopic and contains a very large amount of individual photons, each contributing to a tiny jump. In this case, it is more appropriate to model the noise as a Wiener process with Gaussian noise without further jumps. In particular, homodyne detection schemes measure a quadrature variable $\hat{X}_\phi = \frac{1}{2}(\hat{a}e^{-i\phi} + \hat{a}^\dagger e^{i\phi})$, with ϕ a free parameter (the relevance of these variables will become clearer in subsection 4.2.1). This leads to trajectories of the form

$$d|\widetilde{\psi}\rangle = \left(-i\hat{H}dt - \frac{\gamma}{2}\hat{a}^\dagger\hat{a}dt + 2\gamma\langle\hat{X}_\phi\rangle\hat{a}e^{-i\phi}dt + \sqrt{\gamma}\hat{a}e^{-i\phi}dW\right)|\psi\rangle \quad (2.42)$$

where dW is a real Wiener process satisfying $dW^2 = dt$.

In heterodyne detection, all quadrature variables are measured with equal weights. This yields a stochastic Schrödinger equation

$$d|\widetilde{\psi}\rangle = \left(-i\hat{H}dt - \frac{\gamma}{2}\hat{a}^\dagger\hat{a}dt + \gamma\langle\hat{a}^\dagger\rangle\hat{a}dt + \sqrt{\gamma}\hat{a}dZ^*\right)|\psi\rangle, \quad (2.43)$$

where dZ is complex Wiener noise satisfying $|dZ|^2 = dt$ and $dZ^2 = 0$. These detection schemes are discussed in more detail in Appendix A.

2.6 Two-time correlation functions: the Onsager-Lax quantum regression theorem

Another useful result that we will use later states that two-time correlation functions can be obtained from knowledge of the evolution of single-time operator values. This is known as the **(Onsager-Lax) quantum regression theorem** [29]: If for some operator \hat{O} ,

$$\langle \hat{O}(t + \tau) \rangle = \sum_j a_j(\tau) \langle \hat{O}_j(t) \rangle, \quad (2.44)$$

then

$$\langle \hat{O}_i(t) \hat{O}(t + \tau) \hat{O}_k(t) \rangle = \sum_j a_j(\tau) \langle \hat{O}_i(t) \hat{O}_j(t) \hat{O}_k(t) \rangle. \quad (2.45)$$

There has been some discussion as to whether this statement should truly be considered a theorem, but at least in the case of weak Markovian coupling with a reservoir, it holds to very good approximation [30, 31].

2.7 Further extensions

2.7.1 NON-MARKOVIAN DISSIPATION

For the methods in the previous sections to be valid, a number of approximations had to be made. However, there has been considerable work regarding extensions to more general setups. In particular the criterion of Markovianity is not always satisfied, meaning that the environment can retain correlations (note that this is equivalent with the presence of coloured noise in the Fourier domain, or a frequency dependent coupling Hamiltonian) [6, 32]. The duality between methods on the level of the master equation or individual trajectories persists largely, though. On the level of the master equation, projection operator techniques as the *Nakajima-Zwanzig* method or time-convolutionless modifications are typically used. Non-markovian quantum trajectories can be constructed by working in a *doubled* Hilbert space or considering reverse jumps [6, 32]. Although we focus with the Gaussian Trajectory Approach in this work on Markovian setups, we believe that exploiting the same Gaussian ansatz might also be useful to the non-Markovian extensions.

2.7.2 RELATIVISTIC METHODS

Other extensions include relativistic methods. As a starting point, the *Schwinger-Tomogana equation* is commonly used, where quantum states are considered a functional on the set of spacelike hypersurfaces in Minkowski space. In this context, the locality of measurements becomes an important aspect [6].

Many-body open quantum systems and their numerical description

In the last decade, an increasing amount of attention has been devoted to the study open many-body systems, where physics richer than in closed systems can arise. Several experimental platforms are studied in this regard. Computational resources are often a constraint, although a variety of methods exist to date, with each their advantages and drawbacks.

3.1 Many-body open quantum systems

The systems considered in chapter 2 have, to large extent, arisen in a quantum optics context with few degrees of freedom. More recently, there is an increased interest in systems where both the open and the many-body aspects are important, meaning that insights of quantum optics must be merged with those of condensed matter physics and statistical physics. Even if the exact Lindblad or quantum trajectory evolution can no longer be tracked, a number of general results exist to date, of which we will highlight a few important ones here. In section 3.2 we highlight some important experimental platforms in this context and in section 3.3 we will then give an overview of existing methods to overcome this many-body problem in open quantum systems.

A (non-exhaustive) number of features that may arise in open many-body systems that distinguish them from closed systems:

- **Spohn’s theorem:** A Liouvillian \mathcal{L} for a finite system has a unique steady-state which is reached after (real) time evolution, provided the quantum-dynamical semigroup is irreducible [33–35]. The last requirement corresponds,

loosely speaking, with the fact that the jump operators can connect all possible states and is typically satisfied. Equation (2.15) can be formally integrated i.e.

$$\hat{\rho}(t) = e^{\mathcal{L}t} \hat{\rho}(0) \quad (3.1)$$

while the steady state is the lowest eigenvector of \mathcal{L} (it has eigenvalue zero in fact, by the requirement of stationarity). (Minus the real part of) the first excited eigenvalue denotes the Liouvillian gap λ and yields the slowest timescale in the system ¹ and is important in the context of dissipative phase transitions (we will study these more deeply in Part II). Spohn’s theorem, however, does not state that the decay should be fast: especially in the context of glasses, dynamics can be extremely slow, i.e. much slower than the timescale of the experiment and the system is in a metastable state [37]. A number of more exotic dissipation mechanisms, that don’t satisfy the criteria for Spohn’s theorem and don’t reach a unique steady state, have also recently received attention [38, 39]. In the thermodynamic limit of infinite occupation, even simple loss processes can lead to *dissipative time-crystals* [40, 41].

- In the trivial case of a thermal bath and no driving, this steady state will also be an equilibrium (Boltzmann-Gibbs) state. Note that typically, in thermal equilibrium the Markov-Born approximations are in fact not valid. More interestingly, an interplay of driving and dissipation, or more complex dissipation mechanisms, tend to result in genuinely non-equilibrium behavior. In this context, we should highlight that the concept of a ‘steady state’ refers to the ensemble $\hat{\rho}$, individual experimental realizations (trajectories) can display a variety of dynamical effects (for example, the presence of vortex trains [42, 43]).
- Detailed balance is generally not satisfied, implying that the system can a priori be much more sensitive to microscopic dynamics [44, 45].
- A corollary is that also equilibrium fluctuation-dissipation theorems can be violated. Some observable-dependent alternatives exist [46].
- Reciprocity of susceptibilities can be broken [47].

¹Very recently, a counterexample was found relating to the Liouvillian skin effect [36].

- Densities-of-states can be negative, at least when interpreted as the imaginary part of the Green's function (spectral function). This relates to a combination of a steady-state with population inversion and interactions [48].

In summary, while open quantum systems naturally go to a steady state on short or long timescales²³, their dynamics, especially in a driven-dissipative context, can be very rich compared to closed or thermal quantum states.

3.2 Experimental platforms

3.2.1 NON-EQUILIBRIUM PHYSICS OF ATOMIC CONDENSATES

While for many theoretical descriptions of Bose-Einstein condensates with cold atoms [49], it is not necessary to include interaction with the environment explicitly, there are some cases where this is highly relevant. For example, in order to perform successful laser (Doppler) cooling to prepare such systems experimentally, one needs to overcome the recoil temperature limit, something that is possible by trapping the atomic wavefunction in a dark state [6, 50]. Also the physics of cold atoms in optical cavities and cavity arrays is important, including optical lattices and the heating dynamics therein. These descriptions often give rise to spin models such as the Dicke model [24, 51]. More recently, there has been a surging interest for genuine non-equilibrium features of cold-atom systems [52]. Often, the term 'dissipation' is used here without explicit reference to Markovian coupling with a reservoir, but particle losses can become highly relevant [53, 54].

3.2.2 EXCITON-POLARITON CONDENSATES

Bose-Einstein condensation has also been observed in the-solid state, in the form of exciton-polaritons with a series of experiments in 2006 [55]. Some of the main experimental motivations to study this system has been the possibility to reach condensation and study superfluid properties [56] at standard cryogenic temperatures or even room temperature (as opposed to the nanokelvin regime for cold gases), and that tracking real-time dynamics from the leaking light is possible. Because of the important optical component (polaritons are coherent

²In closed systems, one needs to invoke advanced notions as *eigenstate thermalization* in a somewhat ad hoc way to achieve this result, as the Schrödinger equation (2.13) predicts oscillatory behaviour.

³In a different sense, the closest analogy to a steady state for Hamiltonian dynamics is the ground state, which is reached after infinite *imaginary* time-evolution instead of real.

superpositions of a photon and an exciton), polariton condensates are also known as *quantum fluids of light*. A detailed review of the early experiments is given in Ref. [57]. In practice, it is mostly experimentally realized in planar microcavities such that the system is effectively two-dimensional and the confinement in the z-dimension gives the particles an effective mass. Because particles leak out, new ones have to be pumped in continuously. This can take place either coherently (a term in the Hamiltonian) or incoherently (as another Markovian jump process) and gives polariton condensates a genuine driven-dissipative character [57], so that features of non-equilibrium condensation can become highly relevant. For example, vortices in polariton condensates, a typical witness of superfluidity, [58] can be self-propelling [43]. More recently, the interest has grown to achieve polariton condensation in optical micropillars and arrays of these for quantum information processing [59], as such polariton systems can provide a proper implementation of cavity QED systems with a Kerr nonlinearity. This Kerr ($\chi^{(3)}$)-nonlinearity stems from the interaction of the excitonic component that exhibits a bound state [60]. It is necessary for thermalization [57], but by itself often considered rather weak for the purposes of information processing. For this purpose, the interaction strength can be drastically enhanced by exploiting interference effects known as *unconventional photon blockade* [61, 62] and its dynamical extensions [63].

3.2.3 DYE-MICROCAVITY PHOTON CONDENSATES

An alternative approach to the Bose-Einstein condensation of light is by a strong absorption- and emission rate with a thermal environment consisting of dye-molecules, making the photon-photon collisions from polariton condensates abundant (realized in 2010) [64]. Both absorption and emission processes are incoherent (jumps). The low mass allows for condensation at room temperature, even for standard setups. Although thermal reservoirs lead, in general, to equilibrium behaviour, the dynamics in this system are, as we will see in Part III of this thesis, far from trivial.

3.2.4 SUPERCONDUCTING QUANTUM OPTICS

Apart from optical photons, and around the same time as previous platforms, much work has been done in parallel with microwave photons in superconducting circuits. This work is known as *Circuit QED* [65] and largely parallels cavity QED. The nonlinearity is achieved through superconducting q-bits based on Josephson

junctions, with which high nonlinearities can easily be achieved [66].

3.2.5 OTHER EXPERIMENTAL PLATFORMS

Similar physics to neutral atoms in optical lattices has also been studied with **ions**. Because of their charged nature, potential wells can become deeper, which has allowed for an overall better controllability [67, 68]. Sticking to neutral atoms, **Rydberg atoms**, mediating photon interactions, have recently gained a lot of attention in the context of non-equilibrium dynamics [69] and quantum technologies [70]. These Rydberg atoms are atoms with an electron in a highly excited state, giving them ‘exaggerated atomic properties’. By itself the study of these atoms goes back to the early days of spectroscopy [71], whereas more recently, it has been realized that their controllability [72] is a strong advantage when seeking individual atoms to manipulate. Very high nonlinearities for the photons are achieved because of the ‘Rydberg blockade’ mechanism [73]. Finally, another line of research in this context, that has been intensively studied the last decade, are optomechanical devices (‘**optomechanics**’) that exploit radiation pressure [74]. Here, photons are coupled to mechanical oscillators ‘springs’ (moving mirrors, in practice typically cantilevers, nanobeams or membranes). Also the interferometry for gravitational-wave detectors can be understood in this context [75]. Another intriguing question that is also investigated with such optomechanical systems concerns the fate of quantum coherence and decoherence for progressively larger systems [76].

3.3 Contemporary analytical and numerical methods

3.3.1 EXACT DIAGONALIZATION

For a number of models, exact analytical solutions can be found [13, 77–79]. In principle, any Liouvillian could be written out in an explicit matrix representation, which can be diagonalized by brute force with standard numerical software packages. This approach is however strongly limited to small systems. In addition to the exponential scaling of closed quantum mechanics, the computational cost is even quadratically larger because of the need to work with density matrices. Use of the stochastic simulation method (exact quantum trajectories) reduces the cost for a single evolution to the one of the Schrödinger equation for a closed system, at the expense of the need to average over many trajectories if one is interested in

ensemble statistics.

3.3.2 MEAN-FIELD

A much simpler approach is the (coherent) mean-field approximation, which also exists in closed systems. Fluctuations are disregarded by replacing a field operator by its expectation value. This comes down to the ansatz of a coherent state (see subsection 4.2.1). For BEC physics, this leads, for example, to the generalized Gross-Pitaevskii equation [49, 57]. For complicated, spatially extended, systems, such approaches may be the only ones accessible. Its validity is strongly limited to semiclassical behaviour, typically arising in the limit of large occupation.

3.3.3 LOCALLY EXACT MASTER-EQUATION BASED APPROACHES

A straightforward approach to simplify the brute-force solution of the master equation is the (mean-field) Gutzwiller density matrix approach that assumes factorized solutions [80–82]⁴. If symmetries are present and one is interested in the steady state, it is only necessary to solve the master equation for a single independent site, while replacing couplings with other sites by the obtained expectation values self-consistently [83].

In the study of phase transitions (see section 6.1), Gutzwiller theory is known to predict critical exponents properly from the upper critical dimension onwards (often more than 3), and it was also widely believed that such approach becomes asymptotically exact for an infinitely-dimensional setup. Recently though, strong concerns have arisen as to whether critical points of non-equilibrium systems are accurately detected by such approaches in this limit [84]. More generally, the assumption of a factorized solution poses strong constraints on the non-local correlations that can be captured.

In the study of many-body systems in closed quantum systems, there has further been a lot of attention to DMRG (Density-Matrix Renormalization Group) as a tool for lattice models the last decades. More generally, this has been formalized in Tensor Networks, such as MPS (Matrix-Product States) or MPO (Matrix-Product operators) in 1D and PEPS (Projected Entangled-Pair States) in 2D. The central idea in tensor networks is that the state of the full system can be written exactly as a contraction over local tensors. This method can be generalized

⁴In the literature, both the coherent-state ansatz and the Gutzwiller approach are sometimes referred to as 'Mean-field'. In this thesis, we will only stick to this terminology for the former approach.

quite straightforwardly to the master equation in open quantum systems [85–89]. By itself, this tensor decomposition does not provide a computational advantage. However, a crucial insight is that physical states tend not to occupy the full, exponentially large, Hilbert space, but are typically restricted to a 'physical corner' where entanglement is local. This realization justifies a truncation in bond dimension that leads to the computational reduction. Tensor networks are generally considered as a very powerful and well-controlled tool in the study of lattice models with short-range correlations (bond dimension cannot be truncated so easily in presence of long-range correlations, such as near a critical point [90]). Also non-Markovian extensions exist [91]. Drawbacks are that tensor networks tend to perform worse in systems where higher occupations can be present and in situations where long-range correlations are important. Furthermore, the numerical implementation of tensor networks can become a daunting task when studying systems with a dimension larger than 1.

The same realization, that the important physical states are restricted to the 'physical corner' of Hilbert space, can also be exploited in a somewhat more lightweight tool known as the Corner-Space Renormalization (CSR) method [92]. The approach works as follows: a small lattice system can be solved exactly. Out of this solution, the most relevant eigenvectors are selected, and the others are disregarded. Now, this lattice is doubled in size, and the procedure is repeated, up to the point where convergence is attained for the proper lattice of interest. While much simpler to implement for higher-dimension lattices than tensor networks, the CSR method retains difficulties in accessing systems with higher occupation per mode, and where the state has a strongly mixed character.

3.3.4 LOCALLY EXACT TRAJECTORY-BASED APPROACHES

Some similar approaches have also been applied on the level of individual trajectories [24]. The assumption of a factorized solution, for example, leads to a Gutzwiller monte carlo approach [93–95]. As opposed to the level of the master equation, symmetry can now be broken, meaning that in each trajectory, the solutions on the different sites differ. The added value of starting from trajectories rather than the master equation, is that the classical fluctuations are not restricted by the ansatz, these can thus be sampled much better. The cost is that simulations must be repeated up to proper statistical convergence. A straightforward generalization is the Cluster Gutzwiller method, where the ansatz is used that the trajectory can be written as a product of exact solutions of small 'clusters' of a few lattice

sites [47]. Similarly, also tensor networks can be combined with the trajectory formalism [96–98], with as an advantage, parallel to Gutzwiller monte carlo, the improved description of classical fluctuations. A possible drawback is that if one is only interested in the steady state of the master equation, one still needs to study the dynamics with a trajectory approach.

3.3.5 CUMULANT EXPANSION

Knowledge on the state of a system is equivalent to knowledge of the probability density function of the state over operators (in practice the field–creation and annihilation– operators), which is in turn fully characterized by its moments. Cumulant expansion exploits this by evolving coupled equations for these moments. In practice, these moments form an hierarchy of correlations, similar to the BBGKY hierarchy in classical systems [99]. As typically, the lower moments (mean and variance) are the most important, one can truncate this hierarchy. Up to now, this principle has been mainly applied to the evolution of the master equation. Only truncation at the first (coherent state, equivalent to the mean-field result from subsection 3.3.2) or second (Gaussian) level (Bogoliubov theory), however, leads to well-defined variational states [45, 100].

3.3.6 PHASE-SPACE METHODS

As we will explain more deeply in subsection 4.2.1, quantum mechanical states can also be described as quasi-probability distributions in optical phase-space. Directly translating the master equation of a multi-mode system to phase space, results in a high-dimensional Fokker-Planck-like partial differential equation. By itself, this typically does not make computations more easy. A significant improvement can however be obtained from the Feynman-Kac formula that allows one to map this Fokker-Planck equation onto stochastic differential equations under proper circumstances. To meet these constraints, a number of approximations typically have to be made that are not always well controlled [9, 57, 101]. Of particular importance is the Truncated Wigner Approximation [57, 102–104]. The approximation in this case consists of neglecting derivatives of order higher than two, typically proportional to interaction constants. Alternative derivations, for example from the Keldysh formalism (subsection 3.3.7), exist as well [105, 106]. Remarkably, the deterministic part of the TWA method is almost identical to the Gross-Pitaevskii equation. Noise enters both in the initial conditions and in the

dissipative evolution. This method is especially useful in the semiclassical limit of high occupation and positive Wigner functions. The TWA approach has been particularly successful for the study of BECs of cold atoms and polaritons [57, 102, 107–110] and optical waveguides [111, 112]. Despite these successes, TWA and similar methods are not always reliable and may lead sometimes to unphysical results [45]. Some improvements, with limited practical use so far, have also been introduced [113, 114].

3.3.7 OTHER METHODS

On the analytical side, another sophisticated and powerful approach is the **(Schwinger-)Keldysh field theory**. It was first introduced by Keldysh [115] and Kadanoff and Baym [116] in the 60s as a non-equilibrium extension to the diagrammatic Green’s function methods that are a standard tool in quantum field theory and solid-state physics. More recently, it was realized that this formalism is also very useful to describe driven-dissipative setups, as reviewed in Ref. [117].

Results obtained with this formalism also connect to the **Renormalization-group flow**: Many interesting phenomena take place at long length scales and it is unnecessary to track all microscopic degrees of freedom. In such cases, it is useful to study the asymptotic behaviour of the system under scale transformations. The underlying differential equations were first derived in Ref. [118] and later adapted to a driven-dissipative context [119, 120]. This formalism also provides a convenient picture to distinguish equilibrium from non-equilibrium: in the former, real and imaginary parts of the different coupling constants retain the same ratio under scaling, while this is no longer the case outside of equilibrium.

Regarding numerical approaches, as in closed quantum systems [121], a different approach consists of the **quantum monte carlo** method to sample the density matrix evolution [122]. The samples are by themselves unphysical, and this method should not be confused (despite the name) with wavefunction monte-carlo (quantum trajectories). While being less controlled than tensor-network approaches, quantum monte-carlo approaches are easier to implement in more than one dimension and have been able to find good results in some cases [123]. So far, these methods have only been applied to the determination of the steady state.

A further recent insight from multiple groups in parallel, which leads to improvement and conceptual understanding, is that the quantum monte-carlo approach can efficiently be combined with a variational **neural network ansatz**

[124–127].

Several other approaches and results have also been introduced. It is for example argued that the variational principle for the steady state constitutes minimizing $\|\hat{\mathcal{L}}\hat{\rho}_{\text{trial}}\|$, where $\|\cdot\|$ is a suitable operator norm [128]. This principle is extended to variational evolution of the master equation in Ref. [129]. Another approach directly constructs a variational master equation [130, 131]. Variational optimization has also been studied [132]. Recent work has addressed finding the steady-state through mapping on a closed system [133] and Ref. [134] takes a Geometric approach.

The interested reader can find a few reviews on methods for open many-body systems in Refs. [24, 117, 135].

Gaussian states

Gaussian states have a simple description, can exhibit some notorious non-classical features and have been an important object of study in quantum optics and quantum information. Wick's theorem reduces calculations with Gaussian states considerably. In addition to the standard (quadrature variables) Gaussian states, we also introduce density-phase Gaussian states.

4.1 The Gaussian distribution in classical statistics

The Gaussian probability density function has attained an extremely important role in statistics. An important reason for this is the Central Limit theorem (Independently of the distribution of a variable x , with average \bar{x} and finite standard deviation σ , the average of a large number of measurements N of the variable x converges to a Gaussian distribution around the average \bar{x} with a standard deviation equal to σ/\sqrt{N}), that give the corresponding normal distribution a wide applicability. There is a second feature of Gaussian states, known as the **Isserlis' theorem** or **Wick's theorem** [136]¹: If (X_1, \dots, X_n) is a zero-mean multivariate normal random vector, then

$$E[X_1 X_2 \dots X_n] = \sum_{p \in \mathcal{P}_n^2} \prod_{\{i,j\} \in p} E[X_i X_j], \quad (4.1)$$

where $E[\cdot]$ denotes the expectation value, the sum is over all the pairings of $\{1, \dots, n\}$ and the product is over all the pairs contained in p . This is extremely useful, as all higher moments (and hence full knowledge of the distribution) are readily available from the displacement (transformation to zero-mean vector in the

¹There is also a different, but related, theorem named after 'Wick' about ordering contracted pairs of creation and annihilation operators [137].

theorem above) and covariance matrix. Wick's theorem can readily be applied to bosonic field operators. For fermionic correlation functions (not explicitly studied in this thesis, although extension of the formalism should be straightforward), additional minus signs from the commutators appear, as fermionic operators rather satisfy anti-commutation relations.

4.2 Gaussian states in quantum optics

4.2.1 QUANTUM-OPTICAL PHASE SPACE

In order to introduce the Gaussian state in quantum optics, it is useful to first look at the phase space representation of quantum optics which is able to provide a simple picture of such states, and compare the Gaussian state with some other important states. We first restrict ourselves to a single mode for convenience.

When studying the harmonic oscillator in first quantization, typically one introduces at some point the ladder operators $\hat{a}_{HO} = \sqrt{\frac{m\omega}{2}} (\hat{x} + \frac{i}{m\omega}\hat{p})$, $\hat{a}_{HO}^\dagger = \sqrt{\frac{m\omega}{2}} (\hat{x} - \frac{i}{m\omega}\hat{p})$ to facilitate the calculations.

In second quantization, every bosonic mode is treated as a harmonic oscillator and one works with similar creation and annihilation operators (also known as field operators) \hat{a}^\dagger, \hat{a} that create and destroy excitations of the field (particles) and follow the same algebra $[\hat{a}, \hat{a}^\dagger] = 1$; $\hat{n} = \hat{a}^\dagger \hat{a}$ is now the number operator. In analogy with the position and momentum variables in first quantization, similar Hermitian operators

$$\hat{X} = \frac{\hat{a} + \hat{a}^\dagger}{2} \quad (4.2)$$

$$\hat{P} = \frac{\hat{a} - \hat{a}^\dagger}{2i} \quad (4.3)$$

can be introduced satisfying

$$[\hat{X}, \hat{P}] = \frac{i}{2}. \quad (4.4)$$

These are known as the *quadrature variables*². These are mathematically analogous to position and momentum operators, but do not correspond to a physical position and momentum of a particle. As Hermitian operators, \hat{X} and \hat{P} must correspond to a physical quantity, these are the real and imaginary parts of the field, and can be measured with homodyne techniques (Appendix A).

²Other normalization conventions are in use as well.

It is often convenient to exploit this analogy by working in phase space. Phase space is naturally regarded as a key concept in classical Hamiltonian mechanics, where a system is completely defined by a point in this space. Quantum mechanics usually uses the Hilbert space as an alternative construction (section 2.2). However, it is possible to describe quantum mechanics in phase space as well [138]. The difference with classical mechanics is that Heisenberg uncertainty prevents (also pure) quantum states to map to single points in phase space, rather, they are quasi-probability distributions. The ‘quasi’ here partly refers to the fact that these functions do not have to be positive for every pair (X, P) .

In the Hilbert space of wavefunctions, position and momenta eigenstates (plane waves in their Fourier-transformed domains), both form a complete basis. In the Hilbert space of operators, such a basis exists in the form of *Displacement operators*

$$\hat{D}(\alpha, \alpha^*) = e^{\alpha \hat{a}^\dagger - \alpha^* \hat{a}} = e^{-i(X\hat{P} - P\hat{X})}. \quad (4.5)$$

This also implies that (at least in principle) any operator, including the density matrix, can be written out as a power series in \hat{a}, \hat{a}^\dagger (or equivalently, \hat{X}, \hat{P}) [9, 12]. Replacing this pair of conjugate operators by classical variables then leads to the quasi-probability distribution. There is however a catch, in that classical variables X, P commute whereas \hat{X}, \hat{P} don't. To resolve this ambiguity, the operators need to be ordered in a particular way before being substituted by classical variables. Different choices are possible, leading to different quasi-probability distributions of which Glauber-Sudarshan P-distribution (density matrix with antinormal ordering), the Husimi Q-distribution (density matrix with normal ordering) and the Wigner W-function (symmetric ordering) are the most important [9]. The W-function is unique in the sense that it predicts the proper marginals, i.e.

$$|\psi(X)|^2 = \int W(X, P) dP, \quad (4.6)$$

and similar for $|\psi(P)|^2$. The Wigner function has also been studied much earlier and outside a quantum optics context [139]. Explicitly, it can be computed by first defining the characteristic function as the expectation value over the displacement operator (4.5)

$$\chi_w(\beta, \beta^*) = \text{tr}[\rho \hat{D}(\beta, \beta^*)] \quad (4.7)$$

and then taking its Fourier transformation

$$W(\alpha, \alpha^*) = \frac{1}{\pi^2} \int \int d\beta d\beta^* e^{-\beta\alpha^* + \beta^*\alpha} \chi_W(\beta, \beta^*). \quad (4.8)$$

Another useful property are the transformation rules [9]

$$\hat{a}_i \hat{\rho} \leftrightarrow \left(\alpha_i + \frac{1}{2} \frac{\partial}{\partial \alpha_i^*} \right) W(\vec{\alpha}, \vec{\alpha}^*) \quad (4.9)$$

$$\hat{a}_i^\dagger \hat{\rho} \leftrightarrow \left(\alpha_i^* - \frac{1}{2} \frac{\partial}{\partial \alpha_i} \right) W(\vec{\alpha}, \vec{\alpha}^*) \quad (4.10)$$

$$\hat{\rho} \hat{a}_i \leftrightarrow \left(\alpha_i - \frac{1}{2} \frac{\partial}{\partial \alpha_i^*} \right) W(\vec{\alpha}, \vec{\alpha}^*) \quad (4.11)$$

$$\hat{\rho} \hat{a}_i^\dagger \leftrightarrow \left(\alpha_i^* + \frac{1}{2} \frac{\partial}{\partial \alpha_i} \right) W(\vec{\alpha}, \vec{\alpha}^*). \quad (4.12)$$

that make it easy to map the master equation to phase space, as for example for the truncated Wigner approximation (subsection 3.3.6). We will perform this mapping for a concrete example in section 7.3.

With this in mind, let us look at some important states in quantum optics (Figure 4.1).

- The most trivial state is the **vacuum state** $|0\rangle$ of an empty cavity. It is a pure state, completely isotropic in phase space, and the variances on X and P are both equal to $1/2$. $|0\rangle$ is an eigenstate of both \hat{a} and \hat{n} .
- Next, there is **thermal light** $\hat{\rho}_{\text{therm}} = \exp\{-\beta\omega(\hat{n}+1/2)\}$. It retains the phase-symmetry, both the uncertainties on \hat{X} and \hat{P} are larger (there are thermal fluctuations on top of the quantum fluctuations) such that the state is no longer pure.
- **Fock states** $|n\rangle$ are eigenstates of \hat{n} . Although this seems simple, they can exhibit highly quantum-mechanical features. Their Wigner functions are circularly symmetric and radially oscillating. It is surprisingly hard to produce Fock states in experiment, especially a large amount of work has been devoted to the construction of reliable single-photon sources, which could be useful for quantum information processing [141].
- **Coherent states**: By letting a displacement operator (4.5) operate on the

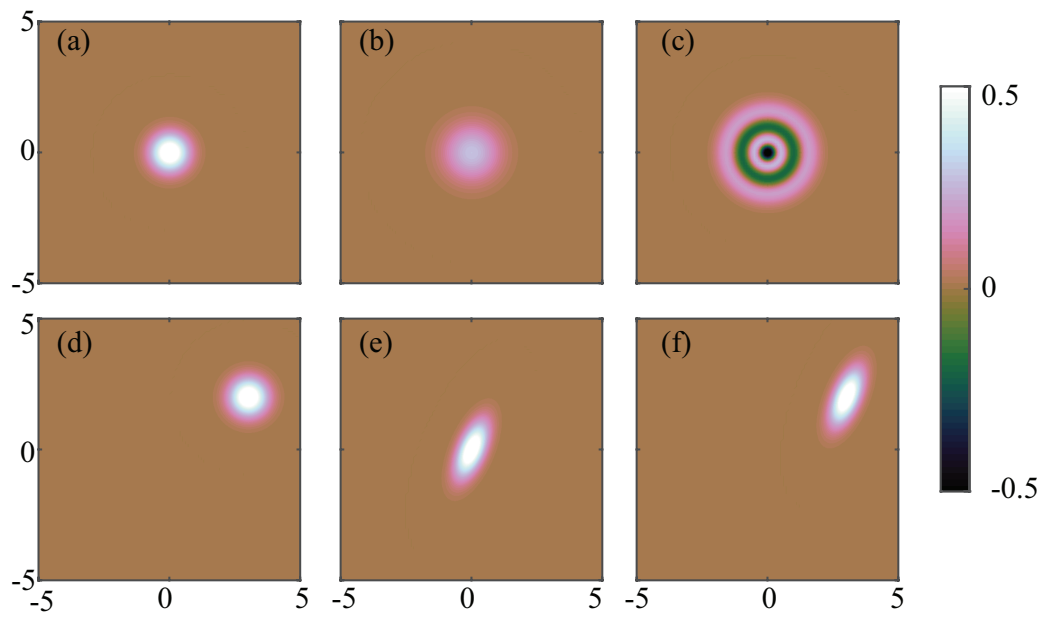


FIGURE 4.1: *W*-functions of some important quantum-optical states: (a) vacuum state, (b) thermal state with $\beta\omega = 1$, (c) $\hat{n} = 3$ Fock state, (d) $\alpha = 3 + 2i$ displaced (coherent) state, (e) $\zeta = 0.3(1 - i)$ squeezed vacuum, (f) $\alpha = 3 + 2i, \zeta = 0.3(1 - i)$ displaced squeezed state, a generic single mode XP-Gaussian state. Colour scheme from Ref. [140].

vacuum, we obtain a state

$$|\alpha\rangle = \hat{D}(\alpha, \alpha^*) |0\rangle. \quad (4.13)$$

the shape of the W-function does not change but it is displaced from the origin to a complex value α . Note that $\hat{a}|\alpha\rangle = \alpha|\alpha\rangle$: coherent states are eigenvectors of the annihilation operator. This means that coherent states are unaffected by the loss of a photon. Also in mean-field descriptions as the Gross-pitaevskii equations, where one substitutes $\hat{\psi}$ by $\psi = \langle \hat{\psi} \rangle$, this can be seen as the variational ansatz that $\hat{\psi}$ is in a coherent state. Furthermore, coherent states are typically used to represent the light field of a laser³.

- Apart from displacement, the vacuum can also be **squeezed**, by an operation

$$|0, \zeta\rangle = \hat{S}(\zeta) |0\rangle = e^{\frac{\zeta^*}{2} \hat{a}^2 - \frac{\zeta}{2} \hat{a}^{\dagger 2}} |0\rangle. \quad (4.14)$$

Interestingly, such states allow for the experimental detection of the vacuum fluctuations [143].

4.2.2 SQUEEZED AND DISPLACED LIGHT

Of course, it is possible to perform both squeezing (4.14) and displacement (4.13) operations subsequently on the vacuum, to

$$|\alpha, \zeta\rangle = \hat{D}(\alpha) \hat{S}(\zeta) |0\rangle. \quad (4.15)$$

This leads to squeezed, displaced states, the most general pure Gaussian state (mixed Gaussian states are obtained by squeezing and displacement of a thermal state). The fact that both $\hat{D}(\alpha)$ and $\hat{S}(\zeta)$ are of no higher than second order of \hat{a}, \hat{a}^\dagger in their exponent hints to the reason why such states are considered Gaussian. Also the W-function and other phase-space distributions themselves have a Gaussian shape. In fact, because of a result known as **Hudson's theorem**, Gaussian states are the only pure states with a W-function that is non-negative everywhere [144].

In practice, we will find it more useful to work directly with the second moments $\langle \hat{a} \hat{a} \rangle$ and $\langle \hat{a}^\dagger \hat{a} \rangle$ in addition to the first moment $\alpha = \langle \hat{a} \rangle$ (the relation of how ζ relates to the Gaussian variances is e.g. given explicitly in ref. [145]).

³Some doubts have arisen as to whether coherent states truly exist at optical frequencies. In any case, this remains a useful picture for practical purposes [142].

In fact, by defining fluctuation operators as $\hat{\delta}_O = \hat{O} - \langle \hat{O} \rangle$, we have access to the second *central* moments or cumulants $\langle \hat{\delta}_{\hat{a}} \hat{\delta}_{\hat{a}} \rangle = \langle \hat{a} \hat{a} \rangle - \alpha^2$ and $\langle \hat{\delta}_{\hat{a}}^\dagger \hat{\delta}_{\hat{a}} \rangle = \langle \hat{a}^\dagger \hat{a} \rangle - |\alpha|^2$. For the remainder of this thesis, we will drop the subscript 'a' for fluctuations. Importantly, fluctuations $\hat{\delta}$ are zero-mean variables, so the application of Wick's theorem (4.1) is clear.

As an explicit example, we apply Wick's theorem to the fourth moment $\langle \hat{a}^\dagger \hat{a}^\dagger \hat{a} \hat{a} \rangle$:

$$\langle \hat{a}^\dagger \hat{a}^\dagger \hat{a} \hat{a} \rangle = \langle (\alpha^* + \hat{\delta}^\dagger)(\alpha^* + \hat{\delta}^\dagger)(\alpha + \hat{\delta})(\alpha + \hat{\delta}) \rangle \quad (4.16)$$

$$= |\alpha|^4 + \alpha^{*2} \langle \hat{\delta} \hat{\delta} \rangle + \alpha^2 \langle \hat{\delta} \hat{\delta} \rangle^* + 2|\alpha|^2 \langle \hat{\delta}^\dagger \hat{\delta} \rangle + \langle \hat{\delta}^\dagger \hat{\delta}^\dagger \hat{\delta} \hat{\delta} \rangle \quad (4.17)$$

$$= |\alpha|^4 + 2|\alpha|^2 \langle \hat{\delta}^\dagger \hat{\delta} \rangle + 2 \operatorname{Re} \left[\alpha^2 \langle \hat{\delta} \hat{\delta} \rangle^* \right] + \left| \langle \hat{\delta} \hat{\delta} \rangle \right|^2 + 2 \langle \hat{\delta}^\dagger \hat{\delta} \rangle^2 \quad (4.18)$$

where we have also used that all odd cumulants of a Gaussian state vanish. Extension of this approach to a multimode system is entirely straightforward and only requires adding subscripts to denote the modes and, of course, properly taking into account the commutation relation $[\hat{\delta}_i, \hat{\delta}_j^\dagger] = \delta_{ij}$, where the δ on the right-hand side is the kronecker delta. When studying multimode systems, we will use the shorthand notation

$$u_{ij} = u_{ji} = \langle \hat{\delta}_i \hat{\delta}_j \rangle = \langle \hat{a}_i \hat{a}_j \rangle - \alpha_i \alpha_j \quad (4.19)$$

$$v_{ij} = v_{ji}^* = \langle \hat{\delta}_i^\dagger \hat{\delta}_j \rangle = \langle \hat{a}_i^\dagger \hat{a}_j \rangle - \alpha_i^* \alpha_j. \quad (4.20)$$

QUADRATURE NOTATION, COVARIANCE MATRIX AND PURITY

In an alternative formulation, the same states can be described with hermitian fluctuations on the quadrature variables, as is more commonly used in some works on the quantum information of Gaussian states [146]. Explicitly, transformations are obtained using $\hat{\delta}^{(j)} = \hat{\delta}_x^{(j)} + i \hat{\delta}_p^{(j)}$ to be

$$\langle \hat{\delta}_i \hat{\delta}_j \rangle = \langle \hat{\delta}_x^{(i)} \hat{\delta}_x^{(j)} \rangle - \langle \hat{\delta}_p^{(i)} \hat{\delta}_p^{(j)} \rangle + i \left(\langle \hat{\delta}_x^{(i)} \hat{\delta}_p^{(j)} \rangle_{\text{sym}} + \langle \hat{\delta}_x^{(j)} \hat{\delta}_p^{(i)} \rangle_{\text{sym}} \right) \quad (4.21)$$

$$\langle \hat{\delta}_i^\dagger \hat{\delta}_j \rangle = \langle \hat{\delta}_x^{(i)} \hat{\delta}_x^{(j)} \rangle + \langle \hat{\delta}_p^{(i)} \hat{\delta}_p^{(j)} \rangle + i \left(\langle \hat{\delta}_x^{(i)} \hat{\delta}_p^{(j)} \rangle_{\text{sym}} - \langle \hat{\delta}_x^{(j)} \hat{\delta}_p^{(i)} \rangle_{\text{sym}} \right) - \frac{\delta_{ij}}{2} \quad (4.22)$$

or conversely,

$$\langle \hat{\delta}_x^{(i)} \hat{\delta}_x^{(j)} \rangle = \frac{1}{2} \text{Re} \left(\langle \hat{\delta}_i^\dagger \hat{\delta}_j \rangle + \langle \hat{\delta}_i \hat{\delta}_j \rangle \right) + \frac{\delta_{ij}}{4} \quad (4.23)$$

$$\langle \hat{\delta}_p^{(i)} \hat{\delta}_p^{(j)} \rangle = \frac{1}{2} \text{Re} \left(\langle \hat{\delta}_i^\dagger \hat{\delta}_j \rangle - \langle \hat{\delta}_i \hat{\delta}_j \rangle \right) + \frac{\delta_{ij}}{4} \quad (4.24)$$

$$(4.25)$$

$$\langle \hat{\delta}_x^{(i)} \hat{\delta}_p^{(j)} \rangle_{\text{sym}} = \frac{1}{2} \text{Im} \left(\langle \hat{\delta}_i \hat{\delta}_j \rangle + \langle \hat{\delta}_i^\dagger \hat{\delta}_j \rangle \right). \quad (4.26)$$

The subscript ‘sym’ denotes the symmetrized expectation value. If we denote the matrices of these variances by square brackets, the matrix

$$\Sigma = \begin{pmatrix} \left[\langle \hat{\delta}_x^2 \rangle \right] & \left[\langle \hat{\delta}_x \hat{\delta}_p \rangle_{\text{sym}} \right]^T \\ \left[\langle \hat{\delta}_x \hat{\delta}_p \rangle_{\text{sym}} \right] & \left[\langle \hat{\delta}_p^2 \rangle \right] \end{pmatrix} \quad (4.27)$$

becomes the covariance matrix of $(\vec{X}, \vec{P})^T$ [146]. For an m-mode system, the purity is equal to $\mu = \text{tr}\{\hat{\rho}^2\} = 2^{-2m} \det\{\Sigma\}^{-1/2}$, meaning that pure Gaussian states satisfy

$$\det\{\Sigma\} = 2^{-4m}, \quad (4.28)$$

or for a single mode

$$\langle \hat{\delta}_x^2 \rangle \langle \hat{\delta}_p^2 \rangle - \langle \hat{\delta}_x \hat{\delta}_p \rangle_{\text{sym}}^2 = \frac{1}{16}. \quad (4.29)$$

For convenience, we note that in terms of our original variables u_{ij} and v_{ij} , we can construct a similar matrix

$$\tilde{\Sigma} = \begin{pmatrix} \left[\text{Re}\{v\} + \frac{\delta_{ij}}{2} \right] & [u] \\ [u^*] & \left[\text{Re}\{v\} + \frac{\delta_{ij}}{2} \right] \end{pmatrix} \quad (4.30)$$

for which pure states satisfy

$$\det\{\tilde{\Sigma}\} = 2^{-2m}, \quad (4.31)$$

or for a single mode

$$\langle \hat{\delta}^\dagger \hat{\delta} \rangle + \langle \hat{\delta} \hat{\delta}^\dagger \rangle = \left| \langle \hat{\delta} \hat{\delta} \rangle \right|^2. \quad (4.32)$$

The main practical use of the purity to our purpose is that it can either be

used to eliminate one independent variable, or as an independent numerical check on the convergence of the simulations. Similar results exist for the entropy of a Gaussian state [146, 147]. If, in a multimode Gaussian state, some modes are traced out, the reduced state for the remaining modes will remain a (mixed) Gaussian state. Gaussian states thus facilitate an easy computation of entanglement entropy (subsection 2.2.4).

In particular, the von-Neumann entropy (subsection 2.2.2) of an individual Gaussian mode k with thermal occupation n_k is

$$S_{vn}^{(k)} = (n_k + 1) \log n_k + 1 - n_k \log n_k. \quad (4.33)$$

A multimode system can be *symplectically* diagonalized to

$$\Sigma = S^T \begin{pmatrix} \text{diag}(d_k) & 0 \\ 0 & \text{diag}(d_k) \end{pmatrix} S \quad (4.34)$$

The values $\pm d_k$ are obtained as the eigenvalues of $iJ\Sigma$, where

$$J = \begin{pmatrix} 0 & -\mathbb{1} \\ \mathbb{1} & 0 \end{pmatrix}. \quad (4.35)$$

The occupation of mode k is $d_k - 1/4$, and the total entropy is [146, 147]

$$S_{vn} = \sum_k S_{vn}^{(k)}. \quad (4.36)$$

This procedure to obtain S_{vn} can be used either on all modes of the Gaussian state as alternative to the purity, or on a Gaussian subsystem for the entanglement entropy. We highlight, though, that (4.36) is only the entropy of an individual trajectory and does not include the classical fluctuations that are additionally present in the master equation. The full entropy of the ensemble that includes these contributions can in principle be obtained from the overlap elements between elements [148] but we have found that this procedure does not converge properly without using an exponentially large amount of trajectories.

EXPLICIT CONSTRUCTION OF GAUSSIAN STATES

As we have seen, Gaussian states can be constructed explicitly, for example in truncated Fock base (or its product space for multimode systems), by executing

squeezing and displacement operators on the vacuum or a thermal state.

The Wigner-function of such Gaussian state can also be easily written down in terms of the displacement and the covariances, both for a single mode [9] as in the multimode case [146].

As it turns out, the density matrix for all mixed Gaussian states can be written as

$$\hat{\rho}_G = \mathcal{N} e^{-\beta \hat{H}_{\text{eff}}}, \quad (4.37)$$

for some ‘effective Hamiltonian’ \hat{H}_{eff} [147] (not to be confused with the operator carrying the same name in chapter 2), and β being inverse temperature. Pure states correspond to the limit $\beta \rightarrow \infty$. They can be obtained as the ground state (lowest eigenvector) of \hat{H}_{eff} .

For the case of a single mode for example, \hat{H}_{eff} would look like [9]

$$\begin{aligned} \hat{H}_{\text{eff}} &\propto \left(\langle \hat{\delta}^\dagger \hat{\delta} \rangle + \frac{1}{2} \right) (\hat{a}^\dagger - \alpha^*)(\hat{a} - \alpha) + \frac{1}{2} \langle \hat{\delta} \hat{\delta} \rangle (\hat{a}^\dagger - \alpha^*)^2 + \frac{1}{2} \langle \hat{\delta} \hat{\delta} \rangle^* (\hat{a} - \alpha)^2, \\ &\propto (\hat{X} - X)^2 \left\langle \hat{\delta}_p \hat{\delta}_p \right\rangle + (\hat{P} - P)^2 \left\langle \hat{\delta}_x \hat{\delta}_x \right\rangle \\ &\quad - (\hat{X} - X)(\hat{P} - P) \left\langle \hat{\delta}_x \hat{\delta}_p \right\rangle_{\text{sym}} - (\hat{P} - P)(\hat{X} - X) \left\langle \hat{\delta}_x \hat{\delta}_p \right\rangle_{\text{sym}}, \end{aligned} \quad (4.38)$$

where the proportionality constant is irrelevant.

4.3 Gaussian states in quantum information

As we know from Hudson’s theorem, Gaussian states have positive Wigner functions and have thus inherently a semiclassical nature. Nevertheless, a squeezed multimode Gaussian state displays entanglement, a feature that is surely non-classical. As such, Gaussian states play a crucial role in continuous-variable quantum information. For a full description, we refer to Refs. [146, 147, 149]. Some convenient formulas are also obtained in that context, including some of the preceding section (although care must be taken about normalization conventions).

4.4 As a variational ansatz: Hartree-Fock-Bogoliubov method

In closed quantum many-body systems, Gaussian states have been known as a standard tool for both bosons and fermions, both for the statics and the dynamics

and both in the solid-state (for example the BCS theory of superconductivity) as in the nuclear physics context. For an overview, see Ref. [150]. Such approaches often go under the name 'Hartree-Fock-Bogoliubov'.

It is further interesting to note that Generalized Gibbs Ensembles [151], entropy-maximizing states that have recently found applicability to integrable quantum systems, are often Gaussian states [152].

4.4.1 A NOTE ON THE TERM 'VARIATIONAL'

In variational methods, one selects a lower-dimensional manifold embedded in the full Hilbert space in which states can be characterized by many fewer degrees of freedom (variational parameters). By tuning these parameters, one tries to find a state in the manifold that is as close as possible to the exact state of interest. Such methods appear in two flavours: for static variational methods that try finding the ground state, one minimizes the energy. For the time-dependent variational principle instead, at each timestep the evolution leaves the manifold and is subsequently projected back on it (equivalent with stationarity of the action). With Gaussian states, this projection is achieved by exploiting Wick's theorem [150, 153].

4.5 Density-phase Gaussian states

In quantum hydrodynamics, a framework commonly used in the context of Bose-Einstein condensation, it is common to introduce a (Dirac) phase by

$$\hat{a} =: e^{i\hat{\theta}}\sqrt{\hat{n}} \quad (4.40)$$

and describe the dynamics in terms of density and phase as two real variables instead of the quadratures [49]. Similar to \hat{X} and \hat{P} , \hat{n} and $\hat{\theta}$ are conjugate variables implying

$$[\hat{n}, \hat{\theta}] = i. \quad (4.41)$$

Because of this mathematical symmetry (symplectic structure), the formulas from the preceding sections on XP-Gaussian states can be straightforwardly transferred to density-phase states as well (if care is taken about the slightly different normalization convention). For a single mode, for example, the independent (real) expectation values to take into account are $\langle \hat{n} \rangle$, $\langle \hat{\delta}_n \hat{\delta}_n \rangle = \langle \hat{n} \hat{n} \rangle - \langle \hat{n} \rangle^2$, $\langle \hat{\theta} \rangle$, $\langle \hat{\delta}_\theta \hat{\delta}_\theta \rangle = \langle \hat{\theta} \hat{\theta} \rangle - \langle \hat{\theta} \rangle^2$ and $\langle \hat{\delta}_n \hat{\delta}_\theta \rangle_{\text{sym}} = \langle \hat{n} \hat{\theta} \rangle / 2 + \langle \hat{\theta} \hat{n} \rangle / 2 - \langle \hat{n} \rangle \langle \hat{\theta} \rangle$.

The use of Wick's theorem is, by itself, the same as with the XP -Gaussian states. Because of the decompositions (4.40), the correlators to expand are not guaranteed to be polynomials in \hat{n} and $\hat{\theta}$. A few useful properties are that

$$e^{ik\hat{\theta}} f(\hat{n}, \hat{\theta}) e^{-ik\hat{\theta}} = f(\hat{n}+k, \hat{\theta}) \quad (4.42)$$

and

$$[f(A), B] = [A, B] \frac{\partial f}{\partial A} \quad (4.43)$$

if $[A, [A, B]] = 0$.

Terms that still remain non-polynomial should be expanded with their Taylor series, in $\hat{\delta}_n/\hat{n}$ and $\hat{\delta}_\theta$ before applying Wick's theorem. For example,

$$\begin{aligned} \langle \sqrt{\hat{n}} e^{-i\hat{\theta}} \rangle &\approx \sqrt{\langle \hat{n} \rangle} e^{-i\langle \hat{\theta} \rangle - \frac{\langle \hat{\delta}_\theta \hat{\delta}_\theta \rangle}{2}} \\ &\times \left(1 + \frac{1}{2\langle \hat{n} \rangle} \left(\frac{1}{2} - i \langle \hat{\delta}_n \hat{\delta}_\theta \rangle_{\text{sym}} \right) - \frac{\langle \hat{\delta}_n \hat{\delta}_n \rangle}{8\langle \hat{n} \rangle^2} \right). \end{aligned} \quad (4.44)$$

Here, phase-phase correlations were kept up to all orders (such exact resummation turns out to be possible rather generally), while phase-density correlations were truncated at second order. This approximation is valid when the average particle number is sufficiently large. The full set of expanded correlators that we will encounter is given in Appendix B.

When using density and phase operators, care must be taken regarding their definition nevertheless. \hat{X} and \hat{P} both have a continuous spectrum from $]-\infty, \infty[$. In truth however, the eigenvalues of \hat{n} are only positive integers. Worse, $\hat{\theta}$ is, related to the periodicity of phase and singularity in the origin, ill-defined [154]. Therefore, density-phase decompositions are only valid at sufficient particle number (we have already seen the traces of this in the expansion of the correlators) and if the state is localized in phase space. From an operational perspective, the fact that the phase is ill-defined can also lead to problems in general, as the phase operator obtained through the Dirac recipe (4.41) cannot be written down in an explicit matrix representation in Fock base. To overcome this issue, we will introduce an *Adaptive Pegg-Barnett phase* in section 11.3.

Gaussian Quantum Trajectories for the variational simulation of open quantum systems

The central chapter of the thesis: we combine the quantum trajectory method with Gaussian ansatzes (XP-Gaussian and NΘ-Gaussian), and compare their performances for different unravelings against exact results and those obtained by the TWA, for some simple problems in a single driven-dissipative Kerr resonator.

5.1 Combining quantum trajectories with a Gaussian ansatz

5.1.1 QUANTUM TRAJECTORIES FOR EXPECTATION VALUES

As noted for the case of the cumulant expansion (subsection 3.3.5), knowledge of a quantum state is equivalent to knowing all moments in a convenient operator basis. We will utilize a similar procedure here, where the ‘quantum state’ of which we study the moments is no longer the density matrix $\hat{\rho}$, but individual trajectories $|\psi(t)\rangle$

Explicitly, equations of motions for expectation values are obtained by starting from the stochastic Schrödinger equation (similar derivations are possible starting from the Heisenberg picture [155]) as

$$d\langle\hat{O}\rangle = d\left(\langle\psi|\hat{O}|\psi\rangle\right) = d(\langle\psi|\hat{O}|\psi\rangle) + \langle\psi|\hat{O}d(|\psi\rangle) + d(\langle\psi|)\hat{O}d(|\psi\rangle) \quad (5.1)$$

and keeping terms of first order in dt , keeping in mind Itô calculus (for real Wiener

noise, $dW^2 = dt$, for complex Wiener noise $|dZ|^2 = dt$ while $dZ^2 = 0$ and for Poisson processes $dN^2 = dN$).

As we have seen, trajectory wavefunctions are often unnormalized according to the simplest standard formulas. Whether one uses the norm-conserving equivalents of the exact trajectory wavefunctions before transferring the evolution correlation functions, or first translate the equations of motions to correlation functions and correct those to be norm-conserving (we will see an example below) is equivalent.

PHOTON-COUNTING UNRAVELING

Let us illustrate this with the photon counting unraveling (subsection 2.5.1).

In terms of unnormalized expectation values, the deterministic evolution (2.40) corresponds to the evolution

$$d\langle\widehat{O}\rangle = i\langle\widehat{[\hat{H}, \hat{O}]}\rangle dt - \frac{\gamma}{2}\langle\widehat{\hat{a}^\dagger \hat{a} \hat{O}}\rangle dt - \frac{\gamma}{2}\langle\widehat{\hat{O} \hat{a}^\dagger \hat{a}}\rangle dt. \quad (5.2)$$

By choosing $\hat{O} = 1$, we see that the evolution for the normalized expectation value $\langle\hat{O}\rangle = \langle\widehat{\hat{O}}\rangle/\langle\widehat{1}\rangle$ is given by

$$d\langle\hat{O}\rangle = i\langle\widehat{[\hat{H}, \hat{O}]}\rangle dt - \frac{\gamma}{2}\langle\widehat{\hat{a}^\dagger \hat{a} \hat{O}}\rangle dt - \frac{\gamma}{2}\langle\widehat{\hat{O} \hat{a}^\dagger \hat{a}}\rangle dt + \gamma\langle\widehat{\hat{a}^\dagger \hat{a}}\rangle\langle\hat{O}\rangle dt. \quad (5.3)$$

Meanwhile, according to (2.41), a jump (photon detection) affects the expectation value $\langle\hat{O}\rangle$ by

$$\langle\hat{O}\rangle \xrightarrow{J} \frac{\langle\widehat{\hat{a}^\dagger \hat{O} \hat{a}}\rangle}{\langle\widehat{\hat{a}^\dagger \hat{a}}\rangle} = \frac{\langle\widehat{\hat{a}^\dagger \hat{O} \hat{a}}\rangle}{\langle\widehat{\hat{a}^\dagger \hat{a}}\rangle}. \quad (5.4)$$

An equivalent result is obtained from SDE (2.39).

HOMO- AND HETERODYNE UNRAVELINGS

Analogously to the deterministic part of photon-counting, Eqs. (2.42),(2.43) can be translated to the evolution of normalized expectation values, yielding for the

heterodyne unraveling

$$\begin{aligned} d\langle\hat{O}\rangle = & i\langle[\hat{H},\hat{O}]\rangle dt \\ & -\frac{\gamma}{2}\langle\hat{n}\hat{O}\rangle dt -\frac{\gamma}{2}\langle\hat{O}\hat{n}\rangle dt +\gamma\langle\hat{a}^\dagger\hat{O}\hat{a}\rangle dt \\ & +\sqrt{\gamma}\left(\langle\hat{a}^\dagger\hat{\delta}_O\rangle dZ +\langle\hat{\delta}_O\hat{a}\rangle dZ^*\right), \end{aligned} \quad (5.5)$$

where again $\hat{\delta}_O = \hat{O} - \langle\hat{O}\rangle$. For the homodyne unraveling, dZ should be replaced by $e^{i\phi} dW$ in this expression.

5.1.2 CLOSING AT GAUSSIAN LEVEL

Equations (5.3), (5.4) or (5.5) will generally introduce an infinite hierarchy of correlation functions, similar to the cumulant expansions (subsection 3.3.5). By restricting ourselves to the Gaussian manifold (chapter 4) and exploiting Wick's theorem, only the first and second moment are required to obtain all information on the state.

Because of the presence of the second moments, a Gaussian ansatz is by nature one order higher than the mean-field approach that corresponds to a coherent ansatz. Formally then, the Gaussian methods are of the same order as Bogoliubov theory. Nevertheless, we can expect these Gaussian trajectory methods to provide a more refined description of the whole state because the second-order expansion is done at the level of individual trajectories instead of on the level of the ensemble. In the next section, we will illustrate this with the example of optical bistability in a Kerr nonlinear cavity. Where the Bogoliubov theory is only able to describe the fluctuations around one of the two stable branches, the variational Gaussian method is also capable of describing the switching between the branches.

5.2 Optical bistability and the XP -Gaussian methods

As a first example, we look at a driven-dissipative cavity with Kerr non-linearity, described by the Hamiltonian

$$\hat{H} = -\Delta\hat{a}^\dagger\hat{a} + \frac{U}{2}\hat{a}^\dagger\hat{a}^\dagger\hat{a}\hat{a} + Fa^\dagger + F^*\hat{a} \quad (5.6)$$

where Δ the cavity-laser detuning in the frame rotating at pump frequency, U the photon-photon interaction and F the classical laser amplitude. Furthermore,

photons leak to the vacuum with rate γ as described in section 2.5.

Exact solutions for the expectation values $\langle \hat{a}^{\dagger m} \hat{a}^n \rangle_{\hat{\rho}}$ of the stationary state, as well as a semi-classical model, were calculated in [77] (the notation $\langle \cdot \rangle_{\hat{\rho}}$ emphasizes that the expectation value is taken over the whole ensemble). Interestingly, at the classical level, this system features a bistability regime where, given all other parameters, two stable solutions for the density exist.

Such a Kerr-cavity provides a model for polariton condensates (subsection 3.2.2), for which it has been shown that trajectory methods can provide an adequate description [156, 157]. Also coupled arrays of these cavities are an object of current interest [158] and it is in these systems that the TWA method has been proven insufficient [45].

Here, we will first use the method with the ordinary Gaussian states (Gaussian in the quadrature variables) or ‘XP-Gaussian states’, as the most straightforward Gaussian ansatz.

From (5.3) and after applying Wick’s theorem to close the set of equations, we obtain for photon-counting the deterministic evolution

$$\partial_t \alpha = \left(\frac{-\gamma}{2} + i\Delta \right) \alpha - Ui \left(|\alpha|^2 \alpha + 2\alpha \langle \hat{\delta}^\dagger \hat{\delta} \rangle + \alpha^* \langle \hat{\delta} \hat{\delta} \rangle \right) - iF - \gamma \left(\alpha \langle \hat{\delta}^\dagger \hat{\delta} \rangle + \alpha^* \langle \hat{\delta} \hat{\delta} \rangle \right) \quad (5.7)$$

$$\partial_t \langle \hat{\delta} \hat{\delta} \rangle = (2i\Delta - \gamma) \langle \hat{\delta} \hat{\delta} \rangle - Ui \left(\alpha^2 (1 + 2 \langle \hat{\delta}^\dagger \hat{\delta} \rangle) + \langle \hat{\delta} \hat{\delta} \rangle (1 + 4|\alpha|^2 + 6 \langle \hat{\delta}^\dagger \hat{\delta} \rangle) \right) - 2\gamma \langle \hat{\delta}^\dagger \hat{\delta} \rangle \langle \hat{\delta} \hat{\delta} \rangle \quad (5.8)$$

$$\partial_t \langle \hat{\delta}^\dagger \hat{\delta} \rangle = 2U \operatorname{Im} \left[\alpha^2 \langle \hat{\delta} \hat{\delta} \rangle^* \right] - \gamma \left(\langle \hat{\delta}^\dagger \hat{\delta} \rangle + \langle \hat{\delta}^\dagger \hat{\delta} \rangle^2 + \left| \langle \hat{\delta} \hat{\delta} \rangle \right|^2 \right). \quad (5.9)$$

This deterministic evolution is propagated until the norm, evolving through (5.2), becomes $\widetilde{\langle 1 \rangle} = \xi$ (the random number as defined in 2.5.1). Then, according to (5.4), jumps occur as

$$\alpha \xrightarrow{J} \frac{|\alpha|^2 \alpha + 2\alpha \langle \hat{\delta}^\dagger \hat{\delta} \rangle + \alpha^* \langle \hat{\delta} \hat{\delta} \rangle}{|\alpha|^2 + \langle \hat{\delta}^\dagger \hat{\delta} \rangle} \quad (5.10)$$

$$\langle \hat{\delta} \hat{\delta} \rangle \xrightarrow{J} \frac{|\alpha|^4 \langle \hat{\delta} \hat{\delta} \rangle + 2|\alpha|^2 \langle \hat{\delta}^\dagger \hat{\delta} \rangle \langle \hat{\delta} \hat{\delta} \rangle - \alpha^2 \langle \hat{\delta}^\dagger \hat{\delta} \rangle^2 + 3 \langle \hat{\delta}^\dagger \hat{\delta} \rangle^2 \langle \hat{\delta} \hat{\delta} \rangle - \alpha^{*2} \langle \hat{\delta} \hat{\delta} \rangle^2}{|\alpha|^4 + 2|\alpha|^2 \langle \hat{\delta}^\dagger \hat{\delta} \rangle + \langle \hat{\delta}^\dagger \hat{\delta} \rangle^2} \quad (5.11)$$

$$\langle \hat{\delta}^\dagger \hat{\delta} \rangle \xrightarrow{J} \frac{|\alpha|^4 \langle \hat{\delta}^\dagger \hat{\delta} \rangle - 2 \operatorname{Re} \left[\alpha^2 \langle \hat{\delta} \hat{\delta} \rangle^* \langle \hat{\delta}^\dagger \hat{\delta} \rangle \right] + \langle \hat{\delta}^\dagger \hat{\delta} \rangle \left| \langle \hat{\delta} \hat{\delta} \rangle \right|^2 + 2|\alpha|^2 \langle \hat{\delta}^\dagger \hat{\delta} \rangle^2 + 2 \langle \hat{\delta}^\dagger \hat{\delta} \rangle^3}{|\alpha|^4 + 2|\alpha|^2 \langle \hat{\delta}^\dagger \hat{\delta} \rangle + \langle \hat{\delta}^\dagger \hat{\delta} \rangle^2}. \quad (5.12)$$

In the heterodyne unraveling on the other hand, the evolution of the mean-field (5.5) is given by

$$d\alpha = \left[\left(\frac{-\gamma}{2} + i\Delta \right) \alpha - U i \left(|\alpha|^2 \alpha + 2\alpha \langle \hat{\delta}^\dagger \hat{\delta} \rangle + \alpha^* \langle \hat{\delta} \hat{\delta} \rangle \right) - iF \right] dt + \sqrt{\gamma} \left(\langle \hat{\delta}^\dagger \hat{\delta} \rangle dZ + \langle \hat{\delta} \hat{\delta} \rangle dZ^* \right). \quad (5.13)$$

Generally, one would expect similar stochastic equations for $\langle \hat{\delta} \hat{\delta} \rangle$ and $\langle \hat{\delta}^\dagger \hat{\delta} \rangle$. Remarkably, they are entirely deterministic (unlike equations for the correlators $\langle \hat{a} \hat{a} \rangle$ and $\langle \hat{a}^\dagger \hat{a} \rangle$) and, moreover, are identical to the deterministic part of photon-counting equations (5.11), (5.12). It should be noted, however, that the equations of motion are different for more general homodyne detection schemes: for those, the equations for $d \langle \hat{\delta} \hat{\delta} \rangle$ and $d \langle \hat{\delta}^\dagger \hat{\delta} \rangle$ contain additional terms

$$- \gamma \left(\langle \hat{\delta}^\dagger \hat{\delta} \rangle^2 e^{2i\phi} + \langle \hat{\delta} \hat{\delta} \rangle^2 e^{-2i\phi} \right) dt \quad (5.14)$$

and

$$- \gamma \left(\langle \hat{\delta}^\dagger \hat{\delta} \rangle \langle \hat{\delta} \hat{\delta} \rangle^* e^{2i\phi} + \langle \hat{\delta} \hat{\delta} \rangle \langle \hat{\delta}^\dagger \hat{\delta} \rangle e^{-2i\phi} \right) dt, \quad (5.15)$$

respectively.

For all unravelings, as a slightly more efficient and stable alternative to evolving $\langle \hat{\delta}^\dagger \hat{\delta} \rangle$ along explicitly through (5.12), one can obtain it from $\langle \hat{\delta} \hat{\delta} \rangle$ by asserting that the state remains pure, corresponding to the condition (4.32). For an initially pure state, this relation remains exactly satisfied through heterodyne measurement as well as through the deterministic evolution between photon jumps, although the purity

$$\operatorname{tr}[\hat{\rho}^2] = \left(1 + 4 \left(\langle \hat{\delta}^\dagger \hat{\delta} \rangle + \langle \hat{\delta} \hat{\delta} \rangle^2 - \left| \langle \hat{\delta} \hat{\delta} \rangle \right| \right) \right)^{-1/2} \quad (5.16)$$

briefly decreases at a jump after which it tends to relax back to 1. Relation (4.32) remains fulfilled at a jump up to order $|\alpha|^{-5}$ so that only in systems where there is a significant jump rate at zero density, it is better to evolve $\langle \hat{\delta}^\dagger \hat{\delta} \rangle$ explicitly with Eq. (5.12).

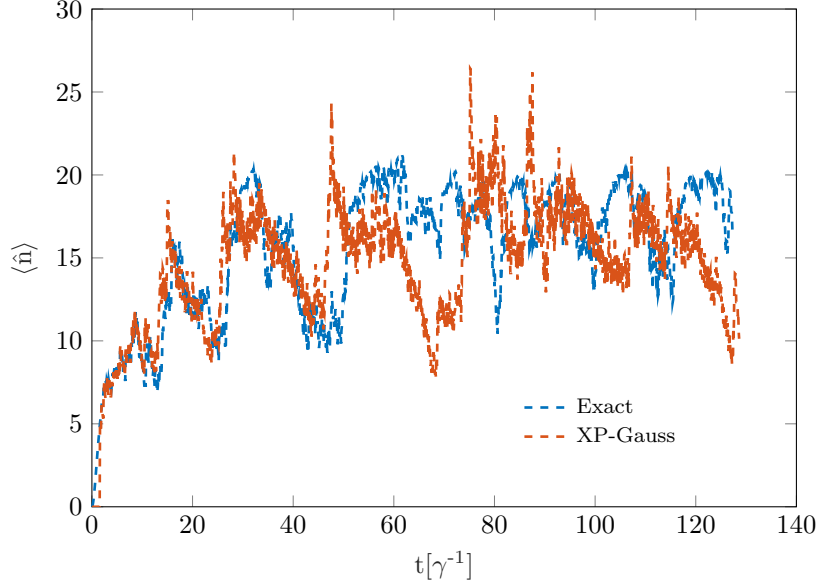


FIGURE 5.1: Numerically exact trajectory (up to particle number truncation) with its corresponding XP-Gaussian approximation for a photon-counting process with parameters $U/\gamma = 0.05$, $\Delta/\gamma = 1$ and $F/\gamma = 2.235$.

In Fig. 5.1, we show a comparison between single trajectories that were obtained with the numerically exact evolution of the wave function and the Gaussian variational ansatz where for the jumps in both simulations (waiting times) identical random numbers were used. Initially, there is a very strong correspondence with the XP-Gaussian variational method, while at later evolution times, due to an accumulation of the deviations, an offset in time emerges and the good correspondence is lost. Qualitatively though, the behavior remains similar so that approximate correspondence in the weak sense (for the whole ensemble) is remain fulfilled.

To verify this, in figure 5.2 densities $\langle \hat{a}^\dagger \hat{a} \rangle_\rho$ and density correlations $g^{(2)} = \frac{\langle \hat{a}^\dagger \hat{a}^\dagger \hat{a} \hat{a} \rangle_\rho}{\langle \hat{a}^\dagger \hat{a} \rangle_\rho^2}$ are plotted as function of F throughout the bistability regime of the Kerr-model. We see that the XP-Gaussian methods can provide reasonable to very good predictions of the exact correlation functions from [77]. In this regime of relatively low density these XP-Gaussian methods are mostly outperformed by the TWA method, though. It is also seen that the predictions on the statistics of the ensemble as a whole depend (weakly) on the choice of unraveling, whereas this is independent for exact trajectories. We should note that, because of the low

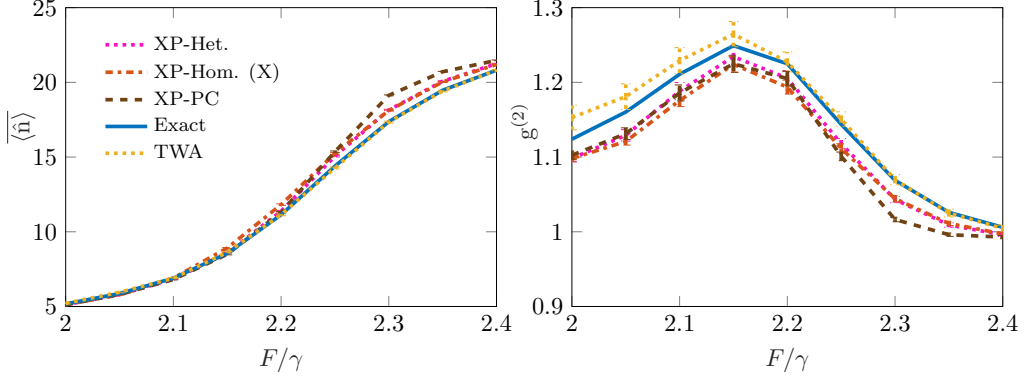


FIGURE 5.2: Stationary ensemble expectations of photon number (left) and instantaneous second-order correlation (right) as function of F through the bistability regime for parameters $U/\gamma = 0.05$, $\Delta/\gamma = 1$. Results were obtained by averaging over 10^4 samples after $t = 100\gamma^{-1}$ of evolution from the vacuum. The exact solution is the analytical result from [77]. While there are some quantitative deviations, all qualitative features are reflected by the GTA.

density, simulation with exact trajectories can also still easily be performed. It is the opposite, high-density, limit where Gaussian ansatzes will provide a better description as well as where exact trajectories become computationally unfeasible.

5.2.1 BENCHMARKS ON A DIMER

In Ref. [159], the TWA method was benchmarked for the dimer (two coupled Kerr resonators 1,2 each with Hamiltonian (5.6) and an additional coupling term $J(\hat{a}_1^\dagger \hat{a}_2 + \hat{a}_2^\dagger \hat{a}_1)$), by moving away from the mean-field limit of high particle number by increasing U while UF^2 is kept constant. In Figure 5.3 we have reproduced this result, and compare with the predictions from our GTA method. Whereas the GTA has a small deviation already in the low- U regime, this remains bounded for increasing U . The TWA method becomes much worse for strong interactions. Interestingly, the deviations of both methods are opposite, suggesting that if a system is studied with both methods, the true result is likely in between the ones obtained with both methods.

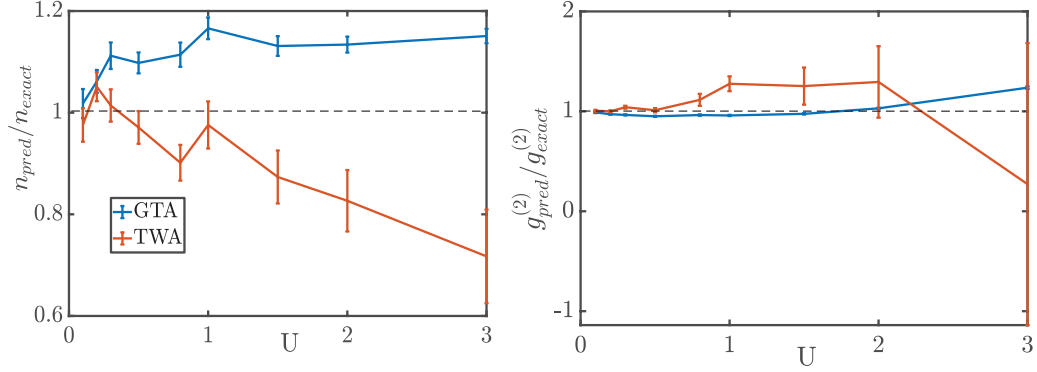


FIGURE 5.3: Ratio of n and $g^{(2)}$ as predicted by the GTA or TWA methods in a dimer, with respect to the exact solution. $UF^2/\gamma^3 = 2.465$ is kept constant while $\Delta/\gamma = 0.1$ and coupling $J/\gamma = 0.9$. The benchmarking of the TWA method in this parameter range has previously been done in ref. [159]

5.3 Phase diffusion and the $N\Theta$ -Gaussian method

5.3.1 PHASE SPACE EVOLUTION

As a second example, we look at the time-evolution of a freely evolving Kerr cavity: we envision an initial state present in system (5.6) where at $t = 0$ the pump is turned off, i.e. $F = F_{on}\Theta(-t)$. Without the pump, $\mathcal{U}(1)$ symmetry is restored, allowing the phase to diffuse freely.

The challenging nature of this problem for our Gaussian variational ansatz can be appreciated from the Wigner distributions of a single exact realization after some time, shown in Fig. 5.4. Panel (a) shows that the phase space distribution has almost spread out over a full circle, implying the loss of phase coherence. The difference between the left and right hand panels, obtained with photon counting and heterodyne detection respectively (Appendix A), shows how the phase space distribution is kept more concentrated under heterodyne measurement as compared to the photon counting. This is expected, because only the heterodyne measurement gives phase information. These statements can be made more precise in the language of subsection 2.4.3. In this example, we clearly see the importance of the unraveling on the applicability of a Gaussian approximation. Unfortunately for the parameters of Fig. 5.4, even for the heterodyne measurement, a Gaussian approximation is very crude. The applicability of the GTA is directly related to Var_1 of the phase. Only $\text{Var}(\hat{O})$ can be measured without unraveling the dynamics and it is the only one that is accessible within the master equation description

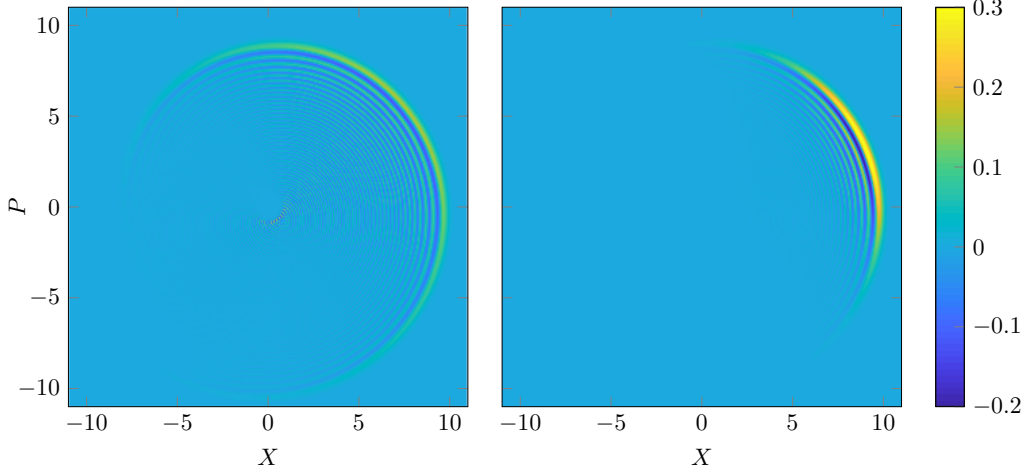


FIGURE 5.4: Wigner function snapshots of a typical single exact trajectory (obtained by numerical integration in truncated Fock space) after $t=0.1\gamma^{-1}$ phase diffusion out of an initial coherent $|\alpha\rangle = |10\rangle$ state ($F/\gamma = 0$, $U/\gamma = 1$, $\Delta/\gamma = 100$), for photon-counting (left) and heterodyne detection (right). It is clear to see that these states are not XP -Gaussian, firstly because they are bent and secondly because the W -function exhibits Fock-like negative parts. Note that the intra-sample variance Var_1 of the phase is smaller for a heterodyne sample, its inter-sample Var_2 variance is larger. Therefore, heterodyne detection is slightly less problematic for the XP -Gaussian states.

(and hence the TWA).

The parameter regime where the width of the phase space distribution is expected to become small can be found by requiring that the phase diffusion rate is much smaller than the rate at which phase information is obtained: $U\sqrt{\langle\hat{a}^\dagger\hat{a}\rangle} \ll \gamma\langle\hat{a}^\dagger\hat{a}\rangle$. For the parameters of Fig. 5.4, we have $U/(\sqrt{\langle\hat{a}^\dagger\hat{a}\rangle}\gamma) = 0.1 \ll 1$, but still the phase space distribution cannot be accurately approximated by a Gaussian.

5.3.2 $N\Theta$ -GAUSSIAN STATES

The shape of the Wigner distribution suggests that a Gaussian description in terms of density and phase may provide a better approximation to the quantum trajectory wave functions, these are exactly the states we have defined in section 4.5.

Using the given set of expectation values, derivation of the stochastic equations of motion, similarly to the case of XP -Gaussian states, proceeds as described in section 5.1. For example, for the deterministic evolution under photon-counting

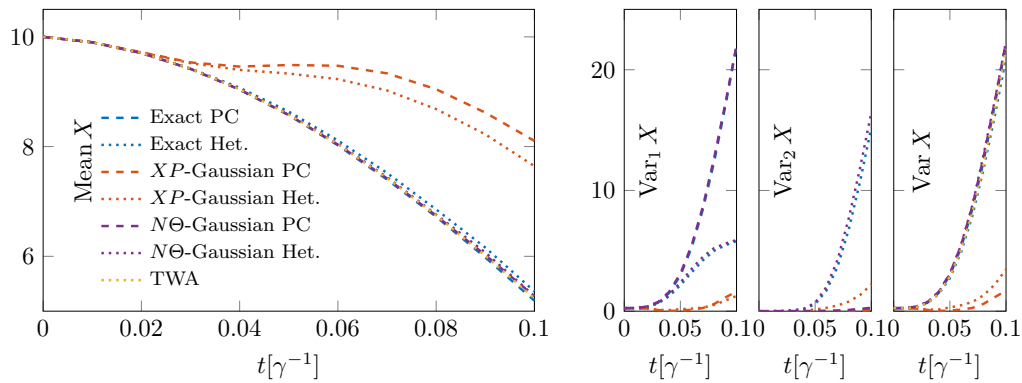


FIGURE 5.5: Mean (left panel) and inner-sample-, between-sample- and total variances (right panel) of the X -quadrature obtained by the numerically exact trajectory methods (in a truncated Fock space) and TWA as well as XP -Gaussian and $N\Theta$ -Gaussian variational methods as function of time after free evolution from a coherent initial state $|\alpha\rangle = |10\rangle$ (same parameters as Fig. 5.4). Averages are taken over 10^3 samples (10^4 for the TWA). It is clear that the $N\Theta$ -variational method provides an accurate description of the true dynamics, both on the level of the whole ensemble as on the level of its constitution in pure states (lines overlap completely or almost completely), whereas the latter cannot be obtained from the TWA method. Very similar behavior is present regarding P and its variances as well as for the X, P -covariances.

we obtain for the density

$$\partial_t \langle \hat{n} \rangle = -\gamma \langle \hat{\delta}_n \hat{\delta}_n \rangle + 2 \operatorname{Im} \left[F \left\langle \sqrt{\hat{n}} e^{-i\hat{\theta}} \right\rangle \right] \quad (5.17)$$

while jumps

$$\langle \hat{n} \rangle \xrightarrow{J} \langle \hat{n} \rangle - 1 + \frac{\langle \hat{\delta}_n \hat{\delta}_n \rangle}{\langle \hat{n} \rangle} \quad (5.18)$$

occur when $\langle \hat{1} \rangle = R$. The full set of equations of motion can be found in subsection 5.3.2, with an analytical solution for the $F = 0$ case. From a different starting point, coupled equations for the evolution of density, phase and their variances have also been used in Ref. [160].

The update rules for the quantum jumps are all exact except the one for $\langle \hat{\delta}_\theta \hat{\delta}_\theta \rangle$ where an expansion in orders of \hat{n}^{-1} must be performed. However, in the case of a pure state (or more generally constant purity) it can be omitted and, similar to the XP -Gaussian case, computed from the other expectation values by the relation

$$\langle \hat{\delta}_n \hat{\delta}_n \rangle \langle \hat{\delta}_\theta \hat{\delta}_\theta \rangle - \langle \hat{\delta}_n \hat{\delta}_\theta \rangle_{\text{sym}}^2 = \frac{1}{4} \quad (5.19)$$

which is the equivalent of (4.29). For a state that is initially pure, relation (5.19) again remains satisfied up to order $\langle \hat{n} \rangle^{-5}$ after a jump.

Equations of motion for heterodyne measurement of density-phase Gaussian states are also given in subsection 5.3.2, for example for the density,

$$\begin{aligned} d \langle \hat{n} \rangle = & \left[2 \operatorname{Im} \left[F \left\langle \sqrt{\hat{n}} e^{-i\hat{\theta}} \right\rangle \right] - \gamma \langle \hat{n} \rangle \right] dt \\ & + 2 \operatorname{Re} \left[\left(\langle \hat{\delta}_n \sqrt{\hat{n}} e^{-i\hat{\theta}} \rangle - \langle \sqrt{\hat{n}} e^{-i\hat{\theta}} \rangle \right) \sqrt{\gamma} dZ \right] \end{aligned} \quad (5.20)$$

is obtained.

In Figure 5.5 (a) the expected evolution of quadrature variable \hat{X} is shown. The right panels show the intra-sample variance Var_1 , inter-sample variance Var_2 and total variances for the evolution of a state that was originally coherent. We see here that the XP -Gaussian methods for both the photon-counting and the heterodyne unraveling strongly underestimate the phase diffusion, the description of which is worse for the photon-counting description.

Only in regimes where the importance of losses is much higher than the importance of dephasing can XP -Gaussian states provide a suitable description.

On the other hand, we see that the $N\Theta$ -methods are able to capture the phase diffusion on the level of the ensemble as well as TWA. This relative success of the $N\Theta$ -methods with respect to the XP -methods is somewhat reminiscent of a similar observation for number-phase phase-space methods of monitored quantum systems [161, 162]. What distinguishes the $N\Theta$ - Gaussian method from TWA however, is that the $N\Theta$ -Gaussian method is able to show the composition of the ensemble: it maintains information of individual trajectories, which is lost in TWA (we note that in practice under appropriate conditions, a single TWA sample may still be representative for some experimental realizations [101, 163]).

FULL EQUATIONS FOR $N\Theta$ -GAUSSIAN TRAJECTORIES

For the photon-counting unraveling, expectation values evolve as

$$\begin{aligned}
 \partial_t \langle \hat{n} \rangle &= -\gamma \langle \hat{\delta}_n \hat{\delta}_n \rangle + 2 \operatorname{Im} [FC_1] \\
 \partial_t \langle \hat{\delta}_n \hat{\delta}_n \rangle &= 4 \operatorname{Im} [FC_2] - 2 \operatorname{Im} [FC_1] \\
 \partial_t \langle \hat{\theta} \rangle &= \left(\Delta + \frac{U}{2} \right) - U \langle \hat{n} \rangle - \gamma \langle \hat{\delta}_n \hat{\delta}_\theta \rangle_{\text{sym}} - \operatorname{Re} [FC_3] \\
 \partial_t \langle \hat{\delta}_\theta \hat{\delta}_\theta \rangle &= -2U \langle \hat{\delta}_n \hat{\delta}_\theta \rangle_{\text{sym}} - 2 \operatorname{Re} [FC_4] + \frac{1}{2} \operatorname{Im} [FC_5] \\
 \partial_t \langle \hat{\delta}_n \hat{\delta}_\theta \rangle_{\text{sym}} &= -U \langle \hat{\delta}_n \hat{\delta}_n \rangle + 2 \operatorname{Im} [FC_6] - \operatorname{Re} [FC_7] \\
 \partial_t \langle \widetilde{1} \rangle &= -\gamma \langle \hat{n} \rangle \langle \widetilde{1} \rangle,
 \end{aligned} \tag{5.21}$$

where correlators C are given with an expansion in $\langle \hat{n} \rangle$ in Appendix B.

Jumps when $\langle \widetilde{1} \rangle = R$ are given by

$$\begin{aligned}
 \langle \hat{n} \rangle &\xrightarrow{J} \langle \hat{n} \rangle - 1 + \frac{\langle \hat{\delta}_n \hat{\delta}_n \rangle}{\langle \hat{n} \rangle} \\
 \langle \hat{\delta}_n \hat{\delta}_n \rangle &\xrightarrow{J} \langle \hat{\delta}_n \hat{\delta}_n \rangle \left(1 - \frac{\langle \hat{\delta}_n \hat{\delta}_n \rangle}{\langle \hat{n} \rangle^2} \right) \\
 \langle \hat{\theta} \rangle &\xrightarrow{J} \langle \hat{\theta} \rangle + \frac{\langle \hat{\delta}_n \hat{\delta}_\theta \rangle_{\text{sym}}}{\langle \hat{n} \rangle} \\
 \langle \hat{\delta}_\theta \hat{\delta}_\theta \rangle &\xrightarrow{J} \langle \hat{\delta}_\theta \hat{\delta}_\theta \rangle - \frac{\langle \hat{\delta}_n \hat{\delta}_\theta \rangle_{\text{sym}}^2}{\langle \hat{n} \rangle^2} + \frac{1}{4 \langle \hat{n} \rangle} \left\langle \frac{1}{\hat{n}} \right\rangle \approx \langle \hat{\delta}_\theta \hat{\delta}_\theta \rangle + \frac{1}{\langle \hat{n} \rangle^2} \left(\frac{1}{4} - \langle \hat{\delta}_n \hat{\delta}_\theta \rangle_{\text{sym}}^2 \right) + \frac{\langle \hat{\delta}_n \hat{\delta}_n \rangle}{4 \langle \hat{n} \rangle^4} \\
 \langle \hat{\delta}_n \hat{\delta}_\theta \rangle_{\text{sym}} &\xrightarrow{J} \langle \hat{\delta}_n \hat{\delta}_\theta \rangle_{\text{sym}} \left(1 - \frac{\langle \hat{\delta}_n \hat{\delta}_n \rangle}{\langle \hat{n} \rangle^2} \right).
 \end{aligned} \tag{5.22}$$

In the $F = 0$ case, evolution (5.21) can be solved exactly to

$$\begin{aligned}
 \langle \hat{n} \rangle(t) &= \langle \hat{n} \rangle(0) - \gamma \langle \hat{\delta}_n \hat{\delta}_n \rangle t & (5.23) \\
 \langle \hat{\delta}_n \hat{\delta}_n \rangle(t) &= \langle \hat{\delta}_n \hat{\delta}_n \rangle(0) \\
 \langle \hat{\theta} \rangle(t) &= \langle \hat{\theta} \rangle(0) + \left(\Delta + U \left(\frac{1}{2} - \langle \hat{n} \rangle(0) \right) - \gamma \langle \hat{\delta}_n \hat{\delta}_\theta \rangle_{\text{sym}}(0) \right) t + U \gamma \langle \hat{\delta}_n \hat{\delta}_n \rangle t^2 \\
 \langle \hat{\delta}_\theta \hat{\delta}_\theta \rangle(t) &= \langle \hat{\delta}_\theta \hat{\delta}_\theta \rangle(0) - 2U \langle \hat{\delta}_n \hat{\delta}_\theta \rangle_{\text{sym}}(0) t + U^2 \langle \hat{\delta}_n \hat{\delta}_n \rangle t^2 \\
 \langle \hat{\delta}_n \hat{\delta}_\theta \rangle_{\text{sym}}(t) &= \langle \hat{\delta}_n \hat{\delta}_\theta \rangle_{\text{sym}}(0) - U \langle \hat{\delta}_n \hat{\delta}_n \rangle t \\
 \langle \overline{1} \rangle(t) &= \exp \left(-\gamma \langle \hat{n} \rangle(0) t + \frac{\gamma^2}{2} \langle \hat{\delta}_n \hat{\delta}_n \rangle t^2 \right).
 \end{aligned}$$

By equating $\langle \overline{1} \rangle(t_j) = R$, we find the time to the next jump to be

$$t_j = \gamma^{-1} \frac{\langle \hat{n} \rangle(0)}{\langle \hat{\delta}_n \hat{\delta}_n \rangle} \left(1 - \sqrt{1 + \frac{2 \langle \hat{\delta}_n \hat{\delta}_n \rangle \ln(R)}{\langle \hat{n} \rangle(0)^2}} \right). \quad (5.24)$$

In the heterodyne unraveling, equations for the evolution are given by

$$\begin{aligned}
 d \langle \hat{n} \rangle &= [2 \operatorname{Im} [FC_1] - \gamma \langle \hat{n} \rangle] dt & (5.25) \\
 &\quad + 2 \operatorname{Re} [(C_2 - C_1) \sqrt{\gamma} dZ] \\
 d \langle \hat{\delta}_n \hat{\delta}_n \rangle &= \left[4 \operatorname{Im} [FC_2] - 2 \operatorname{Im} [FC_1] - 2\gamma \langle \hat{\delta}_n \hat{\delta}_n \rangle + \gamma \langle \hat{n} \rangle \right] dt \\
 &\quad - 2\gamma |C_2 - C_1|^2 dt \\
 &\quad + 2\sqrt{\gamma} \operatorname{Re} \left[D_3 - 2C_2 + C_1(1 - \langle \hat{\delta}_n \hat{\delta}_n \rangle) dZ \right] \\
 d \langle \hat{\theta} \rangle &= \left[\left(\Delta + \frac{U}{2} \right) - U \langle \hat{n} \rangle - \operatorname{Re} [FC_3] \right] dt \\
 &\quad + 2\sqrt{\gamma} \operatorname{Re} [C_6 dZ] \\
 d \langle \hat{\delta}_\theta \hat{\delta}_\theta \rangle &= \left[-2U \langle \hat{\delta}_n \hat{\delta}_\theta \rangle_{\text{sym}} - 2 \operatorname{Re} [FC_4] + \frac{1}{2} \operatorname{Im} [FC_5] + \frac{\gamma}{4} \langle \hat{n}^{-1} \rangle \right] dt \\
 &\quad - 2\gamma |C_6|^2 dt \\
 &\quad + 2\sqrt{\gamma} \operatorname{Re} \left[(D_1 - \langle \hat{\delta}_\theta \hat{\delta}_\theta \rangle C_1) dZ \right] \\
 d \langle \hat{\delta}_n \hat{\delta}_\theta \rangle_{\text{sym}} &= \left[-U \langle \hat{\delta}_n \hat{\delta}_n \rangle + 2 \operatorname{Im} [FC_6] - \operatorname{Re} [FC_7] - \gamma \langle \hat{\delta}_n \hat{\delta}_\theta \rangle_{\text{sym}} \right] dt
 \end{aligned}$$

$$\begin{aligned}
 & - 2\gamma \operatorname{Re} [(C_2 - C_1)C_6^*] dt \\
 & + 2\sqrt{\gamma} \operatorname{Re} \left[\left(-C_6 - (\langle \hat{\delta}_n \hat{\delta}_\theta \rangle_{\text{sym}} + \frac{i}{2})C_1 + D_2 \right) dZ \right].
 \end{aligned}$$

5.4 Numerical considerations

Because of the few simple update rules (five real variables-four if purity constraints are used), the computational cost for evolving a single variational trajectory is of the same order as the cost for a single TWA sample (two real variables) given the same set of parameters. For an exact trajectory $D = 2N_{\text{levels}}$ real variables must be evolved for the same single mode, where N_{levels} is the amount of occupation levels considered. If the dimension of configuration space d increases, the dimension of Hilbert space correspondingly grows as $D \propto e^d$, so that large simulations easily become limited by computational load. The dimension of the corresponding phase space on the other hand only grows $\propto d$, making it far more efficient for large systems. For our variational methods it is the amount of distinct Gaussian correlation functions that is the relevant quantity of complexity and this scales in principle as $\propto d^2$. In many large systems, only correlations between neighbouring sites are important and other ones can be neglected. If this is the case, scaling $\propto d$ is retrieved, as in Gutzwiller- or tensor-network ansatzes (see also section 3.3).

So far, we have only discussed the evolution of a single sample. As Gaussian trajectories, like exact trajectories, have a finite spread in Wigner phase-space, they contain more information than a TWA-sample which is just a point. Therefore, it can be expected that less samples are required to obtain an accurate description of the ensemble dynamics. We can estimate the difference in statistics as follows: take a trajectory method (exact or variational) of which N_{traj} independent trajectories are evolved. For the trajectory methods, the statistical uncertainty [164] is

$$\sigma_{\langle \hat{O} \rangle, \text{traj}}^2 = \frac{\operatorname{Var}_2(\hat{O})}{N_{\text{traj}}}, \quad (5.26)$$

whereas the analogous uncertainty for TWA is

$$\begin{aligned}
 \sigma_{\langle O \rangle_{\text{sym}}, \text{TWA}}^2 &= \frac{\operatorname{Var}_{\text{TWA}}(O_{\text{sym}})}{N_{\text{TWA}}} = \frac{\operatorname{Var}(\hat{O})}{N_{\text{TWA}}} \\
 &= \frac{\operatorname{Var}_1(\hat{O}) + \operatorname{Var}_2(\hat{O})}{N_{\text{TWA}}}.
 \end{aligned} \quad (5.27)$$

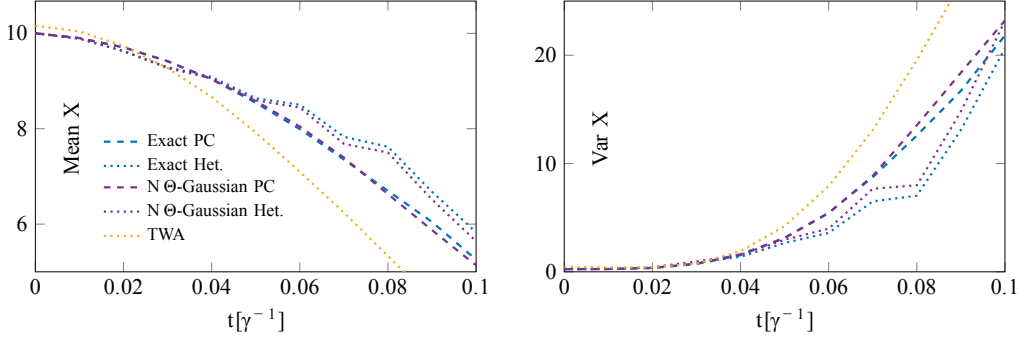


FIGURE 5.6: Same process as figure 5.5 simulated with ten samples of exact/variational trajectories as well as TWA. It is clear that trajectory methods are more tolerant for low statistics than TWA. Corresponding to criterion (5.28), we see that photon-counting is still more tolerant than heterodyne detection, corresponding with the fact that $\text{Var}_1(X) \gg \text{Var}_2(X)$ for this photon-counting unraveling, as opposed to heterodyne. Note that the initial state already has a deviation from the true value for TWA but not for the trajectory methods: criterion (5.28) for the needed ratio of samples diverges there.

The ratio of N_{traj} and N_{TWA} needed for the same precision can be found by equating (5.26) and (5.27) to be

$$\frac{N_{\text{TWA}}}{N_{\text{traj}}} = 1 + \frac{\text{Var}_1(\hat{O})}{\text{Var}_2(\hat{O})}. \quad (5.28)$$

In this sense, variational trajectories may even outperform TWA computationally. As an example, on figure 5.6 the same process as on figure 5.5 is simulated with only ten samples of the exact/variational trajectories and ten samples of TWA. It is clear that TWA provides a bad estimate with such a low number of samples. The performance of trajectory methods with regard to the minimal amount of samples, though observable- and unraveling-dependent, is better. The amount of improvement depends on \hat{O} and the unraveling: as seen from Eq. (5.28), the photon counting unraveling performs best because $\text{Var}_1(X) \gg \text{Var}_2(X)$ as can be appreciated from figure 5.5.

When it is a phase-space distribution itself in which one is interested, it can again be challenging to compute it from an exact density matrix or wavefunction, when the particle number is not low [165]. If a state is Gaussian, particularly in the XP -sense, distributions for individual samples are given by straightforward Gaussian formulas [9] that can be added up for the distribution of the whole

ensemble. The TWA method is by construction surely also very well suited to plot the Wigner-quasi-probability function, but binning as a histogram is necessary there, meaning that again a much larger amount of samples is required for a result of high resolution (this is highly relevant if one is interested in the parity-operator $\Pi = e^{i\pi \hat{a}^\dagger \hat{a}}$ or its displaced versions, for which the phase-space representation is a δ -function [146]).

As a final note, all simulations discussed have been performed by trajectories representing pure states. It is also possible to work with trajectories using mixed states, either corresponding to initial classical uncertainty or to imperfect measurements [6]. The exact solution of these would require a density matrix, undoing the computational advantage of the stochastic simulation method. For the variational trajectories, the only difference between evolving pure or mixed states is whether the same purity-constraints are valid or not. Evolving mixed states increases $\text{Var}_1(\hat{O})$ with respect to $\text{Var}_2(\hat{O})$ so that less statistics are required according to (5.28), at the expense of resolution of the individual trajectories. This would come down to a crossover from pure trajectories to a description on the level of the master equation. Whether such a description is accurate will depend on the system dynamics. For the example of the bistability, if there is not sufficient information on the branch that the system is in, the Gaussian approximation will fail to accurately describe the state, that evolves toward a mixture of the system in the lower and upper branch.

5.5 Discussion and summary

We have shown how Gaussian variational quantum trajectory methods can provide a computationally efficient description of open quantum systems. We have explicitly derived the dynamics for both XP - and $N\Theta$ - Gaussian states, and applied them as an example to a driven-dissipative cavity. XP -Gaussian states are always well-defined, though they may be too rigid to describe states with much phase-diffusion. $N\Theta$ -states on the other hand, exist only by approximation, but often provide a very good description for the true state as long as the density is sufficiently high. Computationally, the cost of a Gaussian trajectory scales similar to TWA, but typically less samples are needed. XP -Gaussian methods, like TWA, are limited to the semiclassical regime where the Wigner function is always positive. $N\Theta$ -Gaussian methods on the other hand can describe the interference patterns similar to Fock-states. As these variational methods, unlike TWA, ensure that the state

remains physically well-defined, we expect them to keep predicting accurate results to a broader class of problems such as coupled cavities. As we have shown, accuracy can be strongly improved by proper choice of the ansatz. Also similar ansatzes, that can for example be Gaussian in other variables [166], may be suitable dependent on the problem. As for exact trajectories, the choice of unraveling greatly determines the amount of samples needed for a proper description. In addition, we have seen that this choice of unraveling can also influence the accuracy of the variational method. In general, terms in the Hamiltonian that are linear and bilinear in the Gaussian variables, are known to correspond with ‘Gaussian operations’, and should be tracked exactly with the Gaussian trajectories. The same holds for linear measurement operators (‘Gaussian measurements’) that include homodyne and heterodyne detection schemes, but not photon counting. This partly explains why the former unravelings work better overall within the XP -Gaussian ansatz. Furthermore, the role of the unraveling is that it translates quantum fluctuations, that may be subject to non-Gaussian deviations, to classical fluctuations that are less restricted. Ideally, the measurement scheme is thus able to measure all relevant degrees of freedom before their quantum uncertainty becomes too large. Again, heterodyne detection has the advantage in this regard that it localizes the state in phase space without preferential direction. As we have seen, accuracy can be described on two levels: either regarding the average behaviour (ensemble expectation values, ‘weak correspondence’) or for the single-shot (e.g. Figure 5.1 ‘strong correspondence’). The criteria for both are similar, although more stringent in the latter case, which is also more vulnerable to accumulation of deviations over time.

In the following parts, we will now study more advanced set-ups with the XP -Gaussian method and the $N\Theta$ -Gaussian method.

PART

II

KERR LATTICES WITH QUADRATIC
DRIVING: AN APPLICATION OF THE
XP-GAUSSIAN METHOD

W. Verstraelen, R. Rota, V. Savona, and M. Wouters, “Gaussian trajectory approach to dissipative phase transitions: the case of quadratically driven photonic lattices”, *Phys. Rev. Research (Rapid communication)* **2**, 022037 (R) (2020).

W. Verstraelen and M. Wouters, “Classical critical dynamics in quadratically driven kerr resonators”, *Phys. Rev. A* **101**, 043826 (2020).

Driven-dissipative phase transition in Kerr lattices with two-photon driving

In addition to thermal phase transitions in classical systems and quantum phase transitions in closed quantum systems, open quantum systems have the notion of dissipative phase transitions. Driven-dissipative Kerr resonators are experimentally relevant systems, useful to access this physics.

6.1 Dissipative phase transitions

6.1.1 INTRODUCTION: PHASES OF MATTER

Even though an extensive amount of physical research is devoted to microscopic models of matter, it are oftentimes a few accessible macroscopic observables that are truly of interest (‘Is it a solid or a liquid?’, ‘What are the magnetic properties?’, ‘Does it superconduct?’...). The latter questions all enquire on the macroscopic *phase* of a substance. Upon tuning of a system parameter (the *control parameter*) g across a certain *criticality* g_c , the macroscopic properties can exhibit a dramatic (non-analytic) change: a *phase transition* occurs. One such macroscopic property σ is taken as a witness of the phase transition: the *order parameter* which should satisfy $\sigma = 0$ for $g < g_c$ and $\sigma \neq 0$ for $g > g_c$ (this order parameter is an additional, extensive and experimentally accessible, variable that can appear in the thermodynamics because of symmetry reduction). The way this occurs defines the *order* of the phase transition: a case where $\sigma(g)$ is discontinuous is for example a first-order transition (e.g. melting and freezing), whereas a continuous but not continuously differentiable $\sigma(g)$ is a second-order phase transition (e.g.

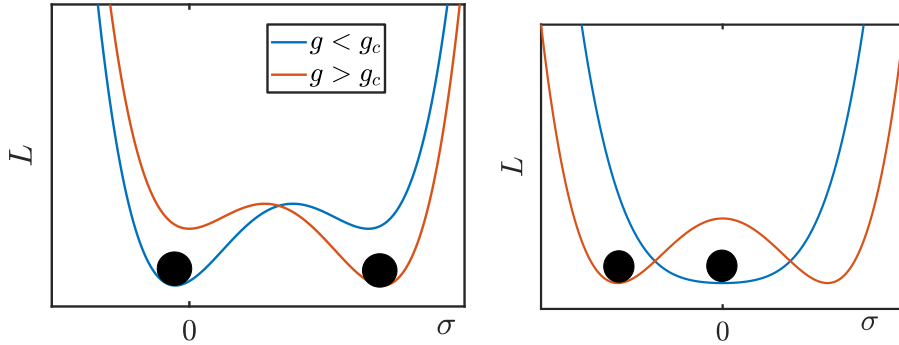


FIGURE 6.1: Examples of a Landau free energy on two different sides of the criticality. The black ball, denoting the system, takes a configuration where L is minimal. Left, a 1st order phase transition (for example: freezing of water to ice): the continuous deformation from the blue curve to the red curve, changes which of two existing local minima is lower, leading to a discrete jump in σ . Right, a second-order phase transition (for example cooling a magnet below the Curie temperature): the unique local minimum splits into two that gradually move away, thus σ changes continuously. The system also displays spontaneous symmetry-breaking: the system randomly chooses one of the two minima in the $g > g_c$ phase.

magnetism across the Curie temperature)¹. A convenient phenomenological picture to understand these phase transitions, is given by the Landau free energy $L_g(\sigma)$, or L for brevity (Figure 6.1). It acts as an effective potential parametrized by g , of which the system seeks the minimum, reflected in the value of σ . Because phases themselves are macroscopically extended over the system, it is easy to grasp that phase transitions can be long-wavelength phenomena. This is especially the case for second-order transitions, where large fluctuations can occur because there is no barrier in L to overcome. This makes second-order transitions very interesting, so we will focus on these. On a more technical level, the *correlation length* ξ diverges at g_c , leading to *scale invariance* in the renormalization group [99]. Close to the criticality, $g - g_c$, ξ and σ are all related to each other by a power-law, e.g. $\xi \sim |g - g_c|^{-\nu}$ and $\sigma \sim |g - g_c|^\beta$. *Critical exponents* as ν and β define a *universality class*: systems with the same dimensionality and symmetries will be in the same class and have the same values for the exponents, regardless of microscopic details.

¹Another category are infinite-order phase transitions such as the BKT (Berezinskii-Kosterlitz-Thouless) transition that occurs in certain rotor models, of topological nature [167].

6.1.2 FROM CLASSICAL AND QUANTUM PHASE TRANSITIONS TO DISSIPATIVE PHASE TRANSITIONS

Let us now make this discussion a bit more concrete. Phase transitions exist in many different flavours and it is convenient to interpret these as relating to the origin of L . First, there are classical phase transitions. The configuration of equilibrium thermodynamic systems, at finite temperature T , is the minimum of their (Helmholtz) free energy $\mathcal{F} = E - TS$, where E is the energy (favouring an ordered configuration) and S the entropy (favouring disorder). Whether E or S dominates \mathcal{F} thus crucially depends on the temperature T , which is therefore a convenient control parameter [99]. Secondly, even at $T \equiv 0$, where the system is always in the ground state, different phases may occur because of competing terms in the Hamiltonian which now takes the role of L (specifically $\text{tr}[\hat{\rho} \hat{H}]$ is minimized). In order for this competition to take place, such terms must be necessarily non-commuting and hence the quantum nature of the system is important. By perturbing such quantum phase transitions with a small finite temperature, one either obtains, depending on the system, that the transition vanishes or is continuously connected to a classical phase transition. Close to the quantum critical point, a *quantum critical region* occurs, where, regardless of whether a true phase transition still takes place, long-range quantum correlations are significant [167].

A third flavour of phase transition can be added to this list. As we have seen in the previous part, systems interacting with a Markovian environment decay to a (non-equilibrium) steady state instead as we know from Spohn's theorem, and this steady state is the lowest eigenvector of the Liouvillian. Similar to the other kinds of phase transitions above, different terms in the Liouvillian $\hat{\mathcal{L}}$ compete. The steady state solution satisfies $\hat{\mathcal{L}}\hat{\rho} = 0$, implying it minimizes $\|\hat{\mathcal{L}}\hat{\rho}\|$ (for any properly defined operator norm $\|\cdot\|$) which therefore takes the role of L here. The phase transitions that occur here from the competition between different coherent and dissipative processes are *dissipative phase transitions*.

6.1.3 STATE-OF-THE-ART ON DISSIPATIVE PHASE TRANSITIONS

Because phase transitions are defined in the thermodynamic limit (infinitely large system) for which the driven-dissipative experimental context is relatively recent, the explicit study of dissipative phase transitions is rather young. The non-trivial interplay between the Hamiltonian evolution, driving and dissipative processes in

open quantum many-body systems has given rise to several fundamental questions about the respective roles of quantum and classical fluctuations across a dissipative phase transition [168–170]. Some early experimental observations are lasing and the BEC transition of exciton-polaritons in a microcavity. In the last years, the possibility of realizing strongly correlated states in photonic cavity arrays [57, 171, 172] has stimulated a deeper investigation of driven-dissipative phase transitions, which have been discussed theoretically in photonic systems [78, 106, 159, 173–183], lossy polariton condensates [119, 184, 185] and spin models [186–194]. From the experimental point of view, remarkable results have been recently obtained with driven circuit quantum electrodynamics systems [195] and semiconductor microcavities [196, 197], showing the possibility to observe dissipative phase transitions in real open quantum many-body systems. These more explicit studies tend to follow two different directions. The first one is the search for exotic non-equilibrium phenomena. A first example by Diehl et al. [80] considers for example a Bose-Hubbard lattice consisting of atoms in an optical trap, where a particularly engineered Lindblad operator favours order. A few other examples are Ref. [198] finding an experimental platform to study percolation theory and Ref [199] predicting the emergence of an oscillating order parameter.

The second direction aims at understanding the fate of quantum phase transitions in the presence of more common noise mechanisms and how this compares to thermal fluctuations. Mitra et al. [200] derive for example that at least certain magnets subject to a dissipative current exhibit a thermal-like criticality to first order. On the other hand, Dalla Torre et al. [201, 202] argue that the very common $1/f$ noise, unlike thermal fluctuations, is only marginal in a Josephson junction circuit and ions in a 1D optical lattice: it does not affect the universality class. In follow-up work [203], the same authors nuance their claim. Higher-order contributions of a non-linear coupling do lead to some thermal behaviour and in [46] they note that driven-dissipative systems may display effective temperatures in particular at low frequencies, but without thermal equilibrium between the different components. Also ref. [191] shows that a transition in dissipative spin-lattices displays signatures of both quantum (such as entanglement) as classical (entropy) critical behaviour. Some other results pointing in the direction of equilibrium behaviour were obtained regarding the phase of free exciton-polariton condensates [106, 119, 204, 205], spin models [190] and the Dicke model [206–208]. Recent work also shows the occurrence of thermalization from non-markovian noise [209]. On the other hand, the authors of Refs. [119, 184, 210–212] find that, among others,

the BEC transitions in driven-dissipative systems (e.g. polaritons) belong to a non-equilibrium universality class instead. According to Ref. [117], equilibrium corresponds to a strongly attractive fixed point in terms of the renormalization group here (meaning that long-wavelength phenomena tend towards it), but it is not the whole story as dynamical responses retain a difference. Many 2D-systems are not attracted to the equilibrium fixed point under renormalization, but rather to the non-equilibrium KPZ (Kardar-Parisi-Zhang) universality class, even at weak noise levels [117, 213, 214]. In Ref. [215], the authors further show, with the example of a polariton condensate, that tuning of the coherent drive can move the system to different universality classes. Finally, a different nonequilibrium class was recently found that relates to exceptional points: bifurcations in the Liouvillian spectrum [216].

As we have noted, correlation length ξ diverges at criticalities. Likewise, also the correlation time τ diverges (a phenomenon known as *critical slowing-down*). In the case of quantum phase transitions, this slowing down corresponds directly to a *closing of the (Hamiltonian) gap* [167]. For a proper characterization of dissipative phase transitions, it is of course desirable that similarly, the *Liouvillian gap* should close [169].

6.1.4 STRUCTURE OF PART II

This part of the thesis is structured as follows. The remainder of this chapter is devoted to introducing the system of consideration. In chapter 7 we describe the application of the Gaussian Trajectory method to this system, and also derive truncated Wigner equations for comparison. Chapter 8 focusses on the static properties of the transition (spatial correlations). In chapter 9 we then turn towards the dynamical properties and the Liouvillian gap, where we show that also the *way* in which it closes bears a deep similarity with Hamiltonian quantum phase transitions.

6.2 Quadratically-driven Kerr resonators

In this debate on the role of dissipation to universality, arrays of nonlinear photonic resonators in presence of two-photon – i.e., quadratic in the field – driving have recently attracted a certain attention, as these systems undergo a dissipative phase transition which belongs to a quantum universality class in a suitable regime of parameters [182].

6.2.1 SINGLE CAVITY

Before turning to lattices of two-photon driven Kerr lattices, let us first discuss the single site problem. The system is very similar to the ordinary (single-photon driven) Kerr cavity studied in chapter 5, except for the driving term. Explicitly, the Hamiltonian of such a system is given by

$$\hat{h} = -\Delta \hat{a}^\dagger \hat{a} + \frac{U}{2} \hat{a}^{\dagger 2} \hat{a}^2 + \frac{G}{2} \hat{a}^{\dagger 2} + \frac{G^*}{2} \hat{a}^2, \quad (6.1)$$

where Δ is the detuning between half of the two-photon driving field frequency and the resonant cavity frequency, U is the photon-photon interaction energy associated to the Kerr nonlinearity and G is the two-photon driving field amplitude. Whereas a single-photon pump completely lifts the $\mathcal{U}(1)$ phase symmetry, two-photon driving leaves a \mathbb{Z}_2 symmetry, because it only fixes the *square* of the phase. In addition to the Lindblad operator $\sqrt{\gamma} \hat{a}$, one may generally expect also incoherent two-photon losses to take place as described by the jump operator $\sqrt{\eta} \hat{a}^2$. Both dissipation mechanisms are consistent with the mentioned symmetry. This system has been thoroughly investigated and exact solutions for the steady state are known both without [217] and with an additional single-photon pump [78], even in the presence of feedback mechanisms. We will restrict ourselves to the case without single-photon driving here, as we are seeking the occurrence of spontaneous symmetry breaking.

In the limit $\gamma = \Delta = 0$ (i.e. no single-photon processes), the steady states of this system form a manifold² spanned by the ‘even and odd Schrödinger-cat’ states

$$|C_\alpha^\pm\rangle = \frac{|\alpha\rangle \pm |-\alpha\rangle}{\sqrt{2(1 \pm e^{-2|\alpha|^2})}}, \quad (6.2)$$

where $|\alpha\rangle, |-\alpha\rangle$ is a set of coherent states with opposite displacement [218, 219]. The name of $|C_\alpha^\pm\rangle$ name stems from the fact that they are not only eigenvectors from \hat{a}^2 with eigenvalue α^2 , but also from the *Parity operator*

$$\hat{\Pi} = e^{i\pi \hat{a}^\dagger \hat{a}} \quad (6.3)$$

with eigenvalues ± 1 , meaning that the cat states have deterministically either an even or odd photon number.

²This is possible because the two-photon processes don’t mix the even and odd solutions, hence the criteria of Spohn’s theorem are unsatisfied.

For $\alpha \gg 0$, the coherent states

$$|\pm\alpha\rangle \langle\pm\alpha| \approx |C_\alpha^+\rangle \langle C_\alpha^+| \pm |C_\alpha^-\rangle \langle C_\alpha^-| \quad (6.4)$$

are, to a good approximation, also steady states.

In mean-field approximation, the values of $\alpha = |\alpha|e^{i\phi}$ are given by [182]

$$|\alpha|^2 = \frac{|G|}{\sqrt{U^2 + \eta^2}} \quad (6.5)$$

$$\phi = \frac{i}{2} \ln \frac{i\eta - U}{\sqrt{U^2 + \eta^2}} + \frac{\theta_G}{2}, \quad (6.6)$$

where $G = |G|e^{i\theta_G}$. In the following, we will assume G to be positive and real.

Even the presence of moderate single-photon losses does not change this picture too much in the sense that the coherent states remain metastable [217]³. The Schrödinger cat states, by contrast, are rapidly destroyed since $\hat{a}|C_\alpha^\pm\rangle = |C_\alpha^\mp\rangle$. The difference between these two decompositions becomes manifest when studying the quantum trajectories with different unraveling schemes [220].

This single site problem, in fact, does allow for defining a thermodynamic limit, by setting $U = \bar{U}/N$ and $\eta = \bar{\eta}/N$ and considering the limit $N \rightarrow \infty$. N here corresponds to the mean-field photon number (6.5). For suitable values of Δ and γ , the derivative of $\chi = \langle \hat{a}^\dagger \hat{a} \rangle / N$ diverges and the Liouvillian gap closes, marking a ‘second-order phase transition’ [78, 169]. However, this thermodynamic limit of high particle number is the rather trivial mean-field limit, where spatial correlations cannot be studied.

6.2.2 ARRAYS

Now that we understand the physics of a single Kerr cavity with two photon driving, we turn towards lattices of these. A lattice of N coupled bosonic modes is described by a Bose-Hubbard model, whose Hamiltonian contains a local term \hat{h}_i acting on the i -th cavity, and a non-local term modelling the photon hopping between different cavities:

$$\hat{H} = \sum_{i=1}^N \hat{h}_i - \sum_{\langle ij \rangle} \frac{J}{z} (\hat{a}^\dagger_i \hat{a}_j + \hat{a}^\dagger_j \hat{a}_i). \quad (6.7)$$

³this is actually generic behaviour for coherent states, as they are ‘pointer states’ for photon losses [8].

Here, \hat{a}_i (\hat{a}_i^\dagger) is the annihilation (creation) operator acting on the i -th site⁴ and the last sum runs over the nearest-neighbor pairs $\langle ij \rangle$, J and z being, respectively, the hopping strength and the coordination number (number of neighbouring sites). Assuming all losses to be local, the jump operators are of the form $\{\sqrt{\gamma} \hat{a}_i\}$, $\{\sqrt{\eta} \hat{a}_i^2\}$, so that the dynamics of $\hat{\rho}(t)$ is described by a Liouvillian $\hat{\mathcal{L}}$ of the Lindblad form (2.20). As in the single-site case, \mathcal{L} presents a \mathbb{Z}_2 symmetry coming from its invariance under a global change of sign of the annihilation operators, $\hat{a}_i \rightarrow -\hat{a}_i \forall i$. Now, a different thermodynamic limit to the one of subsection 6.2.1 can be taken, where parameters (and hence the photon number per cavity) retain their finite value, while instead the limit of an infinitely large lattice is taken.

In this limit of an infinite lattice, the \mathbb{Z}_2 symmetry can be spontaneously broken for large values of G/γ and J/γ , as indicated by a Gutzwiller mean-field master equation (subsection 3.3.3) analysis [181]. This leads to the emergence of a transition between a phase with a \mathbb{Z}_2 -symmetric steady state (i.e. $\text{Tr}(\hat{\rho}_{SS} \sum_i \hat{a}_i) = 0$) and a coherent phase with non-zero expectation value of the Bose field (i.e. $\text{Tr}(\hat{\rho}_{SS} \sum_i \hat{a}_i) \neq 0$).

The nature of the dissipative phase transition can be investigated in terms of an approximate spin model, where two Schrödinger-cat states with opposite parity play the role of the two $s = 1/2$ -spin states with opposite magnetization [182]. When projecting the bosonic Hamiltonian in Eq. (6.7) onto the basis spanned by the Schrödinger-cat states, we recover the Hamiltonian of a quantum transverse XY model, where the photon hopping term plays the role of an anisotropic spin coupling in the xy plane (the coupling can be either ferromagnetic [182] or antiferromagnetic [221], according to the sign of J) and the detuning Δ plays the role of a transverse magnetic field in the z -direction. This model is known to present a phase transition belonging to the universality class of the quantum transverse Ising model [222]. Indeed, also the dissipative phase transition in a quadratically-driven Kerr lattice has numerically shown to belong to this same universality class in the limit where γ is much smaller than the Hamiltonian parameters: a regime where the properties of the dissipative phase transition are very reminiscent to its closed-system quantum phase transition counterpart⁵. In recent work [221], the simulation of frustrated antiferromagnetism is proposed by using $J < 0$.

⁴Explicitly, $\hat{a}_i = 1 \otimes \dots \otimes 1 \otimes \hat{a} \otimes 1 \otimes \dots \otimes 1$, with \hat{a} as the i th factor in the tensor product.

⁵In fact, even phase transitions in a ‘closed system’ need an infinitesimal amount of decoherence for macroscopic symmetry-breaking to occur [223].

6.2.3 FURTHER STATE-OF-THE-ART IN TWO-PHOTON-DRIVEN SYSTEMS

Although full lattices of quadratically driven resonators have not yet been created, the basic ingredients have been realized with superconducting circuits: coupling a circuit with an auxiliary, 'readout' mode with twice the system frequency, and tracing it out results in an effective two-photon drive in the circuit [224]. The possibility of quantum correlations between sites, is shown by production of mode-entangled $(|\alpha\rangle_A |\alpha\rangle_B \pm |-\alpha\rangle_A |-\alpha\rangle_B)/\sqrt{2}$ states in a dimer, where A,B mark the two circuits [225].

Several works have considered the possibility of exploiting the \mathbb{Z}_2 symmetry of this system in order to simulate the behaviour of quantum spin systems for technological purposes as annealing (finding the ground state of the Hamiltonian of a spin problem by adiabatically lower temperature or an equivalent with quantum fluctuations) [226–229] or as a platform for noise-resilient quantum code [224].

Going beyond two-photon driving, the study of n -photon driving [169] is currently an ongoing field of research.

6.3 Annealing and spin models

As noted, one of the first proposed application for these quadratically-driven systems was not the physics of dissipative phase transitions but annealing. It is therefore worthwhile to explain this concept a bit deeper, setting also the broader context of our work.

Many complex-optimization problems (travelling salesman, graph colouring finding a Nash equilibrium, finding the optimal protein threading figure, finding the best matching DNA sequence...) cannot be solved on a classical computer within polynomial time and are thus considered *NP-hard* [230, 231]⁶. Being able to solve one of these *NP-hard* problems would allow for solving all of them with only polynomial overhead.

Interestingly, one kind of such optimization problems with physical relevance occurs in finding the ground state of a spin-glass model [232]: the simplest case is an arbitrary lattice of classical Ising spins (2-level systems) with irregular interactions J_{ij} that can both be positive and negative between the sites. Finding the ground

⁶On a more technical level, *NP-hard* means 'at least as hard as the hardest *NP*-problems', where *NP*-problems are the ones of which a solution can be *verified* within polynomial time (as opposed to *P*-problems, which can be deterministically solved in polynomial time) [231]. It is widely believed that $P \neq NP$ although the formal proof is still one of the most important open problems in mathematics [230].

state of such spin glasses experimentally is thus very helpful in solving a variety of complex optimization problems. However, trying to achieve this by quenching the temperature to $T = 0$ instantly will typically trap the system in a metastable state. Instead, one wants to have just enough fluctuations to ensure that the system is able to end up in the true ground state (at least most of the time if the procedure is repeated). This leads to protocols of gently cooling down the system (using the adiabatic theorem), known as *annealing*. The Ising model can also be upgraded to a quantum version, where fluctuations arise from a non-commuting term instead of temperature [233]. Remarkably, such quantum correlations are not necessary for the system to be suitable for annealing. ‘Classical’ spin models also work as long as the spin itself can only take discrete values (otherwise finding the ground state would only be an algebraic problem) [234].

As an experimental platform to implement such a spin lattice, two-level systems with good controllability are sought. A few other proposals that achieve this using photons include degenerate parametric oscillators ([235–237]) and optical bistability [238, 239]. In quadratically driven Kerr resonators at least, the latest evidence does show an additional speedup when using quantum correlations over classical ones. [240]).

Describing quadratically driven kerr lattices with Gaussian trajectories

The Gaussian Trajectory Approach is able to describe both high and low dissipation regimes in a quadratically driven Kerr lattice, and it displays the predicted quadratic scaling. On the other hand, corner-space renormalization is only able to access the low dissipation regime whereas the TWA method fails to describe an ordered phase even in the semiclassical, high dissipation, regime.

7.1 Accessing the high-loss regime with the GTA method

As discussed in chapter 6, the system under consideration is described by a master equation

$$\frac{\partial \hat{\rho}}{\partial t} = \mathcal{L}\hat{\rho}, = -i[\hat{H}, \hat{\rho}] + \sum_{j,k} \hat{\Gamma}_{j,k} \hat{\rho} \hat{\Gamma}_{j,k}^\dagger - \frac{1}{2} \left\{ \hat{\Gamma}_{j,k}^\dagger \hat{\Gamma}_{j,k}, \hat{\rho} \right\}, \quad (7.1)$$

where \hat{H} is given by (6.7), $\Gamma_{1,k} = \sqrt{\gamma} \hat{a}_k$ and $\Gamma_{2,k} = \sqrt{\eta} \hat{a}_k^2$.

From a computational perspective, the numerical solution of master equation (7.1) becomes intractable even for small lattices. The corner-space renormalization method (subsection 3.3.3), has been used to study quadratically driven-dissipative lattices with large nonlinearities and small loss rates [182], but it fails in the description of regimes characterized by a large photon occupancy per cavity and a highly mixed steady state, which are the regimes we consider here.

As an alternative, we will therefore apply the Gaussian Trajectory Approach to this system. As described in chapter 5, two choices must be made.

First, the class of Gaussian states. Because we are dealing with coherent driving processes (and hence a limited Var_1 of the phase), potential occupations of order one or less, and a multimode system for which the amount of perturbative coefficients as in Appendix B would become large, we choose XP -Gaussian states over $N\Theta$ -Gaussian states. Secondly, the unraveling. We don't envision a particular experimental measurement configuration to mimic, so that the choice remains free. As we noted, the unraveling can be highly important to the success of the Gaussian ansatz though. In Ref. [220], it was shown that the trajectories in a single quadratically-driven Kerr cavity are close to coherent states $|\alpha\rangle, |-\alpha\rangle$ under homodyne unraveling, whereas photon-counting trajectories track the Schrödinger cat states $|\mathcal{C}_\alpha^\pm\rangle$ instead. The former kind of states are obviously better described by a Gaussian than the latter. In order not to introduce a preferential quadrature, we will work with the heterodyne unraveling, equivalent to two conjugate homodyne measurements (Appendix A). There is a more physical reason for this unraveling as well: the heterodyne unraveling measures conjugate variables with equal weights and as such, the way it localizes the state in phase space corresponds the most to a classical limit [241] (it is no coincidence that this unraveling is closely related to stochastic collapse models, as discussed in subsection 2.4.4). In particular, in the context of phase transitions this allows for individual trajectories to track the order parameters optimally [242].

We note that the \mathbb{Z}_2 symmetry of the Liouvillian must not be preserved in an individual quantum trajectory (it is a weak symmetry), but it is restored only after averaging many trajectories. Therefore, it is possible to obtain non-trivial results in the calculation of a suitable order parameter along an individual trajectory at long times. The study of the distribution of the latter expectation values over the whole set of sampled trajectories is helpful to understand the emergence of collective phases in different regimes of the physical parameters, and hence provides an important insight into the critical behavior in the thermodynamic limit [193].

7.2 Implementation and performance

Following the approach of chapter 5, the evolution of a generic expectation value $\langle \hat{O} \rangle$ under heterodyne unraveling for all decay channels is given by

$$d \langle \hat{O} \rangle = i \left\langle \left[\hat{H}, \hat{O} \right] \right\rangle dt - \frac{1}{2} \sum_{j,k} \left(\left\langle \left\{ \hat{\Gamma}_{j,k}^\dagger \hat{\Gamma}_{j,k}, \hat{O} \right\} \right\rangle - 2 \left\langle \hat{\Gamma}_{j,k}^\dagger \hat{O} \hat{\Gamma}_{j,k} \right\rangle \right) dt$$

$$+ \sum_{j,k} \left(\langle \hat{\Gamma}_{j,k}^\dagger (\hat{O} - \langle \hat{O} \rangle) \rangle dZ_{j,k} + \langle (\hat{O} - \langle \hat{O} \rangle) \hat{\Gamma}_{j,k} \rangle dZ_{j,k}^* \right), \quad (7.2)$$

where $dZ_i = \frac{1}{\sqrt{2}}(dW_{x,i} + i dW_{p,i})$ is a complex Wiener process satisfying $|dZ_i|^2 = dt$. By assuming a Gaussian ansatz, Wick decompositions are performed and the trajectory is expressed entirely in terms of the first and second central moments $\alpha_n = \langle \hat{a}_n \rangle$, $u_{nm} := \langle \hat{\delta}_n \hat{\delta}_m \rangle = \langle \hat{a}_n \hat{a}_m \rangle - \alpha_n \alpha_m$, $v_{nm} := \langle \hat{\delta}_n^\dagger \hat{\delta}_m \rangle = \langle \hat{a}_n^\dagger \hat{a}_m \rangle - \alpha_n^* \alpha_m$. Note that $u_{nm} = u_{mn}$ and $v_{nm} = v_{mn}^*$. Using (7.2), the evolution of Gaussian moments is given by

$$\begin{aligned} d\alpha_n = & \left[\left(-\frac{\gamma}{2} + i\Delta \right) \alpha_n + i \frac{J}{z} \sum_{n'} \alpha_{n'} - (\eta + Ui) (|\alpha_n|^2 \alpha_n + 2\alpha_n v_{nn} + \alpha_n^* u_{nn}) - iG \alpha_n^* \right] dt \\ & + \sqrt{\gamma} \sum_i \left(v_{in} dZ_i^{(1)} + u_{in} dZ_i^{(1)*} \right) \\ & + 2\sqrt{\eta} \sum_i \left(\alpha_i^* v_{in} dZ_i^{(2)} + \alpha_i u_{in} dZ_i^{(2)*} \right) \end{aligned} \quad (7.3)$$

$$\begin{aligned} du_{nm} = & \left[(-\gamma + 2i\Delta) u_{nm} + i \frac{J}{z} \left(\sum_{n'} u_{n'm} + \sum_{m'} u_{nm'} \right) - iG (v_{nm} + v_{mn} + \delta_{n,m}) \right. \\ & \left. - (\eta + Ui) \left(v_{nm} (\alpha_n^2 + u_{nn}) + v_{mn} (\alpha_m^2 + u_{mm}) + 2u_{nm} (|\alpha_n|^2 + |\alpha_m|^2 + v_{nn} + v_{mm}) \right) \right. \\ & \left. + \delta_{n,m} (\alpha_n \alpha_m + u_{nm}) \right] \\ & - \gamma \sum_i (u_{mi} v_{in} + u_{ni} v_{im}) \\ & - 4\eta \sum_i |\alpha_i|^2 (u_{mi} v_{in} + u_{ni} v_{im}) \Big] dt \\ & + 2\sqrt{\eta} \sum_i \left(v_{in} v_{im} dZ_i^{(2)} + u_{in} u_{im} dZ_i^{(2)*} \right) \end{aligned}$$

$$\begin{aligned} dv_{nm} = & \left[iU \left(2v_{nm} (|\alpha_n|^2 - |\alpha_m|^2 + v_{nn} - v_{mm}) + u_{nm} (\alpha_n^{*2} + u_{nn}^*) - u_{nm}^* (\alpha_m^2 + u_{mm}) \right) \right. \\ & \left. - \eta \left(2v_{nm} (|\alpha_n|^2 + |\alpha_m|^2 + v_{nn} + v_{mm}) + u_{nm} (\alpha_n^{*2} + u_{nn}^*) + u_{nm}^* (\alpha_m^2 + u_{mm}) \right) \right. \\ & \left. - i \frac{J}{z} \left(\sum_{n'} v_{n'm} - \sum_{m'} v_{nm'} \right) + iG (u_{nm} - u_{nm}^*) - \gamma v_{nm} \right. \\ & \left. - \gamma \sum_i (v_{ni} v_{im} + u_{ni}^* u_{im}) \right. \\ & \left. - 4\eta \sum_i |\alpha_i|^2 (v_{ni} v_{im} + u_{ni}^* u_{im}) \right] dt \end{aligned}$$

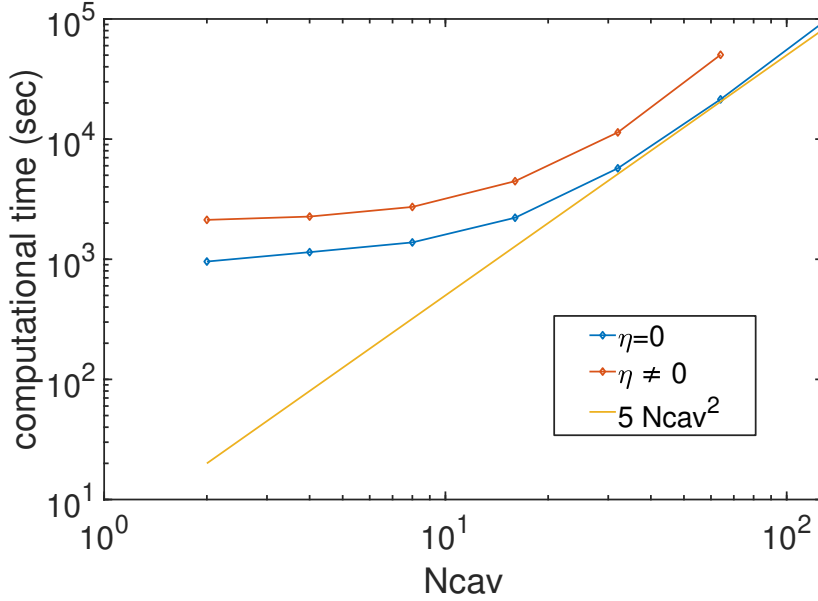


FIGURE 7.1: Computational time needed to recover 100 Gaussian trajectories on a desktop computer as function of system size. For every system size, the trajectories were evolved for $100 \gamma^{-1}$ with numerical (Euler-Mayurama, which coincides with the Milstein scheme at least in the $\eta = 0$ case (section C.2)) timestep $h = 10^{-4} \gamma^{-1}$. The results are consistent with quadratic scaling.

$$+ 2\sqrt{\eta} \sum_i \left(u_{ni}^* v_{mi}^* dZ_i^{(2)} + v_{ni} u_{im} dZ_i^{(2)*} \right),$$

where primed indices refer to nearest-neighbours only. Recalling that the stochasticity of the heterodyne unraveling is fully contained in the Wiener noise terms, equations (7.3) form a complete description of the time-evolution and no further jumps are required. In Fig. 7.1, we benchmark the numerical performance of the method as function of system size. The scaling of required resources tends to quadratic, as predicted (section 5.4). We also observe that disregarding the two-photon loss ($\eta = 0$) results in a speedup of order two. Indeed, about half of the terms in (7.3) are proportional to η .

7.3 Is TWA a valid alternative?

In the semiclassical parameter regime, one may expect the Truncated Wigner Approximation (TWA) to be appropriate (subsection 3.3.6). The Standard TWA-equations [109, 110], taking in account only one-photon processes, are summarized

in [57]. Using the operator correspondences (subsection 4.2.1), we can generalize this approach to two-photon processes. For notational simplicity, we first consider a single mode and assume G to be real.

The two-photon pumping gives a contribution to the Master equation

$$\begin{aligned}
[\hat{H}_p, \hat{\rho}] &= \frac{G}{2} \left(\hat{a}^{\dagger 2} \hat{\rho} - \hat{\rho} \hat{a}^{\dagger 2} + \hat{a}^2 \hat{\rho} - \hat{\rho} \hat{a}^2 \right) \\
&\leftrightarrow \frac{G}{2} \left[\left(\alpha_w^* - \frac{1}{2} \frac{\partial}{\partial \alpha_w} \right)^2 - \left(\alpha_w^* + \frac{1}{2} \frac{\partial}{\partial \alpha_w} \right)^2 + \left(\alpha_w + \frac{1}{2} \frac{\partial}{\partial \alpha_w^*} \right)^2 - \left(\alpha_w - \frac{1}{2} \frac{\partial}{\partial \alpha_w^*} \right)^2 \right] W(\alpha_w, \alpha_w^*) \\
&= G \left(-\alpha_w^* \frac{\partial}{\partial \alpha_w} + \alpha_w \frac{\partial}{\partial \alpha_w^*} \right). \tag{7.4}
\end{aligned}$$

Using Feynman-Kac, this results in a deterministic contribution

$$d\alpha_w = \dots + iG\alpha_w^* dt \tag{7.5}$$

to the evolution of the Wigner field α_w .

The Lindblad terms become

$$\begin{aligned}
\hat{a} \hat{a} \hat{\rho} \hat{a}^\dagger \hat{a}^\dagger &\leftrightarrow \left(\alpha_w^2 + \alpha_w \frac{\partial}{\partial \alpha_w^*} + \frac{1}{4} \frac{\partial^2}{\partial \alpha_w^{*2}} \right) \left(\alpha_w^{*2} + \alpha_w^* \frac{\partial}{\partial \alpha_w} + \frac{1}{4} \frac{\partial^2}{\partial \alpha_w^2} \right) W \\
&= \left(\alpha_w^{*2} + \alpha_w^* \frac{\partial}{\partial \alpha_w} + \frac{1}{4} \frac{\partial^2}{\partial \alpha_w^2} \right) \left(\alpha_w^2 + \alpha_w \frac{\partial}{\partial \alpha_w^*} + \frac{1}{4} \frac{\partial^2}{\partial \alpha_w^{*2}} \right) W \\
\hat{\rho} \hat{a}^\dagger \hat{a}^\dagger \hat{a} \hat{a} &\leftrightarrow \left(\alpha_w^2 - \alpha_w \frac{\partial}{\partial \alpha_w^*} + \frac{1}{4} \frac{\partial^2}{\partial \alpha_w^{*2}} \right) \left(\alpha_w^{*2} + \alpha_w^* \frac{\partial}{\partial \alpha_w} + \frac{1}{4} \frac{\partial^2}{\partial \alpha_w^2} \right) W \\
&= \hat{a} \hat{a} \hat{\rho} \hat{a}^\dagger \hat{a}^\dagger - 2\alpha_w \frac{\partial}{\partial \alpha_w^*} \left(\alpha_w^{*2} + \alpha_w^* \frac{\partial}{\partial \alpha_w} + \frac{1}{4} \frac{\partial^2}{\partial \alpha_w^2} \right) W \\
\hat{a}^\dagger \hat{a}^\dagger \hat{a} \hat{a} \hat{\rho} &\leftrightarrow \left(\alpha_w^{*2} - \alpha_w^* \frac{\partial}{\partial \alpha_w} + \frac{1}{4} \frac{\partial^2}{\partial \alpha_w^2} \right) \left(\alpha_w^2 + \alpha_w \frac{\partial}{\partial \alpha_w^*} + \frac{1}{4} \frac{\partial^2}{\partial \alpha_w^{*2}} \right) W \\
&= \hat{a} \hat{a} \hat{\rho} \hat{a}^\dagger \hat{a}^\dagger - 2\alpha_w^* \frac{\partial}{\partial \alpha_w} \left(\alpha_w^2 + \alpha_w \frac{\partial}{\partial \alpha_w^*} + \frac{1}{4} \frac{\partial^2}{\partial \alpha_w^{*2}} \right) W. \tag{7.6}
\end{aligned}$$

The dissipator then becomes

$$\begin{aligned}
\hat{a} \hat{a} \hat{\rho} \hat{a}^\dagger \hat{a}^\dagger &- \frac{1}{2} (\hat{\rho} \hat{a}^\dagger \hat{a}^\dagger \hat{a} \hat{a} + \hat{a}^\dagger \hat{a}^\dagger \hat{a} \hat{a} \hat{\rho}) \\
&\leftrightarrow \left[\alpha_w \frac{\partial}{\partial \alpha_w^*} \left(\alpha_w^{*2} + \alpha_w^* \frac{\partial}{\partial \alpha_w} + \frac{1}{4} \frac{\partial^2}{\partial \alpha_w^2} \right) + \text{c.c.} \right] W(\alpha_w, \alpha_w^*). \tag{7.7}
\end{aligned}$$

By neglecting the third-order derivative (actually, these terms are exactly the same as those proportional to U , except that here there is a plus sign in between instead of a minus sign), we retain

$$\begin{aligned} & \left[(|\alpha|^2 + 1) \left(\alpha_w^* \frac{\partial}{\partial \alpha_w^*} + \alpha_w \frac{\partial}{\partial \alpha_w} \right) + 4|\alpha|^2 + 2|\alpha|^2 \frac{\partial^2}{\partial \alpha_w \partial \alpha_w^*} \right] W(\alpha_w, \alpha_w^*) \\ &= \frac{\partial}{\partial \alpha_w} [(|\alpha_w|^2 - 1) \alpha_w W(\alpha_w, \alpha_w^*)] + \frac{\partial}{\partial \alpha_w^*} [(|\alpha_w|^2 - 1) \alpha_w^* W(\alpha_w, \alpha_w^*)] \\ & \quad + \frac{1}{2} \frac{\partial^2}{\partial \alpha_w \partial \alpha_w^*} [4|\alpha_w|^2 W(\alpha_w, \alpha_w^*)]. \end{aligned} \quad (7.8)$$

For truncated wigner simulations, this corresponds to contributions¹

$$d\alpha_w = -\eta(|\alpha_w|^2 - 1)\alpha_w dt + \sqrt{2\eta}\alpha_w dZ^{(2)}. \quad (7.9)$$

Hence, including all parameters, The TWA equations are given by

$$\begin{aligned} d\alpha_w^{(n)} = & \left[\left(-\frac{\gamma}{2} + i\Delta \right) \alpha_w^{(n)} + i\frac{J}{z} \sum_{n'} \alpha_w^{(n')} - (\eta + Ui)(|\alpha_w^{(n)}|^2 - 1)\alpha_w^{(n)} - iF - iG\alpha_w^{(n)*} \right] dt + \\ & + \sqrt{\frac{\gamma}{2}} dZ_n^{(1)} + \sqrt{2\eta}\alpha_w^{(n)} dZ_n^{(2)}, \end{aligned} \quad (7.10)$$

where n' again runs over the nearest-neighbours of n .

In fact, both noise terms can be combined to a single

$$\sqrt{\frac{\gamma}{2} + 2\eta|\alpha_w|^2} dZ_n. \quad (7.11)$$

In Figure 7.2, we compare individual exact heterodyne trajectories, GTA trajectories and TWA samples for a single site. Even though the steady state properties seem similar for all three methods here, the TWA method dramatically overestimates the switching rate between branches. This leaves serious doubts as to whether this method will be able to describe phase transitions properly. At least one can expect that critical slowing down (closing of the gap) cannot be predicted correctly. In Figure 7.3, we compare some stationary expectation values obtained with both methods for a dimer of two coupled cavities. We see that local quantities are reasonably captured by both methods, overall slightly better by the GTA. However, the abundant fluctuations destroy the correlations between the

¹The phase of the diffusion coefficient is arbitrary.

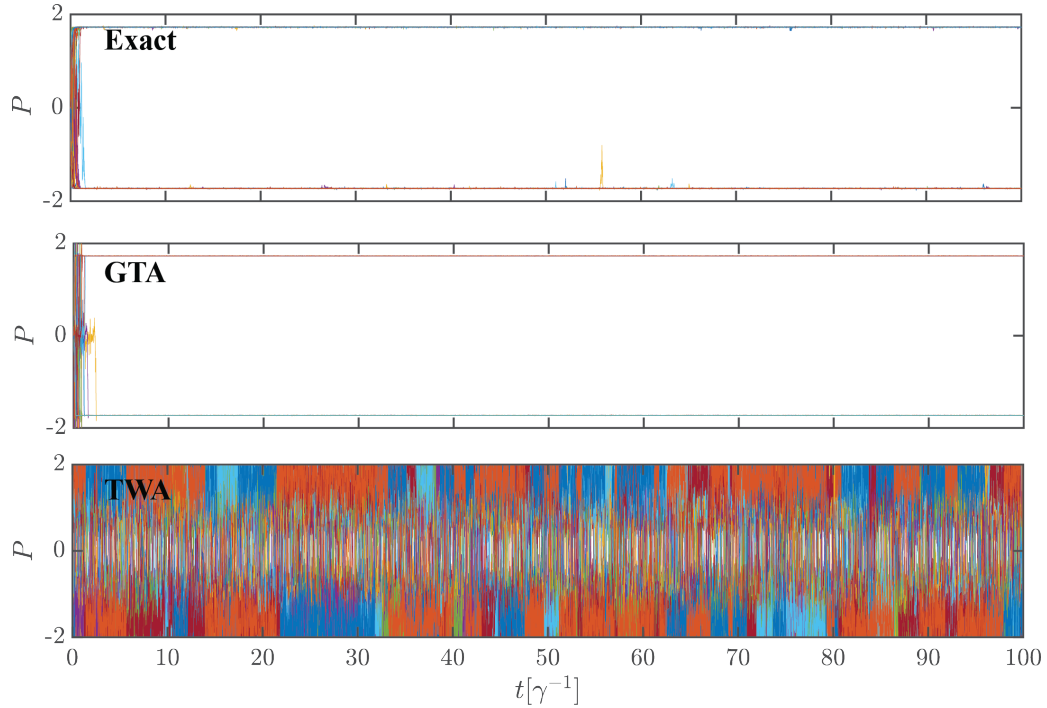


FIGURE 7.2: *Example time evolution in a single cavity through different methods, for parameters $G/\gamma = 50, U/\gamma = \eta/\gamma = 10, \Delta = 0$ (parameters also used in Ref. [220]). $P = \text{Im}[\alpha]$ is plotted for 100 trajectories each time. Both the exact heterodyne trajectories and their Gaussian (GTA) counterparts quickly stabilize in one of the two branches of $P \approx \pm 1.73$, without any switching on the combined timescale of the simulations. The TWA samples on the other hand, not only display the local quantum fluctuations around the branches, but also show a far more frequent switching between the branches.*

sites. As we will consequently see in subsection 8.2.1, the method is not able to predict an ordered phase.

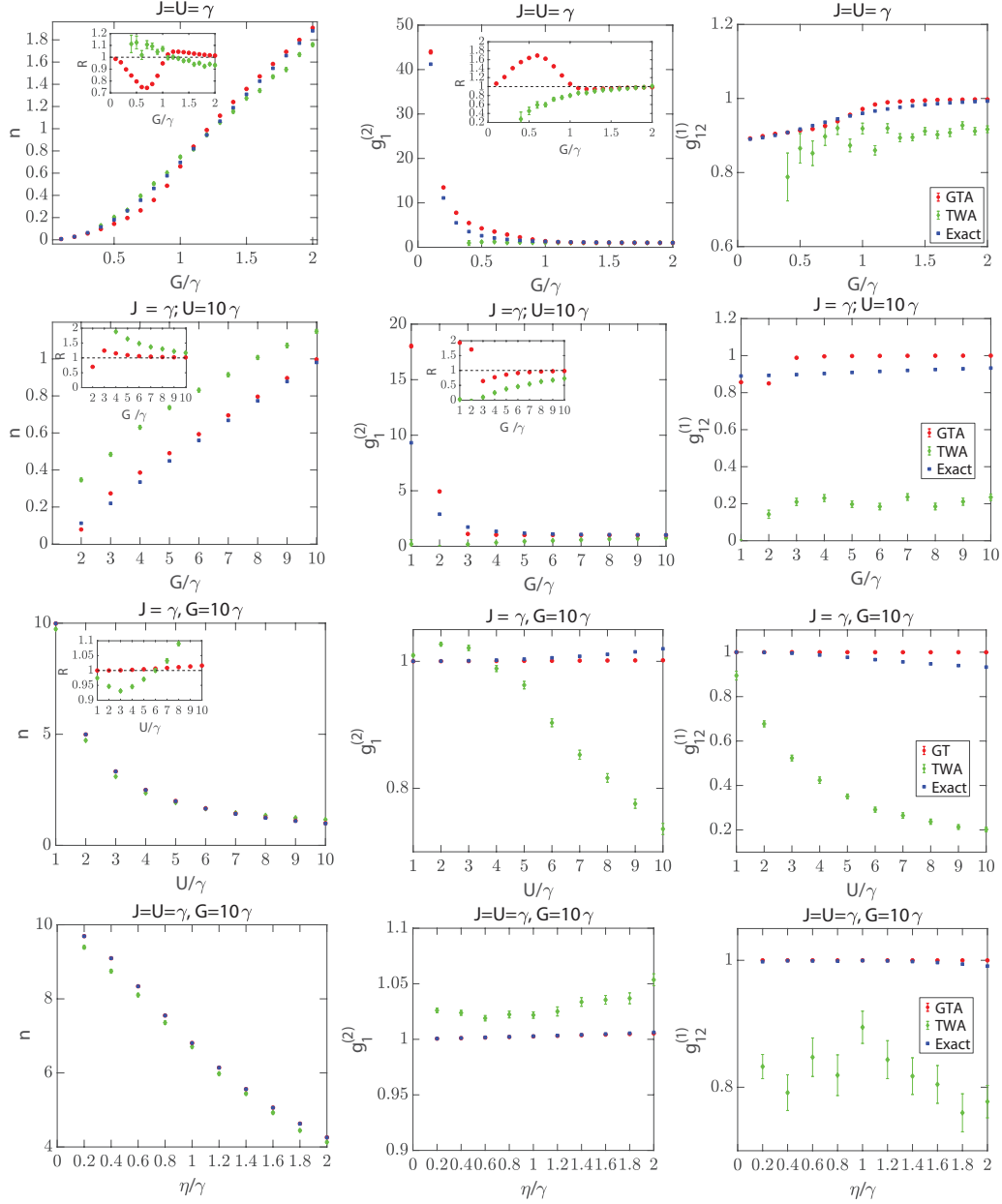


FIGURE 7.3: Benchmarking of the methods in a Bose-hubbard dimer for different parameter values. The left two panels display average photon number $n = \langle \hat{a}_1^\dagger \hat{a}_1 \rangle_\rho$ and second-order correlation function $g_1^{(2)} = \langle \hat{a}_1^\dagger \hat{a}_1^\dagger \hat{a}_1 \hat{a}_1 \rangle_\rho / n^2$ in site 1. The comparison between the methods in terms of accuracy slightly favours the GTA method, although the TWA often produces reasonable results as well. On the right panel, we see however from $g_{12}^{(1)} = \langle \hat{a}_1^\dagger \hat{a}_2 \rangle_\rho / n$ that the TWA is, unlike the GTA, unable to properly describe correlations between the two sites. Insets denote the values relative to the exact result. In all, simulations, $\Delta = -J$ to avoid bistable behaviour. For the upper three studies we have taken $\eta = 0$, in the bottom benchmark we see that the effect of two-photon losses can also be accurately described.

The critical behaviour of quadratically driven photonic lattices

Using the GTA, we reproduce the result that in the low-dissipation regime, the phase transition belongs to the quantum-Ising universality class. In the high dissipation result by contrast, we find that individual trajectories clearly break the symmetry with a transition that belongs to the classical-Ising universality class. The combination of both results provides strong evidence of dissipation acting as an effective temperature.

8.1 The GTA reproduces quantum critical behaviour in the low-loss limit

We apply the GTA formalism to the study of the quadratically-driven dissipative Bose-Hubbard model in 2D square lattices of different size, with periodic boundary conditions. In this section, we apply the GTA to the study the lattice of quadratically driven Kerr resonators in regimes where the one-photon losses is small with respect to the Hamiltonian and we benchmark it with the results obtained in Ref. [182] using corner-space renormalization. Foremost, we want to demonstrate that the GTA is not limited to the description of classically correlated states in open quantum systems, but can be applied also in the study of dissipative phase transitions with a quantum criticality: indeed, as noted in chapter 4, Gaussian states are able to feature multimode entanglement and as such are also used in quantum information. Additionally, we show that two-photon losses do not play a relevant role in the emergence of the dissipative phase transition, considering the critical behaviour of the system for $\eta = 0$.

In Figure 8.1, we show the results for the steady-state expectation value of the parity $\Pi = \langle \exp\{i\pi \hat{a}^\dagger \hat{a}\} \rangle$, as obtained with the GTA, for the following set of parameters: $U = 40\gamma, J = 20\gamma, \Delta = -20\gamma, \eta = 0$ (i.e. the same regime of parameter considered in Ref. [182], except for the value of the two-photon loss rate). The condition $\Delta = -J$ assures that the two-photon driving is resonant with the $k = 0$ mode of the single-particle energy band of the closed system, and is useful to avoid any bistable behaviour. The results show the emergence of a critical point at $G_c \simeq 1.2\gamma$, with the critical exponents of the quantum (transverse) Ising model. This quantum Ising model has Hamiltonian [167]

$$\hat{H}_{QI} = -J \sum_{\langle ij \rangle} \hat{\sigma}_i^{(x)} \hat{\sigma}_j^{(x)} + h \sum_i \hat{\sigma}_i^{(z)}, \quad (8.1)$$

where the matrices $\hat{\sigma}$ denote Pauli matrices: a lattice of spin-1/2 particles with ferromagnetic coupling in the x -direction and quantum fluctuations induced by coupling with an external magnetic field in the z -direction.

HOW DOES FINITE-SIZE SCALING WORK?

At phase transitions in infinite lattice systems, the correlation length ξ is known to diverge. Close to the critical point, ξ is still much larger than the lattice parameter a , which allows for efficient descriptions in terms of the renormalization group [99] where microscopic dynamics must not be taken into account (the *scaling hypothesis*). However, in finite systems, the system size L comes in as an additional length scale. A useful theory is still obtained if one assumes finite-size corrections as function of the dimensionless quantity ξ/L , as was first realized by Fisher and Barber [243].

For example, here we interpret Π as an ‘order parameter’ characterizing the disordered phase, somewhat analogous to M_z , the z -magnetization in the transverse Ising model (8.1). In an infinite system, one has close to the critical point $\Pi \sim |G - G_c|^\beta \sim \xi^{-\beta/\nu}$ (we have introduced these exponents in subsection 6.1.1, for a definition of all critical exponents, see for example ref. [99]). In a lattice of length L , there is a finite size correction described by

$$\Pi = \xi^{-\beta/\nu} \tilde{f}(\xi/L), \quad (8.2)$$

where \tilde{f} is a *scaling function* [244]. By using $\xi \sim |G - G_c|^{-\nu}$ and ensuring that the

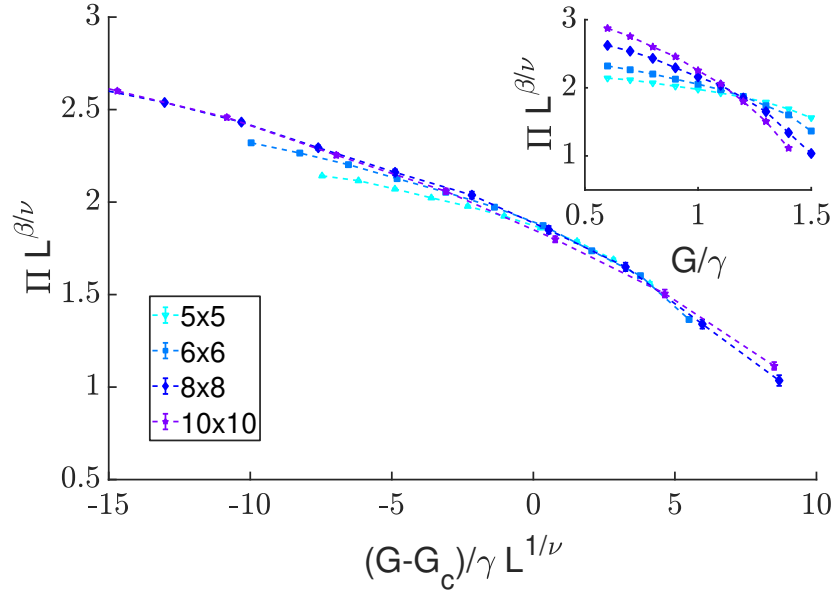


FIGURE 8.1: Rescaled Parity obtained with gaussian trajectories for lattices of different sizes ($U = 40\gamma, J = 20\gamma, \Delta = -20\gamma, \eta = 0$). The critical exponents which allow to recover the universal behaviour of the rescaled quantities are $\nu = 0.62997$ and $\beta = 0.32642$, i.e. the critical exponents for the correlation length and the order parameter of the 2D quantum transverse Ising model. Note that for Gaussian states, Π is obtained by the expectation of the Wigner-function value in the origin of multimode phase-space [146]. Note that in a finite system, the order parameter remains analytical. Its change becomes increasingly sharper for larger lattices, leading to non-analytic behaviour at G_c in the thermodynamic limit.

dimensions are consistent, we obtain

$$\Pi = L^{-\beta/\nu} f(L^{1/\nu} |G - G_c|), \quad (8.3)$$

where f is another scaling function.

If one has data points for corresponding values of Π and G , a plot of $\Pi L^{\beta/\nu}$ as function of $(G - G_c)L^{1/\nu}$ should reveal f , which, sufficiently close to the critical point, should be independent of L : the functions f for different values of L *collapse* for the appropriate values of the critical exponent, with improving agreement for larger values of L . Note that in a first step, it is useful to rescale only the vertical axis in order to find the critical value G_c : at $G = G_c$ the argument of f becomes zero independent of system size, so that a crossing of the curves (more precisely, a limit point) can be observed, as we have done in the inset of Figure 8.1.

It turns out that finite-size scaling is rarely relevant in an experimental context, but it is known to be very useful for numerical simulations as in our case [244].

8.2 New result: classical critical behaviour in the high-loss regime

Now that we have established the validity of the method, even to describe quantum critical behaviour, we turn to the main objective: investigate the dissipative phase transition in regimes where the loss rates are comparable with the Hamiltonian parameters. We therefore set $U/\gamma = J/\gamma = 1$, $\Delta = -J$ here. As we have seen in the previous section that two-photon losses are not expected to play an important role in the emergent criticality [182], we set again $\eta = 0$ to speed up the calculations (Figure 7.1).

Naively, we would apply the same Π -analysis as in the previous section in this new parameter regime. However, as we see on Figure 8.2 (left panel) no crossing is found as Π quickly becomes vanishingly small for finite G , seemingly suggesting the absence of a phase transition. We note, though, that the Parity operator is only able to characterize quantum paramagnetic behaviour, a many-mode Schrödinger cat state. Instead, strong classical fluctuations that arise from the losses mix the even and odd eigenstates of the steady-state density matrix at all values of G , such that $\Pi \approx 0$ on both sides of a phase transition.

A possible way to access the quantum correlations in the system more directly, consists of considering the average entanglement entropy (subsection 2.2.4, subsec-

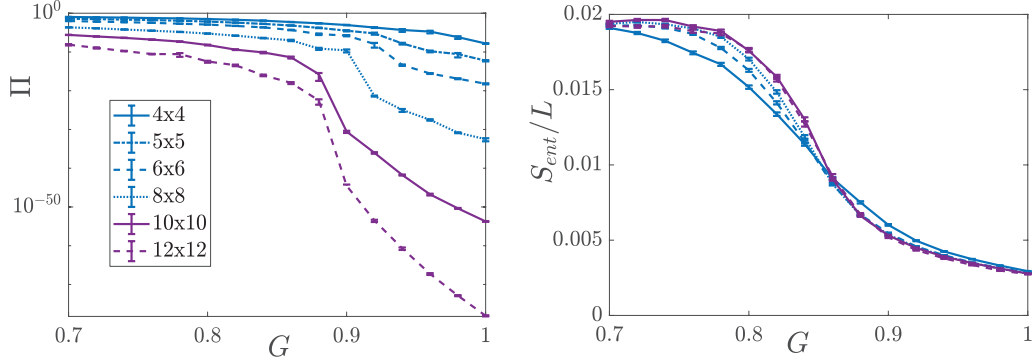


FIGURE 8.2: *Left: the parity Π in the parameter regime $U = J = \gamma = 1, \Delta = -1$ quickly becomes exponentially small for any finite G (note that this result, unlike the ones of Figure 8.1, is plotted on a logarithmic scale). No exponent is able to result in a common crossing point: this quantity cannot be used to characterize the transition. Nevertheless, a drop occurs around the region where criticality can be expected, increasingly sharp for larger lattices. Right: The average entanglement entropy S_{ent} between 'left' and 'right' half of the lattice in an individual trajectory, normalized by L . Remarkably, the amount of quantum correlations actually decreases towards the regime where an ordered phase might be expected. Curves seem to be crossing in this same region around a value $G \approx 0.86$*

tion 4.2.2) between two halves of the lattice, within individual trajectories [245]. This quantity is plotted on the right panel of Figure 8.2. A crossing for different lattice sizes seems to be present around $G \approx 0.86$. But surprisingly, the main observation is that the amount of quantum correlations actually *decreases* for increasing G , the regime where symmetry breaking was predicted from a Gutzwiller study, and where we found ferromagnetic order in the low-loss regime. But similar to Π , S_{ent} is unable to capture *classical correlations*.

In order to have a more complete understanding of the correlations, we plot in Figure 8.3 the first-order correlation function in a 12x12 lattice as function of distance Δx between two cavities, for different values of G . It is clear that long-range correlations emerge. These are dominated by their classical contribution, while quantum correlations decrease. This result suggests that ferromagnetic order is still possible, despite the low entanglement.

To verify this, we plot in Fig. 8.4, the steady-state expectation value for the

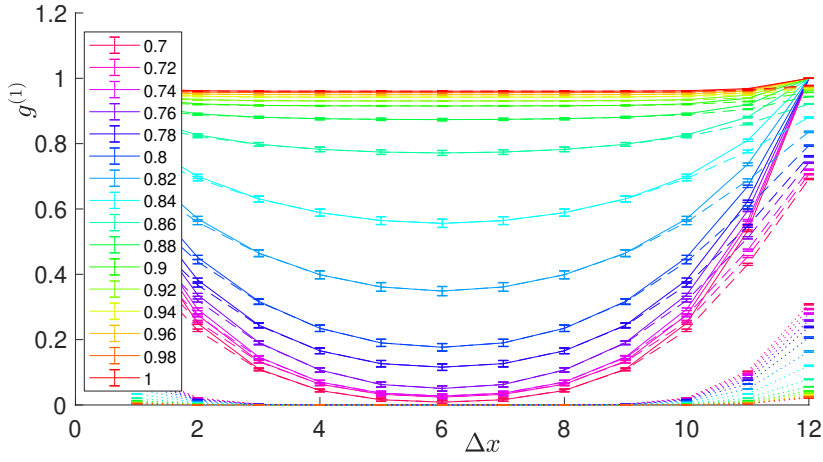


FIGURE 8.3: First order correlation function in a 12x12 lattice with periodic boundary conditions for multiple values of G/γ : $g^{(1)}(\Delta x) = \frac{\langle \hat{a}^\dagger_i \hat{a}_{i+\Delta x} \rangle_{i,\hat{\rho}}}{\langle \hat{a}^\dagger_i \hat{a}_i \rangle_{i,\hat{\rho}}}$ (full line), separated in its classical contribution $\frac{\langle \alpha_i^* \alpha_{i+\Delta x} \rangle_{i,\hat{\rho}}}{\langle \hat{a}^\dagger_i \hat{a}_i \rangle_{i,\hat{\rho}}}$ (dashed lines) and its quantum contribution $\frac{\langle v_{i,i+\Delta x} \rangle_{i,\hat{\rho}}}{\langle \hat{a}^\dagger_i \hat{a}_i \rangle_{i,\hat{\rho}}}$ (dotted lines). We see long-range order emerging for large driving G/γ , which is clearly dominated by the classical contribution. Notation $\langle \cdot \rangle_{i,\hat{\rho}}$ denotes an average over both the lattice sites and the ensemble.

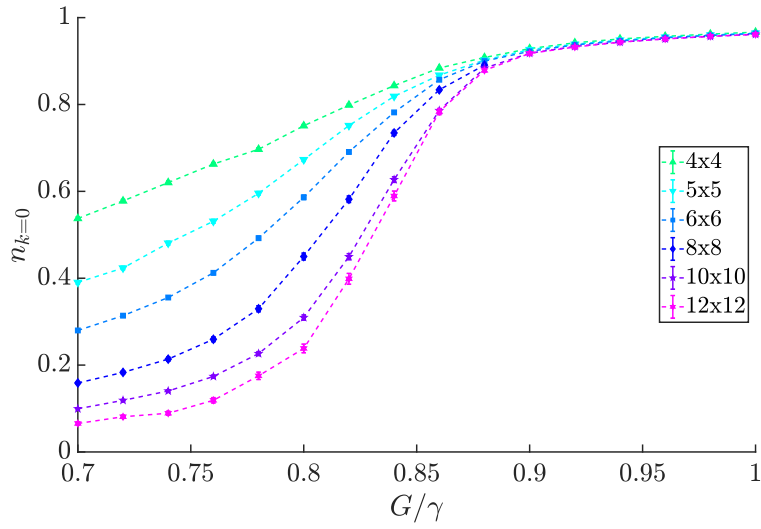


FIGURE 8.4: The steady-state relative occupation of the $k = 0$ -mode increases as a function G/γ , as computed in lattices of different size. Results are obtained from 1000 trajectories (500 for the 12x12 lattice), each evolved over a total time $t = 100\gamma^{-1}$. For each quantum trajectory, the vacuum is chosen as initial state and the two-photon driving is switched on slowly to the desired value, in order to reduce the formation of defects which would appear from strong quenching [246]. The steady-state expectation values are computed averaging the results obtained in a time interval from a size-dependent initial time t_{relax} to the final time $t_{\text{fin}} = 100\gamma^{-1}$.

relative occupation of the $k = 0$ mode

$$n_{k=0} = \frac{\sum_{jj'} \text{Tr} (\hat{\rho}_{SS} \hat{a}^\dagger_j \hat{a}_{j'})}{\left[\sum_j \text{Tr} (\hat{\rho}_{SS} \hat{a}^\dagger_j \hat{a}_j) \right]^2} \quad (8.4)$$

as a function of the driving amplitude G for different lattice sizes. At large values of G/γ , we notice that $n_{k=0} \simeq 1$, independently of the size of the lattice. This result indicates that the steady state of the dissipative system in this limit is a coherent state characterized by long-range order, since the local Bose fields in each cavity assume the same value. This is in agreement with the picture of the spontaneous symmetry breaking obtained in the Gutzwiller calculation [181]. At smaller values of G/γ , $n_{k=0}$ decreases when the lattice size increases, suggesting that $n_{k=0} \rightarrow 0$ in the thermodynamic limit. This behaviour supports the hypothesis of the presence of a disordered \mathbb{Z}_2 -symmetric phase for small values of the driving amplitude.

Given this last result, it is convenient to describe the behaviour of the system across the phase transition in terms of an order parameter, which is related to the average value of the Bose fields on the different cavities. We thus define

$$\bar{\alpha} = \frac{1}{N} \sum_i \text{Im} \alpha_i, \quad (8.5)$$

i.e. the expectation value of the average Bose field in a single quantum trajectory (we consider its imaginary part in order to have a real-valued order parameter): this quantity has a clear physical meaning, as it corresponds to the outcome of a heterodyne unraveling in real experiments. In Fig. 8.5-(a-d), we plot the time evolution of $\bar{\alpha}$ on single trajectories in a 6×6 lattice, choosing the vacuum as the initial state at $t = 0$, for different values of the driving amplitude. For $G = 0.7\gamma$ [Fig. 8.5-(a)], we notice a behaviour supporting the emergence of a disordered phase, as the order parameter exhibits Gaussian fluctuations around the value $\bar{\alpha} = 0$. For $G = 0.8\gamma$ [Fig. 8.5-(b)], the situation is similar, but we can see the presence of longer intervals of time where the value of $\bar{\alpha}$ fluctuates around non-zero values, suggesting the appearance of a bimodal character in the steady-state distribution of the order parameter. At larger values of the driving amplitude [$G \geq 0.9\gamma$, Fig. 8.5-(c-d)], the behaviour of $\bar{\alpha}(t)$ is completely different: after a first transient where the value of $\bar{\alpha}$ changes notably in time, at long time we see that the order parameter fluctuates around a non-zero value, which can be either negative [as in Fig. 8.5-(c)] or positive [as in Fig. 8.5-(d)] according to the particular realization of the noise in the stochastic differential equation. This behaviour suggest the

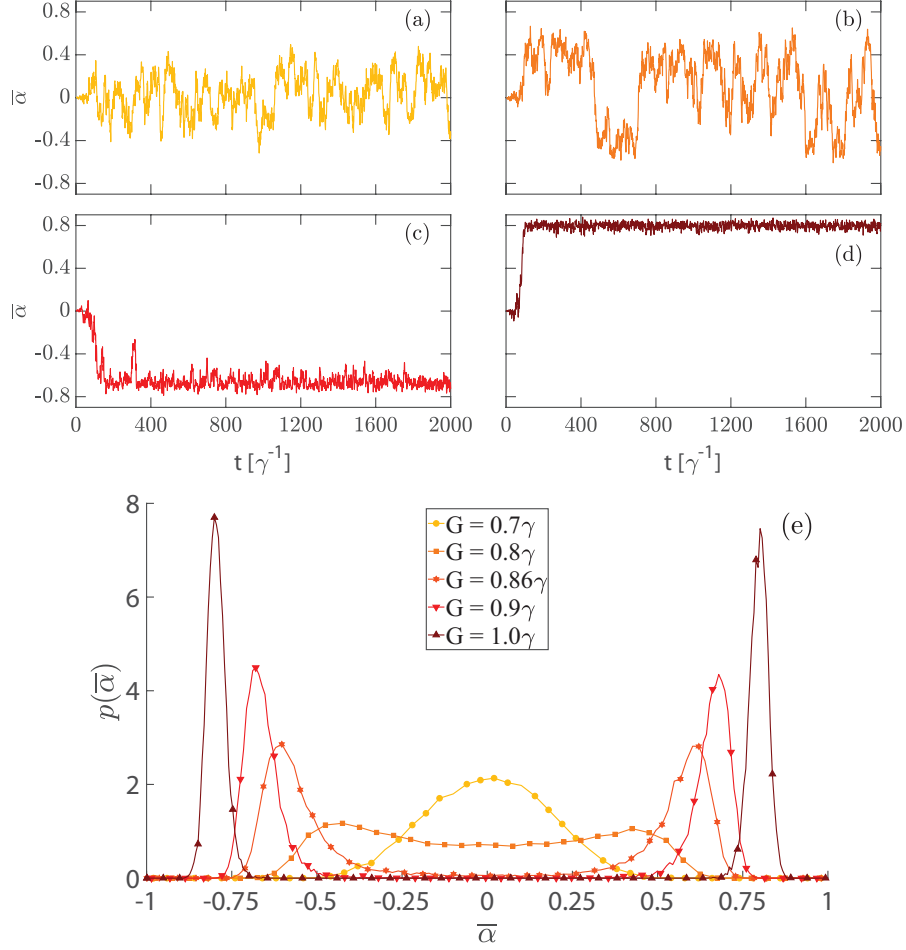


FIGURE 8.5: (a-d): Time evolution of the order parameter $\bar{\alpha}$ along a single Gaussian trajectory in a 6×6 lattice, for different values of the driving amplitude: (a) $G/\gamma = 0.7$, (b) $G/\gamma = 0.8$, (c) $G/\gamma = 0.9$, (d) $G/\gamma = 1.0$. (e) Probability distribution $p(\bar{\alpha})$ of the order parameter for different values of G . For each value of G , we consider 1000 trajectories each evolved over a time $t = 400$ and we collect the data for $\bar{\alpha}(t)$ for $t \geq 20$, i.e. for long times in which the density matrix of the dissipative system has reached the steady state. The distribution $p(\bar{\alpha})$ is obtained as the histogram of the collected data. As G increases, a qualitative transition from monomodal to bimodal distribution is evident.

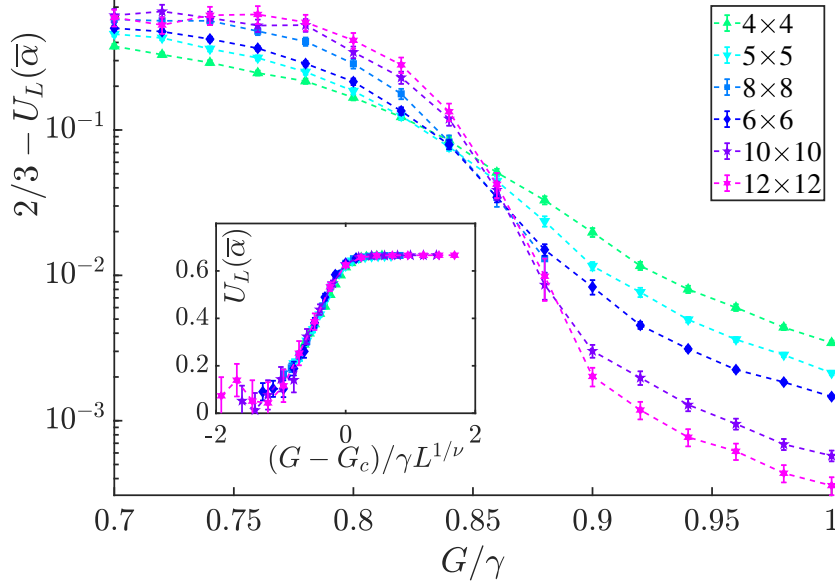


FIGURE 8.6: Binder cumulant U_L as a function of the two-photon driving amplitude G , for different lattice sizes L . A crossing of the curves for different lattice sizes can be seen, signaling the emergence of a critical point at $G = G_c$ (the difference $2/3 - U_L$ is shown on a logarithmic scale). Inset: The curves for different sizes show an universal behaviour when plotted as a function of $(G - G_c)L^{1/\nu}$, with $\nu = 1$ the critical exponent for the correlation length in the classical 2D Ising model

emergence of an ordered phase with broken symmetry in this regime of parameters. However, when considering an ensemble of many trajectories at given G , half of them will stabilize at long time around a positive value for $\bar{\alpha}$ and the other half around the opposite value $-\bar{\alpha}$, retrieving thus a \mathbb{Z}_2 -symmetric steady-state density matrix, as expected for a system of finite size. This behaviour becomes clear from sampling $p(\bar{\alpha})$, the probability distribution of $\bar{\alpha}$, as shown in Fig. 8.5-(e). Although $p(\bar{\alpha})$ is always an even function, we notice that, when increasing G , the character of the distribution changes from a monomodal to a bimodal behaviour.

A more quantitative analysis can be performed from the Binder cumulant, defined as $U_L = 1 - \mu_4/(3\mu_2^2)$, where $\mu_m = \int d\bar{\alpha} \bar{\alpha}^m p(\bar{\alpha})$ denotes the m -th moment of the probability distribution $p(\bar{\alpha})$ [247, 248]. A big advantage of this quantity is its dimensionless nature, because of which finite-size scaling is possible without rescaling the vertical axis. As such this universal function of ξ/L has been widely

used in the finite-size scaling analysis of spin models in presence of a paramagnetic-to-ferromagnetic phase transition [247]. This means that at a critical point, where the correlation length diverges in the thermodynamic limit, the Binder cumulant itself becomes independent of the lattice size L : therefore, the finite-size scaling analysis of U_L is a useful approach to track the emergence of the criticality in our system. In Fig. 8.6, we plot U_L as a function of the driving amplitude G for lattices of different size. We find that all the different curves cross at the common point $G_c = 0.86\gamma$, confirming the presence of a dissipative phase transition in our model. Some insight about the universality class of the phase transition can be obtained by plotting the same data for $U_L(\bar{\alpha})$ as a function of $(G - G_c)L^{1/\nu}$, where ν is the critical exponent of the correlation length. From the results shown in Fig. 8.6 (inset), we notice that setting $\nu = 1$ makes all the curves collapse, confirming the expected universal behaviour of $U_L = f(\xi/L)$. The value $\nu = 1$ corresponds to the critical exponent of the correlation length for a 2D *classical (thermal)* Ising model. This classical Ising model has an energy

$$H = -J \sum_{\langle ij \rangle} \sigma_i \sigma_j, \quad (8.6)$$

where $\sigma_i, \sigma_j = \pm 1$. The ground state of (8.6) is trivial, but interesting physics occurs at finite temperature T , where the equilibrium is obtained by minimizing the free energy $\mathcal{F} = -k_B T \log \mathcal{Z}$, with partition function $\mathcal{Z} = \sum_{\text{conf}} e^{-H/k_B T}$, where the sum is over all possible configurations of the lattice.

8.2.1 FAILURE OF THE TWA METHOD

For comparison, we have also studied the transition with the Truncated Wigner method for the same parameters as in section 8.2. However, as we already anticipated in section 7.3, we see in Fig. 8.7 that it appears to be fundamentally incapable of describing the ordered phase

- (a) the occupation of the k_0 mode does not go to 1 for even the largest G studied (note that we go up to higher values than in section 1). Instead, some plateau values are reached which decrease with lattice size.
- (b) the binder cumulant shows a very similar behaviour, and exhibits no crossing.

The clear failure of this method is remarkable, because of its wide successful use among driven-dissipative systems (subsection 3.3.6).

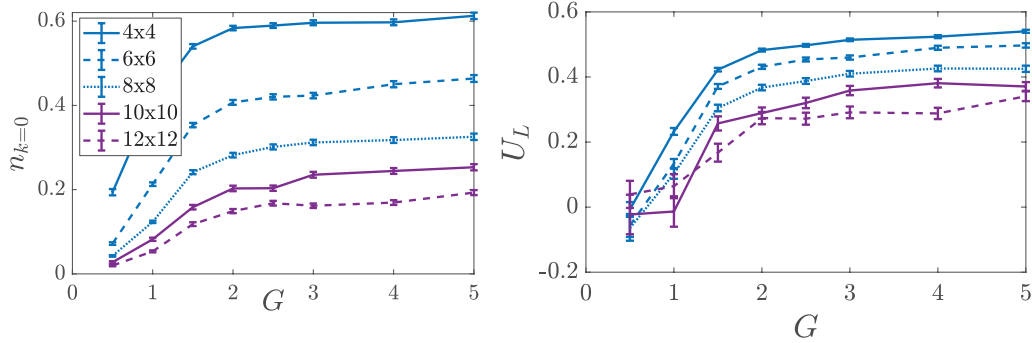


FIGURE 8.7: k_0 -occupation and Binder cumulant for $U = J = \gamma = 1, \Delta = -1, \eta = 0$: as opposed to our GTA result, we see that this method misses the occurrence of an ordered phase, even very deep in the ferromagnetic parameter regime

8.3 Interpretation: losses act as an effective temperature

Putting together the results obtained in section 8.1 and section 8.2, we have found that system (7.1) exhibits a phase transition in all the regimes studied. It belongs to the universality class of the quantum 2D-Ising model (8.1), and the thermal 2D-Ising model (8.6), respectively.

This picture is very similar to the one that describes the fate of a quantum phase transition at finite temperature [167, 249]: an increasing amount of classical fluctuations takes over the role of quantum fluctuations in destroying order, as explained in Figure 8.8. The loss rate γ can thus be interpreted as an effective temperature.

As noted in subsection 6.1.3, similar pictures of losses acting as an effective temperature were recently obtained in a number of other systems. A clear advantage of our analysis is that we were able to study a single system with a single method in multiple parameter regimes. Regarding the nature of the crossover between the high-loss and low-loss regimes, we might expect, when decreasing the relative loss rate, classical behaviour from the losses to be only relevant at longer and longer length scales. This means that for sufficiently large systems, a classical criticality may be expected for G very close to G_c and quantum critical behaviour slightly further away from the critical point. As the 1D classical Ising model does not exhibit a phase transition, our model doesn't either. For higher dimensions, it can

8.3 - INTERPRETATION: LOSSES ACT AS AN EFFECTIVE TEMPERATURE

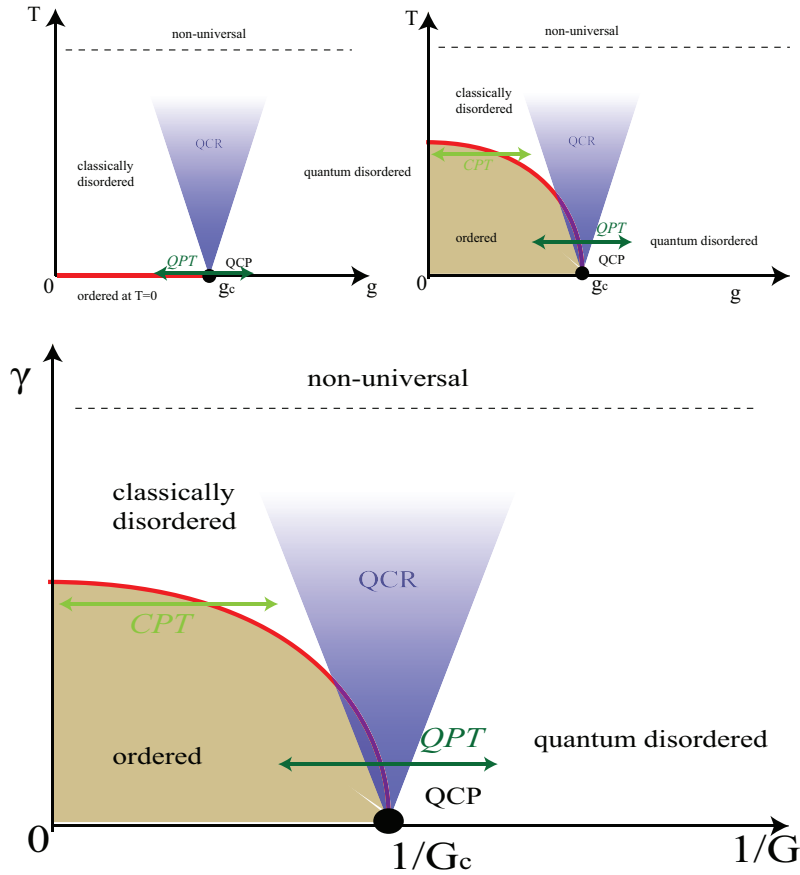


FIGURE 8.8: Top: either quantum phase transitions at temperature $T = 0$ do not correspond to any transition at finite T as any amount of thermal fluctuations destroys the ordered phase (left, e.g. the 1D Ising model); or the phase transition is continuously connected to a classical phase transition (right e.g. the 2D Ising model) [167, 249]. Perturbatively close to the quantum-critical point (QCP), there is always a quantum-critical region (QCR) in parameter space, where long-range quantum correlations are important. At small temperature then, the phase boundary is still within the QCR and the phase transition is still in the quantum universality class. For higher temperature, thermal fluctuations take over the role of quantum fluctuations and the phase boundary leaves the QCR. Phase transitions here belong to the classical universality class. Bottom: our quadratically-driven Kerr lattice displays physics very similar to the equilibrium transition of the 2D quantum Ising model at finite T , when G is used as the control parameter and γ the role of temperature: for small γ quantum critical behaviour is observed whereas the transition has a classical (thermal) nature for higher loss rate γ . Note that in all cases, for extremely high values of T or γ , all universal arguments on phase transitions break down as the microscopic dynamics becomes important.

be expected to converge to the mean-field prediction [181].

Dynamical scaling in quadratically driven kerr-lattices: the Kibble-Zurek effect

The GTA equations readily allow for an investigation of the dynamical aspects of the phase transition. First, we study the formation of domains as function of quench speed, and extract the dynamical critical exponent from a Kibble-Zurek argument. This exponent matches with metropolis dynamics in the classical Ising model. Secondly, from slow decay to the steady state, we extract the Liouillian gap and show that it satisfies the same scaling relations as function of correlation length and distance to the critical point as the Hamiltonian gap in quantum phase transitions.

9.1 Dynamics of phase transitions

Here, we are concerned with extending the conclusions in the large-dissipation limit to the *dynamical* aspects of the phase transition. In particular, we are interested in the dynamical critical exponent z that relates the correlation time, and in closed quantum systems the Hamiltonian gap, to the control parameter and the correlation length. As we have mentioned in section 6.1, not only the correlation length, but also the correlation time diverges near a critical point, leading to the occurrence of critical slowing down. Some current works have addressed the latter effect in a dissipative context for optical bistability (a *first-order* dissipative phase transition) [159, 175, 197], fermionic lattices [250], optical lattice clocks [251] and miscellaneous spin lattices [193, 252].

The value of z does not follow as a simple corollary of knowledge on static

exponents β, ν and their universality class. In the wording of Ref. [117]: *While the static universal critical behaviour is determined by the symmetries and the dimensionality of the problem, the dynamical critical behaviour is sensitive to additional dynamical conservation laws.* The latter statement is in fact already valid for classical systems at equilibrium [253].

For our study of the quadratically driven Kerr lattice, we will use two separate approaches. First, we address the occurrence of the Kibble-Zurek (KZ) effect. Because of the critical slowing down, domains are formed when the control parameter (photon driving in our case) is tuned through the transition at finite speed. According to a dynamical scaling hypothesis based on the KZ effect [254, 255], we are able to extract z from square lattices subject to a linear quench and obtain $1.9 < z < 2.3$. Secondly, we study the slow relaxation dynamics to the steady state. This latter timescale is known to correspond directly to the inverse Liouvillian gap [169]. We here find scaling with $1.8 < z < 2.3$. The fact that both values are consistent implies that the Liouvillian gap exhibits the same scaling relations as the Hamiltonian gap in closed quantum systems.

The two-dimensional classical Ising model (8.6) is known as a paradigmatic example of the second-order phase transition, both in terms of its historical importance as for its pedagogical value [99, 256, 257]. In numerical simulations, it is typically implemented with a somewhat heuristic update rule, which is not uniquely defined by the steady state properties. Moreover, different update rules applied to the same model result in different values of z . The most well-known of these rules is the single-site update rule or Metropolis algorithm, which is consistent with experimental observations of the critical dynamics in an iron film [258]. The same value of z is found in the Hohenberg-Halperin model A dynamics [253] as well as in ϕ^4 -theory [259].

We find here that the value of z extracted from quadratically-driven Kerr resonators is indeed consistent with the value $z_m \approx 2.18$ from the Metropolis algorithm and model A dynamics. This correspondence between our nonequilibrium critical dynamics and model A dynamics is in line with Ref. [106] on critical dynamics of a driven-dissipative Bose-Hubbard model.

9.2 Kibble-Zurek scaling for a linear quench

When a parameter in a thermodynamic system is slowly varied, the adiabatic theorem assures that the system remains at all times in an equilibrium state at

constant entropy. The minimal ramp time for equilibrium to be preserved is given by the relaxation time. When a parameter is quenched through a second order phase transition, the relaxation time diverges, adiabaticity always breaks down and domains with different values of the symmetry-breaking order parameter are formed. This mechanism is known as the Kibble-Zurek (KZ) mechanism [254]. Originally introduced in a cosmological context [260], it has been developed further mainly in condensed matter systems, with first applications to liquid helium [261] and rotor models, where the defects are vortices [254]. More recently, the KZ mechanism has been applied to more generic systems where the defects take the form of domain walls [262, 263]. Extensions to quantum phase transitions have also been developed [152, 255, 264–266].

More specifically, the KZ mechanism works as follows (Fig. 9.1). We envision a continuous quench where, starting from the steady-state solution at some value G_0 for the two-photon driving in the paramagnetic regime, G is increased linearly up to G_c in a total time T :

$$G(t) = G_0 + vt \quad 0 \leq t \leq T, \quad (9.1)$$

where $v = \frac{G_c - G_0}{T}$. As G_c is approached, the correlation time diverges as $\tau \sim (G - G_c)^{-z\nu}$ while the correlation length scales as $\xi \sim (G - G_c)^{-\nu}$. From some point in time during the quench $T - \hat{t}$ onward, $\tau(G) > \hat{t}$: the dynamics freezes as the time available for the dynamics drops below the correlation time. The correlation length is then unable to increase beyond $\xi_c \sim (G(T - \hat{t}) - G_c)^{-\nu}$, setting the final domain size. Crucially, the lower v , the larger $G(T - \hat{t})$ and thus the larger the domains. The former arguments assume universality in an infinite lattice. An example of such domain formation after quenching with different v from a given initial state is given in Fig. 9.2.

Focussing on the steady-state properties of a more realistic finite lattice system, we recall from our discussion in section 8.1, that there are three distinct length scales present: the lattice spacing $a = 1$, the correlation length ξ and system size L . Close to criticality, one has $\xi \gtrsim a$ leading to the scaling hypothesis that all quantities can be expressed as a function of the dimensionless ratio ξ/L [244]. This approach was sufficient to study our system in the previous chapter.

For dynamic scaling, we now follow the scaling approach introduced in ref. [255]. Similar to length, three different timescales are present. τ_a relates to the local individual Hamiltonian processes and loss rate, τ the true correlation time of

the system, and τ_L the slowest scale of the finite system, above which adiabaticity is restored. In general, universal behaviour for ξ and τ , and hence standard Kibble-Zurek scaling, can be expected for $\tau_a < \hat{t} < \tau_L$ (Fig. 9.1). Each of these timescales is associated with velocity scales [255]:

On the order of the lattice spacing ¹, $v_a \sim J^2 a^{-(z+1/\nu)} = J^2$ marks the transition speed between possibly microscopic dynamics and long-range universal behaviour. The second scale is the quench speed v . Third, there is the Kibble-Zurek speed $v_{KZ}(L) \sim J^2 L^{-(z+1/\nu)}$: marking the speed where domain size becomes comparable with the lattice size (below $v_{KZ}(L)$ the dynamics remain adiabatic). Now, two separate scaling functions appear for the square order parameter after the quench ($t = T$) in different regimes [255]. If the quench is sufficiently slow for the microscopic processes to be unimportant ($v \lesssim v_a$), one expects universal scaling as a function of v/v_{KZ} :

$$\langle \bar{\alpha}^2 \rangle_{\hat{\rho}} = L^{-2\beta/\nu} f_1(vL^{z+1/\nu}), \quad (9.2)$$

where $\langle \cdot \rangle_{\hat{\rho}}$ denotes a statistical expectation value over trajectories. On the other hand, if the quench is sufficiently fast for the finite size to be unimportant ($v \gtrsim v_{KZ}(L)$), universal scaling of v/v_a is expected, leading to

$$\langle \bar{\alpha}^2 \rangle_{\hat{\rho}} = L^{-d} f_2(v^{-1}). \quad (9.3)$$

In the overlapping region $v_{KZ} \lesssim v \lesssim v_a$, both scaling functions overlap with a power-law dependence $\langle \bar{\alpha}^2 \rangle_{\hat{\rho}} \propto v^{-x}$ with exponent

$$x = \frac{d - 2\beta/\nu}{z + 1/\nu}. \quad (9.4)$$

The above arguments have extensively been verified for thermal systems, but the generic nature of arguments suggests that they should also work out of equilibrium. In order to verify the KZ mechanism in the two-photon driven dissipative Hubbard model, we have simulated quenches in the amplitude of the two-photon drive of the Bose-Hubbard model from $G_0 = 0.7J$ to $G_c = 0.86J$.

In Fig. 9.3, the extracted slow and fast scaling functions f_1 and f_2 are shown for different square lattice sizes, and collapse is observed for both when using exponents $\beta = 0.125$, $\nu = 1$, $z \approx 2.18$. The former two numbers are static critical

¹More precisely, v_a relates to the energy scales of individual Hamiltonian processes and dissipation rate, which we all take of order one.

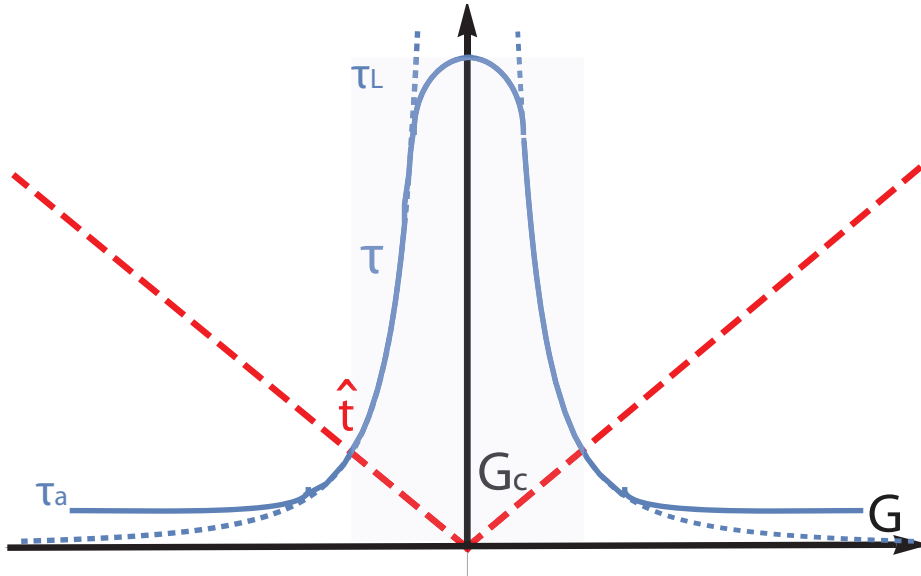


FIGURE 9.1: *The Kibble-Zurek effect: when G is linearly increased, the time until G_c is reached (red, dashed line) becomes less than the diverging correlation time τ (blue line) at \hat{t} . From \hat{t} onwards, the dynamics freezes (blue region). In a finite system, the true value of τ (full line) only follows the universal behaviour for intermediate velocities v for which the crossing occurs at $\tau_a < \tau < \tau_L$.*

exponents corresponding to the 2D thermal Ising model (chapter 8)). The value of z , the dynamical critical exponent, corresponds to Metropolis dynamics in this model ². In the intermediate regime for v , the predicted power-law (9.4) is further observed, consistent with the aforementioned values of the critical exponents.

We thus have obtained strong evidence for the fact that not only the static, but also the dynamical properties of the two-photon driven Bose-Hubbard model are in the Ising universality class, more precisely of Metropolis dynamics.

9.3 The Liouvillian gap scales with the same exponent

In Hamiltonian systems, the dynamical exponent z is further known to govern the scaling of the gap Δ_H [167]:

$$\Delta_H \sim \xi^{-z} \ \& \ \Delta_H \sim |g - g_c|^{z\nu}, \quad (9.5)$$

²The same classical model can have different simulation algorithms (update rules) with other values of z [255]

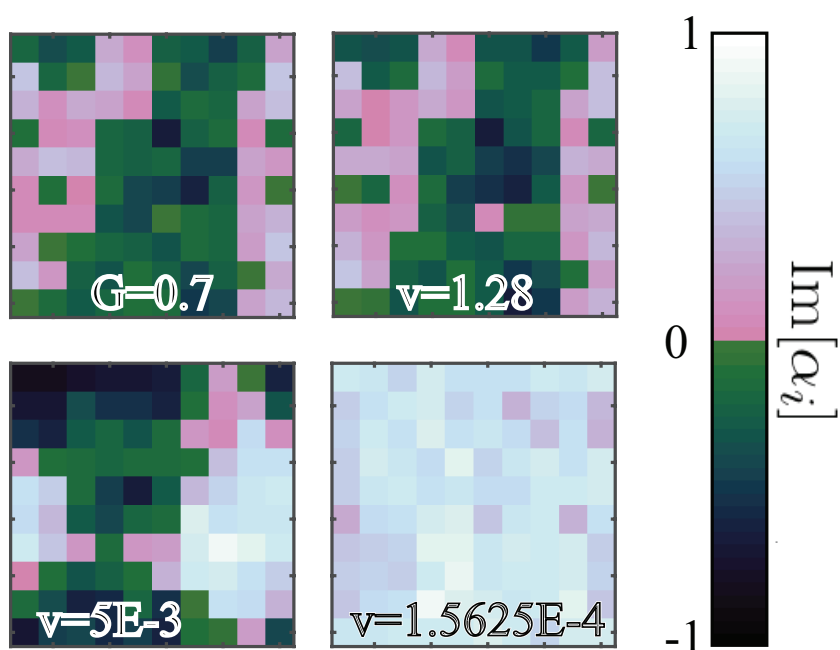


FIGURE 9.2: During the quench protocol, G is increased linearly with time from $G_0 = 0.7J$ to $G_c = 0.86J$, the critical point (section 8.2). The upper left panel shows a Monte Carlo sampling of the steady state at the $G = G_0$. The other panels show a sample of the final state that was evolved with different quench speeds v . For $v \gtrsim 1$, almost no evolution has been able to take place. For decreasing v , the correlations are able to spread further, until for $v \lesssim v_{kz}(L)$ the whole 10×10 lattice is correlated.

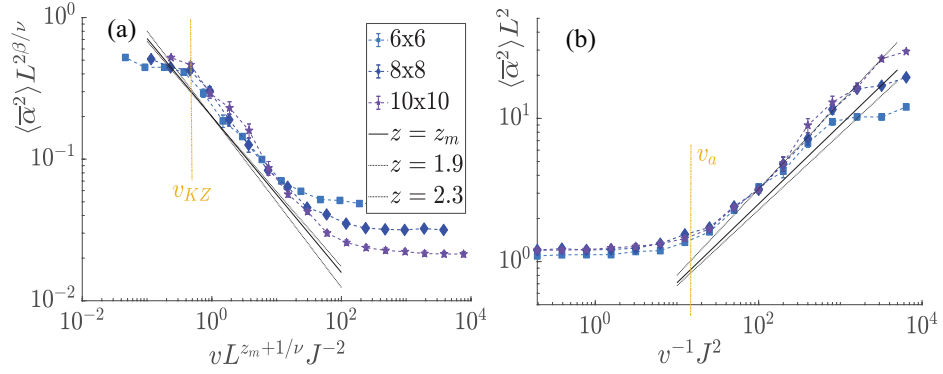


FIGURE 9.3: Dynamic scaling functions for different system sizes showing collapse in the adiabatic (f_1 , (a)) and diabatic limit (f_2 , (b)), for linear quenches from $G_0 = 0.7J$ to $G_c = 0.86J$. In the intermediate regime, there is a universal power-law scaling (black line) with exponent $x = \frac{d-2\beta/\nu}{z+1/\nu}$, where dimension $d = 2$; $\beta = 0.125$, $\nu = 1$ are critical exponents of the universality class of the 2D classical Ising model; and z is the dynamical critical exponent. Results are consistent with $z = z_m \approx 2.18$, the dynamical critical exponent characterizing Metropolis dynamics in the 2D Ising model, this value was also used for the finite-size scaling itself. Parameters: $U = \gamma = J = 1, \Delta = -1$. For the fastest quenches ($v/J^2 \geq 10^{-2}$), 10^3 trajectories were used, and 10^2 trajectories for the slower quenches. The yellow vertical lines denote approximate values for v_{KZ} and v_a , marking the edges of regime where power-law scaling is valid. We find that the prefactor in the definition of v_{KZ} is of order one, whereas $v_a \approx 10J^2$.

where g is the control parameter. Because system (7.1) studied here belongs to a classical universality class due to its driven-dissipative nature, the fate of relations (9.5) is not *a priori* clear. In an open system, the dynamics are governed by the Liouvillian superoperator \mathcal{L} [169]. Likewise, the timescale of slowest relaxation to the steady state is determined by the Liouvillian gap λ , defined as (minus) the real part of the first nonzero eigenvalue of \mathcal{L} . One can thus ask if Δ_H can be replaced by λ in relations (9.5). If this replacement in the first relation of (9.5) is valid, then one must have in a finite system [244]

$$\lambda = \xi^{-z} \tilde{f}(\xi/L) = L^{-z} f(L^{1/\nu}(G - G_c)), \quad (9.6)$$

where \tilde{f}, f are unknown scaling functions.

In order to extract λ from the numerical data, let us take a deeper look at the role that this quantity plays in the dynamics of observables. The Liouvillian, as a linear operator, has a set of eigenvectors $\{\hat{\rho}_i\}$ with corresponding eigenvalues $\{\lambda_i\}$, i.e. $\hat{\mathcal{L}}\hat{\rho}_i = \lambda_i\hat{\rho}_i$ ³. We will, without loss of generality, assume these eigenvalues to be ordered for increasing absolute value of the real part. Any physical density matrix can be written as $\hat{\rho} = \sum_i c_i \hat{\rho}_i$. The time-evolution becomes

$$\hat{\rho}(t) = e^{\hat{\mathcal{L}}t} \hat{\rho}(0) = \sum_i c_i(0) e^{\lambda_i t} \hat{\rho}_i. \quad (9.7)$$

For the steady-state $\hat{\rho}_0$, one easily sees that $\lambda_0 = 0$. For all other eigenvalues, one has $\text{Re}\{\lambda_i\} < 0$ [6], meaning that (9.7) results in an exponential decay of all excited states towards $\hat{\rho}_0$, possibly combined with oscillatory behaviour for the higher excited modes. It is easy to see that $\lambda := -\text{Re}\{\lambda_1\}$ determines the slowest decay scale. Slow timescales typically correspond to long-wavelength behaviour, therefore we access this slowest mode in our system by studying the decay from a fully polarized ($\alpha_j = 1i, \forall j$) state. In order to obtain values of λ for different values of G and L numerically, we thus start from this fully polarized state, and let the system evolve freely. An exponential $\sim e^{-\lambda t}$ is then fitted to the slow relaxation process towards the steady state, as illustrated for a 10x10 lattice in the left panel of Fig. 9.4.

Validity of Eq. (9.6) implies a collapse of curves for different system sizes when plotting $L^z \lambda$ as function of $L^{1/\nu}(G - G_c)$. In the right panel of Fig. 9.4, we see that

³Because $\hat{\mathcal{L}}$ is a superoperator, some aspects of the linear algebra are less intuitive, for example all excited eigenvectors $\hat{\rho}_{i>0}$ are traceless and not necessarily hermitian. For the full spectral theory, see Ref. [169].

this is indeed the case for $\nu = 1$, $z = z_m$, the same values as in the previous section.

Furthermore, relation (9.6) also directly relates λ to control parameter G . In the limit of large system sizes, we observe indeed (black line on Fig. 2)

$$\lambda \sim |G - G_c|^{z\nu}, \quad (9.8)$$

where the numerical result is specifically good in the regime $\xi < L$. This means that both relations (9.5) are valid for the considered Liouvillian dynamics.

The fact that these scaling relations for λ , with exponent z obtained from the Kibble-Zurek scaling are found in this case study, is not too surprising because λ was directly connected to a slow timescale. This is generally the case for dissipative phase transitions, so we may expect these scaling relations to hold very broadly. However, very recently a disconnection between gap and decay time has been found in some systems [36], so that exotic counterexamples cannot be fully excluded.

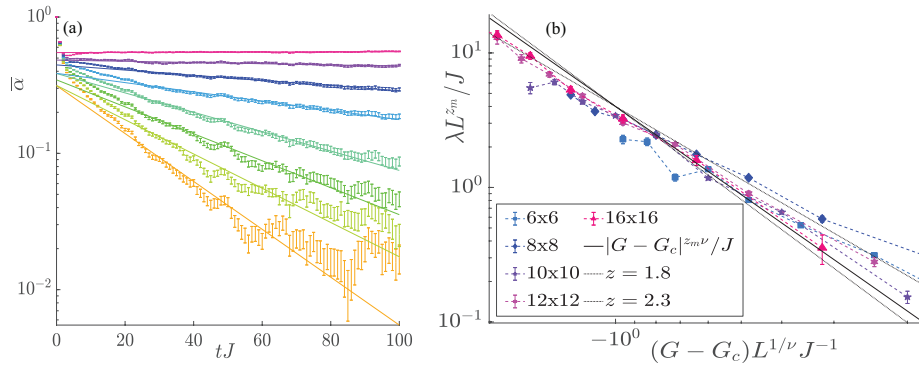


FIGURE 9.4: (a): Errorbars show the decay of $\bar{\alpha}$ to the steady state value (0) in a 10×10 lattice after initialization in a polarized $\alpha_j = 1i, \forall j$ state, average over trajectories. From bottom to top, G values run increment from $0.74J$ with steps $0.02J$ to $0.86J$. Full lines in corresponding colors: fits $\propto e^{-\lambda t}$, with fitting from $tJ = 20/30/40$ onwards ($6 \times 6/10 \times 10/12 \times 12/16 \times 16$) ($tJ = 10 - 50$ for the 8×8 case). (b): extracted values of λ , rescaled assuming $z = z_m$ as function of rescaled G . Especially in the $\xi < L$ regime (where the function argument less than -1), collapse is very clear and in agreement with power-law behaviour (9.8). Closer to the critical point, the data collapse becomes worse. It should be noted that in this regime, the time scales become very long and the extracted decay rate may be less accurate. Moreover, the slow dynamics is more sensitive to rare events, that may not be sufficiently sampled. 10^3 trajectories were used in the simulations up to 12×12 lattices and 10^2 for the 16×16 case.

Quadratically driven lattices: Summary and outlook

In Part II, we have applied the *XP*-Gaussian trajectory approach to the study of quadratically driven photonic lattices of up to 144 sites, in a parameter regime with a highly mixed steady state that is inaccessible with other methods such as corner-space renormalization or the truncated Wigner approximation. The system at hand is particularly interesting because it displays a second-order dissipative phase transition. Its investigation is easily performed with the GTA, because the displacements $\{\alpha_i\}$ form a natural order parameter that is spontaneously broken as function of driving amplitude. In the low-loss regime, the GTA method confirms, with a finite-size scaling of the parity, the finding of a quantum criticality, demonstrating the ability of the method to deal with long-range quantum correlations. In a regime of higher losses, we have found, on the other hand, from an analysis of the statistics of the order parameter with the Binder cumulant, critical behaviour of classical nature, but different from the Gutzwiller mean-field prediction, revealing again the ability of the method to describe the many-body correlations arising among the photons. In fact, the GTA method provides a simple picture to distinguish quantum from classical correlations: whereas quantum correlations are reflected by the Gaussian moments u_{ij} and v_{ij} , classical correlations arise from the stochastic expectation value over trajectories $E[\alpha_i\alpha_j]$.

More specifically, the universality classes in the low- and high loss regimes for this model correspond, respectively, to the quantum and classical Ising model: one of the most paradigmatic spin systems commonly used for the study of phase transitions. This confirms a scenario in which, similarly to the case at thermal equilibrium, a crossover between quantum and classical criticality in the non-equilibrium steady state occurs, depending on the scale of the loss rate relative to the Hamiltonian energy scale; contributing to the general understanding of the crossover from quantum to classical critical behaviour in dissipative phase transitions.

In a following step, we have studied the dynamical properties of the phase transition in the high-loss regime in two ways. First, we have observed the occurrence of the Kibble-Zurek effect in this dissipative phase transition with a linear quench in G . Similar to how it is commonly known in equilibrium, finite domains are formed in the ordered phase depending on the quench speed. From this, we extract, with a slightly more exotic finite-size scaling approach, the value of the dynamical critical exponent z (very recently, the Kibble-Zurek effect has now also been observed a different driven-dissipative context, namely the BKT-transition in a polariton condensate [267]). Second, from relaxation of a polarized initial state to the paradigmatic steady state, we extract the Liouvillian gap λ that governs the slowest timescale. Remarkably, we find that λ scales with z , in a manner that is identical to the scaling of Hamiltonian gaps in quantum phase transitions. To what extent this scaling behaviour is generic for open quantum systems is an interesting open problem: because the close connection between closing of the gap and divergence of correlation time, we might expect it to hold at least in the most typical cases. The extracted value of z corresponds to metropolis dynamics, an important dynamical universality class also matching the classical Ising model, that corresponds to the simplest update rule commonly used in simulations. Overall, our study of this model shows that it behaves as an Ising spin model at finite temperature. This has been assumed before in the different context of annealing, and our work can also be interpreted as a justification. Even within a classical regime, optical simulation of the Ising model has been proposed to solve NP-hard tasks [232] with degenerate parametric oscillators [235–237], a system with an analogous symmetry breaking to ours. With respect to this application, our results also confirm that, especially in absence of an all-to-all connected setup, care must be taken when driving through the transition that $v < v_{KZ}$ in order to find the true steady state (Ising ground state) and not a metastable state with Kibble-Zurek domains. Recently, also implementations of the Ising model in a Kerr resonator have been proposed [238] where optical bistability in the single-photon driven case is mapped to the two spin states. Unlike in this proposal, the \mathbb{Z}_2 symmetry is exact in Kerr resonators with two-photon driving studied here, which might benefit the accuracy of the results of such optimization algorithms.

It is further interesting to note that there are alternatives to metropolis updates in classical Ising simulations, with different values of z (different dynamical universality classes for the same static universality class), which can converge to the steady state faster (Swendsen-Wang, Wolff) or slower (East). One may wonder

if suitable reservoir engineering would allow simulation of these as well. This could be useful to speed up or slow down relaxation to the same steady state numerically or experimentally. A possibility would be exploiting the difference between coupling to a common bath or to independent baths, which has shown to reflect at least on the decoherence time of an open quantum system [268].

It would also be interesting to see how the dynamical criticality behaves in the quantum regime, where Kibble-Zurek effect can exhibit richer behaviour [266], as has also been suggested to study experimentally with trapped ions [269]. Recently, also anti-Kibble Zurek behaviour was found under certain circumstances in open quantum systems [270, 271].

PART

III

THE DYE-CAVITY PHOTON
CONDENSATE: AN APPLICATION OF
THE $N\Theta$ -GAUSSIAN METHOD

W. Verstraelen and M. Wouters, “Temporal coherence of a photon condensate: a quantum trajectory description”, Phys. Rev. A **100**, 013804 (2019).

Condensation of Photons with dye-molecules

Photons are bosonic particles, so are they are in principle able to form a BEC. The required thermalization mechanism can be provided by repeated absorptions and emissions by a reservoir of dye-molecules. Depending on the reservoir size, the number statistics is either canonical or grand-canonical. Whereas this number statistics can be simulated by simple stochastic rate equations, the phase statistics is studied by a heuristic phasor model.

10.1 Condensation of photons using dye

The last few decades, a vast amount of research has been done to the related phenomena of Bose-Einstein Condensates (BECs) and quantum fluids [49, 272], for reasons of fundamental interest as well as their exploitation for quantum simulation.

The traditional platform for the realization of quantum fluids are ultracold atoms, but another fascinating platform is a BEC of photons. In order to condense photons, one faces two obstacles that are absent for atomic condensates. First, photons are massless particles moving at the speed of light without rest energy. This problem can be overcome by reducing the dimensionality:

The energy of a free photon is given by

$$\omega = c \|\vec{k}\| = c \sqrt{k_x^2 + k_y^2 + k_z^2}, \quad (10.1)$$

with c the phase speed, an expression which is formally identical to the relativistic energy of a massive particle in a 2D universe for $m = k_z/c$. In the non-relativistic

limit, this leads to

$$\omega \approx \omega_0 + \frac{k_x^2 + k_y^2}{2m}. \quad (10.2)$$

Meanwhile, parabolic trap potentials to confine the photons in the x and y directions are obtained by curving the mirrors¹. Because their effective mass is many orders of magnitude lower, condensation can take place at room temperature. The second obstacle is that photons are by themselves non-interacting particles², an integrable system in which statistical physics is not valid and thermalization impossible (as an analogy, the motion of billiard balls in a box becomes chaotic because of collisions). A number of approaches have been used to overcome this. A first successful approach has been to use effective photon-photon interactions in a nonlinear material, resulting in the condensation of polaritons³: coherent superpositions of photons and excitons [57], of which the temporal coherence has been studied in Refs. [275, 276] (see also section 3.2).

An alternative approach, where there is no need for the photons to be hybridized, consists of letting the photons interact with their environment. Indeed, the Planck spectrum of the black-body radiator already describes thermal light. The Planck distribution

$$n(\omega) \propto g(\omega) \frac{1}{e^{\beta\omega} - 1} \quad (10.3)$$

is similar to the Bose-Einstein distribution,

$$n(\omega) \propto g(\omega) \frac{1}{e^{\beta(\omega-\mu)} - 1} \quad (10.4)$$

but with chemical potential $\mu = 0$. $\beta = \frac{1}{T}$ is here the inverse temperature and $g(\omega)$ the density of states (we set $k_B = \hbar = 1$). As a result, the temperature cannot be independently tuned of particle number, and condensation is impossible: when the temperature is lowered to go below the critical temperature at a given density, the density simultaneously decreases such that condensation can never be

¹In fact, any quadratic Hamiltonian can be engineered for photons. Apart from the kinetic term and the potential that we have discussed, effective magnetic terms coupling position and momentum are obtained by using tilted mirrors that emulate spinning the cavity [273], although this mechanism hasn't been applied to dye-microcavity photon condensates yet.

²Actually, photons can scatter in diagrams containing virtual electron-positron pairs, but these effects are negligible at the energy scales of interest [274].

³Formally, the scattering processes are similar to the ones in vacuum, but with electron-positron pairs replaced by electron-hole pairs in a semiconductor, requiring far less energy.

achieved. To overcome this, the dye-molecule reservoir is used as an optically active (gain) medium. Such dye-molecules are two-level systems for optical frequencies, dressed with many rovibrational modes that thermalize from frequent collisions with solvent molecules.

Of the M dye-molecules, M_{\downarrow} (M_{\uparrow}) are in the optical ground (excited) state. As the molecules absorb and emit photons in the cavity, the total excitation number $X = M_{\uparrow} + n$ is approximately conserved, where n is the amount of photons (weak fluctuations of X occur because of photon losses from the cavity, balanced by continuous pumping of the dye with an external laser).

Now, the absorption and emission spectra of the molecules differ and are related by the Kennard-Stepanov law for their Einstein coefficients ($B_{12}(\omega)$ for absorption, $B_{21}(\omega)$ for emission) [277–279]

$$\frac{B_{21}(\omega)}{B_{12}(\omega)} = \frac{w_{\downarrow}}{w_{\uparrow}} e^{-\beta(\omega-\omega_0)}, \quad (10.5)$$

where ω is the frequency of the photon and ω_0 the frequency of the atomic transition between ground and excited state of the dye. $w_{\uparrow,\downarrow}$ are weight coefficients taking into account the internal molecular density of (rovibrational) states in the electronic ground and excited level, with a ratio that we will take to be one (otherwise, they can be absorbed in a renormalization of the transition frequency). Assuming detailed balance $B_{12}M_{\downarrow}n = B_{21}M_{\uparrow}(n+1)$ at equilibrium, we see that the Bose-Einstein distribution (10.4) is retrieved with $\mu = T \log M_{\uparrow}/M_{\downarrow}$ as the chemical potential. This thermalization mechanism is depicted in more detail in Figure 10.1.

The above thermalization process was first achieved in Ref. [64] and Bose-Einstein condensation in this system was reported shortly afterwards in Ref. [280] by Klaers et al. (Bonn, 2010) (a picture of the setup is given in Figure 10.2). On the theoretical side, the thermalization mechanism is detailed in Ref. [281].

The interested reader can find a few other, more detailed albeit less recent, reviews and tutorials of photon condensation with dye molecules in Refs. [282–285].

10.1.1 COMPARISON WITH A LASER

As we are studying many-body coherence with photons, one might wonder to what extent the photon BEC is truly different from a laser. In fact, it has been shown [286, 287] that there is a smooth crossover between the two. In the lasing limit, the external loss rate of photons is large compared to the absorption rate, hence the system is far from equilibrium. In the photon-BEC limit on the other hand,

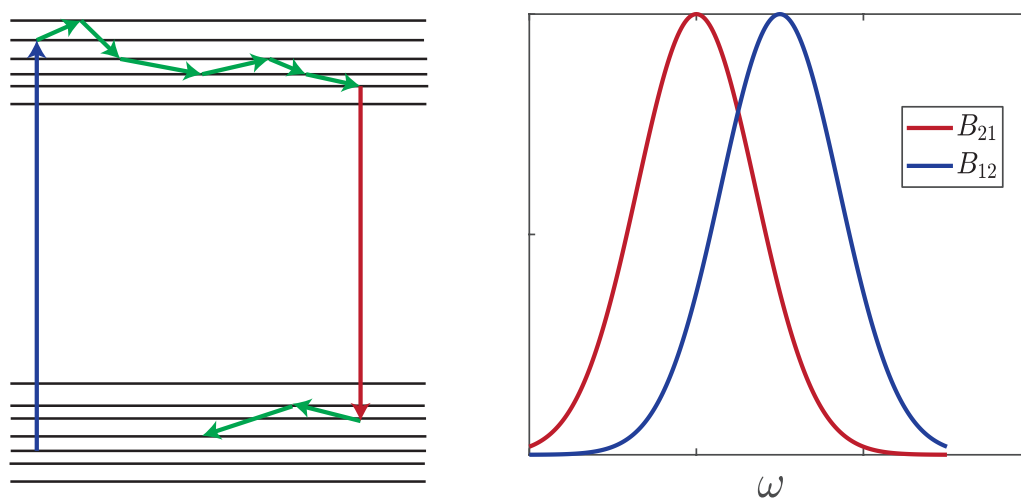


FIGURE 10.1: *Left panel: Thermalization mechanism of photons by dye-molecules. (1) Initially, the dye-molecule is in its optical ground state, with thermal rovibrational excitations. (2) Then, one high energy photon (blue arrow) is absorbed. This excites the molecule optically, and the excessive photon energy pushes the rovibrational modes also out of equilibrium. (3) Collisions with solvent molecules restore the rovibrational occupation to thermal equilibrium (4) From this thermal state, a new photon is emitted with lower energy. (5) Again, collisions with solvent molecules restore the rovibrational occupation to thermal equilibrium. Right panel: As a consequence, emission and absorption spectra differ and are related by the Kennard-Stepanov law.*

the absorption rate is sufficiently large to allow for the repeated interactions with the molecules to cause thermalization and the timescale associated with driving and external losses is much slower. A consequence is that lasers generally need population inversion for the gain medium, whereas a photon BEC does not. A true BEC has a condensed (macroscopically occupied) ground mode and a thermal occupation of the excited modes. For a laser, any mode can be bose-enhanced but the overall distribution will not be thermal. Studying the full phase diagram, it turns out that in a regime where both the driven-dissipative and thermalization mechanisms are strong, multimode condensation may occur [288].

10.1.2 INTERACTIONS IN A PHOTON BEC

As we have noted, condensation of photons does not require direct photon-photon interactions. Nonetheless, such effects can still take place in the dye liquid and have an influence. There are two kinds of nonlinear effects in photon condensates. Most important are usually the *thermo-optical* effects [289], resulting in a delayed interaction. The dye heats slightly from nonradiative relaxation of the excited molecules. This causes the refractive index of the solvent to change locally so that the optical path length decreases, resulting in an increasing potential and thus repulsion of future photons. Interestingly, in a recent experiment using olive oil [290], it has been shown that such thermo-optical effects are able to result in bistable behaviour, similar to the one studied in section 5.2. Although our model could in principle be extended to incorporate such effects, we will not study them as they take place on long timescales compared to our simulations (a mean-field study has recently been performed in Ref. [291]). Instead, we will look here at the influence of a weak (instantaneous) *Kerr-nonlinearity* here, which is known to affect the coherence properties of cold Bose [292] and Fermi [293] gases and exciton-polaritons [275]. A Kerr effect can naturally emerge in experimental setups, where a not entirely decoherent dye induces a natural Kerr effect [294, 295]. Furthermore, it is possible to engineer these interactions on purpose, which makes the photons behave more like polaritons and might open the possibility for effects such as superfluidity [296]. It has also been proposed to realize similar behavior with $\chi^{(2)}$ -nonlinear materials [297]. Although the precise intrinsic value of the Kerr nonlinearity in the commonly used dye molecules is still subject of debate (a recent discussion is given in [295]), we will show that already small values of the Kerr nonlinearity can substantially affect the coherence properties. Because the interaction strength can vary many orders of magnitude, we establish the

interaction scales on which the number and phase dynamics are altered significantly, while the associated energy scale per particle remains small compared to other energy scales.

10.1.3 MISCELLANEOUS STATE-OF-THE ART IN PHOTON BECS

A number of other results have been obtained with photon condensates, both theoretically and experimentally. Regarding the spatial properties, some work regarding the spatial profile and influence of the pump spot is studied in refs. [298, 299]. Experimentally, divergence of the correlation length (an important characteristic of phase transitions, as we have extensively studied in Part II) at the critical point has been measured in Ref. [300] and consistent with predictions for the ideal Bose gas (also divergence of the correlation time has been recently predicted [301], with the peculiarity that slowing down is also present far away from the critical point). Recent measurements of the spatial profile are shown in [302]. Refs. [303, 304] study the polarization aspects. Apart from the diverging correlation length and time, another experimental evidence of the Bose-Einstein phase transition is the observation of a cusp in the specific heat [305]. On the theoretical side, a variety of models exist in addition to mean-field (driven-dissipative Gross-Pitaevskii), from a full nonequilibrium quantum many-body approach in terms of a master equation [286], to a Schwinger-Keldysh formalism (see subsection 3.3.7) [306] and quantum-Langevin approach [307]. Remarkably, the condensation is predicted to occur with even only a few photons [308]. Ref. [309] proposes the simulation of black holes in a photon BEC. Two-mode emission has also been predicted [310].

Refs. [311, 312] predict theoretically the possibility for similar photon condensation in a semiconductor. With a different mechanism, thermalization of photons that leads to condensation can also occur using optomechanical coupling with the mirrors [313, 314]; in equilibrium with atomic gases [315] or by Doppler-cooling these [316]; [317]. Similar 1D condensation has also been studied in microtubes [318] and fibers [317].

10.1.4 STRUCTURE OF PART III

Part III of this thesis is organized as follows: in the remainder of this chapter 10, we will expand on the basic physics in a dye-cavity photon condensate and how it can be simulated with stochastic rate equations and the HPM, also with the

inclusion of a Kerr nonlinearity. In chapter 11 we describe the condensate as an open quantum system and construct a stochastic Schrödinger equation to describe its evolution. At high-densities, we will translate it into equations for an $N\Theta$ -Gaussian variational trajectory, with transitions between exact and variational regime when necessary and compare with the HPM model. Chapter 12 is devoted to a detailed numerical study of the number distribution and τ -temporal coherence, as well as the first-order temporal coherence, where predictions from the different methods are compared with each other and with analytic expressions that we have obtained. Finally, in section 12.3 we discuss some more recent developments that have followed.

We will assume for simplicity the presence of only a single photon mode. In many experimental setups, this is valid because of the lower population of excited modes, the fact that these do not interact and their small overlap with the condensate [319]. Analytical predictions considering only a single mode have also been successful in describing phenomena such as the decay of second-order coherence [284, 320]. As confinement is improving with novel experiments, restriction to a single mode becomes more realistic in practice. Nevertheless, beyond this single-mode description, photonic condensates in some parameter regimes can also exhibit effects arising from multiple modes that lead to interesting physics: if the occupation of other modes is large and the finite size of the reservoir is relevant, mode-competition can become important [321]. Large occupation of other modes in a substantially interacting system, will additionally result in Beliaev-Landau scattering which may give corrections to the single-mode results [49]. In a slightly different context, multimode effects also arise naturally when coupling multiple cavities with a condensate [322], we will discuss some recent insight in this regard in subsection 12.3.1.

10.2 Fluctuations in photon BECs

An interesting, presently realized, feature of photon BECs in a dye microcavity system, as opposed to other BECs, is that the number of photons does not remain fixed through time, even in the absence of losses. If the gain medium is sufficiently large such that saturation effects are small, the condensate will exhibit grand-canonical statistics [279, 323–325]. This is important, because the non-interacting Bose gas is one of the few systems where ensemble equivalence is not satisfied [99].

Along with these statistical fluctuations of the particle number, one observes

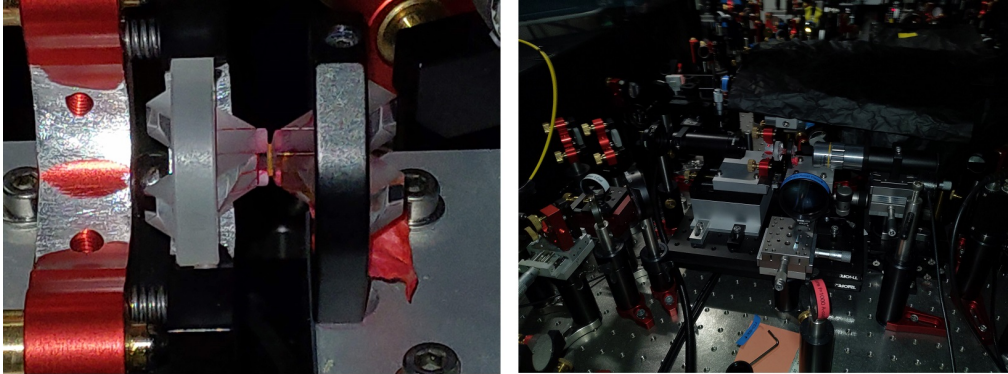


FIGURE 10.2: *Experimental setup in which photon condensation is realized: optical cavity with dye-liquid (left), and the optics for controls and measurement processing (right).*

fluctuations of the phase [284, 320, 326, 327], as first predicted in [328] using the Keldysh formalism. These can be understood from a heuristic phasor model (HPM) which we will explain in section 10.3, originally proposed in laser physics [29, 329], because the phase fluctuations at sufficiently large particle number correspond to the standard Schawlow-Townes broadening [29, 330]. The dynamics seems richer though, because in the grand-canonical regime, the particle number can become zero so that the phase of a subsequent new photon is entirely random, known as a ‘phase jump’. Although predictions from the HPM seem to match experiment so far, the theoretical understanding is still limited.

In particular, the phase jump picture suggests that a dramatic increase of temporal coherence occurs when the second order coherence falls below roughly $g^{(2)}(0) = 1.5$, where the probability of having zero photons in the condensate starts to become exponentially small [326]. We will show here that throughout the crossover between canonical and grand-canonical statistics, the behaviour of the phase coherence time behaves much smoother than expected by the phase jump analysis.

10.2.1 MODEL FOR A DRIVEN-DISSIPATIVE, INTERACTING PHOTON CONDENSATE

We assume a reservoir containing M_{tot} two-level dye molecules, of which M_{\uparrow} (M_{\downarrow}) are in the excited state (ground state). Because of the rapid decoherence due to collisions with solvent molecules [286], these numbers can be treated as classical

integers. We consider this reservoir to be coupled with a single, quantum mechanical, photon mode with number operator \hat{n} . Because we restrict ourselves in this section to number statistics, it is sufficient to consider only number eigenstates (Fock states) with n photons. The corresponding rate equation for the photons is then given by

$$dn = -dN + dM. \quad (10.6)$$

Here dN and dM are Poisson processes describing molecular absorption at rate $B_{12}M_{\downarrow}n$ and molecular emission at rate $B_{21}M_{\uparrow}(n+1)$, respectively, where B_{12} and B_{21} are the modified Einstein coefficients for absorption and emission [279]. For convenience, we define $\gamma := B_{12}M_{\downarrow}$ and $R := B_{21}M_{\uparrow}$. In the absence of losses, the total number of excitations $X = M_{\uparrow} + n$ is conserved such that $dM_{\uparrow} = -dn$ and $dM_{\downarrow} = dn$. For this system, many previous analytical results regarding the number distribution and correlation functions have been summarized in Refs. [284, 320]. In practice, the quality factors of cavities are restricted so that an additional loss at rate $\kappa n(t)$ [280] takes place, which is compensated by an additional pumping of molecules. In a typical experimental setup, $\gamma \gg \kappa$, so that we expect losses not to affect the number statistics significantly. As we are first concerned with ensemble statistics only, we have the freedom to choose the photon-counting unraveling for external losses [9], such that they are also modelled by a Poisson process dK . This results in a rate equation

$$dn = -dN + dM - dK. \quad (10.7)$$

In order to keep the long-time expectation value of X constant, the molecule reservoir is pumped through a process dP with constant rate $\kappa\bar{n}$, where \bar{n} is the average particle number such that

$$dM_{\uparrow} = dN - dM + dP \quad (10.8)$$

and $M_{\downarrow} = M_{tot} - M_{\uparrow}$. From equation (10.7), the average evolution is [284, 320]

$$\frac{\partial n}{\partial t} = B_{21}(X - n)(1 + n) - B_{12}n(M - X + n) - \kappa n \quad (10.9)$$

from which one finds that in the steady state

$$X(\bar{n}) = \frac{B_{12}\bar{n}(M + \bar{n}) + B_{21}\bar{n}(\bar{n} + 1) + \kappa\bar{n}}{B_{12}\bar{n} + B_{21}(\bar{n} + 1)}. \quad (10.10)$$

As we have seen Einstein coefficients B_{12}, B_{21} of the absorption and emission processes are thermodynamically related by the Kennard-Stepanov law (10.5). For noninteracting photons with frequency ω_c , the frequency dependence in (10.5) depends only on the detuning $\omega_c - \omega_0 = \Delta$.

A Kerr effect adds by definition an interaction energy $E_{\text{int}}(n) = \frac{U}{2}n^2$ to the photons. The n th photon now carries a frequency $\omega = \omega_c + [E_{\text{int}}(n) - E_{\text{int}}(n-1)] \approx \omega_c + Un$. As long as the interaction strength and particle number are not excessively large, only the relative difference between $B_{21}(\omega)$ and $B_{12}(\omega)$ is important, so that we can treat B_{12} as constant. With this, we rewrite (10.5) as

$$\frac{B_{21}(n)}{B_{12}} = \frac{w_{\downarrow}}{w_{\uparrow}} e^{-\beta(\Delta+Un)}. \quad (10.11)$$

10.3 The heuristic phasor model

10.3.1 A SEMICLASSICAL MODEL

Next, we proceed to the evolution of the phase. Rate equations (10.7), (10.8) are clearly insufficient in this regard. Some descriptions of the temporal coherence of a photon condensate rely on a heuristic phasor model (HPM, Figure 10.3) [284, 320], originally developed in laser physics [29, 329], that we will repeat here with the addition of Kerr interactions. According to the HPM, one considers the field to be classical such that the state is defined by a single phasor (corresponding to a coherent state as defined in subsection 4.2.1). The energy of a state with n photons, relative to a situation where all excitations are in the dye, is given by

$$E(n) = \Delta n + \frac{U}{2}n^2, \quad (10.12)$$

where Δ is the detuning between the cavity and dye transition. As we treat the phasor as an order parameter, the phase oscillates at speed [49]

$$v_p = \frac{dE}{dn} = \Delta + Un. \quad (10.13)$$

As statistical properties remain the same in a rotating frame, we may replace Δ in numerical simulations by $\Delta' = 0$ (no rotation for the vacuum) or $\Delta' = -U\bar{n}$ (no rotation on average) for convergence. Absorption, stimulated emission and external losses are here treated as deterministic currents that retain the coherence

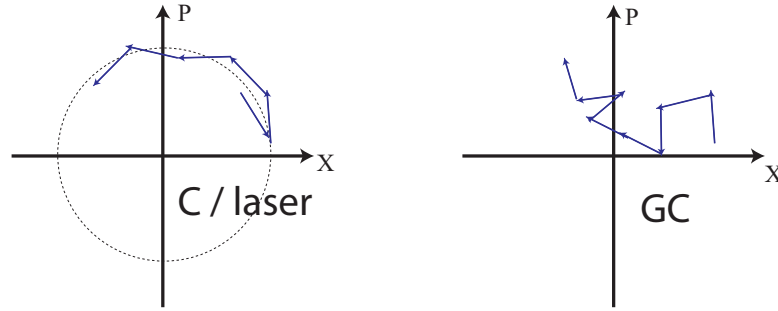


FIGURE 10.3: *The heuristic phasor model: Every timestep, a random phasor is added to the field. Left: in the original description for a laser, the field can only diffuse in the phase direction, while the photon number remains constant. In a canonical PC, the situation remains the same as the deterministic evolution quickly projects the state back to the equilibrium photon number, so that there remains effectively a 1D random walk in phase space. Right: in the grand-canonical regime, the field diffuses freely, a 2D random walk in phase space.*

entirely: they are modeled by an evolution of the particle number

$$dn = (R - \gamma - \kappa)n dt \quad (10.14)$$

where Rn is the rate of stimulated emission, γn the rate of absorption and κn the rate of external losses through the mirrors. Spontaneous emissions into the condensate mode are then taken into account as an additional Poisson process dM_s with expectation $\overline{dM_s} = R dt$. For each spontaneous emission, a vector $e^{i\phi}$ with unit magnitude and random phase is added to the field $\sqrt{n}e^{i\theta}$, with the motivation that this represents an additional photon that is fully incoherent [331]. In fact, such a spontaneous emission does not deterministically change the photon number with one and may even reduce it. As before, R and γ depend on $U\bar{n}$ and M_\uparrow , which is evolved simultaneously with the photon number. Since the photon number now varies continuously, the number of molecules in the ground (M_\downarrow) and excited (M_\uparrow) states are no longer integers.

10.3.2 PREDICTIONS

If M_\uparrow, M_\downarrow are sufficiently large such that R and γ remain approximately constant, the following analytic discussion applies: from geometric reasons, the phase evolves

as [329]

$$d\theta = \frac{1}{\sqrt{n}} \sin(\phi) dM_{\text{spont}}. \quad (10.15)$$

From this, we obtain $d\text{Mean}(\theta) = 0$ and

$$d\text{Var}[\theta] = \frac{\overline{R}}{2n} dt. \quad (10.16)$$

Meanwhile, the photon number evolves as

$$dn = (R - \gamma - \kappa)n dt + (1 + 2\sqrt{n} \cos \phi) dM_s, \quad (10.17)$$

such that

$$d\text{Mean}[n] = d\bar{n} = -(\gamma + \kappa)\bar{n}dt + R(\bar{n} + 1) dt, \quad (10.18)$$

and

$$d\text{Var}[n] = 2(R - \gamma - \kappa) \text{Var}[n] dt + R(2\bar{n} + 1) dt. \quad (10.19)$$

Despite its simplicity, the HPM is able to give a good explanation for Schawlow-Townes phase diffusion [29].

A special case occurs when the particle number vanishes entirely. Here, Eq. (10.16) becomes singular. This means that, in absence of other photons, the phase of the spontaneous emission is entirely random over the interval $[0, 2\pi[$ and a so-called phase jump occurs [284, 320].

In the following chapters, we will introduce a more sophisticated quantum trajectory model, and make a detailed comparison in numerical predictions with the HPM. For now, we note that, the HPM, leaving aside its simplicity and previous successes, suffers from some conceptual difficulties. First of all, by treating the field as classical, any squeezing effects are disregarded. Secondly, the continuous variation of the field is inconsistent with the fact that the emission and absorption are discrete processes at the level of the dye. Thirdly, it is physically dubious that only spontaneous emission and neither absorption nor stimulated emission cause shot noise. In the phasor model, the overly large noise from the spontaneous emission actually mimics the shot noise from all loss and gain processes. Note that even though a single spontaneous emission event adds one photon on average, this number has an uncertainty of \sqrt{n} , such that a spontaneous emission can even decrease the photon number. Finally, regarding the phase, one may wonder what is so special about these spontaneous emission events that they influence θ whereas other processes do not.

Describing photon condensates with $N\Theta$ Gaussian trajectories

To improve on the description of the phasor model, we treat the photon condensate as an open quantum system. Experimental realizations are described by a quantum trajectory model. At low photon numbers, we solve the trajectory exactly, whereas we use the $N\Theta$ -Gaussian variational ansatz, that shows excellent agreement with the exact result, at higher occupations.

11.1 The condensate as an open quantum system

In order to verify the validity of the HPM and to address the questions posed at the end of the previous chapter, we will study the photon field on a fully quantum mechanical level. Because of its driven-dissipative nature, the photon condensate is an open quantum system. The study of an open system starts with the distinction between system and environment (chapter 2). Here, we will treat the condensate mode as the system to be modelled by a quantum-mechanical stochastic wavefunction $|\psi(t)\rangle$. We will use the notation $\langle \cdot \rangle$ to denote quantum expectation values with respect to this wavefunction. The gain medium on the other hand is modeled classically: of the M_{tot} dye molecules, the integer amounts $M_{\uparrow}(t)(M_{\downarrow}(t))$ are in the excited(ground-) state as described by stochastic rate equations given in subsection 10.2.1. This is justified because of the frequent collisions with solvent molecules that lead to thermalization [281]¹.

¹Our model *cannot* be directly translated in a corresponding Lindblad master equation for photons only. This is because we are in a special case where we have actually split the system-environment boundary in two: the dye-molecules do retain a memory (number of excitations), but of an entirely classical nature. The solvent molecules that collide rapidly with the dye are completely untracked by our model.

The coherent evolution of the photons, in the frame rotating at the dye transition frequency, is governed by the Hamiltonian

$$\hat{H} = \Delta \hat{a}^\dagger \hat{a} + \frac{U}{2} \hat{a}^\dagger \hat{a}^\dagger \hat{a} \hat{a}, \quad (11.1)$$

where operators $\hat{a}(\hat{a}^\dagger)$ annihilate (create) a photon, defining also the number operator $\hat{n} = \hat{a}^\dagger \hat{a}$. Again, for numerical purposes we can go to a rotating frame and replace Δ by arbitrary Δ' . In absence of Hamiltonian dynamics, the evolution of the photon field is governed by three processes: gain (corresponding to emission of the dye molecules) occurring at rate $R(\langle \hat{n} \rangle + 1)$, absorption at rate $\gamma \langle \hat{n} \rangle$ and external losses through the mirrors at rate $\kappa \langle \hat{n} \rangle$. Because of the discrete nature of the dye excitations, the first two processes are naturally described through a photon-counting unraveling as if the photon number is ‘measured’ by the dye. External losses are modelled by a heterodyne unraveling, firstly because heterodyne detection is, in experiments where one is interested in the phase properties, typically performed on this leakage current [326]; secondly because it keeps the wave function localized in phase space, which will be helpful; and thirdly because it forms the most natural classical limit, as already discussed in the previous parts (subsection 2.4.4, section 7.1). By combining these processes, we readily obtain a stochastic Schrödinger equation (section 2.4)

$$\begin{aligned} |\tilde{\psi}\rangle = & \left[1 - i \left(\hat{H} - \frac{i}{2} (\gamma + R + \kappa) \hat{n} \right) dt + \kappa \langle \hat{a} \rangle^* \hat{a} dt \right. \\ & \left. + \sqrt{\kappa} \hat{a} dZ^* + \left(\frac{\hat{a}}{\|\hat{a}|\psi\rangle\|} - 1 \right) dN + \left(\frac{\hat{a}^\dagger}{\|\hat{a}^\dagger|\psi\rangle\|} - 1 \right) dM \right] |\psi\rangle. \end{aligned} \quad (11.2)$$

Here again, the tilde denotes that the left hand side describes the unnormalised wavefunction, to be renormalised after every timestep. $dZ = \frac{1}{\sqrt{2}}(dW_x + i dW_p)$ is again a complex (Itô) Wiener noise process such that $|dZ|^2 = dt$ and again, dN , dM describe Poisson processes as defined in subsection 10.2.1, where the role of n is now replaced by $\langle \hat{n} \rangle$.

Because the photon number typically becomes mesoscopic, exact evolution of (11.2) in a truncated Fock basis rapidly becomes computationally unfeasible. A number of variational approaches have been proposed for efficient simulation to this extent, as discussed in subsection 3.3.4. Here, the fact that the system is a single bosonic mode with large occupation, combined with a visual inspection of the Wigner function in Figure 11.1 leads us to model the field as being Gaussian

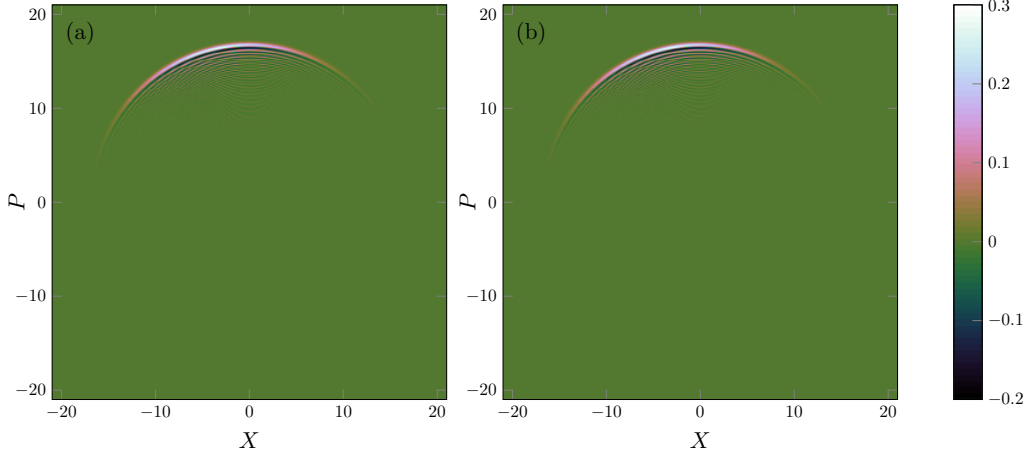


FIGURE 11.1: (a) Wigner function of a representative trajectory wavefunction in the exact regime, about to make the transition to the variational regime. (b): W-function of the corresponding variational trajectory with the same Gaussian moments. The similarity is striking. Note that this optical phase space (subsection 4.2.1) should not be confused with physical phase space, in which the photon BEC has been imaged in Ref. [332].

in particle number and phase: an $N\Theta$ -Gaussian state. Under this assumption, the field $|\psi\rangle$ is entirely characterized by the expectation values $\langle \hat{n} \rangle$, $\langle \hat{\theta} \rangle$, $\langle \hat{\delta}_n \hat{\delta}_n \rangle$, $\langle \hat{\delta}_\theta \hat{\delta}_\theta \rangle$ and $\langle \hat{\delta}_n \hat{\delta}_\theta \rangle_{\text{sym}}$, where $\hat{\delta}_O := \hat{O} - \langle \hat{O} \rangle$ is defined as the fluctuation of operator \hat{O} . The full variational equations for these expectation values are given in section 11.2. Note that if external decay vanishes, or if it is described as a photon-counting process, we find that $\langle \hat{\delta}_n \hat{\delta}_n \rangle \rightarrow 0$, $\langle \hat{\delta}_\theta \hat{\delta}_\theta \rangle \rightarrow \infty$ and the equations reduce to stochastic rate equation as in subsection 10.2.1. Interestingly, it is thus the (small) losses that allow us to define a phase, and avoid the condensate becoming a particle number eigenstate [142]. From Figure 11.1 it is clear that there is a significant amount of number squeezing in the system, unfortunately this seems hard to access with current experimental techniques because of the classical fluctuations of dye-molecule number that are untracked.

Because in the grand-canonical regime the particle number fluctuates also to vanishingly small densities, we will use a combination of both the exact (11.2) and variational (11.4)-(11.8) evolution. That is, we define threshold particle numbers $n_{\text{trans},\searrow}$, $n_{\text{trans},\nearrow}$. When $\langle \hat{n} \rangle < n_{\text{trans},\searrow} = 200$, we perform the exact evolution and when $\langle \hat{n} \rangle > n_{\text{trans},\nearrow} = 240$, we perform the variational evolution. In the intermediate window $n_{\text{trans},\searrow} < \langle \hat{n} \rangle < n_{\text{trans},\nearrow}$, the method of the previous regime remains in

use. The transitions between methods are discussed in more detail in section 11.3. Whereas the variational equations are solved by a straightforward Euler method with direct addition of the Poisson increments, for proper numerical convergence of the exact trajectories, an approach where the deterministic and diffusive evolution is separated from the individual jumps [333] is used (Appendix C).

11.2 The variational evolution

Following the approach of chapter 5 (where the sign convention for the parameter Δ differs, though), the trajectory evolution (11.2) can be recast in terms of (normalized) expectation values $\langle \hat{O} \rangle$ to be

$$\begin{aligned} d \langle O \rangle = & i \langle [H, O] \rangle dt - \frac{\gamma + R + \kappa}{2} (\langle \hat{n} O \rangle + \langle O \hat{n} \rangle) dt + (\gamma + R) \langle O \rangle \langle \hat{n} \rangle dt + \kappa \langle \hat{a}^\dagger O \hat{a} \rangle dt \\ & + \sqrt{\kappa} \left(\langle \hat{a}^\dagger \hat{\delta}_O \rangle dZ + \langle \hat{\delta}_O \hat{a} \rangle dZ^* \right) + \left(\frac{\langle \hat{a}^\dagger O \hat{a} \rangle}{\langle \hat{n} \rangle} - \langle O \rangle \right) dN + \left(\frac{\langle \hat{a} O \hat{a}^\dagger \rangle}{\langle \hat{n} \rangle + 1} - \langle O \rangle \right) dM, \end{aligned} \quad (11.3)$$

where again $\hat{\delta}_O = \hat{O} - \langle O \rangle$. By introducing a Dirac phase through $\hat{a} =: e^{i\hat{\theta}} \sqrt{\hat{n}}$ satisfying $[\hat{n}, \hat{\theta}] = i$ and using Wick's theorem, we obtain for the Gaussian correlation functions $\langle \hat{n} \rangle$, $\langle \hat{\theta} \rangle$, $\langle \hat{\delta}_n \hat{\delta}_n \rangle = \langle \hat{n} \hat{n} \rangle - \langle \hat{n} \rangle^2$, $\langle \hat{\delta}_\theta \hat{\delta}_\theta \rangle = \langle \hat{\theta} \hat{\theta} \rangle - \langle \hat{\theta} \rangle^2$, $\langle \hat{\delta}_n \hat{\delta}_\theta \rangle_{\text{sym}} = \langle \hat{n} \hat{\theta} \rangle / 2 + \langle \hat{\theta} \hat{n} \rangle / 2 - \langle \hat{n} \rangle \langle \hat{\theta} \rangle$ the evolution

$$\begin{aligned} d \langle \hat{n} \rangle = & -(\gamma + R) \langle \hat{\delta}_n \hat{\delta}_n \rangle dt - \kappa \langle \hat{n} \rangle dt + 2 \operatorname{Re} [(C_2 - C_1) \sqrt{\kappa} dZ] \\ & + \left(\frac{\langle \hat{\delta}_n \hat{\delta}_n \rangle}{\langle \hat{n} \rangle} - 1 \right) dN + \left(\frac{\langle \hat{\delta}_n \hat{\delta}_n \rangle}{\langle \hat{n} \rangle + 1} + 1 \right) dM \end{aligned} \quad (11.4)$$

$$\begin{aligned} d \langle \hat{\delta}_n \hat{\delta}_n \rangle = & -2\kappa \langle \hat{\delta}_n \hat{\delta}_n \rangle dt + \kappa \langle \hat{n} \rangle dt - 2\kappa |C_2 - C_1|^2 dt \\ & + 2 \operatorname{Re} [(D_3 - 2C_2 + C_1(1 - \langle \hat{\delta}_n \hat{\delta}_n \rangle)) \sqrt{\kappa} dZ] \\ & - \frac{\langle \hat{\delta}_n \hat{\delta}_n \rangle^2}{\langle \hat{n} \rangle^2} dN - \frac{\langle \hat{\delta}_n \hat{\delta}_n \rangle^2}{(\langle \hat{n} \rangle + 1)^2} dM \end{aligned} \quad (11.5)$$

$$\begin{aligned} d \langle \hat{\theta} \rangle &= \left(-\Delta + \frac{U}{2} \right) - U \langle \hat{n} \rangle - (\gamma + R) \langle \hat{\delta}_n \hat{\delta}_\theta \rangle_{\text{sym}} dt + 2 \operatorname{Re} \left[C_6 \sqrt{\kappa} dZ \right] \\ &\quad + \frac{\langle \hat{\delta}_n \hat{\delta}_\theta \rangle_{\text{sym}}}{\langle \hat{n} \rangle} dN + \frac{\langle \hat{\delta}_n \hat{\delta}_\theta \rangle_{\text{sym}}}{\langle \hat{n} \rangle + 1} dM \end{aligned} \quad (11.6)$$

$$\begin{aligned} d \langle \hat{\delta}_\theta \hat{\delta}_\theta \rangle &= -2U \langle \hat{\delta}_n \hat{\delta}_\theta \rangle_{\text{sym}} + \frac{\kappa}{4} E_1 dt - 2\kappa |C_6|^2 dt + 2 \operatorname{Re} \left[(D_1 - \langle \hat{\delta}_\theta \hat{\delta}_\theta \rangle C_1) \sqrt{\kappa} dZ \right] \\ &\quad + \left(\frac{-\langle \hat{\delta}_n \hat{\delta}_\theta \rangle_{\text{sym}}^2}{\langle \hat{n} \rangle^2} + \frac{E_1}{4 \langle \hat{n} \rangle} \right) dN + \left(\frac{-\langle \hat{\delta}_n \hat{\delta}_\theta \rangle_{\text{sym}}^2}{(\langle \hat{n} \rangle + 1)^2} + \frac{E_2}{4(\langle \hat{n} \rangle + 1)} \right) dM \end{aligned} \quad (11.7)$$

$$\begin{aligned} d \langle \hat{\delta}_n \hat{\delta}_\theta \rangle_{\text{sym}} &= -U \langle \hat{\delta}_n \hat{\delta}_n \rangle - \kappa \langle \hat{\delta}_n \hat{\delta}_\theta \rangle_{\text{sym}} dt - 2\kappa \operatorname{Re} \left[(C_2 - C_1) C_6^* \right] dt \\ &\quad + 2 \operatorname{Re} \left[\left(-C_6 - \left(\langle \hat{\delta}_n \hat{\delta}_\theta \rangle_{\text{sym}} + \frac{i}{2} \right) C_1 + D_2 \right) \sqrt{\kappa} dZ \right] \\ &\quad - \langle \hat{\delta}_n \hat{\delta}_n \rangle \frac{\langle \hat{\delta}_n \hat{\delta}_\theta \rangle_{\text{sym}}}{\langle \hat{n} \rangle^2} dN - \langle \hat{\delta}_n \hat{\delta}_n \rangle \frac{\langle \hat{\delta}_n \hat{\delta}_\theta \rangle_{\text{sym}}}{(\langle \hat{n} \rangle + 1)^2} dM. \end{aligned} \quad (11.8)$$

Here, the coefficients C and D , and E , perturbatively in orders of inverse $\langle \hat{n} \rangle$, are defined in Appendix B.

By considering the measurements to be perfect, we can do a restriction towards pure states, for which relation

$$\langle \hat{\delta}_n \hat{\delta}_n \rangle \langle \hat{\delta}_\theta \hat{\delta}_\theta \rangle - \langle \hat{\delta}_n \hat{\delta}_\theta \rangle_{\text{sym}}^2 = \frac{1}{4} \quad (11.9)$$

is satisfied (Equation 5.19). This constraint allows us to compute $\langle \hat{\delta}_\theta \hat{\delta}_\theta \rangle$ (or another variance) directly from the others.

11.3 How to use a phase operator even though it doesn't exist? Transitions between exact and variational regimes

11.3.1 FROM VARIATIONAL TO EXACT

When $\langle \hat{n} \rangle$ decreases from the variational regime below the threshold $n_{\text{trans}, \searrow}$, the $N\Theta$ -Gaussian state must be explicitly expressed in the Fock basis to continue numerically exact evolution.

As discussed in subsection 4.2.2, the Gaussian state is obtained as the ground state of an effective Hamiltonian, by exploiting the symmetry from (\hat{X}, \hat{P}) to $(\hat{n}, \hat{\theta})$

(section 4.5), we find that it is of the form

$$\begin{aligned} \hat{H}_{\text{eff}} = & (\hat{n} - \langle \hat{n} \rangle)^2 \langle \hat{\delta}_\theta \hat{\delta}_\theta \rangle + (\hat{\theta} - \langle \hat{\theta} \rangle)^2 \langle \hat{\delta}_n \hat{\delta}_n \rangle \\ & - (\hat{n} - \langle \hat{n} \rangle)(\hat{\theta} - \langle \hat{\theta} \rangle) \langle \hat{\delta}_n \hat{\delta}_\theta \rangle_{\text{sym}} - (\hat{\theta} - \langle \hat{\theta} \rangle)(\hat{n} - \langle \hat{n} \rangle) \langle \hat{\delta}_n \hat{\delta}_\theta \rangle_{\text{sym}}. \end{aligned} \quad (11.10)$$

We now encounter the problem that in fact, no hermitian phase operator $\hat{\theta}$ exists, as phase is not a true observable [154]. However, as long as the Fock space is truncated (which is the case here) at level N_{max} , a meaningful phase operator can be obtained through the Pegg-Barnett formalism to be

$$\hat{\theta}_{PB}(\theta_0) = \theta_0 + \frac{N_{\text{max}}\pi}{N_{\text{max}} + 1} + \frac{2\pi}{N_{\text{max}} + 1} \sum_{j \neq k}^{N_{\text{max}}} \frac{\exp\{i(j-k)\theta_0\} |j\rangle \langle k|}{\exp\{i(j-k)2\pi/(N_{\text{max}} + 1)\} - 1} \quad (11.11)$$

[154]. One free parameter, θ_0 , remains, corresponding to the phase-cut. That is, because phase is a periodic variable, there must be a cut where (going counter-clockwise) the phase sharply changes with -2π . In order to avoid spurious effects of this cut, we will use $\theta_0 = \langle \hat{\theta} \rangle - \pi$ such that the $N\Theta$ -Gaussian state is as far from the phase-cut as possible.

Using the operators \hat{n} and $\hat{\theta} := \hat{\theta}_{PB}(\langle \hat{\theta} \rangle - \pi)$, the effective Hamiltonian is constructed. $|\psi\rangle$ is obtained as the eigenvector of \hat{H}_{eff} corresponding to the lowest eigenvalue.

11.3.2 FROM EXACT TO VARIATIONAL

When, in the exact regime, $\langle \hat{n} \rangle = \langle \psi | \hat{n} | \psi \rangle$ increases above $n_{\text{trans},\nearrow}$, the Gaussian moments must be computed. As in the previous case, this is entirely straightforward regarding $\langle \hat{n} \rangle$ and $\langle \hat{\delta}_n \hat{\delta}_n \rangle$. For the phase, we want to use an operator $\hat{\theta}_{PB}(\theta_0)$ again, although it is this time not a priori clear which value of θ_0 to use. We will therefore do an initial guess $\theta_0^{(0)}$ and construct a corresponding $\hat{\theta}_{PB}^{(0)} = \hat{\theta}_{PB}(\theta_0^{(0)})$. We then iteratively use $\theta_0^{i+1} = \langle \psi | \hat{\theta}_{PB}^{(i)} | \psi \rangle - \pi$ and repeat the procedure self-consistently until convergence is reached. The resulting $\hat{\theta}_{PB}(\theta_0^{(f)})$ can then be used to proceed in calculating the Gaussian moments. We have verified that the above procedure results in the expected phase $\arg[\alpha]$ when applied to an arbitrary coherent state $|\alpha\rangle$ (Figure 11.2).

After this transition, we use purity relation (5.19) as a numerical check and as verification for the validity of the Gaussian ansatz.

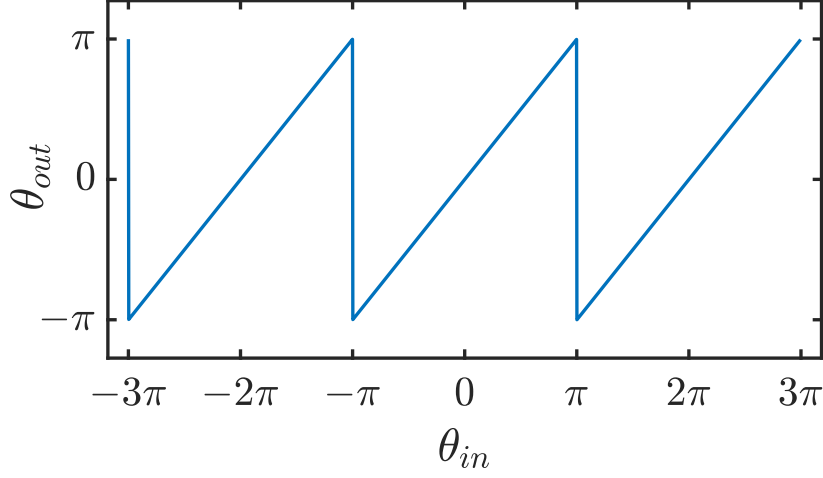


FIGURE 11.2: For coherent states $|\alpha\rangle$ displaced to $\alpha = 1e^{i\theta_{in}}$, the iterative procedure to update Pegg-Barnett phases leads, bearing in mind periodicity, to the expected phase $\theta_{out} = \theta_{in} \pmod{2\pi}$. As a tolerance, the iterations were stopped if the difference between phase predictions in subsequent iterations dropped below $1e-3$.

The fact that two different definitions of a phase operator (Dirac and Pegg-Barnett) are used, causes no problems because the particle number at the transitions is sufficiently large and the trajectory states are sufficiently well-behaved.

11.4 Predictions

Similar to the HPM, we calculate the evolution of the moments of the field while treating γ, R as constant. We will use the variational equations from section 11.2 as a starting point, considering highest order $\mathcal{O}(\langle \hat{n} \rangle) = \mathcal{O}(\langle \hat{\delta}_n \hat{\delta}_n \rangle) = \mathcal{O}(\langle \hat{\delta}_\theta \hat{\delta}_\theta \rangle^{-1})$ (this relation between orders can be seen from a coherent state where $\langle \hat{n} \rangle = \langle \hat{\delta}_n \hat{\delta}_n \rangle$ and relation (5.19)). Under the assumption $\langle \hat{\delta}_n \hat{\delta}_\theta \rangle_{\text{sym}} \equiv 0$ and neglecting noise, one obtains as stationary solution for the phase variance (11.7),

$$\langle \hat{\delta}_\theta \hat{\delta}_\theta \rangle_{\text{stat}} = \frac{1 + \sqrt{2(1 + \frac{\gamma+R}{\kappa})}}{4 \langle \hat{n} \rangle}. \quad (11.12)$$

Substituting in (11.6) results in

$$d \langle \hat{\theta} \rangle = \frac{\kappa + \gamma + R}{2\sqrt{\langle \hat{n} \rangle}} dW_\theta, \quad (11.13)$$

where dW_θ denotes a real Wiener process from which

$$d \text{Mean}[\hat{\theta}] = d \overline{\langle \hat{\theta} \rangle} = 0 \quad (11.14)$$

and

$$d \text{Var}_2 \hat{\theta} = d \left[\overline{\langle \hat{\theta} \hat{\theta} \rangle} \right] - d \left[\overline{\langle \hat{\theta}^2 \rangle} \right] = \frac{\kappa + \gamma + R}{4 \langle \hat{n} \rangle} dt. \quad (11.15)$$

Recall from subsection 2.4.3 that in trajectory simulations, the total variance of an observable $\text{Var}[\hat{O}] = \text{Var}_1 \hat{O} + \text{Var}_2 \hat{O}$ can be decomposed into the intra-trajectory variance $\text{Var}_1 \hat{O} = \overline{\langle \hat{\delta}_\theta \hat{\delta}_\theta \rangle}$ and the inter-trajectory variance $\text{Var}_2 \hat{O} = \text{Var} \langle \hat{O} \rangle$. Here, from our stationary assumption, $d \text{Var}_1 \hat{\theta} = 0$ such that $d \text{Var}[\hat{\theta}] = d \text{Var}_2 \hat{\theta}$.

Similarly, we obtain the stationary solution for the particle number from (11.5):

$$\langle \hat{\delta}_n \hat{\delta}_n \rangle_{\text{stat}} = \frac{\sqrt{\kappa}}{\sqrt{2} \sqrt{\gamma + R}} \langle \hat{n} \rangle, \quad (11.16)$$

where we have used $\kappa \ll \gamma, R$. Substituting in (11.4) results in

$$d \text{Mean}[\langle \hat{n} \rangle] = d \overline{\langle \hat{n} \rangle} = (R - \gamma - \kappa) \overline{\langle \hat{n} \rangle} dt \quad (11.17)$$

and

$$\begin{aligned} d \text{Var} \hat{n} &= d \text{Var}_2 \hat{n} = d \overline{\langle \hat{n} \rangle^2} - d \overline{\langle \hat{n} \rangle^2} \\ &= [2(R - \gamma - \kappa) \text{Var} \hat{n} + (\gamma + R + \kappa) \overline{\langle \hat{n} \rangle}] dt. \end{aligned} \quad (11.18)$$

Comparing Eqs. (11.15), (11.17) (11.18) with the predictions from the HPM (10.16), (10.18), (10.19), the similarity is evident. However, the HPM predicts a variance increase proportional to the gain R , whereas (11.15), (11.18) are symmetrical in R, γ, κ . In the steady-state however, $R \approx \gamma + \kappa$ at least to highest order in $\langle \hat{n} \rangle$, such that the time-averaged result is the same. This correspondence is also reminiscent to the result for a laser [29]: also there, the phasor model predicts a phase diffusion proportional to the gain coefficient R whereas a more detailed quantum-mechanical derivation makes clear that $\frac{R+\kappa}{2}$ is the correct quantity, although both become equivalent at threshold where $R \approx \kappa$.

In Figure 11.3, a comparison between the evolution of phase and particle number in a single HPM sample (a,b,c) and a single trajectory (d,e,f) is given. On short times there is a qualitative difference with the HPM: discrete steps corresponding to emission events are replaced by scale-invariant noise, induced

by the heterodyne detection and fueled by all emission and absorption processes. However, current experiments cannot resolve these small fluctuations on short timescales, as long as they do not affect correlation functions. It is clear from fig. 11.3 that the predictions of both methods become qualitatively indistinguishable on longer timescales. We see also that for both methods, phase diffuses more rapidly at lower photon numbers, as predicted by Eqs. (10.16), (11.15).

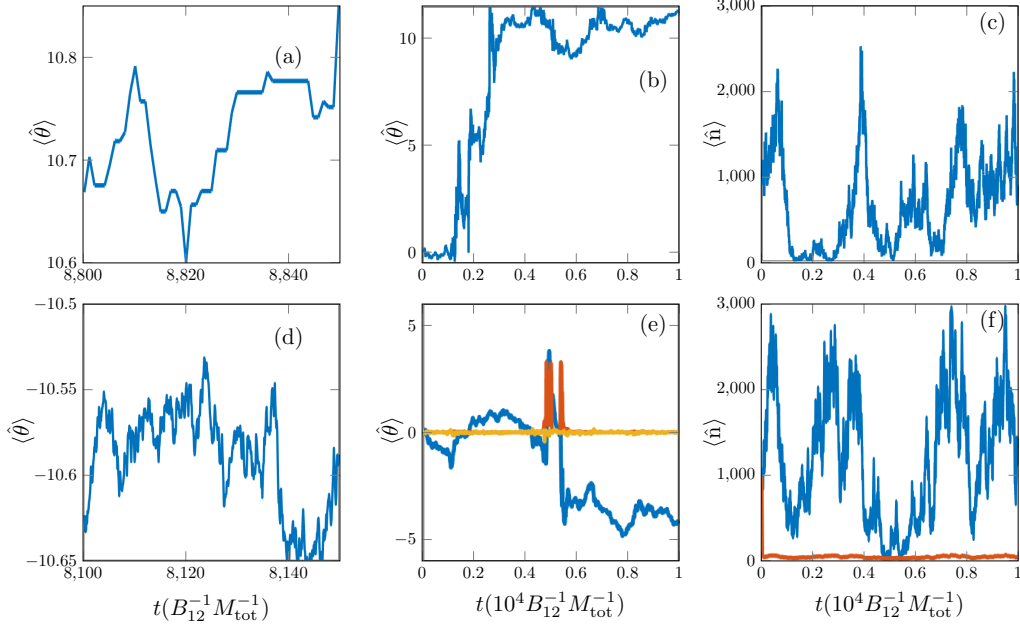


FIGURE 11.3: Some typical single shot realizations, as predicted by (a,b,c) the HPM versus (d,e,f) the quantum trajectories. We see that there is a clear qualitative difference on short timescales: whereas the fluctuations of the phasor model (a) are discrete events corresponding to spontaneous emissions, noise remains on all scales within a quantum trajectory (d). However, this qualitative difference is washed away on longer timescales, where the phase evolution according to the HPM (b) becomes equivalent to the one of a trajectory (e, blue line). Also regarding the photon number, the evolution of the HPM (c) is indistinguishable from the trajectory (f, blue line) on sufficiently large timescales corresponding to typical experiments. Furthermore, it is clear that both according to the HPM and the trajectories, phase fluctuates the most when the photon number is low. For completeness, we have added also the other Gaussian moments of the trajectory: on (e) $\langle \hat{\delta}_\theta \hat{\delta}_\theta \rangle$ (red) and $\langle \hat{\delta}_n \hat{\delta}_\theta \rangle_{\text{sym}}$ (yellow) are typically small but show spikes at phase jumps. On (f), we see that generally $\langle \hat{\delta}_n \hat{\delta}_n \rangle$ (red) $<$ $\langle \hat{n} \rangle$, reflecting number squeezing. Note that $\langle \hat{\theta} \rangle$ is only defined modulo 2π .

Coherence of a photon condensate

We obtain precise expressions for the number distribution in presence of a Kerr nonlinearity, and find that these agree with numerical simulations, even in presence of some external losses. This driven-dissipative aspect does cause a delayed anti-bunching effect nevertheless, as witnessed by the second-order temporal correlation function. First-order correlations that contain phase information decay according to the normal Schawlow-Townes effect in the canonical regime, and only twice as fast in the grand-canonical regime, unlike what was previously believed. Kerr interactions induce an additional Henry phase diffusion.

12.1 Number statistics: effect of interactions and losses

12.1.1 NUMBER DISTRIBUTION

Following the approach of Ref. [279], the steady state number distribution can be found by assuming detailed balance condition

$$R_n \mathcal{P}_n = \gamma_{n+1} \mathcal{P}_{n+1}, \quad (12.1)$$

where \mathcal{P}_n denotes the probability for the condensate mode to contain exactly n photons (note that for fixed M, X ; M_\uparrow, M_\downarrow and consequently R, γ are a function of n as indicated by the subscript). By writing $\gamma_{n+1} = B_{12} M_{\downarrow, n+1} = (M - X + n + 1) B_{12}$ and $R_n = B_{21} M_{\uparrow, n} = (X - n) B_{21}(n)$ we obtain

$$\frac{\mathcal{P}_{n+1}}{\mathcal{P}_n} = \frac{X - n}{M - X + n + 1} \frac{B_{21}(n)}{B_{12}} \quad (12.2)$$

such that using (10.11),

$$\begin{aligned}\frac{\mathcal{P}_n}{\mathcal{P}_0} &= \frac{(M-X)!X!}{(M-X+n)!(X-n)!} e^{-\beta[\Delta n+(U/2)n^2]} \\ &= \frac{\binom{X}{n}}{\binom{M_{\text{tot}}-X+n}{n}} e^{-\beta[\Delta n+(U/2)n^2]},\end{aligned}\quad (12.3)$$

where the expression with binomial coefficients is numerically better conditioned. In the limit of an infinite reservoir, (12.3) reduces to a Bose-Einstein distribution

$$\mathcal{P}_n \propto \left(\frac{\overline{M}_\uparrow}{\overline{M}_\downarrow}\right)^n e^{-\beta E[n]} = \exp\left(-\frac{(\Delta-\mu)n+(U/2)n^2}{T}\right),\quad (12.4)$$

where the chemical potential is $\mu = T \log(\overline{M}_\uparrow/\overline{M}_\downarrow)$.

In Fig. 12.1, we see that the predictions in number distributions (12.3), closely match numerical results from rate equations (10.7), for a set of parameters corresponding to recent experiments [334], as summarized in Tab. 12.1. As for the interaction strength, we have taken the value $U = 10^{-5}\hbar M_{\text{tot}}B_{12}$, corresponding to a dimensionless interaction parameter $\tilde{g} = \frac{U}{\Omega\hbar} \approx 9.95 \times 10^{-5}$ for trapping frequency $\Omega \approx 8\pi \times 10^{10}$ Hz, which is larger than the most common estimates of the natural Kerr effect [295, 319]. Importantly, by defining the effective reservoir size

$$M_{\text{eff}} = \frac{M_{\text{tot}}}{2} [1 + \cosh(\beta(\Delta + U\bar{n}))]^{-1},\quad (12.5)$$

one can distinguish in the noninteracting case a canonical regime with Poissonian number statistics ($\bar{n}^2 \gg M_{\text{eff}}$), a grand-canonical regime with Bose-Einstein statistics ($\bar{n}^2 \ll M_{\text{eff}}$, (12.4)) and a transition region ($\bar{n}^2 \approx M_{\text{eff}}$).

For our parameters in Tab. 12.1, we have an effective reservoir size $M_{\text{eff}} = 7.6 \times 10^7 \gg \bar{n}^2 = 10^6$ such that the system is rather on the grand-canonical side of this crossover.

Definition (12.5) only depends on U to the extent that it changes the average energy per photon, a minor correction for our parameters considered. Nevertheless, also for fixed M_{eff} , the number distribution is significantly altered by interactions: the number fluctuations are reduced, as predicted by Ref. [324]. This can be understood from statistical physics in the grand-canonical regime: by approximating n to be continuous and integrating (12.4) over positive n , we obtain the grand-canonical partition function \mathcal{Z} . From the associated free energy

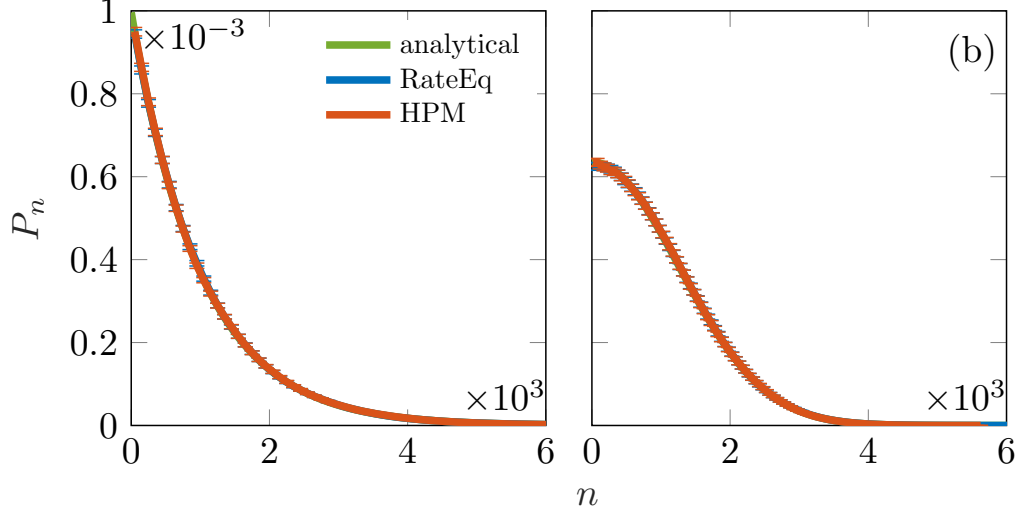


FIGURE 12.1: Particle number distribution (12.3) without (a) and with (b) interactions, for the parameters given in Tab. 12.1. Green lines: analytical results (12.3), covered by the numerical simulation of the rate-equations (10.7), (10.8) (blue) and HPM (red) results. In both cases there is a very good agreement between the analytical prediction and numerical results obtained by rate equations. These are also matched by the predictions from the HPM. Stochastic results are obtained from 10^3 independent samples, each evolving a time $10^5 B_{12}^{-1} M_{tot}^{-1}$.

Parameter	value
B_{12}	2.5 kHz
M_{tot}	10^9
Δ	$-2.4kT/\hbar$
T	300 K
U	$10^{-5} B_{12} M_{tot} = 6.4 \times 10^{-7} k_B T/\hbar$
$w_{\uparrow}/w_{\downarrow}$	1
κ	$2.2 \text{ GHz} = 8.3 \times 10^{-4} B_{12} M_{tot}$

TABLE 12.1: Experimental parameters corresponding to Rhodamin 6G dye at 560 nm. [334]. Further, we have taken for the simulations $\bar{n} = 1000$, which somewhat smaller than in typical experimental setups to reduce the relevant timescales. We have chosen the finite value of interaction strength such that the phase and number statistics are significantly altered ($\sigma = \frac{U\bar{n}^2}{T}$ of order one), while the average interaction energy per particle $U\bar{n}$ remains small compared to other energy scales. The notion of ‘without interactions’ refers to $U = 0$, whereas ‘without losses’ means $\kappa = 0$

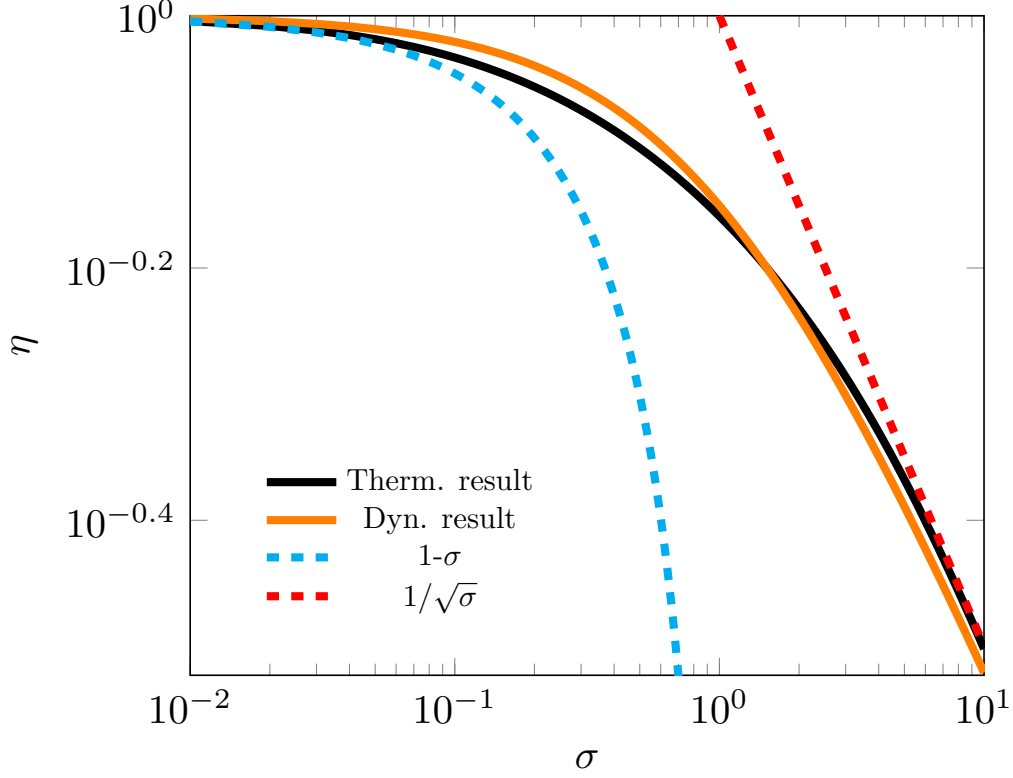


FIGURE 12.2: Amount of fluctuations $\eta = \frac{\sqrt{\bar{n}^2 - \bar{n}^2}}{\bar{n}}$ in a grand-canonical condensate as function of the interaction parameter σ as thermodynamically derived (black), with asymptotics $1 - \sigma$ (cyan,dashed) and $\sigma^{-1/2}$ (red,dashed). Orange: the dynamical approximate result (12.11).

$F = -T \log \mathcal{Z}$, the equation of state $\bar{n}(\mu)$ can be obtained, as well as the amount of number fluctuations $\text{Var}[n](\mu)$. Eliminating μ , the ratio $\eta = \frac{\sqrt{\bar{n}^2 - \bar{n}^2}}{\bar{n}}$ can be expressed as a function of the interaction parameter $\sigma = \frac{U\bar{n}^2}{T}$, as shown on Fig. 12.2. Asymptotically, the relative amount of fluctuations η decreases as $1 - \sigma$ for small σ and as $\sigma^{-1/2}$ for large interactions σ . For our parameters, we find $\sigma = 0.64$, corresponding to $\eta = 0.75$, whereas our noninteracting condensate has $\eta = 0.99$. Thus, interactions that are small enough to modify the single-photon energy only weakly, can still have a strong influence on the system as the total interaction energy $U\bar{n}^2$ can become of the order of the thermal energy.

For a finite reservoir, μ becomes dependent on n , so that the above thermodynamic analysis is no longer valid. η can also be computed from the number distribution (12.3) (fixing \bar{n} for this number distribution can be done self-consistently

using (12.12)), or analytically from the dynamical argument below.

12.1.2 DECAY OF SECOND-ORDER CORRELATIONS

The second order coherence time $\tau_c^{(2)}$, the decay time of $g^{(2)}(\tau) = \frac{\overline{n(t)n(t+\tau)}}{\bar{n}^2}$, can be obtained by an extension of the approach in [284, 320]. In linear approximation $B_{21} = \overline{B_{21}}(1 - \beta U \delta n(t))$, the average fluctuation evolves as

$$\begin{aligned} \frac{\partial}{\partial t} \delta n(t) = & \quad (12.6) \\ & - \left[\frac{\overline{B_{21}} X}{\bar{n}} + (B_{12} + \overline{B_{21}}) \bar{n} + \beta U \overline{B_{21}} M_{\uparrow} (1 + \bar{n}) \right] \delta n(t) \\ & + \mathcal{O}(\delta n(t)^2), \end{aligned}$$

where the driven-dissipative nature has been disregarded. Using the quantum regression theorem (section 2.6) we find that accordingly, the number correlations decay at rate

$$\Gamma_2 = \left[\frac{1 + \sigma}{\bar{n}(1 + e^{\beta(\Delta + U\bar{n})})} + \left(1 + e^{-\beta(\Delta + U\bar{n})}\right) \frac{\bar{n}}{M_{\text{tot}}} \right] B_{12} M_{\text{tot}} \quad (12.7)$$

$$= \left[1 + \sigma + \frac{\bar{n}^2}{M_{\text{eff}}} \right] \frac{B_{12} \overline{M_{\downarrow}}}{\bar{n}}, \quad (12.8)$$

As long as $U\bar{n} \ll \Delta$, the change in $\Gamma_2 = (\tau_c^{(2)})^{-1}$ from a noninteracting condensate is directly proportional to the interaction parameter σ . Note that the same expression (12.7) is also obtained if B_{21} is treated as constant while considering frequency dependence in B_{12} . We verify the validity of decay rate (12.7) by comparison to numerical simulations by rate equations in Fig. 12.3.

For generic parameter values, $g^{(2)}(0) = 1 + \eta^2$ can also be estimated by the stationary solutions of the expectation value of the second moment of the photon number

$$d[\delta n(t)^2] = 2\delta n(t) d[\delta n(t)] + d[\delta n(t)]^2 \quad (12.9)$$

$$= -2\Gamma_2 \delta n(t)^2 dt + R(\bar{n} + \delta n + 1) dt + \gamma(\bar{n} + \delta n), \quad (12.10)$$

from which

$$g^{(2)}(0) - 1 = \eta^2 = \frac{\overline{\delta n^2}}{\bar{n}^2} = \frac{1}{1 + \sigma + \frac{\bar{n}^2}{M_{\text{eff}}}}. \quad (12.11)$$

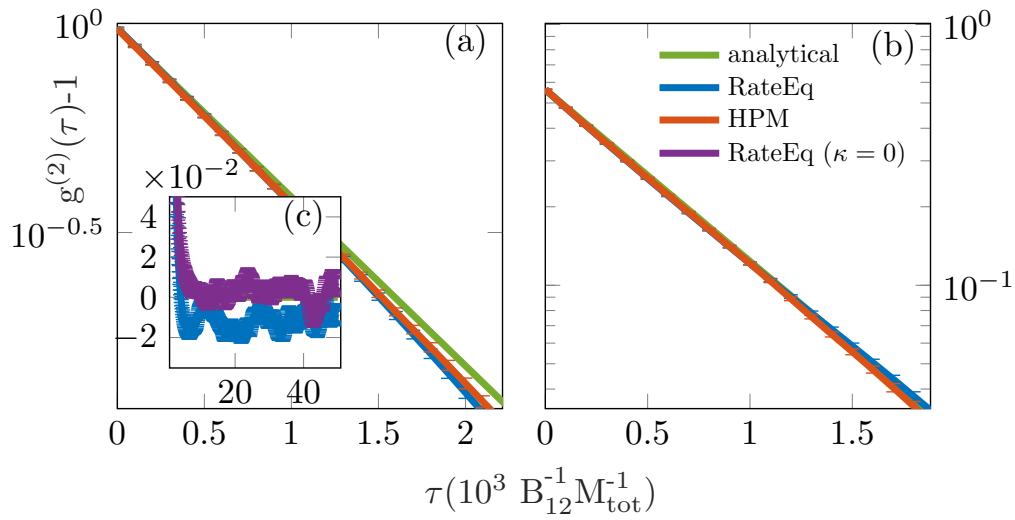


FIGURE 12.3: *Second order correlation functions for the grand-canonical parameters of Tab. 12.1, with the exponential decay (12.7), without (a) and with (b) interactions. Generally there is a good agreement (the plot of the analytical result is completely covered in (b)), though at later times deviations originating from the driven-dissipative character are visible. These results are again matched by the HPM (colors as in Fig. 12.1. Inset (c): $g^{(2)}(\tau_c^{(2)} < \tau < \tau_X) - 1$ becomes negative, while this is not the case without losses ($\kappa = 0$, purple).*

For an infinite reservoir ($M_{\text{eff}}/\bar{n}^2 \rightarrow \infty$), we can compare this dynamical result directly with the thermodynamic result above. As we see in Fig. 12.2, the relative difference in predictions for η remains smaller than 5% for all values of σ , and (12.11) becomes exact in the limit of large σ . We can attribute the deviations at smaller σ to higher order contributions in $d\delta n$.

Such an estimate of η is also useful to initiate the number of excited molecules in the numerical simulations. As can be seen from Eq. (10.10), both the average number of photons and its fluctuations determine the number of excited molecules:

$$M_{\uparrow} = X(\bar{n}) - \bar{n} = \frac{(B_{12}M + \kappa)\bar{n} + (B_{12} + B_{21})\bar{n}^2\eta^2}{B_{21}(\bar{n} + 1 - \beta U\bar{n}^2\eta^2) + B_{12}\bar{n}}. \quad (12.12)$$

12.1.3 LONG- τ (DELAYED) ANTIBUNCHING

In previous analytic discussions, we have disregarded the driven-dissipative nature of the system. Intuitively, one might expect that losses will reduce the second-order coherence time. Such an effect is not observed in the number distribution, as seen in Fig. 12.1.

However, as we see in Fig.12.3, $g^{(2)}(\tau)$ is altered on long timescales compared to the photon correlation time $\tau_c^{(2)}$, where a long- τ antibunching effect appears. This can be explained in the following way: if at $\tau = 0$ the stochastic particle number is $n = \bar{n} + \delta n$, the corresponding fluctuation modifies the excitation number by $\Delta X = -\kappa \delta n \tau_c^{(2)}$. Because $\bar{n} = \bar{n}(X)$, the particle number expectation value is altered to $\bar{n}' = \bar{n} + \frac{\partial \bar{n}}{\partial X} \Delta X$ where from (10.10), $\frac{\partial X}{\partial \bar{n}} \approx \frac{B_{12}B_{21}M_{\text{tot}}}{\bar{n}^2(B_{12}+B_{21})^2}$, so that $g^{(2)}(\tau)$ changes in the order of

$$\frac{\overline{nn'}}{\bar{n}^2} - \frac{\overline{n\bar{n}}}{\bar{n}^2} \approx \frac{\bar{n}^2(B_{12} + B_{21})^2}{B_{12}B_{21}M_{\text{tot}}} \kappa \tau_c^{(2)}, \quad (12.13)$$

where we used that in the grand-canonical regime, $\delta n \sim \bar{n}$. Expression (12.13) predicts a decrease in $g^{(2)}(\tau)$ of about 0.012. We verify this numerically by averaging $g^{(2)}(\tau)$ over a time-interval $10^4 B_{12}^{-1} M_{\text{tot}}^{-1} - 5 \times 10^4 B_{12}^{-1} M_{\text{tot}}^{-1}$, which is sufficiently larger than $\tau_c^{(2)}$ but smaller than the timescale of fluctuations in total excitation number τ_X and obtain a value $g^{(2)}(\tau_c^{(2)}) < \tau < \tau_X) - 1 = -0.012$ for the experimental κ and $g^{(2)}(\tau_c^{(2)} < \tau < \tau_X) - 1 = 0.003$ without losses, in agreement with our results. Of course, one always has $g^{(2)}(\infty) = 1$ as initial and final state become entirely independent, but the relaxation from deviation (12.13) only takes place over the timescale of the dynamics of X , namely $\tau_X = (\kappa \frac{\partial \bar{n}}{\partial X})^{-1}$, which is of order $10^5 B_{12}^{-1} M_{\text{tot}}^{-1}$

in our simulations. Because of the different values for $\tau_c^{(2)}$ and η , this effect is weaker in our simulations of the interacting condensate.

12.2 First-order coherence

In Fig. 12.4, the first order correlation function $g^{(1)}(\tau) = \frac{\overline{\alpha^*(t)\alpha(t+\tau)}}{|\alpha(t)|^2}$ is shown, and again predictions of the HPM agree well with the exact result, obtained by trajectories. In the noninteracting case, the decay of correlations is clearly exponential, whereas it is Gaussian in presence of interactions. The decay can be understood from multiple points of view, let us start with the noninteracting case.

12.2.1 THE GRAND-CANONICAL SCHAWLOW-TOWNES EFFECT, FORMERLY KNOWN AS 'PHASE JUMPS'

According to the HPM picture, absorption and stimulated emission only affect the phasor radially, as $d\sqrt{n} = \frac{dn}{2\sqrt{n}} = \frac{R-\gamma}{2}\sqrt{n} dt$, where we used eq. (10.14), and neglected the external losses. The stochastic evolution of the HPM can then be written in terms of the phasor alone as

$$d\alpha = -\frac{\gamma - R}{2}\alpha dt + dS, \quad (12.14)$$

where dS is additive noise corresponding to the spontaneous emissions. In the grand-canonical limit, γ and R can be treated as constants, so that for the expectation value,

$$d\bar{\alpha} = -\frac{\gamma - R}{2}\bar{\alpha} = \frac{-R}{2\bar{n}}\bar{\alpha}, \quad (12.15)$$

where we have used $\gamma\bar{n} = R(\bar{n} + 1)$ for the second equality. From the quantum regression theorem (section 2.6), it is then clear that

$$g^{(1)}(\tau) = e^{-t/\tau_c^{(1)}}, \quad (12.16)$$

where

$$\frac{1}{\tau_c^{(1)}} = \frac{R}{2\bar{n}} = \frac{B_{21}M_{\uparrow}}{2\bar{n}} \approx \frac{B_{12}M_{\downarrow}}{2\bar{n}} = \frac{B_{12}M_{\text{tot}}}{2\bar{n}(1 + e^{\beta\Delta})}. \quad (12.17)$$

By another line of reasoning, the phase evolution is dominated by large 'phase jumps' when the photon number in the cavity vanishes, as described in Refs. [284, 320, 326]. From estimating the probability of having zero photons in the cavity, one obtains the 'phase jump rate' $\Gamma_{\text{PJ}}^0 = \frac{B_{12}M_{\downarrow}}{\bar{n}^{\zeta}}$. In the grand-canonical limit, $\zeta = 1$, so

that this is consistent with (12.17) up to a scaling factor of order one. The picture of phase jumps would further predict that the phase evolution is suppressed if the probability for the zero-photon state vanishes ($\zeta \rightarrow \infty$), as occurs outside of the grand-canonical limit, towards the canonical regime $M_{\text{eff}} \ll \bar{n}^2$, where M_{eff} is defined as in Eq. (12.5). By additional numerical simulations shown in Fig. 12.5, we see that this is not the case. At most, the first-order coherence time, rescaled with the molecule number, only scales by a factor two. This is not entirely unsurprising as the remaining value corresponds to the standard Schawlow-Townes dephasing mechanism [29, 330] that occurs in the limit where the number distribution is sharply peaked, as can already be seen from (10.16). We are thus led to write generically

$$\Gamma_1 \equiv \frac{1}{\tau_c^{(1)}} = \frac{B_{12}\overline{M}_\downarrow}{\xi\bar{n}}, \quad (12.18)$$

where $\xi = 2$ in the grand-canonical limit and $\xi = 4$ in the canonical limit. Figure 10.3 provides a simple picture for this phenomenon: the canonical and grand-canonical regimes correspond, respectively, to a 1D and 2D random walk in phase space.

Comparing with the decay of second-order coherence (12.7), we find that

$$\frac{\tau_c^{(1)}}{\tau_c^{(2)}} = \frac{\Gamma_2}{\Gamma_1} \quad (12.19)$$

$$= \xi \left[1 + \sigma + \frac{\bar{n}^2}{M_{\text{eff}}} \right] \quad (12.20)$$

$$= \frac{\xi}{\eta^2} = \frac{\xi}{g^{(2)}(0) - 1}, \quad (12.21)$$

where we have used (12.11) for the third equality. However, in the inset of fig. 12.5, we see that on sufficiently short timescales, there is always an initial decay with $\xi = 2$. There is a clear intuition here: while only a few photons have been absorbed/emitted with the dye yet, M_\uparrow is only weakly altered and as such it cannot constrain the dynamics. In general, $\gamma - R = \bar{\gamma} - \bar{R} + (B_{12} + B_{21})\delta n$, where $\delta n = n - \bar{n}$. When, at short timescales, δn remains approximately constant, a similar reasoning to the grand-canonical regime yields

$$g^{(1)}(\tau) = \frac{e^{-\bar{R}\tau/(2\bar{n})}}{\bar{n}} n \exp\left(-\frac{(B_{12} + B_{21})\delta n}{2}\tau\right)$$

$$\begin{aligned}
&\approx e^{\frac{-\bar{R}}{(2\bar{n})}\tau} \left(1 - \frac{\eta^2}{2} (B_{12} + B_{21}) \bar{n} \tau \right) \\
&\approx e^{\frac{-\bar{R}}{(2\bar{n})}\tau}.
\end{aligned} \tag{12.22}$$

At later times, higher-order effects set in and restrict the dynamics.

It is instructive to compare these results with the ones obtained by Whittaker and Eastham [1, 335] in a polariton context. There, a Schawlow-Townes decay is predicted to be of the form

$$\left| g^{(1)}(\tau) \right| = \exp \left[\frac{\eta^2}{4} (e^{-\Gamma_2 \tau} - \Gamma_2 \tau - 1) \right]. \tag{12.23}$$

For $\Gamma_2 \tau \ll 1$, this reduces to an exponential decay at rate $\frac{\eta^2}{2} \Gamma_2$, whereas for $\Gamma_2 \tau \gg 1$, (12.23) decays exponentially at rate $\frac{\eta^2}{4} \Gamma_2$. This can be understood because at short times the number fluctuations contribute to the decay of $g^{(1)}$, but after a time $1/\Gamma_2$ only Schawlow-Townes phase diffusion remains. There remain a few differences between the physics of (12.23) and the photon condensate. First, (12.23) is derived in [1, 335] under the explicit assumption that the whole ensemble has a Gaussian number distribution peaked around \bar{n} ¹. This assumption is physical for the photon condensate only in the canonical regime, where the probability of having zero photons is negligible. This means that the predicted value of ξ equals 4 at late times, in agreement with our prediction for the canonical regime.

Finally, the timescale of the transition between the two decay rates is for photon condensates not determined by Γ_2 , but only by the second term in (12.7), which is responsible for the time-dependence of R and γ . In the grand-canonical limit, this means that a slowing of the decay would only take place at infinitely long times unlike the prediction of (12.23), as is seen on Fig. 12.4.

12.2.2 HENRY DIFFUSION IN AN INTERACTING CONDENSATE

In the presence of finite photon-photon interactions, the decay of first-order coherence is altered, as we see on the right panel of Fig. 12.4. The profile is rather Gaussian than exponential. This is characteristic for the so-called *Henry mechanism* [329], also known as *linewidth enhancement factor* [336]. Whereas Schawlow-Townes decay is attributed to direct fluctuations of the phase, Henry decay results from phase diffusion as a consequence of number fluctuations causing

¹This is different from our ansatz where we consider only individual trajectories as having a Gaussian number distribution.

a change of the interaction energy. For the Henry effect, Ref. [1, 335] on polariton condensation predicts an additional decay

$$\left|g^{(1)}(\tau)\right| = \exp\left[-\frac{\eta^2 U^2}{\Gamma_2^2}(e^{-\Gamma_2 \tau} + \Gamma_2 \tau - 1)\right], \quad (12.24)$$

which reduces to a Gaussian decay with characteristic time $(\sqrt{2}/U\langle\hat{n}\rangle\eta)$ at short timescales. As we see on figure 12.4, there is good agreement with our numerical results on short times, although deviations occur at later times that we can attribute to the non-Gaussian character of the number distribution.

The fact that the prediction of Gaussian decay for short timescales remains valid in the grand-canonical limit can be understood because in a frame rotating at the bare cavity frequency, the expectation value of a phasefactor of a state with n photons at time t is

$$\begin{aligned} \overline{e^{-iU\hat{n}t}} &= \exp\left[\sum_{m=1}^{\infty} k_m \frac{(-i)^m U^m t^m}{m!}\right] \\ &= e^{-iU\bar{n}t} e^{\frac{-1}{2}U^2 t^2 (\overline{n^2} - \bar{n}^2) + \mathcal{O}(Ut)^3}, \end{aligned} \quad (12.25)$$

where k_m is the m th cumulant of the distribution of n . Here, we implicitly assumed that n remains approximately constant on short times.

12.3 Further results

In this section, we highlight some further results from follow-up research on the photon condensate. Part of this research was carried out by collaborators, the author of this thesis was only remotely involved.

12.3.1 ARRAYS OF PHOTON CONDENSATES

So far, we have studied a single condensate mode in one harmonic trap and have found that the heuristic phasor model, as long as it is not overinterpreted, is quantitatively valid for all practical purposes considered. However, recently, the interest has been growing to engineer coupled condensates, in analogy to the optical lattice systems in e.g. Part II that consist of optical micropillars or superconducting circuits. A convenient technology for this purpose was developed in Ref. [337]: by

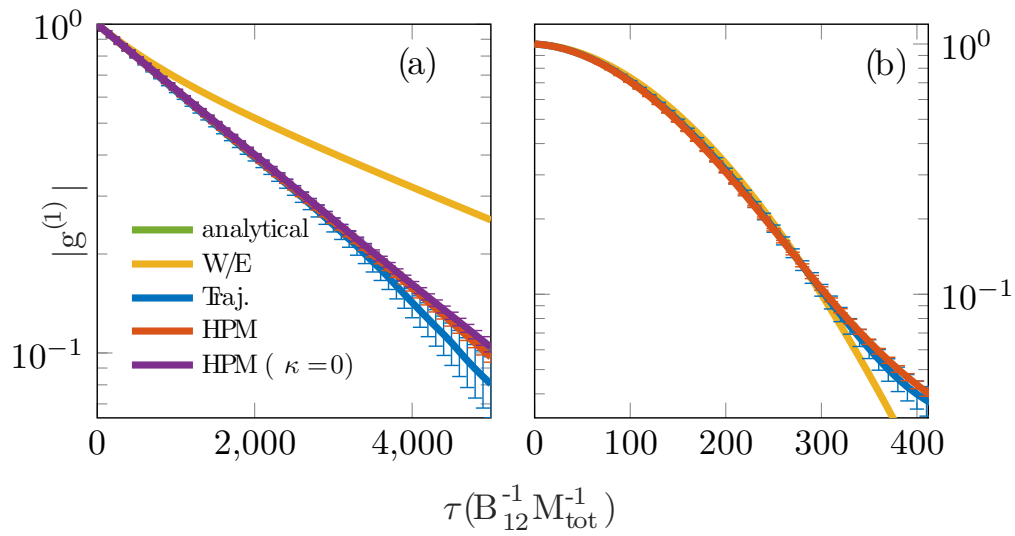


FIGURE 12.4: First order correlation function for the parameters of Tab 12.1, (a) noninteracting and (b) interacting case. Colors as before, Yellow: the polariton result of (12.23) and (12.24) from [1, 335]. The result without losses (purple) is also obtained by the HPM. The quantum-trajectory results are obtained from 84 (noninteracting) or 112 (interacting) independent samples, each evolving a time $10^4 B_{12}^{-1} M_{tot}^{-1}$. The analytical result in (a) is completely covered by the trajectory- and HPM results.

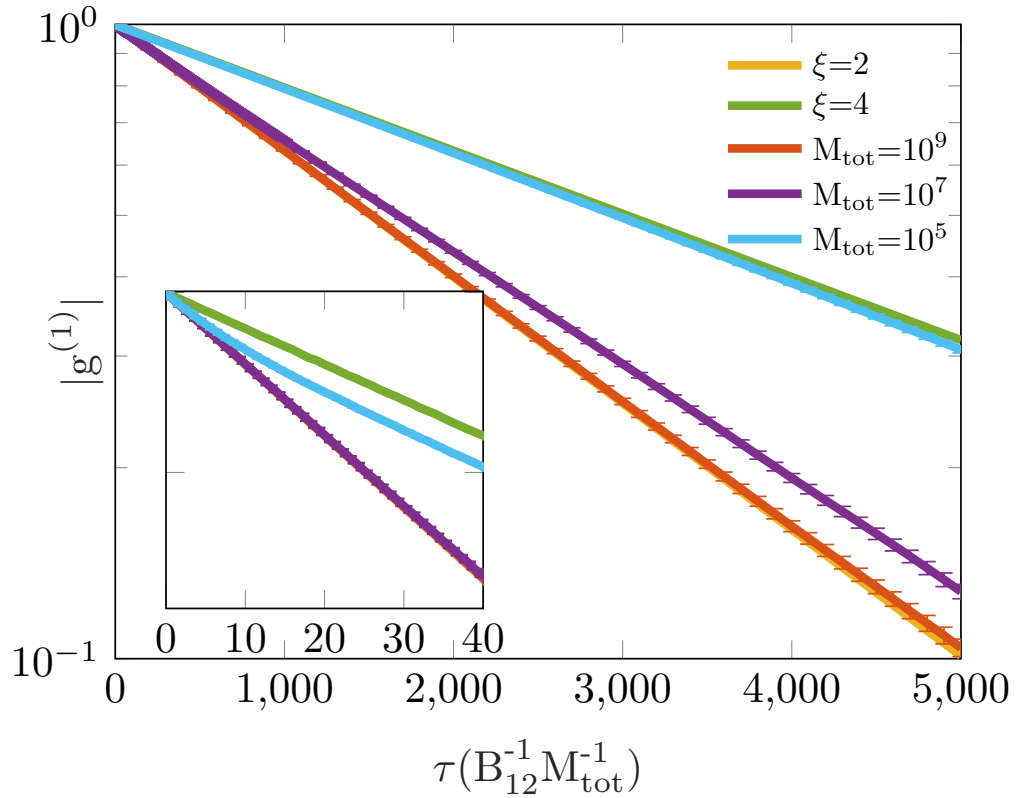


FIGURE 12.5: $g^{(1)}(\tau)$ in absence of interactions, for different values of M_{tot} (10^9 -red, 10^7 -purple, 10^5 -cyan) and hence M_{eff} , together with the asymptotic exponential decays $\xi = 2$ (yellow, line largely covered by the $M_{\text{tot}} = 10^9$ line) and $\xi = 4$ (green). We see that the value of ξ at late times is in between these two limits for any finite molecule reservoir. Again, the other parameters are as in Tab. 12.1 and $\bar{n} = 1000$. Inset: even towards the canonical regime, there is a short initial timespan of grand-canonical ($\xi = 2$) decay of the order of $\tau_c^{(2)}$.

thermo-optical imprinting, local differences in the refraction index of the solvent are induced (a very similar effect to the thermo-optical interactions discussed in subsection 10.1.2). This leads to a position-dependent optical path length, *as if* the mirrors were curved, for example as in parabolic traps. This has very recently also lead to an extensive experimental study of the Josephson junction between two condensates [338], and even mode-entanglement (corresponding to the quantum correlations as in section 8.1) has been claimed [339].

In order to tackle these kinds of systems from a theoretical point of view, the phasor model was recently generalized in Ref. [322] to a classical field method for extended systems. Similar to our handling of a small Kerr effect in the previous sections, the Kennard-Stepanov law is linearized for small βJ , leading to a description of imaginary tunneling (damping). Remarkably, the behavior of relative number fluctuations and phase correlation between two cavities in a dimer is nonmonotoneous as function of J in the canonical regime. For extended 2D lattices, first results show a slower spacial decay of correlations than in 1D lattices, suggesting the presence of a Berezinskii-Kosterlitz-Thouless (topological) phase transition. Results for the grand-canonical regime correspond to the equilibrium result for the ideal Bose gas (some early analytical work in this regard was performed in Ref. [340]).

Apart from the interest from a purely condensed-matter physics point of view, an important feature of arrays of coupled photon condensates is that these may be mapped on spin models and as such could be applicable to solve complex (NP-hard) optimization problems by finding their ground state [235, 338] (see also section 6.3).

12.3.2 IMPROVED CHARACTERIZATION OF THE NUMBER FLUCTUATIONS

We have seen in subsection 12.1.3 that an interplay between the timescales for correlations in photon number n , and the timescale for total occupation number X , leads to peculiar behavior of the $g^{(2)}(\tau)$ function: namely a delayed antibunching effect. In Ref. [341] this is investigated further from both a theoretical and experimental perspective, and it is clear that depending on the system parameters, the antibunching ($g^{(2)}(\tau) < 1$) is damped or oscillations take place. Also Ref. [342] has now reported similar findings in the context of transient phase transitions.

This is also still an ongoing topic of research and even better characterizations of the number fluctuation, and their relation to fluctuation-dissipation theorems [343], are to appear soon.

Photon condensation: Summary and outlook

In Part III, we have applied the method to a photonic Bose-Einstein condensate in a dye-molecule microcavity. More specifically, we have established a model where quantum trajectories are solved exactly (up to Fock-basis truncation) in the low-density parameter regime and variationally with an $N\Theta$ -variational ansatz in the high-density regime. Along the way, we have found a new way to construct a proper phase operator. These trajectories of the photons are coupled to stochastic rate equations for the dye-molecules.

If no phase measurement is performed, the trajectory description for the photon field reduces to stochastic rate equations as well. Regarding the photon number statistics, we have shown thermodynamically and dynamically how Kerr interactions reduce the number fluctuations and calculated the corresponding decay of second-order correlations. The driven-dissipative nature of a realistic photon condensate causes delayed antibunching ($g^{(2)}(\tau) < 1$ at large τ), because of the coupling of the photon number to the slow reservoir dynamics. In the study of the phase properties (heterodyne unraveling on the leaking light), we have studied both Schawlow-Townes (exponential) and Henry (Gaussian) contributions to the decay of first-order correlations in the photon condensate, depending on the interaction strength. As the effect of ‘phase jumps’ is similar to the standard Schawlow-Townes effect, we found no qualitative differences in the coherence between canonical and grand-canonical regimes. We have shown how first- and second-order coherence times are related to the number fluctuations. These analytical formulae were verified with the Gaussian trajectory model.

Furthermore, we have compared the numerical predictions from the trajectories with the ones from a heuristic phasor model (HPM), originally introduced in the context of laser physics. Despite some conceptual difficulties, there is a good match with the exact results within the experimental parameter regimes studied. It provides also a simple picture to distinguish phase diffusion in the canonical

and grand-canonical parameter regimes: a random walk which is, respectively, one-dimensional and two-dimensional in phase space, leading to a factor 2 difference in Schawlow-Townes decay speed. An interesting open question is to what extent the picture above changes in presence of thermo-optical effects. To study the latter, longer evolution times are necessary, but as we have shown an approach based on the numerically efficient heuristic phasor model is likely to be sufficient. Another possible extension is the study of multiple modes. This can either arise in a single-cavity (mode competition: its role could be to add some additional fluctuations to the amount of dye-molecules, strong qualitative differences are not expected and this approximation becomes increasingly better when the total amount of excitations increases), or in lattices of cavities. Some steps in this latter direction have meanwhile been taken with the introduction of a classical field model that generalizes the HPM [322]. Finally, we have assumed here that the absorption and emission processes are Markovian and coupling between the photons and molecules is weak. The introduction of weak Kerr interactions can be seen as a first-order correction on this. It remains an open question to what extent our conclusions remain valid outside of these approximations. Because our conclusions in strong thermal equilibrium and weak losses are similar to a threshold laser far from equilibrium, both regarding the validity of the HPM and the shape of the autocorrelation functions, we expect these conclusions to remain valid for all usual parameter values for photon condensates.

PART

IV

CONCLUSIONS

Conclusions and Outlook

In this thesis, we have introduced a technique to study open quantum systems by combining stochastic quantum trajectories with a Gaussian ansatz. The numerical cost scales only quadratically with system size (number of modes) and is independent of the occupation within a mode. The method takes into account classical fluctuations and correlations, and in addition the dominant quantum fluctuations and correlations (squeezing or Gaussian entanglement). It was introduced with the study of the optical bistability and dephasing in a single driven-dissipative Kerr cavity.

The accuracy of quantitative predictions depends on the unraveling used, and in situations with strong number squeezing, an alternative ansatz, Gaussian in density and phase, is more appropriate. Compared to the widely used truncated Wigner approximation, the GTA method is not always more accurate, but it is overall more robust. There is an additional numerical advantage in the sense that less stochastic samples are required for convergence, but the extent to which this differs is highly dependent on the observables of interest. In addition, the GTA method has direct access to single-shot realizations and is therefore suited to study the experimental process more carefully.

13.1 Results from quadratically driven lattices

In Part II, we have applied the *XP*-Gaussian trajectory approach to the study of extended quadratically driven photonic lattices with more than 100 sites. In particular, this system is interesting because it displays a second-order dissipative phase transition as function of driving amplitude. With the GTA, we are able to study this transition easily in more detail. First, in the low-loss regime, we have reproduced the finding of a quantum criticality (universality class of the quantum

Ising model), demonstrating the ability of the method to describe the relevant long-range quantum correlations (entanglement). Secondly, in a higher-loss parameter regime with a highly mixed steady state, which is inaccessible with other methods (such as corner-space renormalization or the truncated Wigner approximation), the Gaussian trajectories allow us to directly sample a relevant order parameter. Here, we have observed a classical transition, belonging to the universality class of the thermal Ising model. The crossover between both universality classes depending on dissipation rate, suggests that the losses play a role analogous to the one of temperature in an equilibrium system.

In the following step, we have studied dynamical aspects of this phase transition, in the high-loss regime, in two different ways. First, we observe that linear quenches in the driving amplitude lead to the formation of domains as predicted by the Kibble-Zurek mechanism. From this, we extract the dynamical critical exponent z that relates correlation length and time, and obtain a value consistent with the one from metropolis dynamics for the classical Ising model. Second, from the relaxation to the steady state, we obtain the Liouvillian gap, and have shown that it also scales with z , with the same relations as the Hamiltonian gap in a quantum phase transition.

13.2 Results from photon condensates

In Part III, we have studied a photonic Bose-Einstein condensate in a dye-molecule microcavity, by treating the condensate mode as an open quantum system and constructing a trajectory description. If one only measures photon number properties, these trajectories reduce to stochastic rate equations. On the other hand, for the case where one is also interested in phase properties, we solve the trajectories exactly in a truncated Fock basis at low photon numbers and variationally with an $N\Theta$ -variational ansatz at high photon numbers. To perform the transitions between both regimes, we have found a new way to construct a proper phase operator. With numerical simulations, complemented by analytical derivations, we have studied the number distribution and second and first-order temporal coherence. Despite some conceptual issues, a heuristic phasor model has shown to lead to accurate predictions for all these phenomena. Some of the most important findings regarding number statistics are that interactions reduce the number fluctuations similar to a finite reservoir size and that external losses may cause $g^{(2)}(\tau) < 1$. First-order decay is of the exponential Schawlow-Townes form in the canonical

(small dye-molecule reservoir) regime and ‘phase jumps’ only cause a speedup by a factor two in the opposite grand-canonical limit (infinite dye-molecule reservoir). Kerr interactions will introduce an additional Gaussian Henry diffusion.

13.3 The GTA method: overall outlook

We have thus, after first proof-of-principle studies on a single driven-dissipative Kerr cavity, applied the GTA method to more complicated systems where it has demonstrated to be a useful novel tool to access the physics. Of course, these are only the first steps and possibly the method, or variants of it, may find application to a number of other systems. In first instance, we could think of the possibility to use the Gaussian ansatz in the description of strongly correlated photons to open up several ways to the application of our method in quantum many-body physics with light. An interesting perspective for example could be to use Gaussian trajectories to investigate the emergence of collective phenomena in photonic lattices in presence of geometric frustration [221, 344] or disorder [345], both regarding static and dynamical phenomena. Recently, also nonlinear optical networks with random couplings have gained attention in the contexts of annealing and neuromorphic computing [235, 238, 346, 347]: for these systems the method could be useful too. Furthermore, topological photonics is currently a large and active research field that we haven’t touched here, where the method could possibly find applications [348]. Finally, the fact that the GTA-method is trajectory-based makes it also applicable to systems with feedback, another upcoming research field [155]. In fact, closely related approaches have already been used in this context [23, 349]. Related to our study in Part II, we may also think of addressing the true superfluid-to-mott phase transition in an incoherently (so that there is complete phase symmetry) pumped system, especially with the $N\Theta$ -ansatz or similar. In the parameter regimes where this could occur in a photon condensate, we expect the HPM to work well though. But also without photons, there may be relevant systems that could benefit from the method. This includes even fermions in a lattice, for which some descriptions treat inelastic scattering processes as a dissipation channel in the form of two-particle loss [79]. Also spin models can often be mapped on systems of moving particles and have been approximated by Gaussian states, be it in a somewhat less straightforward way [350–352]. They are also commonly used as a toy model for dissipative phenomena, while commonly citing Rydberg atoms as a relevant experimental

platform. Meanwhile, tensor-network approaches have found wide applicability for such systems through. Of course, if Gaussian trajectory approaches for one kind of systems are found suitable, then composite systems of these can also be studied, taking into account classical and Gaussian quantum correlations between the constituents (it would also be very interesting if methods could be devised that include Gaussian correlations between subsystems that are by themselves tracked differently). There are a number of thinkable ways in which the GTA method could further be improved. One possibility is to track higher-order correlations, for example by using higher moments to characterize the trajectory wavefunction. This leads to a cumulant-expansion on the level of individual trajectories instead of the wavefunction. However, the inclusion of higher moments prevents the method to be variational (correlation schemes can be truncated, but not closed) and thus less controlled. Sticking to the Gaussian ansatzes, one could also think of using a different Gaussian ansatz from XP or $N\Theta$, if it is more suitable to a particular system. Finally, we can imagine extending the Gaussian ansatz to non-Markovian techniques.

The extent to which these possibilities will turn out to be realized or if even other directions will be taken, remains to be seen.

Unravelings

As we have described in chapter 2, the evolution of an open quantum system, conditioned on a measurement record (that can either be real or virtual), is a stochastic process known as a quantum trajectory. Different measurement schemes give rise to different unravelings, i.e. different properties to individual trajectories (while the average evolution over all trajectories is the same and consistent with the master equation). We here briefly comment on the nature of the most common unravelings for photon losses. All measurements are considered idealized, i.e. full efficiency, no dark counts and instantaneous.¹

A.1 Photon Counting

The simplest example of an unraveling is photon counting. Here, the detector detects discrete photons leaving the cavity, as discussed in the main text (subsection 2.5.1). Photon counting is an elementary experimental practice to obtain information on the number statistics, including the occurrence of bunching and antibunching [26]. It has also been proposed as a classroom experiment for students [353].

A.2 Homodyne detection

In a different setup, (generalized) homodyne detection can be performed, where the emitted light is interfered with a classical reference signal (local oscillator, LO) resulting in the measurement of quadrature variables (\hat{X} or \hat{P} as defined in

¹The formalism can in principle also be extended outside of these approximations [155]: if only a fraction of the photons are detected for example, one can split γ in multiple contributions of which one is unraveled and the other is not, to obtain a stochastic master equation, trajectories for non-pure states. Application to the GTA method is straightforward.

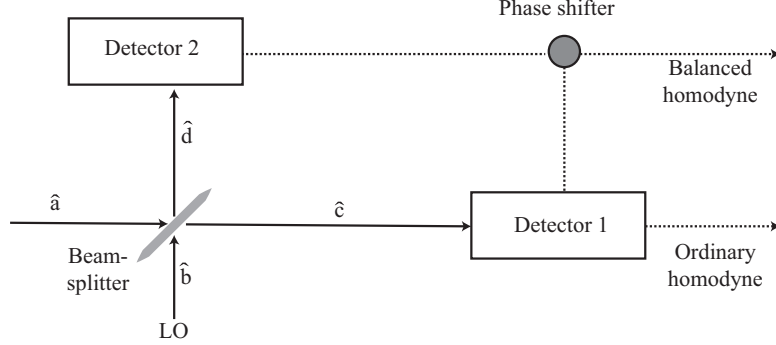


FIGURE A.1: Setup for homodyne (and heterodyne) detection.

subsection 4.2.1, or a linear combination thereof). Following the discussion of Ref. [29], the experimental setup is described more precisely as follows (see Fig. A.1).

Take the quantized input field (the light leaking from the cavity) \hat{a} and the LO \hat{b} . In the beamsplitter, these modes recombine to

$$\begin{aligned}\hat{c} &= \sqrt{T}\hat{a} + i\sqrt{1-T}\hat{b} \\ \hat{d} &= i\sqrt{1-T}\hat{a} + \sqrt{T}\hat{b},\end{aligned}\tag{A.1}$$

where T is the transmissivity and $1-T$ the reflectivity. The signals measured in the two detectors are then given by

$$\begin{aligned}\hat{c}^\dagger\hat{c} &= T\hat{a}^\dagger\hat{a} + (1-T)\hat{b}^\dagger\hat{b} + i\sqrt{T(1-T)}(\hat{a}^\dagger\hat{b} - \hat{b}^\dagger\hat{a}) \\ \hat{d}^\dagger\hat{d} &= (1-T)\hat{a}^\dagger\hat{a} + T\hat{b}^\dagger\hat{b} - i\sqrt{T(1-T)}(\hat{a}^\dagger\hat{b} - \hat{b}^\dagger\hat{a}).\end{aligned}\tag{A.2}$$

As one can see, these operators are time-independent if the local oscillator has the same frequency as the input field. Now, use for the LO mode a coherent state $\hat{b} = |\beta|e^{i\phi_L}$ with large amplitude $|\beta|$ and phase ϕ_L . With this substitution, the last term in the signal operators (A.2) is proportional to

$$\hat{X}_\phi = \frac{1}{2}(\hat{a}e^{-i\phi} + \hat{a}^\dagger e^{i\phi})\tag{A.3}$$

where $\phi = \phi_L + \pi/2$. \hat{X}_ϕ is a general quadrature variable, the most common ones are the conjugate $\hat{X} := \hat{X}_0$ and $\hat{P} := \hat{X}_{\pi/2}$. There are now two possibilities for detection of $\langle \hat{X}_\phi \rangle$. In the so-called *ordinary homodyne detection*, $T \approx 1$ and only the photon flux in detector 1 is measured. The input signal term is negligible with respect to the other terms, and the LO-term is constant except from shot noise

(and can hence be manually subtracted afterwards) so that only the interference term remains. In *balanced homodyne detection*, a beamsplitter with $T = 0.5$ is used instead and the signals of both detectors are directly subtracted.

The corresponding jump operator of Homodyne detection is $\hat{J} = \sqrt{\gamma}(\hat{a} + \beta)$, where $\beta = |\beta|e^{i\phi}$. One readily finds that by inverting this relation towards $\hat{a} = \frac{\hat{J}}{\sqrt{\gamma}} - \beta$ and substituting in (2.38), again an equation in the Lindblad form is retrieved when absorbing a contribution $\sqrt{\gamma} \text{Im}[\beta^* \hat{J}]$ in the Hamiltonian. Therefore, homodyne detection is equally valid as an unraveling of the Master equation. In practice, because β is macroscopic, no individual photons are distinguished but a continuous measurement of the photocurrent is performed. Thus a diffusion approximation of the jumps is justified [6], yielding the stochastic differential equation

$$d|\widetilde{\psi}\rangle = \left(-i \hat{H} dt - \frac{\gamma}{2} \hat{a}^\dagger \hat{a} dt + 2\gamma \langle \hat{X}_\phi \rangle \hat{a} e^{-i\phi} dt + \sqrt{\gamma} \hat{a} e^{-i\phi} dW \right) |\psi\rangle \quad (\text{A.4})$$

Whether ordinary or balanced detection is used has no influence on the quantum trajectory, there only the quadrature variable that is measured is important. Equation (A.4) can also be recast in a norm-conserving way to

$$d|\psi\rangle = -i \hat{H} dt |\psi\rangle + \frac{\gamma}{2} \left(2 \langle \hat{X}_\phi \rangle \hat{a} e^{-i\phi} - \hat{a}^\dagger \hat{a} - \langle \hat{X}_\phi \rangle^2 \right) dt |\psi\rangle + \sqrt{\gamma} \left(\hat{a} e^{-i\phi} - \langle \hat{X}_\phi \rangle \right) dW |\psi\rangle. \quad (\text{A.5})$$

In practical experimental settings, the use of homodyne detection schemes is paramount in a variety of systems. A few notable examples are for the measurements in quantum cryptography [354] and the detection of ‘spooky action at a distance’ (nonlocal wavefunction collapse) [355].

A.3 Heterodyne detection

For heterodyne detection, the condition from homodyne detection that the frequency of the LO matches the input field, is relaxed [9]. This is equivalent with a ϕ oscillating at constant frequency. Measurement information on all quadrature variables is encoded in the signal as fourier components [155]. Also the corresponding trajectory description of heterodyne detection, at sufficient detuning of the LO, is equivalent to a situation where the light leaving the cavity passes a 50/50 beamsplitter where for half the light a homodyne measurement of X is performed

while simultaneously a homodyne measurement of P is performed on the other half of the photocurrent [6]. The stochastic Schrödinger equation is of the form

$$d|\widetilde{\psi}\rangle = \left(-i\hat{H} dt - \frac{\gamma}{2} \hat{a}^\dagger \hat{a} dt + \gamma \langle \hat{a}^\dagger \rangle \hat{a} dt + \sqrt{\gamma} \hat{a} dZ^* \right) |\psi\rangle, \quad (\text{A.6})$$

where $dZ = (dW_X + i dW_P)/\sqrt{2}$ ($dW_X^2 = dW_P^2 = dt$ and $dW_X dW_P = 0$), such that $|dZ|^2 = dt$. An alternative, norm-conserving expression for (A.6) is

$$\begin{aligned} d|\psi\rangle = & -i\hat{H} dt |\psi\rangle + \gamma \left(\langle \hat{a}^\dagger \rangle \hat{a} - \frac{1}{2} \langle \hat{a}^\dagger \rangle \langle \hat{a} \rangle - \frac{1}{2} \hat{a}^\dagger \hat{a} \right) dt |\psi\rangle \\ & + \sqrt{\gamma} (\hat{a} - \langle \hat{a} \rangle) dZ^*. \end{aligned} \quad (\text{A.7})$$

Note that there is gauge freedom involved and a variety of alternative expressions for both homodyne and heterodyne detection schemes can be found in the literature [6, 9, 155].

In an experimental setup, since information on two independent quadratures is retrieved, heterodyne detection is commonly used to obtain phase information. [326, 356]. The technique has also been used for precision metrology with femtosecond frequency combs, leading to the 2015 nobel prize in physics [357].

APPENDIX B

Coefficients

When performing an $N\Theta$ -Gaussian ansatz, the computation of some expectation values is less straightforward, and must sometimes even be performed perturbatively. The following is a list of such expanded correlators that we have encountered in the main text, with a name for convenience. The calculation goes as follows

1. Replace the expressions in brackets by their Taylor series, to obtain a power series. To this extent, note that $\hat{n} = \langle \hat{n} \rangle + \hat{\delta}_{\hat{n}}$ and $\hat{\theta} = \langle \hat{\theta} \rangle + \hat{\delta}_{\hat{\theta}}$.
2. Apply Wick's theorem to each of these terms. Often, this works best by doing this explicitly for some of them and find a general rule.
3. If possible, perform exact resummations. Analytical computational software may be helpful. Of what cannot be resummed, the lowest powers of $\langle \hat{n} \rangle^{-1}$ must be kept (be careful with the other expectation values depending on the problem at hand, for example in the case of Poissonian statistics, $\langle \hat{\delta}_{\hat{n}} \hat{\delta}_{\hat{n}} \rangle$ is of the same order as $\langle \hat{n} \rangle$).

For the expressions below, for expansion up to order $\langle \hat{n} \rangle^{-1}$ between the brackets all Wick contractions are taken into account (resumming over all orders in $\hat{\delta}_{\theta}$), and for order $\langle \hat{n} \rangle^{-2}$ higher order correlators between prefactor and exponential were neglected. Similar expansions were also performed in Ref. [358].

$$\begin{aligned}
 \left\langle e^{-i\hat{\theta}} \right\rangle &= e^{-i\langle \hat{\theta} \rangle - \frac{\langle \hat{\delta}_{\theta} \hat{\delta}_{\theta} \rangle}{2}} & (\text{B.1}) \\
 C_1 := \left\langle \sqrt{\hat{n}} e^{-i\hat{\theta}} \right\rangle &\approx \sqrt{\langle \hat{n} \rangle} e^{-i\langle \hat{\theta} \rangle - \frac{\langle \hat{\delta}_{\theta} \hat{\delta}_{\theta} \rangle}{2}} \left(1 + \frac{1}{2\langle \hat{n} \rangle} \left(\frac{1}{2} - i \langle \hat{\delta}_{\hat{n}} \hat{\delta}_{\theta} \rangle_{\text{sym}} \right) - \frac{\langle \hat{\delta}_{\hat{n}} \hat{\delta}_{\hat{n}} \rangle}{8\langle \hat{n} \rangle^2} \right) \\
 C_2 := \left\langle \hat{\delta}_{\hat{n}} \sqrt{\hat{n}} e^{-i\hat{\theta}} \right\rangle &\approx \sqrt{\langle \hat{n} \rangle} e^{-i\langle \hat{\theta} \rangle - \frac{\langle \hat{\delta}_{\theta} \hat{\delta}_{\theta} \rangle}{2}} \left[\frac{1}{2} - i \langle \hat{\delta}_{\hat{n}} \hat{\delta}_{\theta} \rangle_{\text{sym}} \right]
 \end{aligned}$$

$$\begin{aligned}
 & + \frac{1}{2 \langle \hat{n} \rangle} \left(\langle \hat{\delta}_n \hat{\delta}_n \rangle + \frac{1}{4} - \frac{i}{2} \langle \hat{\delta}_n \hat{\delta}_\theta \rangle_{\text{sym}} - \langle \hat{\delta}_n \hat{\delta}_\theta \rangle_{\text{sym}}^2 \right) \\
 & + \frac{3}{8 \langle \hat{n} \rangle^2} \left(\frac{- \langle \hat{\delta}_n \hat{\delta}_n \rangle}{2} + i \langle \hat{\delta}_n \hat{\delta}_\theta \rangle_{\text{sym}} \langle \hat{\delta}_n \hat{\delta}_n \rangle \right) \Big] \\
 C_3 := & \langle \hat{n}^{-\frac{1}{2}} e^{-i\hat{\theta}} \rangle \approx \frac{e^{-i \langle \hat{\theta} \rangle - \frac{\langle \hat{\delta}_\theta \hat{\delta}_\theta \rangle}{2}}}{\sqrt{\langle \hat{n} \rangle}} \left[1 + \frac{1}{2 \langle \hat{n} \rangle} \left(\frac{-1}{2} + i \langle \hat{\delta}_n \hat{\delta}_\theta \rangle_{\text{sym}} \right) + \frac{3 \langle \hat{\delta}_n \hat{\delta}_n \rangle}{8 \langle \hat{n} \rangle^2} \right] \\
 C_4 := & \langle \hat{n}^{-\frac{1}{2}} \hat{\delta}_\theta e^{-i\hat{\theta}} \rangle \approx \frac{e^{-i \langle \hat{\theta} \rangle - \frac{\langle \hat{\delta}_\theta \hat{\delta}_\theta \rangle}{2}}}{\sqrt{\langle \hat{n} \rangle}} \left[-i \langle \hat{\delta}_\theta \hat{\delta}_\theta \rangle - \frac{1}{2 \langle \hat{n} \rangle} \left(\langle \hat{\delta}_n \hat{\delta}_\theta \rangle_{\text{sym}} + \frac{i}{2} \right) \left(1 - \langle \hat{\delta}_\theta \hat{\delta}_\theta \rangle \right) \right. \\
 & \left. - \frac{3i}{8 \langle \hat{n} \rangle^2} \left(2 \left(\langle \hat{\delta}_n \hat{\delta}_\theta \rangle_{\text{sym}} + \frac{i}{2} \right)^2 + \langle \hat{\delta}_n \hat{\delta}_n \rangle \langle \hat{\delta}_\theta \hat{\delta}_\theta \rangle \right) \right] \\
 C_5 := & \langle \hat{n}^{-\frac{3}{2}} e^{-i\hat{\theta}} \rangle \approx \frac{e^{-i \langle \hat{\theta} \rangle - \frac{\langle \hat{\delta}_\theta \hat{\delta}_\theta \rangle}{2}}}{\sqrt{\langle \hat{n} \rangle}^3} \left[1 + \frac{1}{2 \langle \hat{n} \rangle} \left(\frac{-3}{2} + 3i \langle \hat{\delta}_n \hat{\delta}_\theta \rangle_{\text{sym}} \right) + \frac{15 \langle \hat{\delta}_n \hat{\delta}_n \rangle}{8 \langle \hat{n} \rangle^2} \right] \\
 C_6 := & \langle \sqrt{\hat{n}} \hat{\delta}_\theta e^{-i\hat{\theta}} \rangle \approx \sqrt{\langle \hat{n} \rangle} e^{-i \langle \hat{\theta} \rangle - \frac{\langle \hat{\delta}_\theta \hat{\delta}_\theta \rangle}{2}} \left[-i \langle \hat{\delta}_\theta \hat{\delta}_\theta \rangle + \frac{1}{2 \langle \hat{n} \rangle} \left(\langle \hat{\delta}_n \hat{\delta}_\theta \rangle_{\text{sym}} + \frac{i}{2} \right) \left(1 - \langle \hat{\delta}_\theta \hat{\delta}_\theta \rangle \right) \right. \\
 & \left. + \frac{i}{8 \langle \hat{n} \rangle^2} \left(2 \left(\langle \hat{\delta}_n \hat{\delta}_\theta \rangle_{\text{sym}} + \frac{i}{2} \right)^2 + \langle \hat{\delta}_n \hat{\delta}_n \rangle \langle \hat{\delta}_\theta \hat{\delta}_\theta \rangle \right) \right] \\
 C_7 := & \langle \hat{\delta}_n \hat{n}^{-\frac{1}{2}} e^{-i\hat{\theta}} \rangle \approx \sqrt{\langle \hat{n} \rangle} e^{-i \langle \hat{\theta} \rangle - \frac{\langle \hat{\delta}_\theta \hat{\delta}_\theta \rangle}{2}} \left[\frac{1}{2 \langle \hat{n} \rangle} \left(1 - 2i \langle \hat{\delta}_n \hat{\delta}_\theta \rangle_{\text{sym}} \right) - \frac{\langle \hat{\delta}_n \hat{\delta}_n \rangle}{2 \langle \hat{n} \rangle^2} \right]; \\
 D_1 := & \langle \sqrt{\hat{n}} \hat{\delta}_\theta \hat{\delta}_\theta e^{-i\hat{\theta}} \rangle \approx \sqrt{\langle \hat{n} \rangle} e^{-i \langle \hat{\theta} \rangle - \frac{\langle \hat{\delta}_\theta \hat{\delta}_\theta \rangle}{2}} \left[\left(1 - \langle \hat{\delta}_\theta \hat{\delta}_\theta \rangle \right) \langle \hat{\delta}_\theta \hat{\delta}_\theta \rangle \right. \\
 & - \frac{i}{2 \langle \hat{n} \rangle} \left(3 \langle \hat{\delta}_\theta \hat{\delta}_\theta \rangle - \langle \hat{\delta}_\theta \hat{\delta}_\theta \rangle^2 \right) \left(\langle \hat{\delta}_n \hat{\delta}_\theta \rangle_{\text{sym}} + \frac{i}{2} \right) \\
 & \left. - \frac{1}{8 \langle \hat{n} \rangle^2} \left(\langle \hat{\delta}_n \hat{\delta}_n \rangle \langle \hat{\delta}_\theta \hat{\delta}_\theta \rangle + 2 \left(\langle \hat{\delta}_n \hat{\delta}_\theta \rangle_{\text{sym}} + \frac{i}{2} \right)^2 \right) \right] \\
 D_2 := & \langle \sqrt{\hat{n}} \hat{\delta}_n \hat{\delta}_\theta e^{-i\hat{\theta}} \rangle \approx \sqrt{\langle \hat{n} \rangle} e^{-i \langle \hat{\theta} \rangle - \frac{\langle \hat{\delta}_\theta \hat{\delta}_\theta \rangle}{2}} \left[\left(\langle \hat{\delta}_n \hat{\delta}_\theta \rangle_{\text{sym}} + \frac{i}{2} \right) \left(1 - \langle \hat{\delta}_\theta \hat{\delta}_\theta \rangle \right) \right. \\
 & - \frac{i}{2 \langle \hat{n} \rangle} \left(\langle \hat{\delta}_n \hat{\delta}_n \rangle \langle \hat{\delta}_\theta \hat{\delta}_\theta \rangle + \left(\langle \hat{\delta}_n \hat{\delta}_\theta \rangle_{\text{sym}} + \frac{i}{2} \right)^2 \left(2 - \langle \hat{\delta}_\theta \hat{\delta}_\theta \rangle \right) \right) \\
 & \left. - \frac{3}{8 \langle \hat{n} \rangle^2} \langle \hat{\delta}_n \hat{\delta}_n \rangle \left(\langle \hat{\delta}_n \hat{\delta}_\theta \rangle_{\text{sym}} + \frac{i}{2} \right) \right] \\
 D_3 := & \langle \sqrt{\hat{n}} \hat{\delta}_n \hat{\delta}_n e^{-i\hat{\theta}} \rangle \approx \sqrt{\langle \hat{n} \rangle} e^{-i \langle \hat{\theta} \rangle - \frac{\langle \hat{\delta}_\theta \hat{\delta}_\theta \rangle}{2}} \left[\langle \hat{\delta}_n \hat{\delta}_n \rangle - \left(\langle \hat{\delta}_n \hat{\delta}_\theta \rangle_{\text{sym}} + \frac{i}{2} \right)^2 \right. \\
 & \left. - \frac{i}{2 \langle \hat{n} \rangle} \left(3 \langle \hat{\delta}_n \hat{\delta}_n \rangle \left(\langle \hat{\delta}_n \hat{\delta}_\theta \rangle_{\text{sym}} + \frac{i}{2} \right) - 6 \left(\langle \hat{\delta}_n \hat{\delta}_\theta \rangle_{\text{sym}} + \frac{i}{2} \right)^3 \right) - \frac{3 \langle \hat{\delta}_n \hat{\delta}_n \rangle}{8 \langle \hat{n} \rangle^2} \right], \\
 E_1 := & \left\langle \frac{1}{\hat{n}} \right\rangle \approx \frac{1}{\langle \hat{n} \rangle} \left(1 + \frac{\langle \hat{\delta}_n \hat{\delta}_n \rangle}{\langle \hat{n} \rangle^2} \right) \tag{B.3}
 \end{aligned}$$

$$E_2 := \left\langle \frac{1}{\hat{n}+1} \right\rangle \approx \frac{1}{\langle \hat{n} \rangle + 1} \left(1 + \frac{\langle \hat{\delta}_n \hat{\delta}_n \rangle}{(\langle \hat{n} \rangle + 1)^2} \right). \quad (\text{B.4})$$

Numerical implementation

C.1 Software

All numerical simulations shown in this thesis were carried out in MATLAB (versions 2016b-2019b). For the trajectory description of the photon condensate, .mex (C++) executables were used for a speed-up. The most important part in optimizing the performance of this code was vectorization, either over samples (for single-mode problems), or over lattice sites (many-mode problems). Some code for the solver algorithms is already freely available online as supplementary material to the corresponding papers, the other is available upon request. For a number of analytical computations, Wolfram Mathematica 11 was helpful, for example in resummation over the Wick-expanded coefficients from Appendix B, or for the analytical expressions regarding the number fluctuations of a photon condensate in chapter 12.

Some of the more heavy calculations were performed on a cluster of the Flemish Supercomputing Centre (VSC), in particular the CalcUA service at the University of Antwerp, which I also thank for the support.

C.2 Numerical solution of Stochastic processes

Regarding the convergence properties of numerical methods for Itô stochastic differential equations, one distinguishes the *strong* and *weak orders of convergence* p and p' , respectively defined by [359]

$$E \left\| \vec{X}_k - \vec{X}(t_k) \right\| \leq C(\Delta t)^p \quad (\text{C.1})$$

$$\left\| EF(\vec{X}_k) - EF(\vec{X}(t_k)) \right\| \leq C'(\Delta t)^{p'}, \quad (\text{C.2})$$

where \vec{X}_k is the vector of variables that are evolved, \vec{X}_k its approximation at time t_k and Δt the numerical timestep. F are the functions of \vec{X} in which one is truly interested (i.e. observables). E denotes the expectation value over different solutions. The simplest scheme is the *Euler-Mayurama scheme*, in which equation

$$d\vec{X} = f(\vec{X}, t) dt + \sum_r g_r(\vec{X}, t) dW_r \quad (\text{C.3})$$

is approximately solved by

$$\vec{X}_{k+1} = \vec{X}_k + f(\vec{X}_k, t_k)\Delta t + \sum_r g_r(\vec{X}_k, t_k)\Delta W_{r,k}, \quad (\text{C.4})$$

with $\Delta W_{r,k} = \xi_{r,k}\sqrt{\Delta t}$ where $\xi_{r,k}$ is a random number with standard normal distribution. In general, (C.4) has orders of convergence $p = 1/2$ and $p' = 1$. An alternative scheme with $p = p' = 1$ is the *Milstein scheme*, which adds terms

$$\frac{1}{2} \sum_{r,i} \Lambda_i \vec{g}_r (\Delta W_{r,k} \Delta W_{i,k} - \delta_{ir} \Delta t) \quad (\text{C.5})$$

to (C.4), where $\Lambda_i = (\vec{g}_i \cdot \frac{\partial}{\partial \vec{x}})$. At least for single-photon loss noise however, the additional terms predicted by this scheme are exactly zero for the Gaussian trajectories (the coefficients vanish because noise enters only the equations for $\{\alpha_i\}$, with prefactors that only depend on $\{u_{ij}, v_{ij}\}$) such that both orders of convergence are one. The same holds true for the TWA for which single-photon noise is additive. Far more advanced schemes of higher order for the numerical solution of SDEs exist, and already a number of software packages are specialized in their implementation [359, 360]. However, we have so far found the robustness and controllability of a manual implementation of (C.4) to be advantageous (this furthermore facilitates easy renormalization at every timestep). This may change in the near future as the available software gets more mature for the solution of complex, multi-variate SDEs.

For a jump process alone, the approach of deterministic evolution combined with a jump when the norm has decreased to a random number has been suitable whenever the time-separation between jumps is sufficiently larger than Δt , as was the case for the problems in chapter 5. For the photon condensate evolution (chapter 11) this was not always the case, and the jump process was combined with Wiener noise. Therefore, the proper amount of jumps must be added after every timestep with Poissonian statistics, leading to an expression for the Gaussian

expectation functions very similar to (C.4), with additional Poissonian noise terms $h_1(\vec{X}_k, t_k)\Delta N + h_2(\vec{X}_k, t_k)\Delta M$. Because this scheme is highly unstable for the exact trajectory, we therefore take a slightly different approach. After the deterministic-diffusive evolution with in a timestep, we add both Poisson processes to $dA = dN + dM$, looped through $1 \dots dA$ and for each of these events determine again the nature (absorption or emission) by linear search, and perform them consecutively on $|\psi\rangle$, an approach inspired by Ref. [333]. Finally, note also that generation of random numbers with Poissonian statistics can be computationally much slower than random numbers from a uniform or normal distribution. In the situation where the probability that $\Delta N > 1$ is negligible, it is therefore possible to approximate instead $\Delta N \approx \Theta[\gamma \langle \hat{n} \rangle \Delta t - \zeta]$, where we assume that the expectation value of dN is $\gamma \langle \hat{n} \rangle dt$, ζ a random number from a uniform $[0, 1]$ distribution and Θ the Heaviside theta-function.

List of publications

W. Verstraelen, D. Sels, and M. Wouters, “Unitary work extraction from a generalized gibbs ensemble using bragg scattering”, *Phys. Rev. A* **96**, 023605 (2017).

W. Verstraelen and M. Wouters, “Gaussian quantum trajectories for the variational simulation of open quantum-optical systems”, *Applied Sciences* **8**, *feature paper*, 1427 (2018).

W. Verstraelen and M. Wouters, “Temporal coherence of a photon condensate: a quantum trajectory description”, *Phys. Rev. A* **100**, 013804 (2019).

W. Verstraelen, R. Rota, V. Savona, and M. Wouters, “Gaussian trajectory approach to dissipative phase transitions: the case of quadratically driven photonic lattices”, *Phys. Rev. Research (Rapid communication)* **2**, 022037 (R) (2020).

W. Verstraelen and M. Wouters, “Classical critical dynamics in quadratically driven kerr resonators”, *Phys. Rev. A* **101**, 043826 (2020).

Conference contributions

- talk *The quadratically driven nonlinear photonic lattice and its dissipative phase transition: from quantum to classical*; APS March Meeting 2020 (presentation shared on its online platform, talk physically given at the University of Colorado, Denver).
- talk *Temporal coherence of a photon condensate: a quantum trajectory description*; Quantum matter out-of-equilibrium, Granada, 2019.
- attended Solvay workshop on quantum simulation, Brussels, 2019.
- poster *Gaussian quantum trajectories for the variational simulation of open quantum systems*; Quantum fluids of light and matter, Les Houches, 2018.
- talk *Gaussian Quantum Trajectories as a variational way to simulate open quantum systems*; General meeting of the Belgian Physical Society, Antwerp, 2018.
- poster *Gaussian Quantum Trajectories as a variational way to simulate open quantum systems*; Novel paradigms in many-body physics from open quantum systems, MPI Dresden, 2018.

LIST OF PUBLICATIONS

- poster *Gaussian Quantum Trajectories: a variational Monte Carlo method for efficient simulation of open quantum systems*; Nano and quantum optics, Les Houches, 2017.
- presentations and posters in Theory@sea, Oostduinkerke in 2017 and 2018.

Miscellaneous

- Teaching assistant *Mathematical methods in theoretical physics*, 2016-2020.
- Secretary of the *Antwerp Young Mind Section of the European Physical Society* 2016-2019; I was especially involved in organizing the popular Science quiz in 2018 and 2019, in collaboration with Flemish chemistry and engineering organizations (jong-KVCV and ie-net Jongeren).
- Courses followed include *Leadership and Teamwork*, *Project management*, *Applied Communication*, *Analytic storytelling*, *Grow your future career*, *Optimizing cooperation in international groups*, *Cluster computing*, *Programming techniques for MATLAB* and for *Julia*.

Bibliography

- ¹D. M. Whittaker and P. R. Eastham, “Coherence properties of the microcavity polariton condensate”, *EPL (Europhysics Letters)* **87**, 27002 (2009).
- ²J. J. Sakurai and J. Napolitano, *Modern quantum mechanics* (Cambridge University Press, 2019).
- ³W. Hermanns and A. Einstein, *Einstein and the poet: in search of the cosmic man* (Branden Press, 1983).
- ⁴A. Cabello, “Interpretations of quantum theory: a map of madness”, [10.1017/9781316494233.009](https://arxiv.org/abs/10.1017/9781316494233.009) (2015).
- ⁵D. Lazarou, “Interpretation of quantum theory - an overview”, [arXiv:0712.3466](https://arxiv.org/abs/0712.3466) (2007).
- ⁶H.-P. Breuer and F. Petruccione, *The theory of open quantum systems* (Oxford university press, 2002).
- ⁷H. Wiseman and G. Milburn, *Quantum measurement and control* (Cambridge University Press, 2010).
- ⁸S. Haroche and J. Raimond, *Exploring the quantum: atoms, cavities, and photons*, Oxford Graduate Texts (OUP Oxford, 2006).
- ⁹C. Gardiner and P. Zoller, *Quantum noise: a handbook of markovian and non-markovian quantum stochastic methods with applications to quantum optics (springer series in synergetics)* (Springer, 2004).
- ¹⁰H. J. Carmichael, *Statistical methods in quantum optics 2: non-classical fields*, Theoretical and mathematical physics (Springer, 2008).
- ¹¹T. A. Brun, “A simple model of quantum trajectories”, *American Journal of Physics* **70**, 719–737 (2002).
- ¹²I. Deutsch, *Quantum optics ii, lecture notes*.
- ¹³T. Prosen, “Third quantization: a general method to solve master equations for quadratic open fermi systems”, *New Journal of Physics* **10**, 043026 (2008).
- ¹⁴R. Bausch, “Bewegungsgesetze nicht abgeschlossener quantensysteme”, *Zeitschrift für Physik* **193**, 246–265 (1966).
- ¹⁵V. Gorini, A. Kossakowski, and E. C. G. Sudarshan, “Completely positive dynamical semigroups of n-level systems”, *Journal of Mathematical Physics* **17**, 821–825 (1976).
- ¹⁶G. Lindblad, “On the generators of quantum dynamical semigroups”, *Communications in Mathematical Physics* **48**, 119–130 (1976).

BIBLIOGRAPHY

- ¹⁷E. B. Davies, “Quantum stochastic processes”, *Comm. Math. Phys.* **15**, 277–304 (1969).
- ¹⁸J. Dalibard, Y. Castin, and K. Mølmer, “Wave-function approach to dissipative processes in quantum optics”, *Phys. Rev. Lett.* **68**, 580–583 (1992).
- ¹⁹R. Dum, P. Zoller, and H. Ritsch, “Monte carlo simulation of the atomic master equation for spontaneous emission”, *Phys. Rev. A* **45**, 4879–4887 (1992).
- ²⁰H. Carmichael, *An open systems approach to quantum optics*, Vol. m12, Lecture Notes in Physics (Springer-Verlag, 1993).
- ²¹A. Barchielli and V. P. Belavkin, “Measurements continuous in time and a posteriori states in quantum mechanics”, *Journal of Physics A: Mathematical and General* **24**, 1495 (1991).
- ²²A. Barchielli, M. Gregorati, and M. Licciardo, “Quantum trajectories, feedback and squeezing”, *International Journal of Quantum Information* **06**, 581–587 (2008).
- ²³G. Mazzucchi, S. F. Caballero-Benitez, and I. B. Mekhov, “Quantum measurement-induced antiferromagnetic order and density modulations in ultracold fermi gases in optical lattices”, *Scientific Reports* **6**, Article, 31196 EP – (2016).
- ²⁴A. J. Daley, “Quantum trajectories and open many-body quantum systems”, *Advances in Physics* **63**, 77–149 (2014).
- ²⁵R. E. Wyatt, *Quantum dynamics with trajectories introduction to quantum hydrodynamics* (Springer New York, 2010).
- ²⁶D. F. Walls and G. J. Milburn, *Quantum optics*, 2nd ed. (Springer., 2008).
- ²⁷A. daley, *Continuous measurement and open many-body quantum systems, granada summer school 2019(lecture slides)*.
- ²⁸H. Walther, B. T. H. Varcoe, B.-G. Englert, and T. Becker, “Cavity quantum electrodynamics”, *Reports on Progress in Physics* **69**, 1325–1382 (2006).
- ²⁹M. O. Scully and M. S. Zubairy, *Quantum optics* (Cambridge University Press, 1997).
- ³⁰G. W. Ford and R. F. O’Connell, “There is no quantum regression theorem”, *Phys. Rev. Lett.* **77**, 798–801 (1996).
- ³¹M. Lax, “The lax–onsager regression ‘theorem’ revisited”, *Optics Communications* **179**, 463–476 (2000).
- ³²I. de Vega and D. Alonso, “Dynamics of non-markovian open quantum systems”, *Rev. Mod. Phys.* **89**, 015001 (2017).
- ³³H. Spohn, “Approach to equilibrium for completely positive dynamical semigroups of n-level systems”, *Reports on Mathematical Physics* **10**, 189–194 (1976).
- ³⁴H. Spohn, “An algebraic condition for the approach to equilibrium of an open n-level system”, *Letters in Mathematical Physics* **2**, 33–38 (1977).
- ³⁵D. Nigro, “On the uniqueness of the steady-state solution of the lindblad–gorini–kossakowski–sudarshan equation”, *Journal of Statistical Mechanics: Theory and Experiment* **2019**, 043202 (2019).
- ³⁶T. Haga, M. Nakagawa, R. Hamazaki, and M. Ueda, “Liouvillian skin effect: slowing down of relaxation processes without gap closing”, arXiv:2005.00824 (2020).

- ³⁷J. P. Garrahan, “Aspects of non-equilibrium in classical and quantum systems: slow relaxation and glasses, dynamical large deviations, quantum non-ergodicity, and open quantum dynamics”, *Physica A: Statistical Mechanics and its Applications* **504**, Lecture Notes of the 14th International Summer School on Fundamental Problems in Statistical Physics, 130–154 (2018).
- ³⁸V. V. Albert, B. Bradlyn, M. Fraas, and L. Jiang, “Geometry and response of lindbladians”, *Phys. Rev. X* **6**, 041031 (2016).
- ³⁹B. Buca, J. Tindall, and D. Jaksch, “Non-stationary coherent quantum many-body dynamics through dissipation”, *Nature Communications* **10**, 1730 (2019).
- ⁴⁰C. Lledo, T. K. Mavrogordatos, and M. H. Szymanska, “Driven bose-hubbard dimer under nonlocal dissipation: a bistable time crystal”, *Phys. Rev. B* **100**, 054303 (2019).
- ⁴¹K. Seibold, R. Rota, and V. Savona, “Dissipative time crystal in an asymmetric nonlinear photonic dimer”, *Phys. Rev. A* **101**, 033839 (2020).
- ⁴²A. Amo, S. Pigeon, D. Sanvitto, et al., “Polariton superfluids reveal quantum hydrodynamic solitons”, *Science* **332**, 1167–1170 (2011).
- ⁴³V. N. Gladilin and M. Wouters, “Multivortex states and dynamics in nonequilibrium polariton condensates”, *Journal of Physics A: Mathematical and Theoretical* **52**, 395303 (2019).
- ⁴⁴H. J. Carmichael and D. F. Walls, “Detailed balance in open quantum markoffian systems”, *Zeitschrift für Physik B Condensed Matter* **23**, 299–306 (1976).
- ⁴⁵M. Van Regemortel, W. Casteels, I. Carusotto, and M. Wouters, “Spontaneous beliaev-landau scattering out of equilibrium”, *Phys. Rev. A* **96**, 053854 (2017).
- ⁴⁶E. G. D. Torre, S. Diehl, M. D. Lukin, S. Sachdev, and P. Strack, “Keldysh approach for nonequilibrium phase transitions in quantum optics: beyond the dicke model in optical cavities”, *Phys. Rev. A* **87**, 023831 (2013).
- ⁴⁷D. Huybrechts and M. Wouters, “Cluster methods for the description of a driven-dissipative spin model”, *Phys. Rev. A* **99**, 043841 (2019).
- ⁴⁸O. Scarlatella, A. A. Clerk, and M. Schiro, “Spectral functions and negative density of states of a driven-dissipative nonlinear quantum resonator”, *New Journal of Physics* **21**, 043040 (2019).
- ⁴⁹L. P. Pitaevski and S. Stringari, *Bose-einstein condensation* (Oxford University Press, 2016).
- ⁵⁰F. Bardou, J.-P. Bouchaud, A. Aspect, and C. Cohen-Tannoudji, *Lévy statistics and laser cooling: how rare events bring atoms to rest* (Cambridge University Press, 2002).
- ⁵¹P. Kirton, M. M. Roses, J. Keeling, and E. G. Dalla Torre, “Introduction to the dicke model: from equilibrium to nonequilibrium, and vice versa”, *Advanced Quantum Technologies* **2**, 1800043 (2019).
- ⁵²M. Van Regemortel, H. Kurkjian, M. Wouters, and I. Carusotto, “Prethermalization to thermalization crossover in a dilute bose gas following an interaction ramp”, *Phys. Rev. A* **98**, 053612 (2018).
- ⁵³N. Navon, A. L. Gaunt, R. P. Smith, and Z. Hadzibabic, “Emergence of a turbulent cascade in a quantum gas”, *Nature* **539**, 72–75 (2016).

BIBLIOGRAPHY

- ⁵⁴N. Navon, C. Eigen, J. Zhang, et al., “Synthetic dissipation and cascade fluxes in a turbulent quantum gas”, *Science* **366**, 382–385 (2019).
- ⁵⁵J. Kasprzak, M. Richard, S. Kundermann, et al., “Bose-einstein condensation of exciton polaritons”, *Nature* **443**, 409–414 (2006).
- ⁵⁶A. Amo, D. Sanvitto, F. P. Laussy, et al., “Collective fluid dynamics of a polariton condensate in a semiconductor microcavity”, *Nature* **457**, 291–295 (2009).
- ⁵⁷I. Carusotto and C. Ciuti, “Quantum fluids of light”, *Reviews of Modern Physics* **85** (2013).
- ⁵⁸K. G. Lagoudakis, M. Wouters, M. Richard, et al., “Quantized vortices in an exciton-polariton condensate”, *Nature Physics* **4**, 706–710 (2008).
- ⁵⁹T. Boulier, M. Bamba, A. Amo, et al., “Polariton-generated intensity squeezing in semiconductor micropillars”, *Nature Communications* **5**, 3260 (2014).
- ⁶⁰M. Wouters, “Resonant polariton-polariton scattering in semiconductor microcavities”, *Phys. Rev. B* **76**, 045319 (2007).
- ⁶¹C. Vaneph, A. Morvan, G. Aiello, et al., “Observation of the unconventional photon blockade in the microwave domain”, *Phys. Rev. Lett.* **121**, 043602 (2018).
- ⁶²H. J. Snijders, J. A. Frey, J. Norman, et al., “Observation of the unconventional photon blockade”, *Phys. Rev. Lett.* **121**, 043601 (2018).
- ⁶³S. Ghosh and T. C. H. Liew, “Dynamical blockade in a single-mode bosonic system”, *Phys. Rev. Lett.* **123**, 013602 (2019).
- ⁶⁴J. Klaers, F. Vewinger, and M. Weitz, “Thermalization of a two-dimensional photonic gas in a ‘white wall’ photon box”, *Nature Physics* **6**, 512 EP – (2010).
- ⁶⁵R. J. Schoelkopf and S. M. Girvin, “Wiring up quantum systems”, *Nature* **451**, 664–669 (2008).
- ⁶⁶A. Wallraff, D. I. Schuster, A. Blais, et al., “Strong coupling of a single photon to a superconducting qubit using circuit quantum electrodynamics”, *Nature* **431**, 162–167 (2004).
- ⁶⁷R. Blatt and C. F. Roos, “Quantum simulations with trapped ions”, *Nature Physics* **8**, 277–284 (2012).
- ⁶⁸D. Leibfried, R. Blatt, C. Monroe, and D. Wineland, “Quantum dynamics of single trapped ions”, *Rev. Mod. Phys.* **75**, 281–324 (2003).
- ⁶⁹M. Marcuzzi, E. Levi, S. Diehl, J. P. Garrahan, and I. Lesanovsky, “Universal nonequilibrium properties of dissipative rydberg gases”, *Phys. Rev. Lett.* **113**, 210401 (2014).
- ⁷⁰C. S. Adams, J. D. Pritchard, and J. P. Shaffer, “Rydberg atom quantum technologies”, *Journal of Physics B: Atomic, Molecular and Optical Physics* **53**, 012002 (2019).
- ⁷¹T. F. Gallagher, *Rydberg atoms* (Cambridge University Press, 2005).
- ⁷²A. K. Mohapatra, T. R. Jackson, and C. S. Adams, “Coherent optical detection of highly excited rydberg states using electromagnetically induced transparency”, *Phys. Rev. Lett.* **98**, 113003 (2007).
- ⁷³M. Saffman, T. G. Walker, and K. Mølmer, “Quantum information with rydberg atoms”, *Rev. Mod. Phys.* **82**, 2313–2363 (2010).

- ⁷⁴F. Marquardt and S. Girvin, “Optomechanics”, *Physics* **2**, 10.1103/physics.2.40 (2009).
- ⁷⁵T. Corbitt and N. Mavalvala, “Review: quantum noise in gravitational-wave interferometers”, *Journal of Optics B: Quantum and Semiclassical Optics* **6**, S675–S683 (2004).
- ⁷⁶M. Arndt and K. Hornberger, “Testing the limits of quantum mechanical superpositions”, *Nature Physics* **10**, 271–277 (2014).
- ⁷⁷P. D. Drummond and D. F. Walls, “Quantum theory of optical bistability. i. nonlinear polarisability model”, *J. Phys. A.: Math. Gen.* **13**, 725 (1979).
- ⁷⁸N. Bartolo, F. Minganti, W. Casteels, and C. Ciuti, “Exact steady state of a kerr resonator with one- and two-photon driving and dissipation: controllable wigner-function multimodality and dissipative phase transitions”, *Phys. Rev. A* **94**, 033841 (2016).
- ⁷⁹M. Nakagawa, N. Kawakami, and M. Ueda, “Exact liouvillian spectrum of a one-dimensional dissipative hubbard model”, arXiv:2003.14202 (2020).
- ⁸⁰S. Diehl, A. Tomadin, A. Micheli, R. Fazio, and P. Zoller, “Dynamical phase transitions and instabilities in open atomic many-body systems”, *Phys. Rev. Lett.* **105**, 015702 (2010).
- ⁸¹A. Tomadin, S. Diehl, and P. Zoller, “Nonequilibrium phase diagram of a driven and dissipative many-body system”, *Phys. Rev. A* **83**, 013611 (2011).
- ⁸²L. Joubert-Doriol and A. F. Izmaylov, “Problem-free time-dependent variational principle for open quantum systems”, *The Journal of Chemical Physics* **142**, 134107 (2015).
- ⁸³A. Le Boité, G. Orso, and C. Ciuti, “Steady-state phases and tunneling-induced instabilities in the driven dissipative bose-hubbard model”, *Phys. Rev. Lett.* **110**, 233601 (2013).
- ⁸⁴D. Huybrechts, F. Minganti, F. Nori, M. Wouters, and N. Shammah, “Validity of mean-field theory in a dissipative critical system: liouvillian gap, $\mathbb{P}\mathbb{T}$ -symmetric antigap, and permutational symmetry in the XYZ model”, *Phys. Rev. B* **101**, 214302 (2020).
- ⁸⁵F. A. Y. N. Schröder and A. W. Chin, “Simulating open quantum dynamics with time-dependent variational matrix product states: towards microscopic correlation of environment dynamics and reduced system evolution”, *Phys. Rev. B* **93**, 075105 (2016).
- ⁸⁶M. T. Manzoni, D. E. Chang, and J. S. Douglas, “Simulating quantum light propagation through atomic ensembles using matrix product states”, *Nature Communications* **8**, 1743 (2017).
- ⁸⁷J. Cui, J. I. Cirac, and M. C. Bañuls, “Variational matrix product operators for the steady state of dissipative quantum systems”, *Phys. Rev. Lett.* **114**, 220601 (2015).
- ⁸⁸F. Verstraete, J. J. García-Ripoll, and J. I. Cirac, “Matrix product density operators: simulation of finite-temperature and dissipative systems”, *Phys. Rev. Lett.* **93**, 207204 (2004).
- ⁸⁹M. Zwolak and G. Vidal, “Mixed-state dynamics in one-dimensional quantum lattice systems: a time-dependent superoperator renormalization algorithm”, *Phys. Rev. Lett.* **93**, 207205 (2004).
- ⁹⁰R. Orús, “Tensor networks for complex quantum systems”, *Nature Reviews Physics* **1**, 538–550 (2019).

BIBLIOGRAPHY

- ⁹¹A. Strathearn, P. Kirton, D. Kilda, J. Keeling, and B. W. Lovett, “Efficient non-markovian quantum dynamics using time-evolving matrix product operators”, *Nature Communications* **9**, 3322 (2018).
- ⁹²S. Finazzi, A. Le Boité, F. Storme, A. Baksic, and C. Ciuti, “Corner-space renormalization method for driven-dissipative two-dimensional correlated systems”, *Phys. Rev. Lett.* **115**, 080604 (2015).
- ⁹³W. Casteels and M. Wouters, “Optically bistable driven-dissipative bose-hubbard dimer: gutzwiller approaches and entanglement”, *Phys. Rev. A* **95**, 043833 (2017).
- ⁹⁴W. Casteels, R. M. Wilson, and M. Wouters, “Gutzwiller monte carlo approach for a critical dissipative spin model”, *Phys. Rev. A* **97**, 062107 (2018).
- ⁹⁵H. Pichler, J. Schachenmayer, A. J. Daley, and P. Zoller, “Heating dynamics of bosonic atoms in a noisy optical lattice”, *Phys. Rev. A* **87**, 033606 (2013).
- ⁹⁶A. J. Daley, J. M. Taylor, S. Diehl, M. Baranov, and P. Zoller, “Atomic three-body loss as a dynamical three-body interaction”, *Phys. Rev. Lett.* **102**, 040402 (2009).
- ⁹⁷A. Kantian, M. Dalmonte, S. Diehl, W. Hofstetter, P. Zoller, and A. J. Daley, “Atomic color superfluid via three-body loss”, *Phys. Rev. Lett.* **103**, 240401 (2009).
- ⁹⁸P. Barmettler and C. Kollath, “Controllable manipulation and detection of local densities and bipartite entanglement in a quantum gas by a dissipative defect”, *Phys. Rev. A* **84**, 041606 (2011).
- ⁹⁹K. Huang, *Statistical mechanics* (John Wiley & Sons, 2014).
- ¹⁰⁰W. Casteels, S. Finazzi, A. L. Boité, F. Storme, and C. Ciuti, “Truncated correlation hierarchy schemes for driven-dissipative multimode quantum systems”, *New Journal of Physics* **18**, 093007 (2016).
- ¹⁰¹P. Blakie†, A. Bradley†, M. Davis, R. Ballagh, and C. Gardiner, “Dynamics and statistical mechanics of ultra-cold bose gases using c-field techniques”, *Advances in Physics* **57**, 363–455 (2008).
- ¹⁰²A. Sinatra, C. Lobo, and Y. Castin, “Classical-field method for time dependent bose-einstein condensed gases”, *Phys. Rev. Lett.* **87**, 210404 (2001).
- ¹⁰³A. Polkovnikov, “Phase space representation of quantum dynamics”, *Annals of Physics* **325**, 1790–1852 (2010).
- ¹⁰⁴P. D. Drummond and B. Opanchuk, “Truncated wigner dynamics and conservation laws”, *Phys. Rev. A* **96**, 043616 (2017).
- ¹⁰⁵F. Hebenstreit, “Vortex formation and dynamics in two-dimensional driven-dissipative condensates”, *Phys. Rev. A* **94**, 063617 (2016).
- ¹⁰⁶M. Foss-Feig, P. Niroula, J. T. Young, et al., “Emergent equilibrium in many-body optical bistability”, *Phys. Rev. A* **95**, 043826 (2017).
- ¹⁰⁷A. Sinatra, C. Lobo, and Y. Castin, “The truncated wigner method for bose-condensed gases: limits of validity and applications”, *Journal of Physics B: Atomic, Molecular and Optical Physics* **35**, 3599 (2002).

- ¹⁰⁸M. J. Steel, M. K. Olsen, L. I. Plimak, et al., “Dynamical quantum noise in trapped bose-einstein condensates”, *Phys. Rev. A* **58**, 4824–4835 (1998).
- ¹⁰⁹I. Carusotto and C. Ciuti, “Spontaneous microcavity-polariton coherence across the parametric threshold: quantum monte carlo studies”, *Phys. Rev. B* **72**, 125335 (2005).
- ¹¹⁰M. Wouters and V. Savona, “Stochastic classical field model for polariton condensates”, *Phys. Rev. B* **79**, 165302 (2009).
- ¹¹¹P. D. Drummond and A. D. Hardman, “Simulation of quantum effects in raman-active waveguides”, *EPL (Europhysics Letters)* **21**, 279 (1993).
- ¹¹²S. J. Carter, “Quantum theory of nonlinear fiber optics: phase-space representations”, *Phys. Rev. A* **51**, 3274–3301 (1995).
- ¹¹³L. I. Plimak, M. K. Olsen, M. Fleischhauer, and M. J. Collett, “Beyond the fokker-planck equation: stochastic simulation of complete wigner representation for the optical parametric oscillator”, *Europhysics Letters (EPL)* **56**, 372–378 (2001).
- ¹¹⁴A. Polkovnikov, “Quantum corrections to the dynamics of interacting bosons: beyond the truncated wigner approximation”, *Phys. Rev. A* **68**, 053604 (2003).
- ¹¹⁵L. Keldysh, “Diagram technique for nonequilibrium processes”, *JETP* **20**, 1018 (1965).
- ¹¹⁶L. P. Kadanoff and G. Baym, *Quantum statistical mechanics: greens function methods in equilibrium and nonequilibrium problems* (Perseus Books, 2000).
- ¹¹⁷L. M. Sieberer, M. Buchhold, and S. Diehl, “Keldysh field theory for driven open quantum systems”, *Reports on Progress in Physics* **79**, 096001 (2016).
- ¹¹⁸C. Wetterich, “Exact evolution equation for the effective potential”, *Physics Letters B* **301**, 90–94 (1993).
- ¹¹⁹L. M. Sieberer, S. D. Huber, E. Altman, and S. Diehl, “Dynamical critical phenomena in driven-dissipative systems”, *Phys. Rev. Lett.* **110**, 195301 (2013).
- ¹²⁰J. Marino and S. Diehl, “Quantum dynamical field theory for nonequilibrium phase transitions in driven open systems”, *Phys. Rev. B* **94**, 085150 (2016).
- ¹²¹T. Pang, *An introduction to quantum monte carlo methods*, 2053-2571 (Morgan & Claypool Publishers, 2016).
- ¹²²A. Nagy and V. Savona, “Driven-dissipative quantum monte carlo method for open quantum systems”, *Phys. Rev. A* **97**, 052129 (2018).
- ¹²³W. M. C. Foulkes, L. Mitas, R. J. Needs, and G. Rajagopal, “Quantum monte carlo simulations of solids”, *Rev. Mod. Phys.* **73**, 33–83 (2001).
- ¹²⁴A. Nagy and V. Savona, “Variational quantum monte carlo method with a neural-network ansatz for open quantum systems”, *Phys. Rev. Lett.* **122**, 250501 (2019).
- ¹²⁵M. J. Hartmann and G. Carleo, “Neural-network approach to dissipative quantum many-body dynamics”, *Phys. Rev. Lett.* **122**, 250502 (2019).
- ¹²⁶F. Vicentini, A. Biella, N. Regnault, and C. Ciuti, “Variational neural-network ansatz for steady states in open quantum systems”, *Phys. Rev. Lett.* **122**, 250503 (2019).

BIBLIOGRAPHY

- ¹²⁷N. Yoshioka and R. Hamazaki, “Constructing neural stationary states for open quantum many-body systems”, *Phys. Rev. B* **99**, 214306 (2019).
- ¹²⁸H. Weimer, “Variational principle for steady states of dissipative quantum many-body systems”, *Phys. Rev. Lett.* **114**, 040402 (2015).
- ¹²⁹V. R. Overbeck and H. Weimer, “Time evolution of open quantum many-body systems”, *Phys. Rev. A* **93**, 012106 (2016).
- ¹³⁰D. P. S. McCutcheon, N. S. Dattani, E. M. Gauger, B. W. Lovett, and A. Nazir, “A general approach to quantum dynamics using a variational master equation: application to phonon-damped rabi rotations in quantum dots”, *Phys. Rev. B* **84**, 081305 (2011).
- ¹³¹F. A. Pollock, D. P. S. McCutcheon, B. W. Lovett, E. M. Gauger, and A. Nazir, “A multi-site variational master equation approach to dissipative energy transfer”, *New Journal of Physics* **15**, 075018 (2013).
- ¹³²N. Suri, F. C. Binder, B. Muralidharan, and S. Vinjanampathy, “Speeding up thermalisation via open quantum system variational optimisation”, *The European Physical Journal Special Topics* **227**, 203–216 (2018).
- ¹³³N. Yoshioka, Y. O. Nakagawa, K. Mitarai, and K. Fujii, “Variational quantum algorithm for non-equilibrium steady states”, arXiv:1908.09836 (2019).
- ¹³⁴D. O. Krimer and M. Pletyukhov, “Few-mode geometric description of a driven-dissipative phase transition in an open quantum system”, *Phys. Rev. Lett.* **123**, 110604 (2019).
- ¹³⁵H. Weimer, A. Kshetrimayum, and R. Orús, “Simulation methods for open quantum many-body systems”, arXiv:1907.07079 (2019).
- ¹³⁶S. Janson, *Gaussian hilbert spaces*, Cambridge Tracts in Mathematics (Cambridge University Press, 1997).
- ¹³⁷L. G. Molinari, “Notes on wick’s theorem in many-body theory”, arXiv:1710.09248 (2017).
- ¹³⁸W. Schleich, *Quantum optics in phase space* (b VCH, 2001).
- ¹³⁹D. Sels, “A treatise on wigner distributions: from particles and polarons to fields”, PhD thesis (University of Antwerp, 2014).
- ¹⁴⁰D. A. Green, “A colour scheme for the display of astronomical intensity images”, *Bull. Astron. Soc. India* **39**, 289–295 (2011).
- ¹⁴¹R. V. Meter and J. Touch, “Designing quantum repeater networks”, *IEEE Communications Magazine* **51**, 64–71 (2013).
- ¹⁴²K. Mølmer, “Optical coherence: a convenient fiction”, *Phys. Rev. A* **55**, 3195–3203 (1997).
- ¹⁴³I.-C. Benea-Chelms, F. F. Settembrini, G. Scalari, and J. Faist, “Electric field correlation measurements on the electromagnetic vacuum state”, *Nature* **568**, 202–206 (2019).
- ¹⁴⁴R. Hudson, “When is the wigner quasi-probability density non-negative?”, *Reports on Mathematical Physics* **6**, 249–252 (1974).
- ¹⁴⁵M.-A. Lemonde, N. Didier, and A. A. Clerk, “Antibunching and unconventional photon blockade with gaussian squeezed states”, *Phys. Rev. A* **90**, 063824 (2014).

- ¹⁴⁶A. Ferraro, S. Olivares, and M. Paris, *Gaussian states in quantum information*, Napoli Series on physics and Astrophysics, arXiv:quant-ph/0503237 (Bibliopolis, 2005).
- ¹⁴⁷A. Serafini, *Quantum continuous variables: quantum entanglement, communication and control* (CRC Press, 2017).
- ¹⁴⁸N. S. (<https://physics.stackexchange.com/users/4888/norbert-schuch>), *Von neumann entropy in terms of the mutual overlap?*, Physics Stack Exchange, <https://physics.stackexchange.com/q/498838> (version: 2019-08-26).
- ¹⁴⁹C. Weedbrook, S. Pirandola, R. García-Patrón, et al., “Gaussian quantum information”, *Rev. Mod. Phys.* **84**, 621–669 (2012).
- ¹⁵⁰J.-P. Blaizot and G. Ripka, *Quantum theory of finite systems* (MIT Press, 1986).
- ¹⁵¹E. T. Jaynes, “Information theory and statistical mechanics”, *Phys. Rev.* **106**, 620–630 (1957).
- ¹⁵²A. Polkovnikov, K. Sengupta, A. Silva, and M. Vengalattore, “Colloquium: nonequilibrium dynamics of closed interacting quantum systems”, *Rev. Mod. Phys.* **83**, 863–883 (2011).
- ¹⁵³P. Kramer, “A review of the time-dependent variational principle”, *Journal of Physics: Conference Series* **99**, 012009 (2008).
- ¹⁵⁴M. M. Nieto, “Quantum phase and quantum phase operators: some physics and some history”, *Physica Scripta* **1993**, 5 (1993).
- ¹⁵⁵H. M. Wiseman and G. J. Milburn, *Quantum measurement and control* (Cambridge University Press, 2009).
- ¹⁵⁶M. Wouters, “Wave-function monte carlo method for polariton condensates”, *Phys. Rev. B* **85**, 165303 (2012).
- ¹⁵⁷I. O. Kuznetsov and P. F. Kartsev, “Simulation of equilibrium particle distribution of the bose gas of polaritons using quantum monte carlo”, *Journal of Physics: Conference Series* **941**, 012070 (2017).
- ¹⁵⁸A. Le Boité, “Strongly correlated photons in arrays of nonlinear cavities”, PhD thesis (Université Paris Diderot-Paris 7, 2015).
- ¹⁵⁹F. Vicentini, F. Minganti, R. Rota, G. Orso, and C. Ciuti, “Critical slowing down in driven-dissipative bose-hubbard lattices”, *Phys. Rev. A* **97**, 013853 (2018).
- ¹⁶⁰A. Johnson, S. S. Szigeti, M. Schemmer, and I. Bouchoule, “Long-lived nonthermal states realized by atom losses in one-dimensional quasicondensates”, *Phys. Rev. A* **96**, 013623 (2017).
- ¹⁶¹M. R. Hush, A. R. R. Carvalho, and J. J. Hope, “Number-phase wigner representation for scalable stochastic simulations of controlled quantum systems”, *Phys. Rev. A* **85**, 023607 (2012).
- ¹⁶²M. R. Hush, S. S. Szigeti, A. R. R. Carvalho, and J. J. Hope, “Controlling spontaneous-emission noise in measurement-based feedback cooling of a bose-einstein condensate”, *New Journal of Physics* **15**, 113060 (2013).
- ¹⁶³R. J. Lewis-Swan, M. K. Olsen, and K. V. Kheruntsyan, “Approximate particle number distribution from direct stochastic sampling of the wigner function”, *Phys. Rev. A* **94**, 033814 (2016).

BIBLIOGRAPHY

- ¹⁶⁴K. Mølmer, Y. Castin, and J. Dalibard, “Monte carlo wave-function method in quantum optics”, *J. Opt. Soc. Am. B* **10**, 524–538 (1993).
- ¹⁶⁵S. Krämer, D. Plankensteiner, L. Ostermann, and H. Ritsch, “Quantumoptics.jl: a julia framework for simulating open quantum systems”, *Computer Physics Communications* **227**, 109–116 (2018).
- ¹⁶⁶P. Adam, M. Mechler, V. Szalay, and M. Koniorczyk, “Intelligent states for a number-operator-annihilation-operator uncertainty relation”, *Phys. Rev. A* **89**, 062108 (2014).
- ¹⁶⁷S. Sachdev, *Quantum phase transitions* (Cambridge University Press, 2011).
- ¹⁶⁸E. M. Kessler, G. Giedke, A. Imamoglu, S. F. Yelin, M. D. Lukin, and J. I. Cirac, “Dissipative phase transition in a central spin system”, *Phys. Rev. A* **86**, 012116 (2012).
- ¹⁶⁹F. Minganti, A. Biella, N. Bartolo, and C. Ciuti, “Spectral theory of liouvillians for dissipative phase transitions”, *Phys. Rev. A* **98**, 042118 (2018).
- ¹⁷⁰D. Nigro, D. Rossini, and E. Vicari, “Competing coherent and dissipative dynamics close to quantum criticality”, *Phys. Rev. A* **100**, 052108 (2019).
- ¹⁷¹M. J. Hartmann, “Quantum simulation with interacting photons”, *Journal of Optics* **18**, 104005 (2016).
- ¹⁷²C. Noh and D. G. Angelakis, “Quantum simulations and many-body physics with light”, *Reports on Progress in Physics* **80**, 016401 (2016).
- ¹⁷³H. J. Carmichael, “Breakdown of photon blockade: a dissipative quantum phase transition in zero dimensions”, *Phys. Rev. X* **5**, 031028 (2015).
- ¹⁷⁴J. J. Mendoza-Arenas, S. R. Clark, S. Felicetti, et al., “Beyond mean-field bistability in driven-dissipative lattices: bunching-antibunching transition and quantum simulation”, *Phys. Rev. A* **93**, 023821 (2016).
- ¹⁷⁵W. Casteels, F. Storme, A. Le Boité, and C. Ciuti, “Power laws in the dynamic hysteresis of quantum nonlinear photonic resonators”, *Phys. Rev. A* **93**, 033824 (2016).
- ¹⁷⁶M. Benito, C. Sánchez Muñoz, and C. Navarrete-Benlloch, “Degenerate parametric oscillation in quantum membrane optomechanics”, *Phys. Rev. A* **93**, 023846 (2016).
- ¹⁷⁷W. Casteels and C. Ciuti, “Quantum entanglement in the spatial-symmetry-breaking phase transition of a driven-dissipative bose-hubbard dimer”, *Phys. Rev. A* **95**, 013812 (2017).
- ¹⁷⁸W. Casteels, R. Fazio, and C. Ciuti, “Critical dynamical properties of a first-order dissipative phase transition”, *Phys. Rev. A* **95**, 012128 (2017).
- ¹⁷⁹M. Biondi, G. Blatter, H. E. Türeci, and S. Schmidt, “Nonequilibrium gas-liquid transition in the driven-dissipative photonic lattice”, *Phys. Rev. A* **96**, 043809 (2017).
- ¹⁸⁰A. Biella, F. Storme, J. Lebreuilly, et al., “Phase diagram of incoherently driven strongly correlated photonic lattices”, *Phys. Rev. A* **96**, 023839 (2017).
- ¹⁸¹V. Savona, “Spontaneous symmetry breaking in a quadratically driven nonlinear photonic lattice”, *Phys. Rev. A* **96**, 033826 (2017).
- ¹⁸²R. Rota, F. Minganti, C. Ciuti, and V. Savona, “Quantum critical regime in a quadratically driven nonlinear photonic lattice”, *Phys. Rev. Lett.* **122**, 110405 (2019).

- ¹⁸³J. Gelhausen and M. Buchhold, “Dissipative dicke model with collective atomic decay: bistability, noise-driven activation, and the nonthermal first-order superradiance transition”, *Phys. Rev. A* **97**, 023807 (2018).
- ¹⁸⁴L. M. Sieberer, S. D. Huber, E. Altman, and S. Diehl, “Nonequilibrium functional renormalization for driven-dissipative bose-einstein condensation”, *Phys. Rev. B* **89**, 134310 (2014).
- ¹⁸⁵E. Altman, L. M. Sieberer, L. Chen, S. Diehl, and J. Toner, “Two-dimensional superfluidity of exciton polaritons requires strong anisotropy”, *Phys. Rev. X* **5**, 011017 (2015).
- ¹⁸⁶T. E. Lee, H. Häffner, and M. C. Cross, “Antiferromagnetic phase transition in a nonequilibrium lattice of rydberg atoms”, *Phys. Rev. A* **84**, 031402 (2011).
- ¹⁸⁷T. E. Lee, S. Gopalakrishnan, and M. D. Lukin, “Unconventional magnetism via optical pumping of interacting spin systems”, *Phys. Rev. Lett.* **110**, 257204 (2013).
- ¹⁸⁸C.-K. Chan, T. E. Lee, and S. Gopalakrishnan, “Limit-cycle phase in driven-dissipative spin systems”, *Phys. Rev. A* **91**, 051601 (2015).
- ¹⁸⁹J. Jin, A. Biella, O. Viyuela, et al., “Cluster mean-field approach to the steady-state phase diagram of dissipative spin systems”, *Phys. Rev. X* **6**, 031011 (2016).
- ¹⁹⁰M. F. Maghrebi and A. V. Gorshkov, “Nonequilibrium many-body steady states via keldysh formalism”, *Phys. Rev. B* **93**, 014307 (2016).
- ¹⁹¹R. Rota, F. Storme, N. Bartolo, R. Fazio, and C. Ciuti, “Critical behavior of dissipative two-dimensional spin lattices”, *Phys. Rev. B* **95**, 134431 (2017).
- ¹⁹²V. R. Overbeck, M. F. Maghrebi, A. V. Gorshkov, and H. Weimer, “Multicritical behavior in dissipative ising models”, *Phys. Rev. A* **95**, 042133 (2017).
- ¹⁹³R Rota, F Minganti, A Biella, and C Ciuti, “Dynamical properties of dissipative XYZ heisenberg lattices”, *New Journal of Physics* **20**, 045003 (2018).
- ¹⁹⁴D. Roscher, S. Diehl, and M. Buchhold, “Phenomenology of first-order dark-state phase transitions”, *Phys. Rev. A* **98**, 062117 (2018).
- ¹⁹⁵J. M. Fink, A. Dombi, A. Vukics, A. Wallraff, and P. Domokos, “Observation of the photon-blockade breakdown phase transition”, *Phys. Rev. X* **7**, 011012 (2017).
- ¹⁹⁶S. R. K. Rodriguez, W. Casteels, F. Storme, et al., “Probing a dissipative phase transition via dynamical optical hysteresis”, *Phys. Rev. Lett.* **118**, 247402 (2017).
- ¹⁹⁷T. Fink, A. Schade, S. Höfling, C. Schneider, and A. Imamoglu, “Signatures of a dissipative phase transition in photon correlation measurements”, *Nature Physics* **14**, 365–369 (2018).
- ¹⁹⁸M Marcuzzi, E Levi, W Li, J. P. Garrahan, B Olmos, and I Lesanovsky, “Non-equilibrium universality in the dynamics of dissipative cold atomic gases”, *New Journal of Physics* **17**, 072003 (2015).
- ¹⁹⁹O. Scarlatella, R. Fazio, and M. Schiró, “Emergent finite frequency criticality of driven-dissipative correlated lattice bosons”, *Phys. Rev. B* **99**, 064511 (2019).
- ²⁰⁰A. Mitra, S. Takei, Y. B. Kim, and A. J. Millis, “Nonequilibrium quantum criticality in open electronic systems”, *Phys. Rev. Lett.* **97**, 236808 (2006).

BIBLIOGRAPHY

- ²⁰¹E. G. Dalla Torre, E. Demler, T. Giamarchi, and E. Altman, “Quantum critical states and phase transitions in the presence of non-equilibrium noise”, *Nature Physics* **6**, 806–810 (2010).
- ²⁰²S. Diehl, “Noise gets marginal”, *Nature Physics* **6**, 721–722 (2010).
- ²⁰³E. G. Dalla Torre, E. Demler, T. Giamarchi, and E. Altman, “Dynamics and universality in noise-driven dissipative systems”, *Phys. Rev. B* **85**, 184302 (2012).
- ²⁰⁴M. Kulczykowski and M. Matuszewski, “Phase ordering kinetics of a nonequilibrium exciton-polariton condensate”, *Phys. Rev. B* **95**, 075306 (2017).
- ²⁰⁵P. Comaron, G. Dagvadorj, A. Zamora, I. Carusotto, N. P. Proukakis, and M. H. Szymanska, “Dynamical critical exponents in driven-dissipative quantum systems”, *Phys. Rev. Lett.* **121**, 095302 (2018).
- ²⁰⁶J. Klinder, H. Keßler, M. Wolke, L. Mathey, and A. Hemmerich, “Dynamical phase transition in the open dicke model”, *Proceedings of the National Academy of Sciences* **112**, 3290–3295 (2015).
- ²⁰⁷J. Lang and F. Piazza, “Critical relaxation with overdamped quasiparticles in open quantum systems”, *Phys. Rev. A* **94**, 033628 (2016).
- ²⁰⁸D. A. Paz and M. F. Maghrebi, “Critical dynamics of weakly-dissipative driven systems”, [arXiv:1906.08278](https://arxiv.org/abs/1906.08278) (2019).
- ²⁰⁹J. Lebreuilly, A. Chiochetta, and I. Carusotto, “Pseudothermalization in driven-dissipative non-markovian open quantum systems”, *Phys. Rev. A* **97**, 033603 (2018).
- ²¹⁰U. C. Täuber and S. Diehl, “Perturbative field-theoretical renormalization group approach to driven-dissipative bose-einstein criticality”, *Phys. Rev. X* **4**, 021010 (2014).
- ²¹¹J. Marino and S. Diehl, “Driven markovian quantum criticality”, *Phys. Rev. Lett.* **116**, 070407 (2016).
- ²¹²L. M. Sieberer and E. Altman, “Topological defects in anisotropic driven open systems”, *Phys. Rev. Lett.* **121**, 085704 (2018).
- ²¹³M. Kardar, G. Parisi, and Y.-C. Zhang, “Dynamic scaling of growing interfaces”, *Phys. Rev. Lett.* **56**, 889–892 (1986).
- ²¹⁴P. Strack, “Dynamic criticality far from equilibrium: one-loop flow of burgers-kardar-parisi-zhang systems with broken galilean invariance”, *Phys. Rev. E* **91**, 032131 (2015).
- ²¹⁵A. Zamora, L. M. Sieberer, K. Dunnett, S. Diehl, and M. H. Szymanska, “Tuning across universalities with a driven open condensate”, *Phys. Rev. X* **7**, 041006 (2017).
- ²¹⁶R. Hanai and P. B. Littlewood, “Critical fluctuations at a many-body exceptional point”, [arXiv:1908.03243](https://arxiv.org/abs/1908.03243) (2019).
- ²¹⁷F. Minganti, N. Bartolo, J. Lolli, W. Casteels, and C. Ciuti, “Exact results for schrödinger cats in driven-dissipative systems and their feedback control”, *Scientific Reports* **6**, Article, 26987 EP – (2016).
- ²¹⁸C. C. Gerry, “Non-classical properties of even and odd coherent states”, *Journal of Modern Optics* **40**, 1053–1071 (1993).

- ²¹⁹L. Gilles, B. M. Garraway, and P. L. Knight, “Generation of nonclassical light by dissipative two-photon processes”, *Phys. Rev. A* **49**, 2785–2799 (1994).
- ²²⁰N. Bartolo, F. Minganti, J. Lolli, and C. Ciuti, “Homodyne versus photon-counting quantum trajectories for dissipative kerr resonators with two-photon driving”, *The European Physical Journal Special Topics* **226**, 2705–2713 (2017).
- ²²¹R. Rota and V. Savona, “Simulating frustrated antiferromagnets with quadratically driven qed cavities”, *Phys. Rev. A* **100**, 013838 (2019).
- ²²²A. Dutta, G. Aeppli, B. K. Chakrabarti, U. Divakaran, T. F. Rosenbaum, and D. Sen, *Quantum phase transitions in transverse field spin models: from statistical physics to quantum information* (Cambridge University Press, 2015).
- ²²³B. Zeng, *Quantum information meets quantum matter: from quantum entanglement to topological phases of many-body systems* (Springer, 2019).
- ²²⁴Z. Leghtas, S. Touzard, I. M. Pop, et al., “Confining the state of light to a quantum manifold by engineered two-photon loss”, *Science* **347**, 853–857 (2015).
- ²²⁵C. Wang, Y. Y. Gao, P. Reinhold, et al., “A schrödinger cat living in two boxes”, *Science* **352**, 1087–1091 (2016).
- ²²⁶H. Goto, “Universal quantum computation with a nonlinear oscillator network”, *Phys. Rev. A* **93**, 050301 (2016).
- ²²⁷H. Goto, “Bifurcation-based adiabatic quantum computation with a nonlinear oscillator network”, *Scientific Reports* **6**, 21686 (2016).
- ²²⁸S. E. Nigg, N. Lörch, and R. P. Tiwari, “Robust quantum optimizer with full connectivity”, *Science Advances* **3**, e1602273 (2017).
- ²²⁹S. Puri, C. K. Andersen, A. L. Grimsmo, and A. Blais, “Quantum annealing with all-to-all connected nonlinear oscillators”, *Nature Communications* **8**, 15785 (2017).
- ²³⁰L. Fortnow, “The status of the p versus np problem”, *Communications of the ACM* **52**, 78 (2009).
- ²³¹D. P. Bovet and P. Crescenzi, *Introduction to the theory of complexity* (Prentice Hall, 2000).
- ²³²F. Barahona, “On the computational complexity of ising spin glass models”, *Journal of Physics A: Mathematical and General* **15**, 3241–3253 (1982).
- ²³³T. Kadowaki and H. Nishimori, “Quantum annealing in the transverse ising model”, *Phys. Rev. E* **58**, 5355–5363 (1998).
- ²³⁴S. Bravyi and M. Hastings, “On complexity of the quantum ising model”, *Communications in Mathematical Physics* **349**, 1–45 (2017).
- ²³⁵A. Marandi, Z. Wang, K. Takata, R. L. Byer, and Y. Yamamoto, “Network of time-multiplexed optical parametric oscillators as a coherent ising machine”, *Nature Photonics* **8**, 937–942 (2014).
- ²³⁶T. Inagaki, Y. Haribara, K. Igarashi, et al., “A coherent ising machine for 2000-node optimization problems”, *Science* **354**, 603–606 (2016).

BIBLIOGRAPHY

- ²³⁷P. L. McMahon, A. Marandi, Y. Haribara, et al., “A fully programmable 100-spin coherent ising machine with all-to-all connections”, *Science* **354**, 614–617 (2016).
- ²³⁸O. Kyriienko, H. Sigurdsson, and T. C. H. Liew, “Probabilistic solving of np -hard problems with bistable nonlinear optical networks”, *Phys. Rev. B* **99**, 195301 (2019).
- ²³⁹K. P. Kalinin and N. G. Berloff, “Networks of non-equilibrium condensates for global optimization”, *New Journal of Physics* **20**, 113023 (2018).
- ²⁴⁰M. Kewming, S. Shrapnel, and G. Milburn, “Quantum correlations in the kerr ising model”, [10.1088/1367-2630/ab7255](https://arxiv.org/abs/10.1088/1367-2630/ab7255) (2019).
- ²⁴¹W. T. Strunz and I. C. Percival, “Classical mechanics from quantum state diffusion - a phase-space approach”, *Journal of Physics A: Mathematical and General* **31**, 1801–1813 (1998).
- ²⁴²V. Link, K. Luoma, and W. T. Strunz, “Revealing the nature of nonequilibrium phase transitions with quantum trajectories”, *Phys. Rev. A* **99**, 062120 (2019).
- ²⁴³M. E. Fisher and M. N. Barber, “Scaling theory for finite-size effects in the critical region”, *Phys. Rev. Lett.* **28**, 1516–1519 (1972).
- ²⁴⁴C. J. (ed.), *Finite-size scaling* (Elsevier, 1988).
- ²⁴⁵H. Nha and H. J. Carmichael, “Entanglement within the quantum trajectory description of open quantum systems”, *Phys. Rev. Lett.* **93**, 120408 (2004).
- ²⁴⁶A. del Campo and W. H. Zurek, “Universality of phase transition dynamics: topological defects from symmetry breaking”, *International Journal of Modern Physics A* **29**, 1430018 (2014).
- ²⁴⁷K. Binder, “Finite size scaling analysis of ising model block distribution functions”, *Zeitschrift für Physik B Condensed Matter* **43**, 119–140 (1981).
- ²⁴⁸K. Binder, “Critical properties from monte carlo coarse graining and renormalization”, *Phys. Rev. Lett.* **47**, 693–696 (1981).
- ²⁴⁹M. Vojta, “Quantum phase transitions”, *Reports on Progress in Physics* **66**, 2069–2110 (2003).
- ²⁵⁰M. V. Medvedyeva and S. Kehrein, “Power-law approach to steady state in open lattices of noninteracting electrons”, *Phys. Rev. B* **90**, 205410 (2014).
- ²⁵¹L. Henriot, J. S. Douglas, D. E. Chang, and A. Albrecht, “Critical open-system dynamics in a one-dimensional optical-lattice clock”, *Phys. Rev. A* **99**, 023802 (2019).
- ²⁵²Z. Cai and T. Barthel, “Algebraic versus exponential decoherence in dissipative many-particle systems”, *Phys. Rev. Lett.* **111**, 150403 (2013).
- ²⁵³P. C. Hohenberg and B. I. Halperin, “Theory of dynamic critical phenomena”, *Rev. Mod. Phys.* **49**, 435–479 (1977).
- ²⁵⁴T. Kibble, “Phase-transition dynamics in the lab and the universe”, *Physics Today* **60**, 47–52 (2007).
- ²⁵⁵C.-W. Liu, A. Polkovnikov, and A. W. Sandvik, “Dynamic scaling at classical phase transitions approached through nonequilibrium quenching”, *Phys. Rev. B* **89**, 054307 (2014).
- ²⁵⁶E. Ising, “Beitrag zur theorie des ferromagnetismus”, *Zeitschrift für Physik* **31**, 253–258 (1925).

- ²⁵⁷L. Onsager, “Crystal statistics. i. a two-dimensional model with an order-disorder transition”, *Phys. Rev.* **65**, 117–149 (1944).
- ²⁵⁸M. J. Dunlavy and D. Venus, “Critical slowing down in the two-dimensional ising model measured using ferromagnetic ultrathin films”, *Phys. Rev. B* **71**, 144406 (2005).
- ²⁵⁹W. Zhong, G. T. Barkema, D. Panja, and R. C. Ball, “Critical dynamical exponent of the two-dimensional scalar ϕ^4 model with local moves”, *Phys. Rev. E* **98**, 062128 (2018).
- ²⁶⁰T. Kibble, “Some implications of a cosmological phase transition”, *Physics Reports* **67**, 183–199 (1980).
- ²⁶¹W. H. Zurek, “Cosmological experiments in superfluid helium?”, *Nature* **317**, 505–508 (1985).
- ²⁶²A. Chandran, A. Erez, S. S. Gubser, and S. L. Sondhi, “Kibble-zurek problem: universality and the scaling limit”, *Phys. Rev. B* **86**, 064304 (2012).
- ²⁶³J. Sabbatini, W. H. Zurek, and M. J. Davis, “Causality and defect formation in the dynamics of an engineered quantum phase transition in a coupled binary bose-einstein condensate”, *New Journal of Physics* **14**, 095030 (2012).
- ²⁶⁴J. Dziarmaga, “Dynamics of a quantum phase transition and relaxation to a steady state”, *Advances in Physics* **59**, 1063–1189 (2010).
- ²⁶⁵D. Jaschke, K. Maeda, J. D. Whalen, M. L. Wall, and L. D. Carr, “Critical phenomena and kibble-zurek scaling in the long-range quantum ising chain”, *New Journal of Physics* **19**, 033032 (2017).
- ²⁶⁶P. Silvi, G. Morigi, T. Calarco, and S. Montangero, “Crossover from classical to quantum kibble-zurek scaling”, *Phys. Rev. Lett.* **116**, 225701 (2016).
- ²⁶⁷A. Zamora, G. Dagvadorj, P. Comaron, I. Carusotto, N. P. Proukakis, and M. H. Szymanska, “Kibble-zurek mechanism in driven-dissipative systems crossing a non-equilibrium phase transition”, arXiv:2004.00918 (2020).
- ²⁶⁸D. Jaschke, L. D. Carr, and I. de Vega, “Thermalization in the quantum ising model: approximations, limits, and beyond”, *Quantum Science and Technology* **4**, 034002 (2019).
- ²⁶⁹R. Puebla, O. Marty, and M. B. Plenio, “Quantum kibble-zurek physics in long-range transverse-field ising models”, *Phys. Rev. A* **100**, 032115 (2019).
- ²⁷⁰A. Dutta, A. Rahmani, and A. del Campo, “Anti-kibble-zurek behavior in crossing the quantum critical point of a thermally isolated system driven by a noisy control field”, *Phys. Rev. Lett.* **117**, 080402 (2016).
- ²⁷¹R. Puebla, A. Smirne, S. F. Huelga, and M. B. Plenio, “Universal anti-kibble-zurek scaling in fully-connected systems”, arXiv:1911.06023 (2019).
- ²⁷²A. Bramati and M. E. Modugno, *Physics of quantum fluids new trends and hot topics in atomic and polariton condensates* (Springer Berlin Heidelberg, 2015).
- ²⁷³A. Sommer and J. Simon, “Engineering photonic floquet hamiltonians through fabry–pérot resonators”, *New Journal of Physics* **18**, 035008 (2016).
- ²⁷⁴C. Collaboration, “Evidence for light-by-light scattering and searches for axion-like particles in ultraperipheral pbpb collisions at $\sqrt{s}=5.02\text{TeV}$ ”, *Physics Letters B* **797**, 134826 (2019).

BIBLIOGRAPHY

- ²⁷⁵D. M. Whittaker and P. R. Eastham, “Coherence properties of the microcavity polariton condensate”, *EPL (Europhysics Letters)* **87**, 27002 (2009); A. P. D. Love, D. N. Krizhanovskii, D. M. Whittaker, et al., “Intrinsic decoherence mechanisms in the microcavity polariton condensate”, *Phys. Rev. Lett.* **101**, 067404 (2008).
- ³³⁵A. P. D. Love, D. N. Krizhanovskii, D. M. Whittaker, et al., “Intrinsic decoherence mechanisms in the microcavity polariton condensate”, *Phys. Rev. Lett.* **101**, 067404 (2008).
- ²⁷⁶H. Haug, T. D. Doan, H. T. Cao, and D. B. T. Thoai, “Temporal first- and second-order correlations in a polariton condensate”, *Phys. Rev. B* **85**, 205310 (2012).
- ²⁷⁷E. H. Kennard, “On the thermodynamics of fluorescence”, *Phys. Rev.* **11**, 29–38 (1918).
- ²⁷⁸B. I. Stepanov, “A universal relation between the absorption and fluorescence spectra of complex molecules.”, *Dokl. Akad. Nauk. S. S. S. R. Phys. Sect.* **2**, 81–84 (1957).
- ²⁷⁹J. Klaers, J. Schmitt, T. Damm, F. Vewinger, and M. Weitz, “Statistical physics of bose-einstein-condensed light in a dye microcavity”, *Phys. Rev. Lett.* **108**, 160403 (2012).
- ²⁸⁰J. Klaers, J. Schmitt, F. Vewinger, and M. Weitz, “Bose-einstein condensation of photons in an optical microcavity”, *Nature* **468**, 545 EP – (2010).
- ²⁸¹P. Kirton and J. Keeling, “Thermalization and breakdown of thermalization in photon condensates”, *Phys. Rev. A* **91**, 033826 (2015).
- ²⁸²R. Rajan, P. Ramesh Babu, and K. Senthilnathan, “Photon condensation: a new paradigm for bose-einstein condensation”, *Frontiers of Physics* **11**, 110502 (2016).
- ²⁸³J. Klaers, “The thermalization, condensation and flickering of photons”, *Journal of Physics B: Atomic, Molecular and Optical Physics* **47**, 243001 (2014).
- ²⁸⁴J. Schmitt, “Dynamics and correlations of a bose-einstein condensate of photons”, *Journal of Physics B: Atomic, Molecular and Optical Physics* **51**, 173001 (2018).
- ²⁸⁵R. A. Nyman and B. T. Walker, “Bose-einstein condensation of photons from the thermodynamic limit to small photon numbers”, *Journal of Modern Optics* **65**, 754–766 (2018).
- ²⁸⁶P. Kirton and J. Keeling, “Nonequilibrium model of photon condensation”, *Phys. Rev. Lett.* **111**, 100404 (2013).
- ²⁸⁷J. Schmitt, T. Damm, D. Dung, F. Vewinger, J. Klaers, and M. Weitz, “Thermalization kinetics of light: from laser dynamics to equilibrium condensation of photons”, *Phys. Rev. A* **92**, 011602 (2015).
- ²⁸⁸H. J. Hesten, R. A. Nyman, and F. Mintert, “Decondensation in nonequilibrium photonic condensates: when less is more”, *Phys. Rev. Lett.* **120**, 040601 (2018).
- ²⁸⁹H. Alaeian, M. Schedensack, C. Bartels, D. Peterseim, and M. Weitz, “Thermo-optical interactions in a dye-microcavity photon bose-einstein condensate”, *New Journal of Physics* **19**, 115009 (2017).
- ²⁹⁰Z. Geng, K. J. H. Peters, A. A. P. Trichet, et al., “Universal power law decay in the dynamic hysteresis of an optical cavity with non-instantaneous photon-photon interactions”, *arXiv:1911.00463* (2019).

- ²⁹¹E. Stein, F. Vewinger, and A. Pelster, “Collective modes of a photon bose–einstein condensate with thermo-optic interaction”, *New Journal of Physics* **21**, 103044 (2019).
- ²⁹²A. Sinatra, Y. Castin, and E. Witkowska, “Coherence time of a bose-einstein condensate”, *Phys. Rev. A* **80**, 033614 (2009).
- ²⁹³H. Kurkjian, Y. Castin, and A. Sinatra, “Brouillage thermique d’un gaz cohérent de fermions”, *Comptes Rendus Physique* **17**, Quantum microwaves / Micro-ondes quantiques, 789–801 (2016).
- ²⁹⁴R. A. Nyman and M. H. Szymanska, “Interactions in dye-microcavity photon condensates and the prospects for their observation”, *Phys. Rev. A* **89**, 033844 (2014).
- ²⁹⁵M. Radonjic, W. Kopylov, A. Balaz, and A. Pelster, “Interplay of coherent and dissipative dynamics in condensates of light”, *New Journal of Physics* **20**, 055014 (2018).
- ²⁹⁶O. L. Berman, R. Y. Kezerashvili, and Y. E. Lozovik, “On bose-einstein condensation and superfluidity of trapped photons with coordinate-dependent mass and interactions”, *J. Opt. Soc. Am. B* **34**, 1649–1658 (2017).
- ²⁹⁷A. Majumdar and D. Gerace, “Single-photon blockade in doubly resonant nanocavities with second-order nonlinearity”, *Phys. Rev. B* **87**, 235319 (2013).
- ²⁹⁸J. Marelic and R. A. Nyman, “Experimental evidence for inhomogeneous pumping and energy-dependent effects in photon bose-einstein condensation”, *Phys. Rev. A* **91**, 033813 (2015).
- ²⁹⁹J. Keeling and P. Kirton, “Spatial dynamics, thermalization, and gain clamping in a photon condensate”, *Phys. Rev. A* **93**, 013829 (2016).
- ³⁰⁰T. Damm, D. Dung, F. Vewinger, M. Weitz, and J. Schmitt, “First-order spatial coherence measurements in a thermalized two-dimensional photonic quantum gas”, *Nature Communications* **8**, 158 (2017).
- ³⁰¹B. T. Walker, H. J. Hesten, H. S. Dhar, R. A. Nyman, and F. Mintert, “Noncritical slowing down of photonic condensation”, *Phys. Rev. Lett.* **123**, 203602 (2019).
- ³⁰²S. Greveling, K. L. Perrier, and D. van Oosten, “Density distribution of a bose-einstein condensate of photons in a dye-filled microcavity”, *Phys. Rev. A* **98**, 013810 (2018).
- ³⁰³R. I. Moodie, P. Kirton, and J. Keeling, “Polarization dynamics in a photon bose-einstein condensate”, *Phys. Rev. A* **96**, 043844 (2017).
- ³⁰⁴S. Greveling, F. van der Laan, H. C. Jagers, and D. van Oosten, “Polarization of a bose-einstein condensate of photons in a dye-filled microcavity”, arXiv:1712.08426 (2017).
- ³⁰⁵T. Damm, J. Schmitt, Q. Liang, et al., “Calorimetry of a bose-einstein-condensed photon gas”, *Nature Communications* **7**, 11340 (2016).
- ³⁰⁶A.-W. de Leeuw, H. T. C. Stoof, and R. A. Duine, “Schwinger-keldysh theory for bose-einstein condensation of photons in a dye-filled optical microcavity”, *Phys. Rev. A* **88**, 033829 (2013).
- ³⁰⁷A. Chiocchetta and I. Carusotto, “Quantum langevin model for nonequilibrium condensation”, *Phys. Rev. A* **90**, 023633 (2014).

BIBLIOGRAPHY

- ³⁰⁸B. T. Walker, L. C. Flatten, H. J. Hesten, et al., “Driven-dissipative non-equilibrium bose-einstein condensation of less than ten photons”, *Nature Physics* **14**, 1173–1177 (2018).
- ³⁰⁹L. Liao, E. C. I. van der Wurff, D. van Oosten, and H. T. C. Stoof, “Proposal for an analog schwarzschild black hole in condensates of light”, *Phys. Rev. A* **99**, 023850 (2019).
- ³¹⁰M. Vlaho, H. A. M. Leymann, D. Vorberg, and A. Eckardt, “Controlled two-mode emission from the interplay of driving and thermalization in a dye-filled photonic cavity”, *Phys. Rev. Research* **1**, 033191 (2019).
- ³¹¹A.-W. de Leeuw, E. C. I. van der Wurff, R. A. Duine, D. van Oosten, and H. T. C. Stoof, “Theory for bose-einstein condensation of light in nanofabricated semiconductor microcavities”, *Phys. Rev. A* **94**, 013615 (2016).
- ³¹²S. Barland, P. Azam, G. L. Lippi, R. A. Nyman, and R. Kaiser, “Photon thermalization and a condensation phase transition in an electrically pumped semiconductor microresonator”, arXiv:1912.11358 (2019).
- ³¹³M. Weitz, J. Klaers, and F. Vewinger, “Optomechanical generation of a photonic bose-einstein condensate”, *Phys. Rev. A* **88**, 045601 (2013).
- ³¹⁴M. Fani and M. H. Naderi, “Thermalization and bose-einstein condensation of a photon gas in a multimode hybrid atom-membrane optomechanical microcavity”, *J. Opt. Soc. Am. B* **33**, 1242–1250 (2016).
- ³¹⁵A. Kruchkov and Y. Slyusarenko, “Bose-einstein condensation of photons in an ideal atomic gas”, *Phys. Rev. A* **88**, 013615 (2013).
- ³¹⁶C.-H. Wang, M. J. Gullans, J. V. Porto, W. D. Phillips, and J. M. Taylor, “Theory of bose condensation of light via laser cooling of atoms”, *Phys. Rev. A* **99**, 031801 (2019).
- ³¹⁷R. Weill, A. Bekker, B. Levit, M. Zhurahov, and B. Fischer, “Thermalization of one-dimensional photon gas and thermal lasers in erbium-doped fibers”, *Opt. Express* **25**, 18963–18973 (2017).
- ³¹⁸A. J. Kruchkov, “One-dimensional bose-einstein condensation of photons in a microtube”, *Phys. Rev. A* **93**, 043817 (2016).
- ³¹⁹J. Klaers, J. Schmitt, T. Damm, F. Vewinger, and M. Weitz, “Bose-einstein condensation of paraxial light”, *Applied Physics B* **105**, 17 (2011).
- ³²⁰J. Schmitt, “Dynamik und korrelationen eines bose-einstein-kondensats aus licht”, PhD thesis (Bonn, 2015).
- ³²¹B. T. Walker, H. J. Hesten, R. A. Nyman, and F. Mintert, “Collective excitation profiles and the dynamics of photonic condensates”, *Phys. Rev. A* **100**, 053828 (2019).
- ³²²V. N. Gladilin and M. Wouters, “Classical field model for arrays of photon condensates”, *Phys. Rev. A* **101**, 043814 (2020).
- ³²³J. Schmitt, T. Damm, D. Dung, F. Vewinger, J. Klaers, and M. Weitz, “Observation of grand-canonical number statistics in a photon bose-einstein condensate”, *Phys. Rev. Lett.* **112**, 030401 (2014).
- ³²⁴C. Weiss and J. Tempere, “Grand-canonical condensate fluctuations in weakly interacting bose-einstein condensates of light”, *Phys. Rev. E* **94**, 042124 (2016).

- ³²⁵N. P. Proukakis, D. W. Snoke, and P. B. E. Littlewood, *Universal themes of bose-einstein condensation* (Cambridge university press, 2017).
- ³²⁶J. Schmitt, T. Damm, D. Dung, et al., “Spontaneous symmetry breaking and phase coherence of a photon bose-einstein condensate coupled to a reservoir”, *Phys. Rev. Lett.* **116**, 033604 (2016).
- ³²⁷J. Marelic, L. F. Zajiczek, H. J. Hesten, et al., “Spatiotemporal coherence of non-equilibrium multimode photon condensates”, *New Journal of Physics* **18**, 103012 (2016).
- ³²⁸A.-W. de Leeuw, E. C. I. van der Wurff, R. A. Duine, and H. T. C. Stoof, “Phase diffusion in a bose-einstein condensate of light”, *Phys. Rev. A* **90**, 043627 (2014).
- ³²⁹C. Henry, “Theory of the linewidth of semiconductor lasers”, *IEEE Journal of Quantum Electronics* **18**, 259–264 (1982).
- ³³⁰R. Paschotta, “Schawlow–townes linewidth”, *RP Photonics Encyclopedia - Schawlow-Townes linewidth, single-frequency laser, phase noise* (2020).
- ³³¹N. B. Abraham and S. R. Smith, “Stimulated versus spontaneous emission as a cause of photon correlations”, *Phys. Rev. A* **15**, 421–428 (1977).
- ³³²J. Marelic, B. T. Walker, and R. A. Nyman, “Phase-space views into dye-microcavity thermalized and condensed photons”, *Phys. Rev. A* **94**, 063812 (2016).
- ³³³N. Bruti-Liberati and E. Platen, “Approximation of jump diffusions in finance and economics”, *Computational Economics* **29**, 283–312 (2007).
- ³³⁴J. Schmitt, private communication, 2018.
- ³³⁶R. Paschotta, “Linewidth enhancement factor”, *RP Photonics Encyclopedia - linewidth enhancement factor, amplitude-phase coupling, alpha, semiconductor laser, phase noise, Henry factor* (2020).
- ³³⁷D. Dung, C. Kurtscheid, T. Damm, et al., “Variable potentials for thermalized light and coupled condensates”, *Nature Photonics* **11**, 565–569 (2017).
- ³³⁸B. Kassenberg, M. Vretnar, S. Bissesar, and J. Klaers, “Controllable josephson junction for photon bose-einstein condensates”, *arXiv:2001.09828* (2020).
- ³³⁹C. Kurtscheid, D. Dung, E. Busley, F. Vewinger, A. Rosch, and M. Weitz, “Thermally condensing photons into a coherently split state of light”, *Science* **366**, 894–897 (2019).
- ³⁴⁰A.-W. de Leeuw, O. Onishchenko, R. A. Duine, and H. T. C. Stoof, “Effects of dissipation on the superfluid–mott-insulator transition of photons”, *Phys. Rev. A* **91**, 033609 (2015).
- ³⁴¹F. E. Ozturk, T. Lappe, G. Hellmann, et al., “Fluctuation dynamics of an open photon bose-einstein condensate”, *Phys. Rev. A* **100**, 043803 (2019).
- ³⁴²B. T. Walker, J. D. Rodrigues, H. S. Dhar, R. F. Oulton, F. Mintert, and R. A. Nyman, “Non-stationary statistics and formation jitter in transient photon condensation”, *Nature Communications* **11**, 1390 (2020).
- ³⁴³S. Van Leuven, *Fluctuaties in een bose-einstein condensaat van fotonen in een caviteit gevuld met kleurvloeistof*, 2019.

BIBLIOGRAPHY

- ³⁴⁴M. Biondi, G. Blatter, and S. Schmidt, “Emergent light crystal from frustration and pump engineering”, *Phys. Rev. B* **98**, 104204 (2018).
- ³⁴⁵F. Vicentini, F. Minganti, A. Biella, G. Orso, and C. Ciuti, “Optimal stochastic unraveling of disordered open quantum systems: application to driven-dissipative photonic lattices”, *Phys. Rev. A* **99**, 032115 (2019).
- ³⁴⁶A. Opala, S. Ghosh, T. C. Liew, and M. Matuszewski, “Neuromorphic computing in ginzburg-landau polariton-lattice systems”, *Phys. Rev. Applied* **11**, 064029 (2019).
- ³⁴⁷K. P. Kalinin, A. Amo, J. Bloch, and N. G. Berloff, “Polaritonic xy-ising machine”, arXiv:2003.09414 (2020).
- ³⁴⁸L. Lu, J. D. Joannopoulos, and M. Soljacic, “Topological photonics”, *Nature Photonics* **8**, 821–829 (2014).
- ³⁴⁹G. Mazzucchi, W. Kozłowski, S. F. Caballero-Benitez, and I. B. Mekhov, “Collective dynamics of multimode bosonic systems induced by weak quantum measurement”, *New Journal of Physics* **18**, 073017 (2016).
- ³⁵⁰C. D. Batista and G. Ortiz, “Generalized jordan-wigner transformations”, *Phys. Rev. Lett.* **86**, 1082–1085 (2001).
- ³⁵¹L. B. Madsen and K. Mølmer, “Spin squeezing and precision probing with light and samples of atoms in the gaussian description”, *Phys. Rev. A* **70**, 052324 (2004).
- ³⁵²M. Takahashi, “Modified spin-wave theory of a square-lattice antiferromagnet”, *Phys. Rev. B* **40**, 2494–2501 (1989).
- ³⁵³P. Koczyk, P. Wiewiór, and C. Radzewicz, “Photon counting statistics—undergraduate experiment”, *American Journal of Physics* **64**, 240 (1996).
- ³⁵⁴Q. Xu, P. Gallion, and F. Mendieta, “Optical homodyne detection and applications in quantum cryptography.”, PhD thesis (2009).
- ³⁵⁵M. Fuwa, S. Takeda, M. Zwierz, H. M. Wiseman, and A. Furusawa, “Experimental proof of nonlocal wavefunction collapse for a single particle using homodyne measurements”, *Nature Communications* **6**, Article, 6665 EP – (2015).
- ³⁵⁶G. M. D’Ariano and M. G. A. Paris, “Lower bounds on phase sensitivity in ideal and feasible measurements”, *Phys. Rev. A* **49**, 3022–3036 (1994).
- ³⁵⁷T. W. Hänsch, “Passion for precision”, Nobel Lecture (2005).
- ³⁵⁸C. Mora and Y. Castin, “Extension of bogoliubov theory to quasicondensates”, *Phys. Rev. A* **67**, 053615 (2003).
- ³⁵⁹G. N. Milstein and M. V. Tretyakov, *Stochastic numerics for mathematical physics* (Springer-Verlag, 2010).
- ³⁶⁰C. Rackauckas and Q. Nie, “Differentials.jl – a performant and feature-rich ecosystem for solving differential equations in julia”, *Journal of open research software* **5**, 15 (2017).